METHIONINE SULFOXIDE REDUCTASE IN NEURODEGENERATIVE DISEASE AND LOCOMOTOR–ASSOCIATED DOPAMINE SIGNALING

By

Derek B. Oien

Submitted to the Department of Pharmacology and Toxicology of the University of Kansas in partial fulfillment of the requirements for the degree of Doctor of Philosophy

Dissertation Committee:

_____
Jackob Moskovitz (Chairman)

_____
Stephen C. Fowler

_____
Mary L. Michaelis

_____
Honglian Shi

_____
Michael A. Johnson

Date defended: April 22nd, 2010

Acceptance

The Dissertation Committee for Derek B. Oien certifies
that this is the approved version of the following dissertation:

METHIONINE SULFOXIDE REDUCTASE IN NEURODEGENERATIVE DISEASE AND LOCOMOTOR–ASSOCIATED DOPAMINE SIGNALING

_____
Jackob Moskovitz (Chairman)

_____
Date approved

Abstract

Reactive oxygen species can cause posttranslational modifications to amino acids, including sulfur-containing methionine. Methionine sulfoxide modifications are reduced by methionine sulfoxide reductase enzymes. The redox balance between reactive oxygen species and the methionine sulfoxide reductase system is disrupted in the aging process. This loss of antioxidant homeostasis can result in disease, and neurons may be particularly susceptible to the impact of methionine sulfoxide in proteins. Here we present evidence for the disruption of cell signaling processes in neuronal protein metabolism, and neurodegeneration in organisms lacking the methionine sulfoxide reductase A gene. In addition, we present data supporting the novel concept of the compromising effect of methionine oxidation on dopaminergic receptor function that is linked to movement regulation. Consequently, it is predicted that enhancing the activity of the methionine sulfoxide reductase system may be beneficial in preventing oxidative stress-related changes in brain function and neurodegenerative diseases.

Acknowledgements

I dedicate this work to my parents, Jeffrey M. Oien and Kimberly A. Kyllonen, who have supported my goals and helped me achieve them. I owe a great debt of thanks to my advisor, Jackob Moskovitz, and my committee members Stephen C. Fowler, Mary L. Michaelis, Michael A. Johnson, and Honglian Shi. I could not have accomplished this research without the assistance of Gregory L. Osterhaus, Andrea N. Ortiz, David S. Moore, Heather E. Shinogle, and Brandi L. Lundquist. I would also like thank the Department of Pharmacology & Toxicology and all of its members who could not have been more helpful in supporting my research and education. Finally, I am thankful for the undying support of Heather A. Menchen and Nathan C. Haley.

The research presented here has been supported by funding from the National Institute of Aging AG027363, Higuchi Bioscience Center J.R. and Inez Jay Award, KIDDRC Center Grant HDO2528, Kansas EPSCOR/National Science Foundation, and the Department of Pharmacology & Toxicology.

Common Abbreviations Used

Cys, Cysteine

D1DR, Dopamine D1 receptor

D2DR, Dopamine D2 receptor

DA, Dopamine

FSCV, Fast scan cyclic voltammetry

KO, Knockout

Met, Methionine

MetO, Methionine sulfoxide

Msr, Methionine sulfoxide reductase

MsrA$^{-/-}$, Msr knockout mouse

ROS, Reactive oxygen species

WT, Wild type

Table of Contents

[1-9]Replication or excerpt duplicated respectively from the following:

1. Oien DB, Moskovitz J. Substrates of the methionine sulfoxide reductase system and their physiological relevance. Schatten, GP (ed.), *Current Topics in Developmental Biology*. Academic Press. 2007 Oct; 80:Ch. 3.
2. Pal R, Oien DB, Ersen FY, Moskovitz J. Elevated levels of brain-pathologies associated with neurodegenerative diseases in the methionine sulfoxide reductase A knockout mouse. *Experimental Brain Research*. 2007 Jul; 180(4):765-774.
3. Oien DB, Shinogle HE, Moore DS, Moskovitz J. Clearance and phosphorylation of alpha-synuclein are inhibited in methionine sulfoxide reductase A null yeast cells. *Journal of Molecular Neuroscience*. 2009 Nov; 39(3):323-332.
4. Oien DB, Canello T, Gabizon R, Gasset M, Lundquist BL, Burns JM, Moskovitz J. Detection of oxidized methionine in selected proteins, cellular extracts and blood serums by novel anti-methionine sulfoxide antibodies. *Archives of Biochemistry and Biophysics*. 2009 May; 485(1): 35-40.
5. Moskovitz J, Oien DB. Protein carbonyl and the methionine sulfoxide reductase system. *Antioxidants & Redox Signaling*. 2010 Mar; 12(3):405-415.
6. Oien DB, Wang X, Moskovitz J. Genomic and proteomic analyses of the methionine sulfoxide reductase A knockout mouse. *Current Proteomics*. 2008 Jul; 5(2):96-103.
7. Oien DB, Osterhaus GL, Latif S, Pinkston JW, Fulks J, Johnson M, Fowler SC, Moskovitz J. The *MsrA* knockout mouse exhibits abnormal behavior and brain dopamine levels. *Free Radical Biology and Medicine*. 2008 Jul; 45(2):193-200.
8. Oien DB, Osterhaus GL, Lundquist BL, Fowler SC, Moskovitz J. Caloric restriction alleviates abnormal locomotor activity and dopamine levels in the brain of the methionine sulfoxide reductase A knockout mouse. *Neuroscience Letters*. 2010 Jan; 468(1):38-41.
9. *Manuscript*: Ortiz AN, Oien DB, Moskovitz J, Johnson MA. Reserve pool dopamine mobilization in methionine sulfoxide reductase null mice.
10. Oien DB, Ortiz AN, Rittel AG, Dobrowsky RT, Johnson MA, Fowler SC, Moskovitz J. Dopamine D2 receptor function is compromised in the brain of the methionine sulfoxide reductase A knockout mouse. *Journal of Neurochemistry*. In Press.

I. Introduction

Posttranslational modifications can change a protein's structure, function, and solubility. One specific modification caused by reactive oxygen species (ROS) is the oxidation of the sulfur atom in the methionine (Met) side chain. This modified amino acid is denoted as methionine sulfoxide (MetO). Sulfoxides in proteins are of considerable interest as they are involved in early posttranslational modification events. Thus, various organisms produce specific enzymes that can reverse these modifications. Methionine sulfoxide reductase (Msr) enzymes, known collectively as the Msr system, are the only known enzymes that can reduce MetO. The current research field of methionine redox cycles is consumed with elucidating its role in regulation, redox homeostasis, prevention of irreversible modifications, pathogenesis, and the aging process. (Oien & Moskovitz, 2008)

In 1956, Denham Harman published a theory on free radical damage to organisms and its relation to aging (Harman, 1956). This landmark article has evolved to what is now known as the free radical theory of aging (Harman, 1973). The free radical theory of aging is in accordance with the common hypothesis that aging is a process mediated by oxidative damage, and the controversial idea that age-related disease is linked to oxidative damage.

Oxidative damage to cells can affect multiple cellular components, including lipids and proteins. In general, a chemical modification forming after the genetic expression of a protein is denoted as post-translational modification. Oxidative modifications to proteins are caused by reactive species, such as ROS and reactive nitrogen intermediates. These oxidants are formed by a variety of biological processes within cells and tissues at varying rates, and specific toxins can induce their production. Examples include hydrogen peroxide, superoxide, oxygen, ozone, hypochlorous acid, choramine T (sodium N-chloro-p-toluenesulfonchloramide), N-chlorosuccinimide, hydroxyl radicals, and peroxynitrite (Savige & Fontana, 1977). Modifications via ROS can affect virtually all amino acid side chains and the backbone of the peptide linkage.

However, amino acids vary in their vulnerability to become oxidized. Furthermore, the particular location of amino acid residues within the structure of a protein may determine the sensitivity level towards the oxidants, which contributes to even greater variability.

Common ROS-mediated side chain modifications can be in the form of a carbonyl or the oxidized sulfur atom of Met or cysteine (Cys). Protein-carbonyls are non-enzymatic irreversible modifications. They are often catalyzed by metal ions and tend to form on the side chains of the amino acids proline, arginine, threonine, and lysine (Dalle-Donne et al., 2006). In contrast, the sulfur-containing amino acids are readily oxidized and most modifications are reversible. Modifications of Cys residues have various consequences including the alteration of protein structure, inactivation of proteins, and formation of disulfide bridges (Jacob, Knight, & Winyard, 2006). Reversal of the post-translational modifications to Cys residues can be achieved by several non-enzymatic reductants and reducing enzymes. However, the reduction of MetO is exclusively performed by the Msr system.

A. **Msr System** (Oien & Moskovitz, 2008)

The oxidation of a Met side chain can form either a MetO or a Met sulfone. The former contains an oxygen atom double-bonded to the sulfur atom, and the latter contains two oxygens bonded to the sulfur atom. Met sulfones are formed in more extreme oxidant conditions following the formation of MetO. They are considered irreversible, and cannot be reduced under physiological conditions. In contrast, MetO is readily formed relative to other post-translational modifications and can be reduced by Msr. Oxidation of the Met sulfur atom can form either one of two possible enantiomers; denoted as *S* and *R*. With some specific exceptions, there is no general evidence to date predicting which enantiomer of MetO will be formed when the side chain of Met is oxidized. The *S* and *R* enantiomers can be reduced by the enzymes methionine sulfoxide reductase A and B (MsrA, MsrB), respectively.

The Msr enzymes reduce MetO at the expense of becoming oxidized, and thus inactivate themselves. The first evidence of a reductase that reduced MetO in peptides was shown in 1981 (Brot, Weissbach, Werth, & Weissbach, 1981). The enzymes are reduced and reactivated primarily by thioredoxin (Trx), thioredoxin reductase (Trr), and NAD(P)H. The reduction sequence can be illustrated by the equation:

$$\text{NADPH} + \text{Trr} \rightarrow \text{Trx} \rightarrow \text{Msr} \rightarrow \text{Met (-Methyl-SO to -Methyl-S)}$$

where the arrows depict reduction of each oxidized form of the molecule by the former substance. After the reducing enzymes bind to their substrates, they become oxidized and thus re-enter the reduction cycle. In some forms of human MsrB, specifically hMsrB2 and hMsrB3, thioredoxin has been found less efficient for reduction. In addition, a protein called thionein, especially for hMsrB3 (Sagher, Brunell, Hejtmancik et al., 2006), and certain selenium compounds make better reducing enzymes to activate these reductases (Sagher, Brunell, Brot, Vallee, & Weissbach, 2006). In experimental conditions dithiothreitol is often used to reduce Msr, and lipoic acid also can act as a reductant (Biewenga, Veening-Griffioen, Nicastia, Haenen, & Bast, 1998).

The Cys at position 72 is vital for Msr activity and is highly conserved in most species (Moskovitz et al., 2000). When Msr is inactivated, the Cys residue is oxidized and forms a disulfide bridge with another Cys near the C-terminal (Brot & Weissbach, 2000).

The Msr enzymes are found in many organisms in nature. In a bacterial strain like *Escherichia coli*, there is one form of MsrA and one form of MsrB. However, in mammals there is one form of MsrA and four forms of MsrB, denoted MsrB1, MsrB2, MsrB3A, and MsrB3B. The MsrB1 form is a cytoplasmic selenoprotein (Bar-Noy & Moskovitz, 2002; Moskovitz et al., 2002), MsrB2 and MsrB3B can be targeted to the mitochondria, and MsrB3A is targeted to the endoplasmic reticulum (Kim & Gladyshev, 2004). In addition, MsrA also has a long spliced-

variant form that is transported to the mitochondria (Balog et al., 2003). The *msr* genes are ubiquitously expressed in many organisms, and highly expressed in the liver and kidneys of mammals (Moskovitz et al., 1996). The Msr system is considered to be important for survival under oxidative stress conditions as manifested by *msrA* gene knockouts in various organisms (Moskovitz, 2005).

Oxidation of Met residues can be readily reduced by the Msr system. The latter may prevent changes resulting from Met oxidation, for example alterations in the properties methyl sulfoxide-containing peptides, protein structure, biological function, or a combination of all possibilities. Met is a hydrophobic amino acid, and the hydrophobicity decreases when the sulfur atom is oxidized. However, the sulfoxide formation can alter the native folding and create a more hydrophobic protein (Chao, Ma, & Stadtman, 1997). When Met is present in a protein, it can scavenge/detoxify the ROS, and this may occur with impunity if Msr is present. Thus, it is further speculated that Met residues play a protective role from ROS by their placement on outer faces of certain proteins. In this situation, they may serve as a shield from oxidative modification, protecting the active site of the protein. Furthermore, lack of MsrA has been shown in some organisms to increase protein carbonyl accumulation, an irreversible form of protein oxidation (Moskovitz et al., 2001). There is also evidence that Msr levels decrease in various rat tissues as they age (Petropoulos, Mary, Perichon, & Friguet, 2001), supporting the link between enhanced free radical damaging action and the aging process (Stadtman, Moskovitz, Berlett, & Levine, 2002).

The role of MetO in proteins and the subsequent reduction in the pathogenesis of disease and general aging of cells is not completely known. Hence, the Msr system may prove to be a key component of oxidative prevention, regulation, or a combination of both. The extent of the consequences of these posttranslational modifications and their complete physiological significance still require more research.

B. Physiological Relevance of Msr Substates (Oien & Moskovitz, 2008)

Substrates of the Msr system can be loosely classified by the overall effect of the MetO on the protein. Regulated substrates utilize Met as a molecular switch to modulate activation; scavenging substrates use Met residues to detoxify oxidants and protect important regions of the protein; modified substrates are altered by methionine oxidation resulting in various changes in their properties including function, activity, structure, and degradation resistance.

1. Regulated Substrates

Cell signaling is an important biological mechanism and critical component of cellular regulation. Signaling pathways consist of proteins that can be activated and inactivated to modulate a response. Activity of the protein is often determined by its structure, and overall by the accessibility of reactive site. Modifications that add to cell signaling are covalently bonded and reversible. Well known examples of this phenomenon include tyrosine and serine phosphorylation/dephosphorylation, and Cys redox modulation (Ciorba, Heinemann, Weissbach, Brot, & Hoshi, 1997). It is suggested that the redox properties of Met residues also can contribute to signal pathways. Msr enzymes are generally regarded as repair enzymes, but the following examples show evidence of the enzymes contributing to cellular regulation.

2. Scavenging Substrates

Scavenging substrates do not display any significant loss of biological activity when Met residues are oxidized under physiological conditions. This classification is dedicated to substrates containing Met that are hypothesized to play a protective role against the oxidation of proteins, or other residues of the same protein. Thus, by Met cyclic oxidation and reduction via the Msr system, these substrates are considered to be endogenous antioxidants, or oxidant scavengers. Theoretically, Met residues can effectively scavenge oxidants before reactive species modify residues critical to the structure and function of the substrate (Levine, Mosoni,

Berlett, & Stadtman, 1996). In this perspective, the Met residues act as ‘shields’ to the active site or ‘molecular sinks’ for reactive species balance. Evidence to support this idea is found in the placement of Met residues. They are often described as surface-exposed, protecting an opening to the active site, flanking the active site, or a combination.

3. Modified Substrates with ‘Damaged’ Effects

The proteins in this classification display altered functions, a loss of biological activity, a change in structure, or resistance to degradation after the oxidation of the Met residues. The substrates are often linked to respective diseases, where they are discovered in a ‘damaged’ state. Evidence demonstrates that MetO may contribute to this state. The role that MetO may play in the physical and chemical properties of the protein is based solely on their availability to oxidation. Additionally, it is not always clear to what extent the substrate plays a role in the pathogenesis development of a respective disease, or rather if it is a consequence of a mature pathological state. The Msr system is proposed to play a role in maintaining the integrity of these substrates in their reduced form. The role of the Msr system may include repairing MetO-oxidized proteins by preventing malfunction due to MetO, protecting specific regions of the protein from further irreversible modifications and structural changes, or a combination of both. The ultimate question is: if indeed MetO residues are responsible for this functional alteration, what makes Msr insufficient to counteract this phenomenon? Possibilities include, but are not limited to, the decline of Msr presence, decline of Msr activity, and non-compatable concentrations of reactive species. In some cases, Met oxidation may serve a modulation role, or simply be an ROS scavenger. Evidence may be either lacking in support of these roles or the actual functions of the proteins may still be unknown.

4. Discussion (Oien & Moskovitz, 2008)

In summary, there is a broad spectrum of substrates of the Msr system. The physiological significance of the MetO in conjunction with the Msr system is based on separate evidence. Furthermore, the substrates are classified into the three categories of regulated substrates, scavenging substrates, and modified substrates resulting in various changes in properties. The complete list of substrates is presented in Table 1. In addition, the substrates are subcategorized depending on the experimental evidence of *in vivo/ex vivo* (including *in situ*) and *in vitro*.

The continuing research will provide new information on the role of the Met redox cycle in regulation, redox homeostasis, prevention of irreversible modifications, pathogenesis, and the aging process. Moreover, the characterization of Met oxidation and the Msr system may lead to new targets for therapeutic intervention.

Table 1. Substrates for Msr further classified by type of experimental evidence. The key for abbreviations can be found in Oien & Moskovitz, 2008.

Regulated *in vivo/ex vivo*
α_1-AT[a]
Apo-AI[a]
Calcium-activated potassium channels[a]
IκBα
TM[a]
Voltage-activated potassium channels[a]

Scavenging *in vivo/ex vivo*
GS[a]
GrL
GH[a]
IFN-γ[a]
sHsps[a]

Modified Substrates *in vivo/ex vivo*
αS
APP
Aβ[a]
Cardiotoxin-VII1[a]
Catalase
CCK[a]
CX3
DJ-1
Ffh[a]
Fn[a]
Glucagon[a]
LH[a]
MENK[a]
NYP[a]
PTH[a]
Prolactin[a]
Prp[c]
SSR
VIP[a]

Regulated *in vitro*
Apo-AII[a]
t-PA[a]

Scavenging *in vitro*
α2-PI[a]
α2M[a]
AT III[a]
CS[a]
IFN-α2b[a]
IL-6[a]
15-lipoxygenase[a]
MPI[a]
SCF[a]

Modified Substrates *in vitro*
Actin
ATCH[a]
AF2[a]
β_1-Butx[a]
Bombesin[a]
CT[a]
Chymotrypsin[a]
Complement C5[a]
Cytochrome *c*[a]
Cytochrome *c* oxidase[a]
Echistatin[a]
FVIIa[a]
Hb
HMD-D
HIV-2 protease[a]
L12/L7 (ribosomal proteins)[a]
Lysozyme[a]
Ovoinhibitor[a]
Pepsin[a]
Phosphoglucomutase[a]
PAI-1[a]
RNase A[a]
Secretory leukocyte inhibitor[a]
Subtilisin[a]
Tryptophanase[a]

[a]Substrates that are listed by the review of Levine *et al.* (2000).

D. References

Balog, E. M., Norton, L. E., Bloomquist, R. A., Cornea, R. L., Black, D. J., Louis, C. F., et al. (2003). Calmodulin oxidation and methionine to glutamine substitutions reveal methionine residues critical for functional interaction with ryanodine receptor-1. *J Biol Chem, 278*(18), 15615-15621.

Bar-Noy, S., & Moskovitz, J. (2002). Mouse methionine sulfoxide reductase B: effect of selenocysteine incorporation on its activity and expression of the seleno-containing enzyme in bacterial and mammalian cells. *Biochem Biophys Res Commun, 297*(4), 956-961.

Biewenga, G. P., Veening-Griffioen, D. H., Nicastia, A. J., Haenen, G. R., & Bast, A. (1998). Effects of dihydrolipoic acid on peptide methionine sulfoxide reductase. Implications for antioxidant drugs. *Arzneimittelforschung, 48*(2), 144-148.

Brot, N., & Weissbach, H. (2000). Peptide methionine sulfoxide reductase: biochemistry and physiological role. *Biopolymers, 55*(4), 288-296.

Brot, N., Weissbach, L., Werth, J., & Weissbach, H. (1981). Enzymatic reduction of protein-bound methionine sulfoxide. *Proc Natl Acad Sci U S A, 78*(4), 2155-2158.

Chao, C. C., Ma, Y. S., & Stadtman, E. R. (1997). Modification of protein surface hydrophobicity and methionine oxidation by oxidative systems. *Proceedings of the National Academy of Sciences of the United States of America, 94*(7), 2969-2974.

Ciorba, M. A., Heinemann, S. H., Weissbach, H., Brot, N., & Hoshi, T. (1997). Modulation of potassium channel function by methionine oxidation and reduction. *Proc Natl Acad Sci U S A, 94*(18), 9932-9937.

Dalle-Donne, I., Aldini, G., Carini, M., Colombo, R., Rossi, R., & Milzani, A. (2006). Protein carbonylation, cellular dysfunction, and disease progression. *J Cell Mol Med, 10*(2), 389-406.

Harman, D. (1956). Aging: a theory based on free radical and radiation chemistry. *J Gerontol, 11*(3), 298-300.

Harman, D. (1973). Free radical theory of aging. *Triangle, 12*(4), 153-158.

Jacob, C., Knight, I., & Winyard, P. G. (2006). Aspects of the biological redox chemistry of cysteine: from simple redox responses to sophisticated signalling pathways. *Biol Chem, 387*(10-11), 1385-1397.

Kim, H. Y., & Gladyshev, V. N. (2004). Characterization of mouse endoplasmic reticulum methionine-R-sulfoxide reductase. *Biochem Biophys Res Commun, 320*(4), 1277-1283.

Levine, R. L., Mosoni, L., Berlett, B. S., & Stadtman, E. R. (1996). Methionine residues as endogenous antioxidants in proteins. *Proc Natl Acad Sci U S A, 93*(26), 15036-15040.

Moskovitz, J. (2005). Methionine sulfoxide reductases: ubiquitous enzymes involved in antioxidant defense, protein regulation, and prevention of aging-associated diseases. *Biochim Biophys Acta, 1703*(2), 213-219.

Moskovitz, J., Bar-Noy, S., Williams, W. M., Requena, J., Berlett, B. S., & Stadtman, E. R. (2001). Methionine sulfoxide reductase (MsrA) is a regulator of antioxidant defense and lifespan in mammals. *Proc Natl Acad Sci U S A, 98*(23), 12920-12925.

Moskovitz, J., Jenkins, N. A., Gilbert, D. J., Copeland, N. G., Jursky, F., Weissbach, H., et al. (1996). Chromosomal localization of the mammalian peptide-methionine sulfoxide reductase gene and its differential expression in various tissues. *Proc Natl Acad Sci U S A, 93*(8), 3205-3208.

Moskovitz, J., Poston, J. M., Berlett, B. S., Nosworthy, N. J., Szczepanowski, R., & Stadtman, E. R. (2000). Identification and characterization of a putative active site for peptide methionine sulfoxide reductase (MsrA) and its substrate stereospecificity. *J Biol Chem, 275*(19), 14167-14172.

Moskovitz, J., Singh, V. K., Requena, J., Wilkinson, B. J., Jayaswal, R. K., & Stadtman, E. R. (2002). Purification and characterization of methionine sulfoxide reductases from mouse

and Staphylococcus aureus and their substrate stereospecificity. *Biochem Biophys Res Commun, 290*(1), 62-65.

Oien, D. B., & Moskovitz, J. (2008). Substrates of the methionine sulfoxide reductase system and their physiological relevance. *Curr Top Dev Biol, 80*, 93-133.

Petropoulos, I., Mary, J., Perichon, M., & Friguet, B. (2001). Rat peptide methionine sulphoxide reductase: cloning of the cDNA, and down-regulation of gene expression and enzyme activity during aging. *Biochem J, 355*(Pt 3), 819-825.

Sagher, D., Brunell, D., Brot, N., Vallee, B. L., & Weissbach, H. (2006). Selenocompounds can serve as oxidoreductants with the methionine sulfoxide reductase enzymes. *J Biol Chem, 281*(42), 31184-31187.

Sagher, D., Brunell, D., Hejtmancik, J. F., Kantorow, M., Brot, N., & Weissbach, H. (2006). Thionein can serve as a reducing agent for the methionine sulfoxide reductases. *Proc Natl Acad Sci U S A, 103*(23), 8656-8661.

Savige, W. E., & Fontana, A. (1977). Interconversion of methionine and methionine sulfoxide. *Methods Enzymol, 47*, 453-459.

Stadtman, E. R., Moskovitz, J., Berlett, B. S., & Levine, R. L. (2002). Cyclic oxidation and reduction of protein methionine residues is an important antioxidant mechanism. *Mol Cell Biochem, 234-235*(1-2), 3-9.

II. Msr in Neurodegenerative Disease

Increasing evidence suggests a major role of Met redox cycles in neurodegenerative disease. A neurodegenerative disease is a condition resulting in the deterioration of neurons, ultimately affecting brain function. They often present with problems in movement or memory and dementia. Certain neurodegenerative diseases are associated with a specific brain protein. Examples are amyloid-beta, alpha-synuclein, and prion (J. Moskovitz, 2005). The functions of these brain proteins are unknown, but they are each implicated in a respective neurodegenerative disease. Oxidant-mediated accumulation of modified proteins may be one of the major causes of age-related neurodegenerative disease (Jackob Moskovitz & Bush, 2005). In addition, the Msr system may prevent irreversible protein damage, and thus prevent accumulation of posttranslational modified proteins. Overall, Met redox cycles have been associated with Alzheimer's disease, Parkinson's disease, and Prion-related spongiform encephalopathies. (D. B. Oien & Moskovitz, 2008)

Alzheimer's disease is a data processing disorder associated with neural cell neurofibrillary tangles and the extracellular deposition of the amyloid plaques. Amyloid plaques are extracellular plaque filaments with an amyloid structure, and contain the amyloid-beta peptide. The amyloid-beta peptide is formed by cleavage of the amyloid precursor protein (Goedert & Spillantini, 2006). This cleavage commonly results in an amyloid beta peptide of 40 or 42 residues. Amyloid-beta-40 concentrates in plaques of cerebral arteries. Amyloid-beta-42 is more concentrated in neural plaques. It is neurotoxic and thought to cause neurodegeneration. The toxicity of amyloid-beta-42 is suggested to play a central role in Alzheimer's disease. The formation of amyloid plaques is considered one possible pathway of Alzheimer's disease progression. However, this theory is not conclusive.

Amyloid-beta-42 is a neurotoxin found in extracellular amyloid plaques. It contains 42 amino acids, including one Met at position 35. The neurotoxic properties of amyloid-beta may be a result of reactive species and free radical formation (Pogocki, 2003). Oxidation of Met35 can

reduce the amyloid-beta-42 fibrillation rate (Hou, Kang, Marchant, & Zagorski, 2002). The fibrillation rate may be associated with its ability to form the insoluble plaques, although the exact role is still unclear. The oxidized Met35 alters the peptide structure and decreases the hydrophobicity of the peptide (Barnham et al., 2003). The change in hydrophobicity decreases its ability to penetrate lipid membranes, and may contribute to the peptides altered location. The Msr system may assist in retaining the structure of amyloid-beta-42 (Jackob Moskovitz & Bush, 2005). Moreover, the transduction of MsrA as a fusion protein to cells with amyloid-beta-42 increases the viability of the cultures (Jung et al., 2003). In addition, Msr activity was shown to decrease in Alzheimer's brains (Gabbita, Aksenov, Lovell, & Markesbery, 1999). The higher levels of oxidative stress correlate with the presence of amyloid-beta in the hippocampus and cortex.

Amyloid precursor protein is a glycoprotein expressed throughout the plasma membrane. Mutations in the amyloid precursor protein gene are thought to cause a familial form of Alzheimer's disease. For example, Val717 can be changed to a phenylalanine or glycine. This substitution stimulates G-protein binding and signal transduction in aged human brain membranes (Karelson, Fernaeus, Reis, Bogdanovic, & Land, 2005). The stimulation is weakened in the temporal cortex when a methionine at position 722 is oxidized to a sulfoxide (Reis, Zharkovsky, Bogdanovic, Karelson, & Land, 2007). Furthermore, oxidized Met722 in the V717G mutated peptide causes less mitochondrial damage in neuron cell cultures. The neurotoxcity of this mutation may be mediated by methionine oxidation; thus, the Msr system may also contribute to this regulation.

Parkinson's disease is a neurodegenerative disease that causes alterations in motor function and postural stability. The disease is characterized by a progressive loss of dopaminergic neurons in the substantia nigra (Wood-Kaczmar, Gandhi, & Wood, 2006). The majority of Parkinson's cases are sporadic, and the cause of the disease is unknown. However, over 5% of Parkinson's disease cases are familial, cause by genetic mutations. These cases

include mutations in the alpha-synuclein and DJ-1 genes. Hence, the alpha-synuclein and DJ-1 proteins may also be implicated in sporadic Parkinson's disease.

Alpha-Synuclein is a neural protein that is thought to play a role in multiple diseases, collectively termed synucleinopathies. It is found in the lewy bodies of post-mortem Parkinson's disease patients. Lewy bodies are cytoplasmic inclusions mainly in nigral domaminergic neurons. Alpha-synuclein is soluble, natively unfolded protein that has no ordered structure under physiological conditions (Uversky, Gillespie, & Fink, 2000). Alpha-synuclein has four Met residues at positions 1, 5, 116, and 127 (Glaser, Yamin, Uversky, & Fink, 2005). All four Met residues can be oxidized with hydrogen peroxide, which inhibits alpha-synuclein fibrillation (Uversky et al., 2002). Metals such as titanium, zinc, aluminum, and lead can overcome the inhibited fibrillation of the Met-oxidized protein (Yamin, Glaser, Uversky, & Fink, 2003). If the reversal of Met oxidation can prevent further irreversible modification to other residues, it may be a new target for therapeutic intervention (Jackob Moskovitz & Bush, 2005).

The DJ-1 protein is ubiquitously expressed and has no known function. However, it is associated with various cellular processes, including a oxidative stress response (Lev, Roncevich, Ickowicz, Melamed, & Offen, 2006). Mutations in DJ-1 are associated with a genetic autosomal recessive form of Parkinson's disease, and suggested to cause neurodegeneration. However, patients with sporadic Parkinson's and Alzheimer's disease can accumulate oxidized DJ-1 in frontal cortex brain tissues (Choi et al., 2006). Oxidized modifications are found include Cys and Met residues, and additionally irreversible carbonyls and Met sulfones. It is suggested that irreversible oxidations occur under more extreme oxidant conditions, after Cys and Met are oxidized in a reversible state. Moreover, the levels of DJ-1 are increased in Parkinson's and Alzheimer's brains. All together, reduction systems such as Msr may protect DJ-1 in healthy brains, and elevated oxidant conditions in diseased brains may lead to irreversible residue modifications.

Protease-resistant protein-C is the protein found in prions, which are present in the cells of nervous and immune tissue. Prion is a short name for proteinaceous infectious particle, and C refers to cellular. Protein-resistant protein-Sc is a disease-associated isomer. The Sc refers to scapie, a prion disease in sheep. These proteins can be genetic, sporadic, or infectious. They are known to infect brain neural tissue and induce misfolding of other proteins. Diseases associated with prions are called spongiform encephalopathies, one example being Creutzfeldt-Jakob disease (J. Moskovitz, 2005). Creutzfeldt-Jakob disease is a rapidly progressing neurodegenerative disease characterized by dementia and loss of memory. Protein-resistant protein-C exists in an alpha-helix structure. It can convert into the beta-sheet confirmation of the insoluble Sc isomer, probably by conformational changes involving posttranslational modification (Jackson et al., 1999). In addition, a polymorphism at residue 129 results in either a valine or Met surface exposed amino acid that can affect the susceptibility of developing Creutzfeld-Jakob disease (Hill et al., 2003). Hydrogen peroxide can cause Met oxidation, which interferes with the conformation change (Breydo et al., 2005). Moreover, Met residues in mouse and chicken prion protein can be selectively oxidized and form free radicals by copper (II) ions when they refold *in vitro* (Wong, Wang, Brown, & Jones, 1999). Furthermore, the cellular prion protiein level is higher in *msrA* null mice (Williams, Stadtman, & Moskovitz, 2004). This may be a compensation pathway of additional oxidant stress from the lack of an endogenous antioxidant enzyme (Jackob Moskovitz & Bush, 2005). It has not been determined if Met29 and other Met residues are involved in the prion cascade of events. Prion may function as an antioxidant (Wong et al., 2001) or as a signal to increase endogenous antioxidant systems (Rachidi et al., 2003).

The most advanced evidence of methionine oxidation in neurodegenerative diseases is found in Alzheimer's disease, Parkinson's disease, and spongiform encephalopathies (J. Moskovitz, 2005; D. B. Oien & Moskovitz, 2008). The next two articles from our lab present studies related to Alzheimer's disease and synucleinopathies such as Parkinson's disease. In

the section following these two articles, further evidence in these pathologies and prion-associated changes relating to spongiform encelphalopathies are presented.

A. Elevated Levels of Brain-Pathologies Associated with Neurodegenerative Diseases in the MsrA Knockout Mouse (Pal, Oien, Ersen, & Moskovitz, 2007)

One of the posttranslational modifications to proteins is Met oxidation, which is readily reversible by the Msr system. Thus, accumulation of faulty proteins due to a compromised Msr system may lead to the development of aging-associated diseases like neurodegenerative diseases. In particular, it was interesting to monitor the consequential effects of Met oxidation in relation to markers that are associated with Alzheimer's disease as methionine oxidation was implied to play a role in amyloid-beta toxicity. In this study, the Msr knockout (*MsrA*$^{-/-}$) mouse caused an enhanced neurodegeneration in brain hippocampus relative to its wild-type (WT) control mouse brain. Additionally, a loss of astrocytes integrity, elevated levels of amyloid-beta deposition, and tau phosphorylation were dominant in various regions of the *MsrA*$^{-/-}$ hippocampus but not in the WT. Also, a comparison between cultured brain slices of the hippocampal region of both mouse strains showed more sensitivity of the *MsrA*$^{-/-}$ cultured cells to H_2O_2 treatment. It is suggested that a deficiency in MsrA activity fosters oxidative-stress that is manifested by the accumulation of faulty proteins (via Met oxidation), deposition of aggregated proteins, and premature brain cell death.

1. Introduction

Met oxidation in neurodegenerative diseases. Previously, we have shown that exposing mice to 100% oxygen caused higher elevation of protein-carbonyl adducts in various tissues of *MsrA*$^{-/-}$ than in control mice (J. Moskovitz et al., 2001). These results correlated with the loss of MsrA activity in Alzheimer's diseased brains while elevated levels of protein-carbonyl were observed in normal brains (Gabbita et al. 1999). Met oxidation denatures proteins, and converts the

hydrophobic properties of Met into hydrophilic causing structural alterations (Stadtman, Moskovitz, & Levine, 2003). Two major proteins, amyloid-beta and alpha-synuclein, are involved in the toxicity associated with Alzheimer's and Parkinson's diseases, respectively. Both proteins have been shown to lose their fibrillation rate due to their Met oxidation (Palmblad, Westlind-Danielsson, & Bergquist, 2002; Uversky et al., 2002); and in the case with MetO-alpha-synuclein to re-fibrillate in the presence of metal ions and ROS, *in vitro* (Yamin et al., 2003). Moreover, it appears that oxidation of Met35 in amyloid-beta contributes significantly to its toxicity *in vitro* (Butterfield & Boyd-Kimball, 2005; Schoneich, 2005). It has also been demonstrated that MetO-amyloid-beta adducts are present in post-mortem senile plaques (Dong et al., 2003).

To determine whether the *MsrA*$^{-/-}$ mice exhibit specific protein expression patterns that are associated with markers of AD, the levels of the following proteins were monitored:

(a) Tau protein – Microtubule-associated protein tau is abnormally hyper-phosphorylated and aggregated into neurofibrillary tangles in brains of individuals with Alzheimer's disease and other tauopathies (Blennow, Vanmechelen, & Hampel, 2001). Additionally, developmental and aging-induced alterations in brain oxidative status exhibit a major factor in triggering enhanced predisposition to Alzheimer's disease (Apelt, Bigl, Wunderlich, & Schliebs, 2004).

(b) Synaptophysin – Synaptophysin is a 38 kDa calcium-binding glycoprotein that is present in the presynaptic vesicles of neurons and in the neurosecretory granules of neuroendocrine cells. Decreased levels of synaptophysin in Alzheimer's disease correlate with duration of disease.

(c) Glial fibrillary acidic protein (GFAP) – GFAP is considered to be a highly specific marker for astroglial cells. A high number or enhanced apoptosis of the glial cells may reflect on the overall well-being of the neighboring neuronal cells. Taken together, the current hypothesis is that the occurrence of neurodegenerative diseases is linked to the accumulative damages to proteins that causes them to unfold and aggregate; thereby interfering with normal neuronal functions and survival under oxidative stress conditions.

2. Materials and Methods

Antibodies

The antibodies against the following antigens were purchased from the various companies for immunohistochemistry analysis: phosphorylated-tau at serine 202/199 or threonine 205 (Biosource, USA); synaptophysin (Chemicon, USA); Glial fibrillary acidic protein, GFAP (DAKO, Denmark); amyloid-beta 1-42 (anti-human amyloid-beta, 4G8 monoclonal antibodies, which probe an epitope between residues 17–24 of A_, Abcam, USA).

Tissue processing and immunohistochemistry and staining analysis

All mouse experiments were conducted according to guidelines of the University of Kansas Animal Care and Use Committee. “Principles of Laboratory Animal Care” (NIH publication no. 86–23, revised 1985) were followed, as well as special national laws (e.g. the current version of the German law on the Protection of Animals) where applicable.

For all suggested analyses for both mouse strains, we hemisected 12-month-old postmortem cerebrum and fixed the left hemisphere for histological quantification and immunohistochemistry (using the various primary antibodies above), according to previously described methods (Friedlich et al. 2004).

Generally, coronal brain sections from both mouse strains were processed for immunocytochemistry analysis using a specific primary antibody in each case as follows: mice were perfused with phosphate-buffered solution (PBS) followed by 4% paraformaldehyde in 3.8% sodium borate. After completion of the perfusion, brains were decapitated and immersed in 4% paraformaldehyde and 10% sucrose over night. Then, the brains were sectioned and the slices were washed three times with PBS. For immunohistochemistry analyses, 10 µm-thick sections were treated with 3% hydrogen peroxide in methanol for 30 min. After blocking with 1% bovine serum albumin and 3% goat serum in PBS, the sections were incubated with the primary

antibody for overnight at 4℃. After removal of the primary antibody and rinsing them in appropriate buffer they were sequentially incubated with biotinylated goat anti-rabbit or mouse IgG (depending on the source), avidin–horseradish peroxide solution, 0.015% diaminobenzidine plus 0.001% H_2O_2, and finally counterstained with hematoxylin (Vector Laboratories).

For silver stain analysis parallel brain slices were incubated with 10% silver nitrate for 15 min and then washed three times with distilled water. To the silver nitrate solution, concentrated ammonium hydroxide was added drop-by-drop until the precipitate formed was clear. The slides were stained at 40℃ for 30 min or until sections became dark brown. Then, the slides were incubated with 1% ammonium hydroxide solution for 1 min to stop the reaction. Slides were washed in three changes of distilled water and placed in 5% sodium thiosulfate solution for 5 min.

For Nissl stain analysis, parallel brain slides were immersed into 0.5% Cresyl echt violet solution for 3–5 min. At the end of the staining the slides were rinsed in distilled water.

Following all staining and immunohistochemical procedures, the brain slides were washed in three changes of distilled water and dehydrated through graded ethanols and xylene before mounting them with permount (Vector laboratories Burlingame, CA, USA). The slides were then visualized using an upright Nikon light microscope, and images were photographed for analysis.

Brain-hippocampus slice culture

The procedure to grow brain-hippocampus slices in culture was performed according to previously published method (Stoppini, Buchs, & Muller, 1991) with some modification. Briefly, the brains of 3-week-old mice were dissected-out and transferred immediately into an artificial cerebral spinal fluid (aCSF) media containing 124 mM NaCl, 2.8 mM KCl, 2 mM $CaCl_2$, 2 mM $MgSO_4$, 26 mM $NaHCO_3$, 1.25 mM NaH_2PO_4, and 10 mM glucose at pH 7.4. The brains were sliced to sections of 200 µm thickness and were immersed in the aCSF media. Intact sections were transferred into cell culture inserts that are bathed in fresh growth medium containing 50%

MEM w/glutamine (GIBCO), 25% Hanks Balanced Salt Solution (GIBCO), 25% Horse serum (GIBCO), 4.5 mg/mL glucose (Sigma), 1 mM glutamine (Sigma), and pen strep (Sigma) solution. Every second day, half of the old medium was replaced by equal amount of fresh medium. After 7 days in culture the sections were treated with 400 µM of H_2O_2 for 3 h. Control sections were left untreated. Following the incubation, a propidium iodide staining for quantifying the level of cell death was applied as shown below.

Propidium iodide staining

The above medium ($\pm H_2O_2$) was removed and the slices were rinsed twice with PBS, followed by incubation for 30 min at 37°C in the presence of 2 mM propidium iodide (PI) for 30 min at 37°C. The unbound PI was rinsed several times with PBS before viewing with Zeiss LSM 510 confocal microscope.

3. Results

Deposition of amyloid-beta in brain

Alzheimer's disease is characterized pathologically by numerous region-specific, extracellular amyloid-beta depositions in the brain. An immunohistochemical procedure was followed to assess the formation and localization of deposited amyloid-beta in brains of both *MsrA*$^{-/-}$ and WT mouse strains. Postmortem brains of 12-month-old mice (*MsrA*$^{-/-}$ and WT) were prepared to produce slices suitable for immunohistochemical reactions using primary antibody against amyloid-beta (as described under "Materials and Methods"). As shown in Fig. 1, there were significant differences in the amount and localization of amyloid-beta between the brains of *MsrA*$^{-/-}$ and WT mice. In the WT mice, there was no significant detection of amyloid-beta deposits in the hippocampus region shown (Fig. 1, A1, A2). However, in the *MsrA*$^{-/-}$ mice, the staining revealed 2–4 dark brown aggregates stained by the antibody around the cell-body areas of CA1 hippocampus (Fig. 1, B1, B2). The cell bodies remained free of any staining.

These aggregates were localized in the border of stratum pyramidale and oriens and were described as basket cell interneurons by several authors (Ashwood, Lancaster, & Wheal, 1984; Knowles & Schwartzkroin, 1981; Schwartzkroin & Mathers, 1978). Most interestingly, the antibody also labeled at least 10–12 dark-brown aggregates in the *MsrA*$^{-/-}$ stratum lacuonosum layer (Fig. 1, B1, B2). Although the level of the amyloid-beta depositions in the *MsrA*$^{-/-}$ was lower than in the APP mice, it is important to note that the *MsrA*$^{-/-}$ mice were not manipulated to express high levels of amyloid-beta and that it was tested in mid-aged animals.

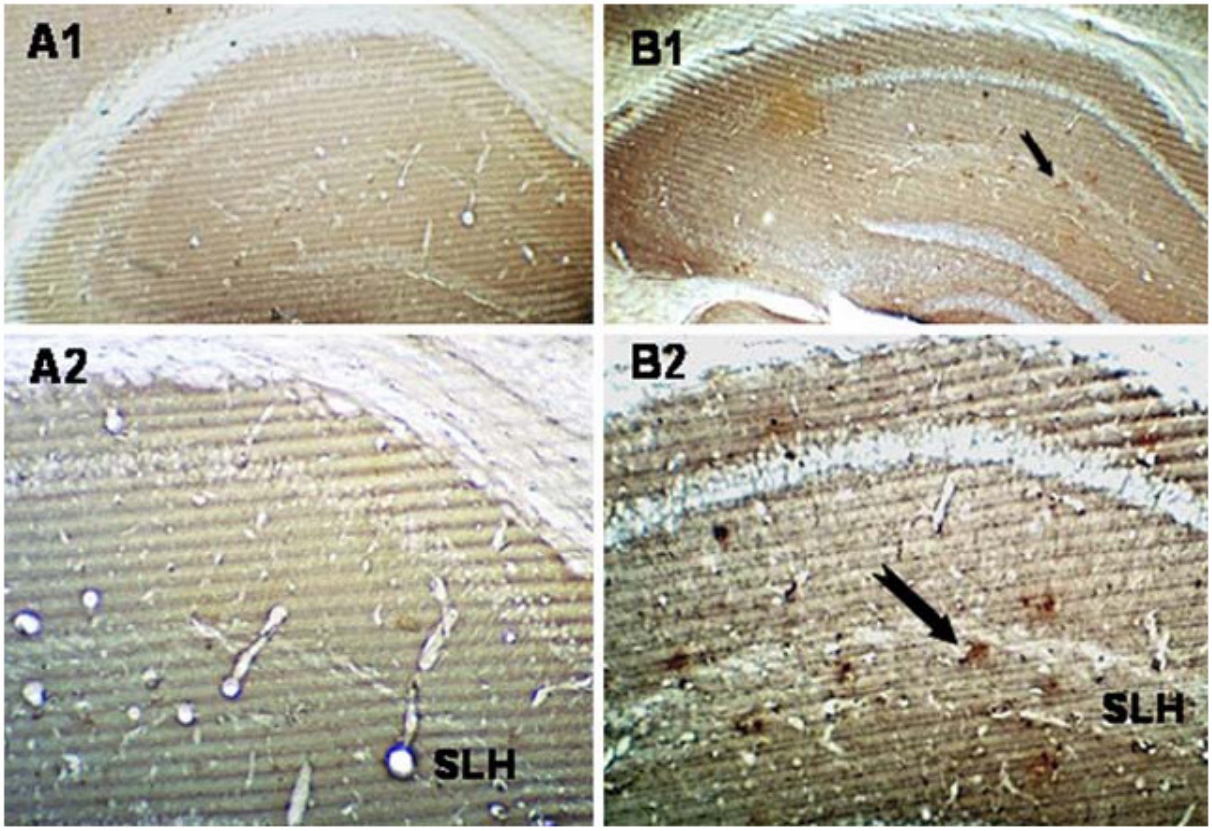

Figure 1. Deposition of amyloid-beta in 12-month-old brains of *MsrA*$^{-/-}$ and WT mice. Brain slices of both mouse strains were stained with monoclonal antibodies 4G8, which probe an epitope between residues 17–24 of amyloid-beta. **A1)** Total WT hippocampal region (40x magnification) **A2)** CA1-hippocampal region of the WT focused on the SLH (100x magnification). **B1**) Total *MsrA*$^{-/-}$ hippocampal region (40x magnification) **B2)** CA1-hippocampus of the *MsrA*$^{-/-}$ focused on the lacunosum of the hippocampus proper SLH (100x magnification). The *arrows* point to typical deposited amyloid-beta.

Tau phosphorylation

To assess the formation and localization of phosphorylated tau in brains of both mouse strains an immunohistochemistry analysis was performed using a mixture of anti-phosphorylated S202 and anti-phosphorylated S199 antibodies (anti-phosphorylated T205 showed very limited reaction, data not shown). As shown in Fig. 2, a significant immunostaining was observed mainly in the hippocampal-CA3 region of the *MsrA*$^{-/-}$ brain (especially in the cell body, dendritic processes of the giant pyramidal neurons, and in the mossy fiber tract), while a much weaker staining was detected in the WT hippocampal-region.

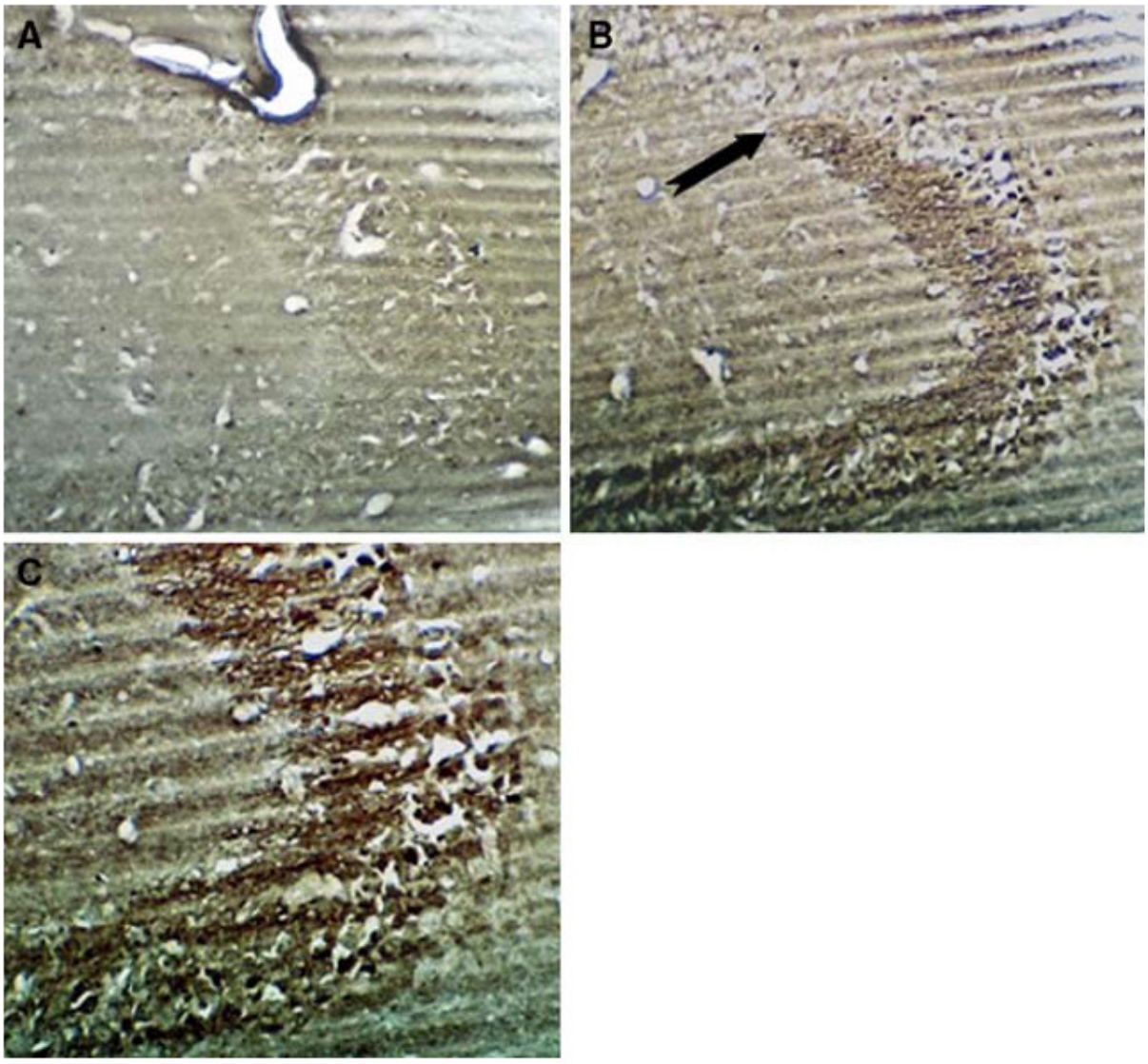

Figure 2. Tau-phosphorylation in 12-month-old brains of *MsrA*$^{-/-}$ and WT mice. Brain slices of both mouse strains were stained with antibodies against P-tau at S199/202 **A)** CA3-hippocampal region of the WT (100x magnification); **B)** CA3-hippocampal region of the *MsrA*$^{-/-}$ (100x magnification). The *arrow* indicates the edge of the staining area by the antibodies in the CA3 region. **C)** CA3-hippocampal region of the *MsrA*$^{-/-}$ (200x magnification, close-up caption of part of the stained region).

Expression of synaptophysin

We have monitored the levels of synaptophysin in hippocampal regions of both mouse strains (at 12 months of age) by immunohistochemistry using antibodies against synaptophysin. As shown in Fig. 3, the immunoreactivity in the hippocampal CA1 and CA3 regions of the WT mice presented a strong staining pattern in and around the hippocampal pyramidal neuronal cell body and dendritic processes (while leaving the perikarya free of staining). The processes were nicely delineated and well defined. In contrast, the relative level of synaptophysin immunostaining decreased and was more diffuse in the *MsrA*$^{-/-}$ in comparison to the WT mice in these hippocampal regions, suggesting an enhanced neurodegeneration in the *MsrA*$^{-/-}$. These results were supported by the silver staining and Nissl staining for neuronal degeneration, as shown in Figs. 5 and 6.

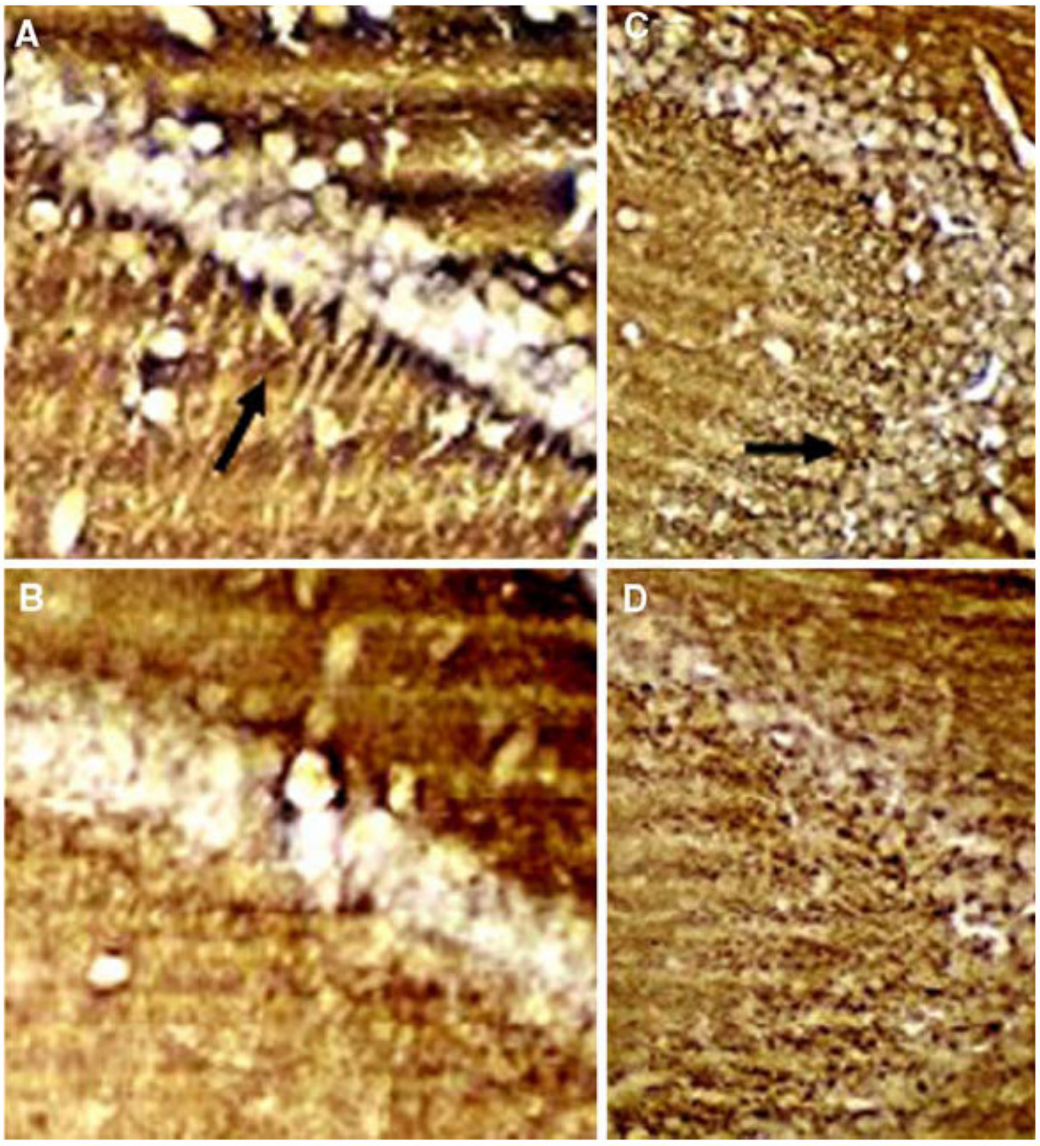

Figure 3. Expression of synaptophysin in 12-month-old brains of *MsrA*$^{-/-}$ and WT mice. Brain slices of both mouse strains were stained with antibodies against syntophysin. **A)** CA1-hippocampal region of WT (200x magnification); **B)**CA1-hippocampal region of the *MsrA*$^{-/-}$ (200x magnification). **C)** CA3-hippocampal region of the WT (200x magnification); **D)** CA3-hippocampal region of the *MsrA*$^{-/-}$ (200x magnification). The *arrows* indicate examples of areas in which synaptophysin staining around the neuronal surfaces was denser and showed an intact structure of the processes and cell bodies in WT mice (A, C). Same areas showed diminished and more defuse staining in the *MsrA*$^{-/-}$ (B, D).

Expression of GFAP

The GFAP antibody labeled both large and small-sized astroglial cells (astrocytes) in or around the pyramidal neurons throughout the hippocampus of the WT mice (Fig. 4). The immunoreactivity of the processes was very strong; the wavy pattern of the processes was clearly outlined by the staining where the nuclei were completely free of any staining. The anti-GFAP antibody stained both type I and type II of the astroglial cells. Most of the immuno-positive cells were located in the stratum oriens and entire radiatum (including distal). The antibody did not label any cells in the pyramidal area. Similar staining was shown for the *MsrA*$^{-/-}$ mice in the same respected regions. However, a substantial damage to astroglial structure was observed and it is possibly due to an enhanced gliosis (Fig. 4). It is clear from the 100x magnification of the hippocampus that at least the same number of total astrocytes is present in the hippocampal region of both mouse strains. Due to the fact that the *MsrA*$^{-/-}$ astrocytes are damaged, it is hard to tell if there are more astrocytes present in the *MsrA*$^{-/-}$ versus the WT hippocampus.

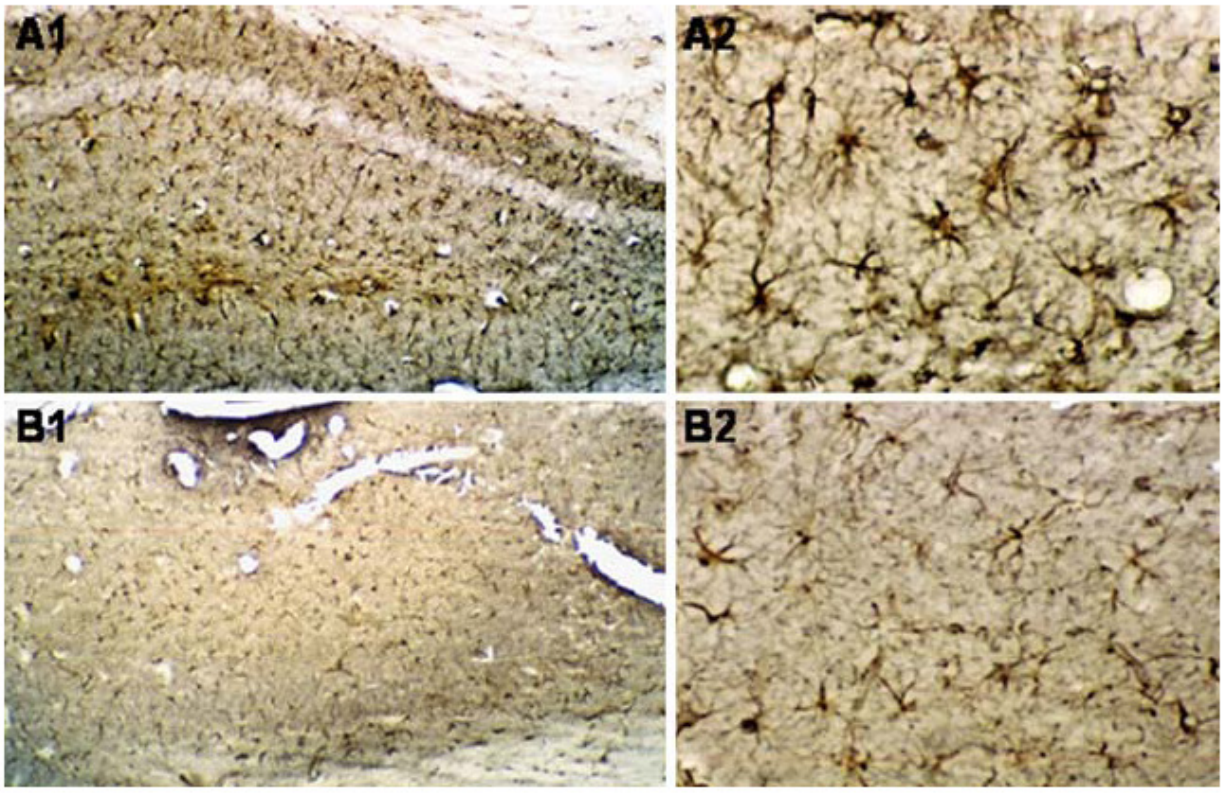

Figure 4. Expression of GFAP in 12-month-old brains of *MsrA*$^{-/-}$ and WT mice. Brain slices of both mouse strains were stained with antibodies against GFAP. **A1)** CA1-hippocampal region of the WT (100x magnification); *A2* CA1-hippocampal region of the WT (200x magnification); *B1* CA1-hippocampal region of the *MsrA*$^{-/-}$ (100x magnification); **B2)** CA1-hippocampal region of the *MsrA*$^{-/-}$ (200x magnification). Note the relative high level of damaged GFAP-stained astrocytes shown in panel B1–B2 in comparison to the astrocytes shown in panel A1–A2, respectively.

Neurodegeneration

We have obtained results with 12-month-old mice of both strains that showed enhanced neurodegeneration in the brains of *MsrA*$^{-/-}$ relative to WT mice. Following Nissl staining (used for the detection of neuronal cells) it is eminent that certain regions of the *MsrA*$^{-/-}$ mouse brain have altered neuronal cell density in comparison to WT control, especially in the hippocampus area. Pyramidal cells are excitatory cells that are enriched in glutamatergic synapses. The stratum pyramidale cells (SP) at the CA2 brain region seemed to be more compact in the WT, relative to the *MsrA*$^{-/-}$ mouse brain (Fig. 5A, A1 vs. B1, respectively). In contrast, the *MsrA*$^{-/-}$ mouse brain had more diffuse and longer pyramidal neurons that seemed to have shorter axonal processes (Fig. 5A, B1). This structural neuronal change may reflect a compensatory mechanism for neuronal cell loss at that brain region by increasing the number of cell layers. Similarly, the neuronal cells in the CA3 region of the WT looked denser with prominent dendritic processes compared to the similar cells in the CA3 region of the *MsrA*$^{-/-}$ mouse (Fig. 5A, A2 vs. B2, respectively). Loss of neuronal cells at the CA3 region of the *MsrA*$^{-/-}$ mouse brain may indicate loss of memory and learning capabilities. The CA1 region of the WT mouse brain showed a thicker and darker staining of the pyramidal cells indicating denser concentration of the cells in comparison to *MsrA*$^{-/-}$ mouse brain (Fig. 5A, A3 vs. B3, respectively). Loss of pyramidal cells at the CA2/CA1 region of the *MsrA*$^{-/-}$ mouse brain may indicate compromised neurotransmission capabilities. Close-up captions of the regions showing differences between the two mouse strains are presented in Fig. 5B, respectively. No apparent difference in neurodegeneration in the cortex region is observed as judged by Nissl staining (Fig. 5C). Complementary results for damaged neurons in regions, where lower neuronal expression was observed, were obtained by using silver staining. Accordingly, the regions of the dentate gyrus (DG), SP, and stratum radiatum (SR), showed a dark dotted staining in the *MsrA*$^{-/-}$ mouse, indicating more neuronal degeneration in comparison to WT, (Fig. 6A, B1 vs. A1, respectively). However, no significant difference in the silver staining of the cortex in brains of the two mouse strains was observed

(Fig. 6A, A2 vs. B2, respectively). The latter result confirms the demonstration of same neuronal cell integrity in the cortex of both mouse strains, as judged by Nissl staining (Fig. 5C). Additionally, heavy silver staining was observed in the auditory nerve region (OPN, olivary pretectal nucleons) of the *MsrA*$^{-/-}$ mouse brain relative to the WT brain, respectively (Fig 6B).

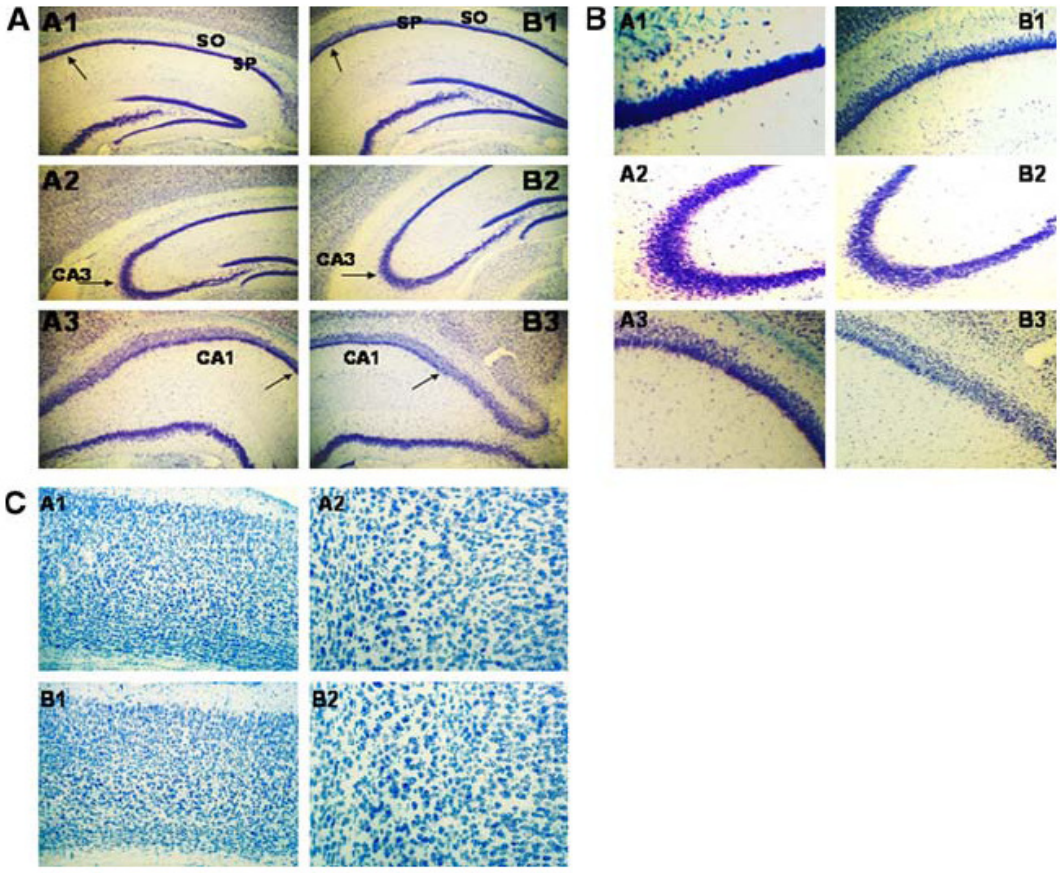

Figure 5. Nissl staining of brain slices of *MsrA*$^{-/-}$ and WT control mice. A) Histological brain sections were performed through the CA1 Weld of the hippocampus (A1, B1; A3, B3), dentate gyrus and CA3 Weld (A2, B2) of a 12-month-old WT mouse (A1–A3) and *MsrA*$^{-/-}$ mouse (B1–B3). Brain sections were stained with methylene blue. *SP* stratum pyramidale; *SO* stratum oriens. Note the compact cell layer of the SP in A1 relative to the SP in A2; the denser cell layer of the CA3 field in A2 relative to CA3 in B2; the loss of pyramidal cells in CA1 field in B3 relative to CA1 Weld in A3. The *arrows* point to examples of regions showing differences between both mouse strains (40x magnification). **B)** A close-up caption of the regions showing differences between the two mouse-strains in A (corresponding to A1–A3 for WT and B1–B3 for *MsrA*$^{-/-}$ mouse, respectively). **C)** *A1–A2*, the cortex region in WT brain (A1, 100x magnification; A2, 200x magnification). B1–B2, the cortex region in *MsrA*$^{-/-}$ brain (*B1* 100x magnification; B2 200x magnification).

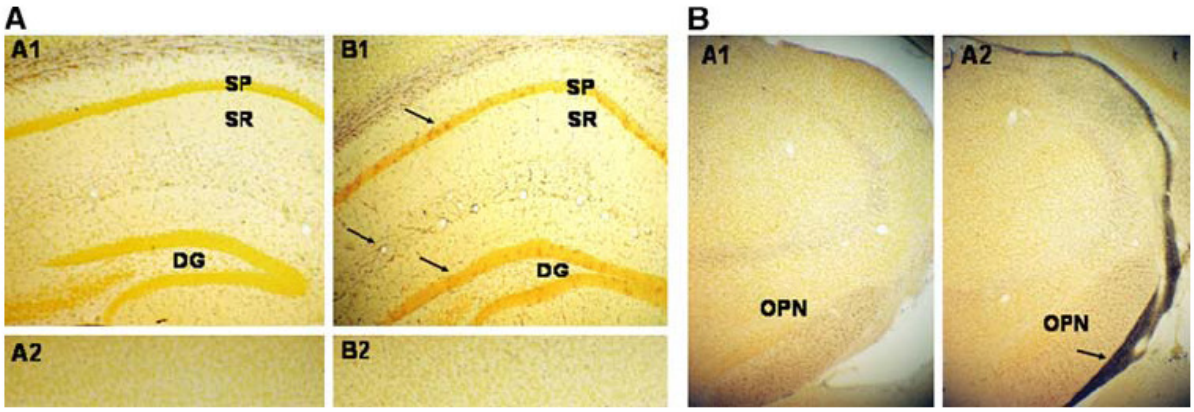

Figure 6. Silver staining of brain slices of *MsrA*$^{-/-}$ and WT control mice. Histological brain sections were performed through various regions of 12-month-old brain stained with cupric silver stain (100x magnification). **A)** CA1/CA2 field and dentate gyrus (A1 for WT and B1 for *MsrA*$^{-/-}$ mouse, respectively); Cortex (A2 for WT and *B2* for *MsrA*$^{-/-}$ mouse, respectively). **B)** Olivary pretectal nucleons (A1 for WT and B1 for *MsrA*$^{-/-}$ mouse, respectively). *SP* stratum pyramidale; *SR,* stratum radiatum; *DG,* dentate gyrus; *OPN,* olivary pretectal nucleons. Note the neuronal changes as manifested by the *dark dots* in the regions shown in A (B1 vs. A1, respectively) and continuous dark area in B (A2 vs. A1, respectively). The *arrows* point to examples of areas in which differences were observed.

Hypersensitivity of hippocampal cells to oxidative stress

We have compared hippocampal cells in cultured brain slices of both mouse strains with oxidative stress that is mediated by H_2O_2. As shown in Fig. 7, following propidium iodide staining for dead cells, the *MsrA*$^{-/-}$ cells were more sensitive than the WT cells to 400 µM H_2O_2 (~double dead cells in the *MsrA*$^{-/-}$ cells).

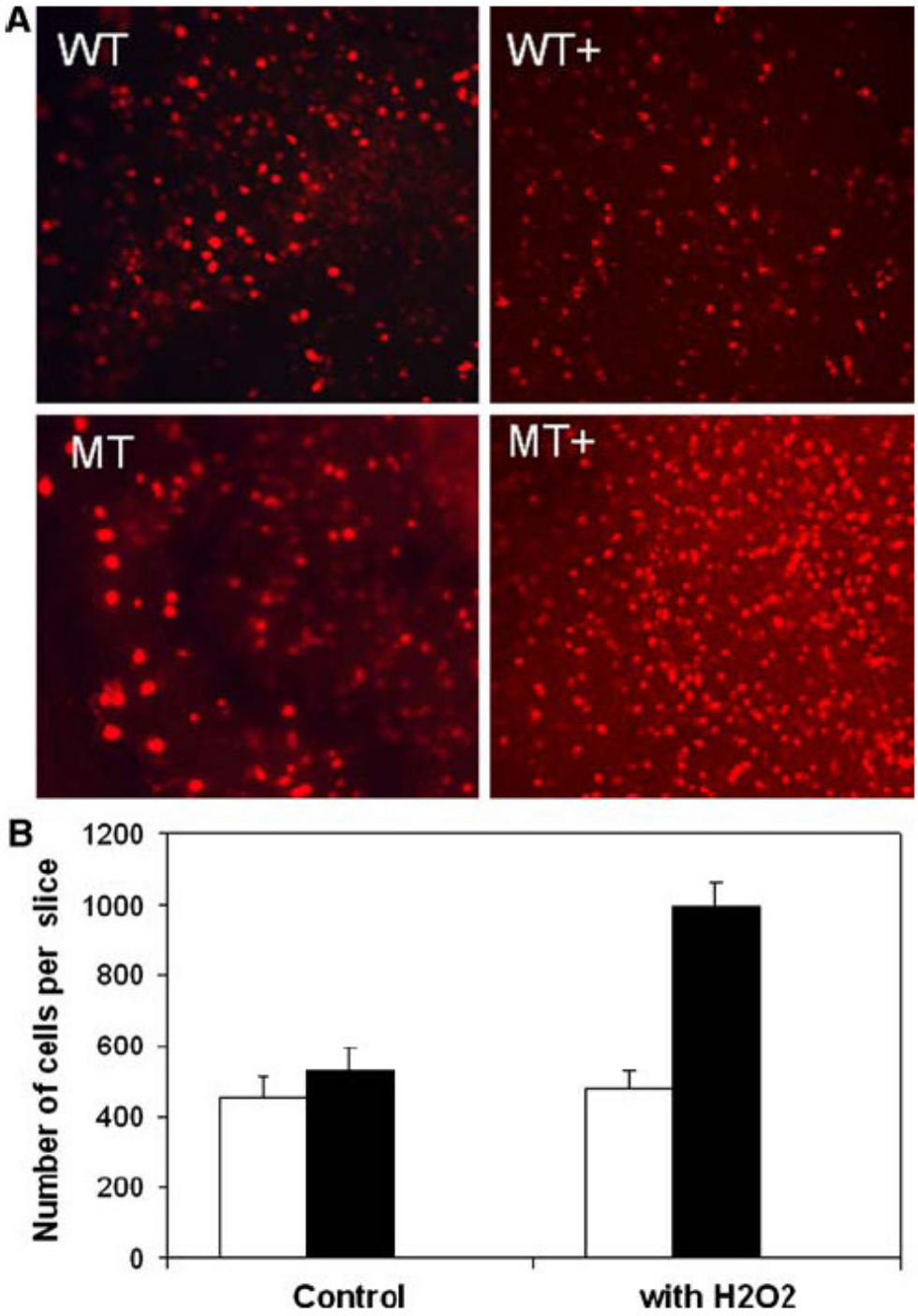

Figure 7. Survival of hippocampal cells in slice brain cultures of *MsrA*$^{-/-}$ and WT control.

Brain slices of both mouse strains were processed for tissue culture and stained with propidium iodide (*PI*) according to the procedures described under "Materials and Methods". The brain sections were treated with 400 µM of H_2O_2 followed by the treatment with PI. Respective control

sections were left untreated with H_2O_2, followed by the treatment with PI. The cells were visualized by confocal microscope and PI-glowing cells were counted. **A)** Pictures of regions in each slice stained with PI; *WT* wild-type; *MT MsrA*$^{-/-}$; the areas of the counted cells were the same in all slices. The + symbol indicates cells treated with H_2O_2. **B)** *White bar*: *WT*; *Black bar*: *MsrA*$^{-/-}$. *Each bar* represents an average of three separate experiments with $P < 0.01$ (using paired student's *t* test).

4. Discussion

The current study shows that there is an elevated level of deposited-amyloid-beta in the hippocampus regions of mid-aged *MsrA*$^{-/-}$ mice (Fig. 1). The aggregates or plaque-like structures that were labeled by the antibodies in the different sub-layers of CA1 pyramidal region of the *MsrA*$^{-/-}$ mice were in consistent with results reported earlier in the brains of Alzheimer's disease transgenic mice model. The neuritic plaques that are preferentially found to be localized in the areas of molecular layers of dentate gyrus and stratum lacunosum may be due to the accumulative aggregates of amyloid-beta. The interneurons of the CA1 hippocampus regions display a high spontaneous discharge rate and a pronounced action potential after hyperpolarization. These interneurons are vulnerable to extreme physiological conditions (like oxidative stress) that might lead to the release of abnormal amount of amyloid-beta and deposition at the sites of dying interneurons. Several amyloid-beta-aggregates were mainly observed in the *MsrA*$^{-/-}$ stratum lacuonosum layer compared to the same brain region in WT (Fig. 1B vs. Fig. 1A, respectively). Previous reports demonstrated that, in this layer, there were some interneurons that showed immunoreactivity with GABA (Gamrani, Onteniente, Seguela, Geffard, & Calas, 1986) and GAD (Kunkel, Hendrickson, Wu, & Schwartzkroin, 1986; Ribak, Vaughn, & Saito, 1978). The latter result is in agreement with the selective deposition of amyloid-beta in the amyloid precursor protein transgenic mouse to various regions of the hippocampus including the SLH and CA2 regions (Su & Ni, 1998). Since stratum lacunosum is known to regulate declarative memory function, any cell death caused by either hyper-excitation or deposited amyloid-beta-aggregates can lead to a memory malfunction. Taken together, it is suggested that the deposited-amyloid-beta in the *MsrA*$^{-/-}$ that were found mainly in the CA1 pyramidal and stratum lacunosum regions may represent part of the hippocampal pathologies associated with Alzheimer's disease. We expect that the observed amyloid-beta deposition and the amyloid plaque burden will be enhanced with age, especially in the *MsrA*$^{-/-}$ mice. Similarly, it is predicted that the level of neurofibrillary tangles in the *MsrA*$^{-/-}$ mice will be increased relative

to WT mice as a function of age. The region-specific amyloid-beta deposition, accompanied by other pathological features is associated clinically with progressive impairment of memory and intellectual function of the disease (Morris et al., 1996). Consequently, we suggest that observed accumulation of amyloid-beta might contribute to the development of Alzheimer's disease-pathology in the *MsrA*$^{-/-}$ mice.

A significant immunostaining of tau-phosphorylation was observed mainly in the hippocampal CA3 region of the *MsrA*$^{-/-}$ brain while not detected in the WT brain (Fig. 2). Among the many kinases that are involved in tau-phosphorylation is the active form of the extracellular signal-regulated kinase (p-Erk). In human and rhesus monkey brains, anti-Erk immunostaining showed that Erk levels are highest in the CA3 region, the mossy fiber zone, and the granule cell layer of the dentate gyrus (Hyman, Elvhage, & Reiter, 1994; Hyman, Reiter, Moss, Rosene, & Pandya, 1994). P-Erk is increased in neurons containing p-tau and NFTs and in dystrophic neuritis in senile plaques in Alzheimer's disease brains and it is linked to oxidative-stress (Ferrer et al., 2001; Hyman, Elvhage et al., 1994; Pei et al., 2002; Perry et al., 1999; Trojanowski, Mawal-Dewan, Schmidt, Martin, & Lee, 1993). Moreover, zinc is found in high levels in the CA3 region and can increase the levels of p-tau and p-Erk (Harris, Brecht, Xu, Mahley, & Huang, 2004). Taken together, it is suggested that the high p-tau level in the hippocampal-CA3 region of the *MsrA*$^{-/-}$ brain has the similar characteristics of the elevated levels of zinc and p-Erk found in Alzheimer's disease brains. To support this finding, it will be important to determine the levels of p-Erk and zinc in the *MsrA*$^{-/-}$ and WT brains. It is expected that the levels of zinc, p-Erk, and tau-phophorylation will be elevated with age relative to WT especially in the CA3 region.

The strong immunoreactivity of the antibody against synaptophysin in the WT mice implies intact membrane structures in the presynaptic vesicles (Fig. 3). Synaptophysin is an integral membrane protein of presynaptic vesicles that interacts with other synaptic proteins. It also participates in the trafficking, docking and fusion of synaptic vesicles to the membranes and facilitates synaptic transmission and exocytosis of transmitters. The overall weak and

diminished synaptophysin immunostaining in the same regions of the *MsrA*$^{-/-}$ mice suggests severe axonal transport impairment and a gross failure in the synaptic transmission. Consequently, it is concluded that the decreased synaptophysin level in the *MsrA*$^{-/-}$ mice (Fig. 3) reflects enhanced neuronal degeneration in the hippocampal areas that are similarly observed in mouse models of Alzheimer's disease and Alzheimer's disease-human brains. Generally, we expect the *MsrA* ablation to accelerate pathology associated with Alzheimer's disease that includes the induction of GFAP level. Significantly greater GFAP levels were found in samples from individuals diagnosed with Alzheimer's disease, mixed dementia, and vascular mediated dementia. Because elevated levels of GFAP reflect astroglial responses to even subtle forms of neural damage, GFAP may provide independent, supporting evidence for the damage underlying dementia, even in the absence of other evidence of neuropathology such as the presence of neuritic plaques (NPs) and neurofibrillary tangles (NFTs). Moreover, enhanced gliosis was observed throughout the course of the illness, and it was attributed to the cleavage of GFAP that may contribute to astrocyte injury and damage in the Alzheimer's disease brain (Hol et al., 2003; Ingelsson et al., 2004; Mouser, Head, Ha, & Rohn, 2006). Indeed, our results in Fig. 4 demonstrate that the *MsrA*$^{-/-}$ hippocampal astrocytes are more damaged than the astrocytes of the WT brain, suggesting the occurrence of a similar gliosis process described in Alzheimer's disease. GFAP is expected to be elevated in the vicinity of plaques. Consequently, it is possible that the activated glia and astrocytes are trying to shift the amyloid-beta deposits but instead release H_2O_2, making the deposited-amyloid-beta stick even more. Moreover, the released H_2O_2 may preferably damage the *MsrA*$^{-/-}$ astrocytes causing their gliosis as they are likely to be more sensitive to H_2O_2 (similarly to *MsrA*$^{-/-}$ hippocampal cells (Fig. 7) and other *MsrA* knockout cells (J. Moskovitz, 2005) that were shown to be more sensitive to H_2O_2.

Generally, it is clear that there is an enhanced neurodegeneration in the *MsrA*$^{-/-}$ hippocampal [Fig. 5A, 5B, 6A (A1, B1)] and auditory (Fig. 6B) regions of the brain of 12-month-old mice. In particular, the hippocampal neurodegeneration is supported by the expression of the particular

markers for Alzheimer's disease as shown above, while the auditory nerve degeneration is a known phenomenon that is indicative of age-related neurodegeneration. Moreover, lack of an obvious difference in neurodegeneration of the cortex between the two mouse strains suggests that cell vulnerability, due to a compromised MsrA function, is region-specific [Figs. 5C, 6A (A2, B2)].

In summary, we expect that all the observed-differences between the *MsrA*$^{-/-}$ and WT mice, with regard to the expression and localization of the molecular markers associated with neurodegenerative diseases, will be exacerbated as a function of age. Additionally, it will be of great interest to compare the hippocampal protein-expression profile between the two mouse strains. This approach will identify proteins that are playing an important role in defense against oxidative stress (by monitoring which protein-expression levels are affected by MsrA, especially in the neurons).

B. Clearance and Phosphorylation of Alpha-Synuclein are Inhibited in MsrA Null Yeast Cells (D. B. Oien, Shinogle, Moore, & Moskovitz, 2009)

Aggregated alpha-synuclein and the point mutations Ala30Pro and Ala53Thr of alpha-synuclein are associated with Parkinson's disease. The physiological roles of alpha-synuclein and Met oxidation of the alpha-synuclein protein structure and function are not fully understood. MsrA reduces methionine sulfoxide residues and functions as an antioxidant. To monitor the effect of Met oxidation to alpha-synuclein on basic cellular processes, alpha-synucleins were expressed in *msrA* null mutant and WT yeast cells. Protein degradation was inhibited in the alpha-synuclein-expressing *msrA* null mutant cells compared to alpha-synuclein-expressing WT cells. Increased inhibition of degradation and elevated accumulations of fibrillated proteins were observed in SynA30P-expressing *msrA* null mutant cells. Additionally, Met oxidation inhibited alpha-synuclein phosphorylation in yeast cells and *in vitro* by casein kinase 2. Thus, a

compromised MsrA function combined with alpha-synuclein overxpression may promote processes leading to synucleinopathies.

1. Introduction

One of the hallmarks of Parkinson's disease is the formation of Lewy bodies (Lucking & Brice, 2000). These neuronal inclusion bodies are composed of aggregated proteins and consist mainly of alpha-synuclein fibrils (Baba et al., 1998). The alpha-synuclein protein is a presynaptic protein of unknown function and its involvement in the pathogenesis of Parkinson's disease is still not clear. However, the alpha-synuclein point mutations Ala30Pro and Ala53Thr are found in autosomal dominant forms of Parkinson's disease (Kruger et al., 1998; Polymeropoulos et al., 1997). Overexpression of alpha-synuclein is also associated with the risk of developing Parkinson's disease (Takeda et al., 1998), and alpha-synuclein locus triplication can cause Parkinson's disease (Singleton et al., 2003). When alpha-synuclein is abnormally expressed or modified, various studies indicate it may cause alterations in mitochondrial and proteasomal function, protein aggregation, and accumulation of ROS (Lindersson et al., 2004; Sawada et al., 2004; Snyder et al., 2005; Vekrellis, Rideout, & Stefanis, 2004).

Yeast cells have been used to study events related to alpha-synuclein biology and toxicity. This toxicity was shown to be mediated by increased cellular ROS and decreased proteasome function (Q. Chen, Thorpe, Ding, El-Amouri, & Keller, 2004; Sharma et al., 2006; Willingham, Outeiro, DeVit, Lindquist, & Muchowski, 2003). The monomeric alpha-synuclein forms fibrils at a relatively slow rate. We hypothesize that modifications alter the physical properties and degradation rate of alpha-synuclein, overall promoting its oligomerization. This is consistent with the associated increase in oxidative stress among Parkinson's disease, aging, and other neurodegenerative diseases. Increased ROS and cellular alpha-synuclein levels promote its aggregation (Giasson et al., 2000; Hsu et al., 2000). The presence of ROS can cause posttranslational modifications, commonly to the sulfur-containing residues Met and Cys. The

alpha-synuclein protein does not have Cys, but does contain four Met residues that can be readily oxidized to MetO *in vitro*. Under conditions of oxidative stress, MetO-alpha-synuclein can form fibrils when triggered by certain metals (e.g. Zn^{2+}, Al^{3+}, etc.) *in vitro* (Yamin et al., 2003). Furthermore, cellular conditions such as higher alpha-synuclein protein concentrations (Fink, 2006) and a saline environment (Munishkina, Henriques, Uversky, & Fink, 2004) could increase the rate of alpha-synuclein fibril formation. Post-translational modifications can alter the solubility of alpha-synuclein, possibly decreasing the clearance of this short-lived protein. Cytoplasmic alpha-synuclein can be degraded by the ubiquitin-proteasome system, the autophagy system, and lysosomic pathway (Giorgi et al., 2006); however, degradation of alpha-synuclein is inhibited in Parkinson's disease. It is plausible the latter inhibition decreases the clearance and promotes aggregation of alpha-synuclein. Modifications to alpha-synuclein may alter its solubility and interfere with its ability to be degraded, thereby resulting in a decreased clearance of alpha-synuclein.

Overexpression of *msrA* may suppress dopaminergic cell death and protein aggregation (Liu et al., 2008). One hypothesis to explain the late onset of certain neurodegenerative diseases, such as Parkinson's disease, is that they occur in aging neurons when the capacity of the quality control system to cope with accumulating misfolded proteins is exceeded (Berke & Paulson, 2003). This situation has been modeled in yeast by increasing alpha-synuclein expression (Outeiro & Lindquist, 2003). Due to the lack of substantial information about MetO-alpha-synuclein *in vivo*, we further explored this by overexpressing alpha-synuclein and two mutants in *msrA* null (*msrA*-KO) yeast cells. The effects of the alpha-synuclein on protein fibril formation, degradation, and phosphorylation were monitored.

2. Materials and Methods

Overexpressing human alpha-synuclein in yeast

The human alpha-synuclein protein and its mutants were overexpressed in *msrA*-KO and WT *Saccharomyces cerevisiae* strains with the pYES6 expression vector used previously (J. Moskovitz, Berlett, Poston, & Stadtman, 1997). This vector harbors the yeast GAL1 promoter for high-level inducible protein expression by galactose. It has a C-terminal peptide encoding a V5 epitope and a polyhistidine (6His) tag for detection and purification of the recombinant fusion alpha-synuclein. This vector contains the ampicillin and blasticidin resistance genes for selection of bacteria and yeast colonies harboring the plasmid, respectively. Three forms of the human alpha-synuclein cDNA (wild-type (α-synuclein), Ala53Thr (SynA53T), and Ala30Pro (SynA30P)) were inserted into the vector keeping the sequence in frame with the 6His peptide. For that purpose, suitable 5' forward and 3' reverse complement primers (harboring *Hind* III and *Xba* I restriction sites, respectively) were used with each of the alpha-synuclein cDNAs (kindly provided by Dr. Mikiei Tanaka, NIH, NHLBI) in a routine PCR procedure. The resulting PCR products were sub-cloned into the suitable complementary restriction sites on the pYES6 and transformed into bacterial cells (DH5α). Each plasmid was isolated from bacterial cells and transformed into WT and *msrA*-KO yeast. Vector-only transformed cells served as controls. Following growth selection on media containing blasticidin (Invivogen), all the transformed yeast strains (WT and *msrA*-KO containing either the vector only, vector containing alpha-synuclein, or vector containing either SynA53T or SynA30P) were grown in induction media containing 2% galactose and 1% raffinose for up to 24 h. At various time points, equal amounts of cells were taken from each culture (determined by optical density (OD_{600nm})) and extracted by glass beads and a bead-beater homogenizer apparatus (BioSpec Products, OK). The alpha-synuclein proteins were purified from the corresponding extracts by using of ProBond™ Nickel-Chelating Resin (Invitrogen). Equal volumes of purified alpha-synuclein proteins were subjected to SDS-gel electrophoresis and detected by western blotting using anti-6His antibodies (Immunology Consultants Laboratories).

Total protein degradation and synthesis in yeast expressing alpha-synuclein

The procedure was performed as done previously (Q. Chen, Ding, & Keller, 2005) with modifications. Yeast cells (WT and *msrA*-KO) expressing the three alpha-synuclein variants (alpha-synuclein, SynA30P, SynA53T) were grown in yeast extract-peptone-dextrose (YPD, Fisher Scientific) medium to mid-logarithmic phase while shaking at 30°C. The media was removed by centrifugation and replaced with 2% galactose and 1% raffinose media lacking Met. Next, 50 µCi [^{35}S]Met (Perkin-Elmer) was added and incubated for additional 30 min. The media was removed and radioactive labeling was chased by media containing Met without radioactive isotopes. At different time intervals, equal aliquots of cells were removed from each culture and homogenized. The corresponding protein extracts were mixed with trichloroacetic acid (TCA) at a final concentration of 20% (v/v). After incubation at 4°C for 1 hour, the samples were centrifuged, and the radioactivity (cpm) of the TCA-insoluble precipitates and soluble material was measured by liquid scintillation counting.

For quantification of protein synthesis, the radioactivity (cpm) of the TCA-insoluble precipitate was measured by liquid scintillation counting after labeling with 50 µCi [^{35}S]Met and immediate precipitation with TCA.

Phosphorylation of alpha-synuclein in yeast (ex-vivo system)

The WT and *msrA*-KO yeast cells expressing alpha-synuclein, SynA30P, and SynA53T were grown in YPD medium to mid-logarithmic phase shaking at 30°C. The medium was removed by centrifugation and substituted with induction media containing 2% galactose and 1% raffinose for 1 h. The cells were then incubated in media with only 10% of the nutrients for 1 h to reduce free phosphate. To each culture 5 µCi/mL [^{32}P]orthophosphoric acid (Perkin-Elmer) was added and incubated 1 h. The cells were harvested and alpha-synuclein was isolated by resin affinity as described above with the addition of NaF and Na_2VO_4 as phosphatase inhibitors. The alpha-synuclein was eluted from the resin with 150 mM imidazole. Equal amounts of each eluted

protein were subjected to an SDS-gel electrophoresis. At the end of electrophoretic separation, the gel was stained with GelCode Blue (Thermo Scientific, Rockford, IL). Bands corresponding to the molecular weight of the alpha-synucleins were excised, added to vials with liquid scintillation cocktail, and their cpm measurements were determined by liquid scintillation counting.

Phosphorylation of alpha-synuclein in vitro

Recombinant alpha-synuclein, SynA30P, and SynA53T (rPeptide) were incubated overnight in 200 mM H_2O_2 at 37℃ in PBS buffer. The H_2O_2 was removed by adding catalase and incubating 30 min (oxidant removal verified by adding alpha-synuclein after oxidants were removed, this served as the non-oxidized alpha-synuclein control). To reduce MetO, recombinant yeast MsrA and PilB were produced as previously described (J. Moskovitz et al., 1997; Olry et al., 2002). These Msrs were added at a concentration of 0.3 mg/mL with 20 mM DTT for 1 h. Each alpha-synuclein was phosphorylated by adding 6 mCi [γ-^{32}P]-ATP (Perkin-Elmer), 20 µM cold ATP, 10 mM $MgCl_2$, and 0.3 µg casein kinase 2 (Upstate) for 1 h. Reactions were stopped by adding an equal volume of protein gel sample buffer. Equal amounts of alpha-synuclein proteins were subjected to an SDS-gel electrophoresis. At the end of the electrophoretic separation, the gel was stained with GelCode Blue Stain reagent and exposed to X-ray film.

Protein fibrillation in yeast strains expressing alpha-synuclein

In the presence of fibrils, Thioflavin T undergoes a ‘red shift’ where it is excited at a wavelength of 442 nm, and emits fluorescence at 482 nm. Yeast cells were grown in YPD and incubated in media with 2% galactose and 1% raffinose for 3 h. The cells were precipitated by centrifugation and resuspended in 1% Thioflavin T solution. Cells were washed in buffer and aliquots were diluted into a 96-well plate. Finally, Thioflavin T fluorescence was imaged and quantified using an IN Cell Analyzer 1000 (GE Healthcare) high content imaging system.

Statistics

Comparison and calculation of P values was performed using student *t*-test analysis. Values of $P < 0.05$ were considered significant.

3. Results and Discussion

Overexpression of alpha-synuclein in yeast

To investigate the effects of MetO on alpha-synuclein and its point mutation variants (alpha-synuclein, SynA30P, SynA53T), they were separately overexpressed in WT or *msrA*-KO yeast cells. Cell aliquots were collected at various time points during the expression period of the alpha-synuclein proteins. Following conditional alpha-synuclein purification from the yeast cells, bands migrating at ~22 kDa and ~16 kDa positions were detected by western blot analysis (Fig. 1). The 22 kDa band corresponds to the full length of alpha-synuclein with the 6His tag moiety, which is known to cause slower migration in gel electrophoresis due to the added mass and positive charge. Accordingly, the 16 kDa and lower detected minor bands correspond to degradation products of the 22 kDa band. The three types of alpha-synuclein are degraded at an increased rate when expressed in the WT compared to the *msrA*-KO strain. The time dependent degradation of the corresponding alpha-synucleins is trailing in the *msrA*-KO relative to WT strain without complete degradation of the 16 kDa band, which is completely degraded in WT strain (Fig. 1). Moreover, among all the types of alpha-synuclein examined, the SynA53T type seems to be the most resistant to degradation in the WT strain while the SynA30P appears to be the most resistant to degradation in the *msrA*-KO strain (Fig. 1). Interestingly, the degradation of the SynA30P into both the 16 kDA peptide and lower mass peptides was inhibited more in the *msrA*-KO strain as shown by the relative lower amounts of the shorter peptides products with time (Fig. 1). The antibodies used in the western blot recognize only

alpha-synuclein protein and derived peptides that still contain the 6His tag, which provides recognition that is not based on alpha-synuclein conformation.

The expression patterns of alpha-synuclein suggests the three types of alpha-synucleins are degraded faster in the WT compared to the *msrA*-KO strain (Fig. 1). Moreover, the SynA30P variant of alpha-synuclein was the most resistant to degradation in the *msrA*-KO strain (Fig. 1). This result is supported by previous studies showing that WT yeast cells overexpressing SynA30P are inhibited in their general protein degradation by the proteasome, compared to non-mutated alpha-synuclein (Q. Chen et al., 2005). We suggest the degradation of alpha-synuclein is inhibited more in *msrA*-KO cells compared to WT cells, which may be an enhanced inhibitory effect of the MetO on cellular degradation. Using MALDI-MS techniques, we have verified that SynA30P and SynA53T expressed in the *msrA*-KO cells had elevated levels of Met oxidation relative to same alpha-synucleins expressed in WT cells (data not shown).

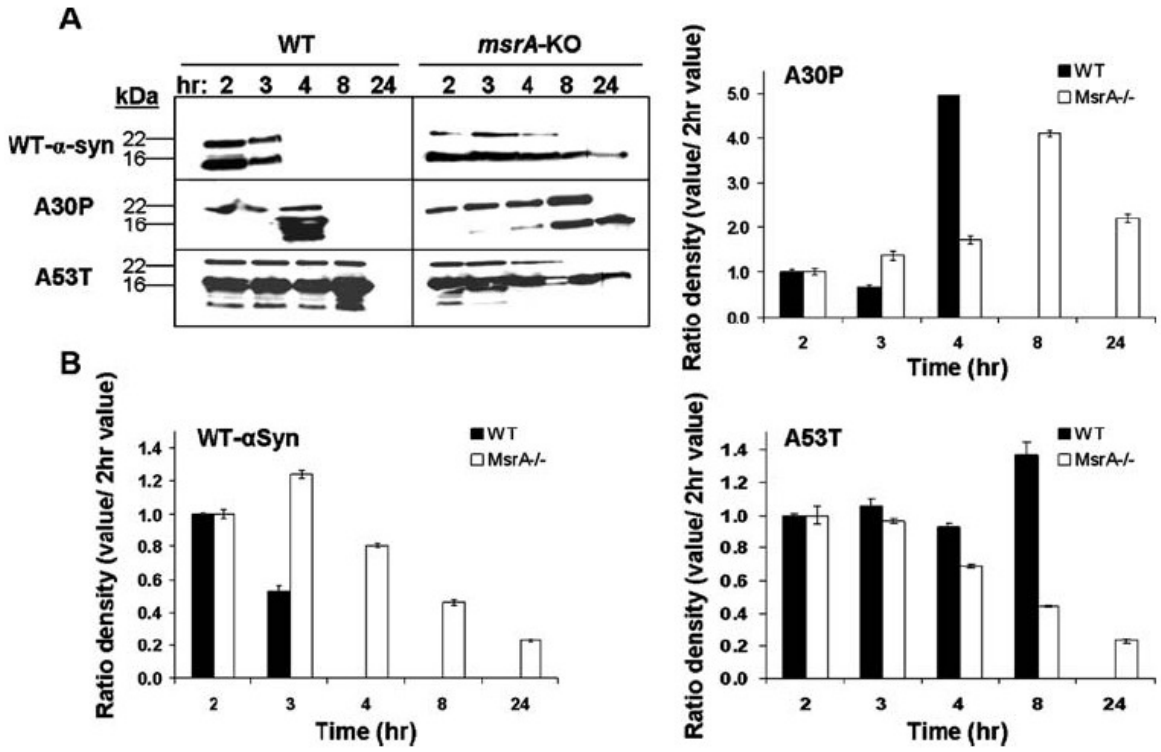

Figure 1. Presence of alpha-synuclein over time isolated from *msrA*-KO and WT yeast cells. Soluble alpha-synucleins (WT-α-syn, A30P, A53T) were isolated from cells at specified time points during alpha-synuclein protein induction. Equal amounts of cells were taken from each culture and alpha-synuclein proteins were isolated by resin from the corresponding extracts. **A)** The alpha-synuclein proteins were detected by western blotting using antibodies specific to the 6His tag. *Left side*: alpha-synuclein from WT yeast cells. *Right side*: alpha-synuclein from *msrA*-KO yeast cells. *Horizontal axis*: Time from start of alpha-synuclein induction period (2, 3, 4, 8, and 24 h). **B)** Densitometry analysis performed on the protein bands shown in panel A. To compare the types of synucleins expressed and cells, the pattern of resistance to degradation over time was demonstrated as a percent ratio of the protein-densitometry for each time point relative to the densitometry value of the 2 h point level (represented 100% expression level).

Protein degradation and synthesis in yeast strains overexpressing alpha-synuclein

The accumulation of alpha-synuclein may be causing a general inhibition of degradation processes that is increased in the *msrA*-KO strain. Following pulse-chase labeling with [^{35}S]Met during the induction period of alpha-synuclein synthesis, all types of expressed alpha-synuclein lowered the percentage levels of acid-soluble labeled material, mostly in *msrA*-KO cells (Fig. 2A; labeled acid-soluble material, soluble degradation products; and labeled non-soluble material, newly synthesized proteins; represent total labeled proteins). While SynA53T was the only type having a significant reduction effect on the WT total protein degradation rate, all types of alpha-synuclein reduced the total degradation rate in the *msrA*-KO strain compared to control (Fig. 2A).

It is noteworthy that the degradation rate over time was elevated in the *msrA*-KO versus WT yeast strain when sham vector was present. One possible explanation is that accumulation of MetO-containing proteins (the case in the *msrA*-KO strain) induces the action of the degradation machinery as an attempt to remove the faulty proteins (Stadtman & Berlett, 1998). However, this response is inhibited by excess levels of specific alpha-synuclein types (Figs. 1 and 2A). The general inhibition of protein degradation was more pronounced in the *msrA*-KO cells expressing native and A30P alpha-synuclein (Fig. 2A). The overexpressed native alpha-synuclein effect on cellular degradation may be relevant to its accumulation that is thought to be a risk factor for Parkinson's disease, and specifically impaired alpha-synuclein degradation may be involved (Singleton et al., 2003).

The mechanism by which the nature of alpha-synuclein and MetO modifications to alpha-synucleins inhibit degradation is not known. The degradation pathways may be inhibited by the cellular localization of alpha-synuclein. In yeast, each alpha-synuclein mutant accumulated at the same level as non-mutated alpha-synuclein, but the cellular distributions differed profoundly. Similar to native alpha-synuclein, SynA53T is concentrated at the plasma membrane, while SynA30P dispersed throughout the cytoplasm (Brandis et al., 2006; Bussell & Eliezer, 2003; Jo, Fuller, Rand, St George-Hyslop, & Fraser, 2002). Therefore, the cytoplasmic localization of

SynA30P may cause the protein to be more prone to oxidation (compared to a membrane region), and accordingly less protected from the accumulation of MetO in the absence of cytoplasmic MsrA. This may also partly explain the special negative effect of MetO-alpha-synuclein accumulations on cytoplasmic degradation, as accumulations of oxidized proteins can inhibit protein degradation (Starke-Reed & Oliver, 1989).

Inhibition of protein synthesis by native and Ala30Pro α-synuclein expressed in yeast cells was previously described (Q. Chen et al., 2005). Therefore, we examined the contribution of *msrA* ablation to the alpha-synuclein inhibitory effect on protein synthesis. Expression of alpha-synuclein caused an overall inhibition of protein synthesis in both strains compared to control cells expressing the sham vector (Fig. 2B). The inhibition levels were similar in both yeast strains expressing either SynA30P or SynA53T. However, a combination of *msr*A ablation and native alpha-synuclein expression in *msrA*-KO cells caused a stronger inhibitory effect on protein synthesis compared to WT cells expressing native alpha-synuclein (Fig. 2B).

As discussed by other groups (Q. Chen et al., 2005), the basis for decreased protein synthesis in cells expressing alpha-synuclein is unknown. They suggest that the impairments in this synthesis may either represent negative feedback (result of impaired protein degradation) or alpha-synuclein induction of endoplasmic reticulum stress impairing protein synthesis (Q. Chen et al., 2005). It is possible that alterations to the structure and function of native alpha-synuclein expressed in *msrA*-KO cells are more effective in fostering inhibition of protein synthesis (Fig. 2B).

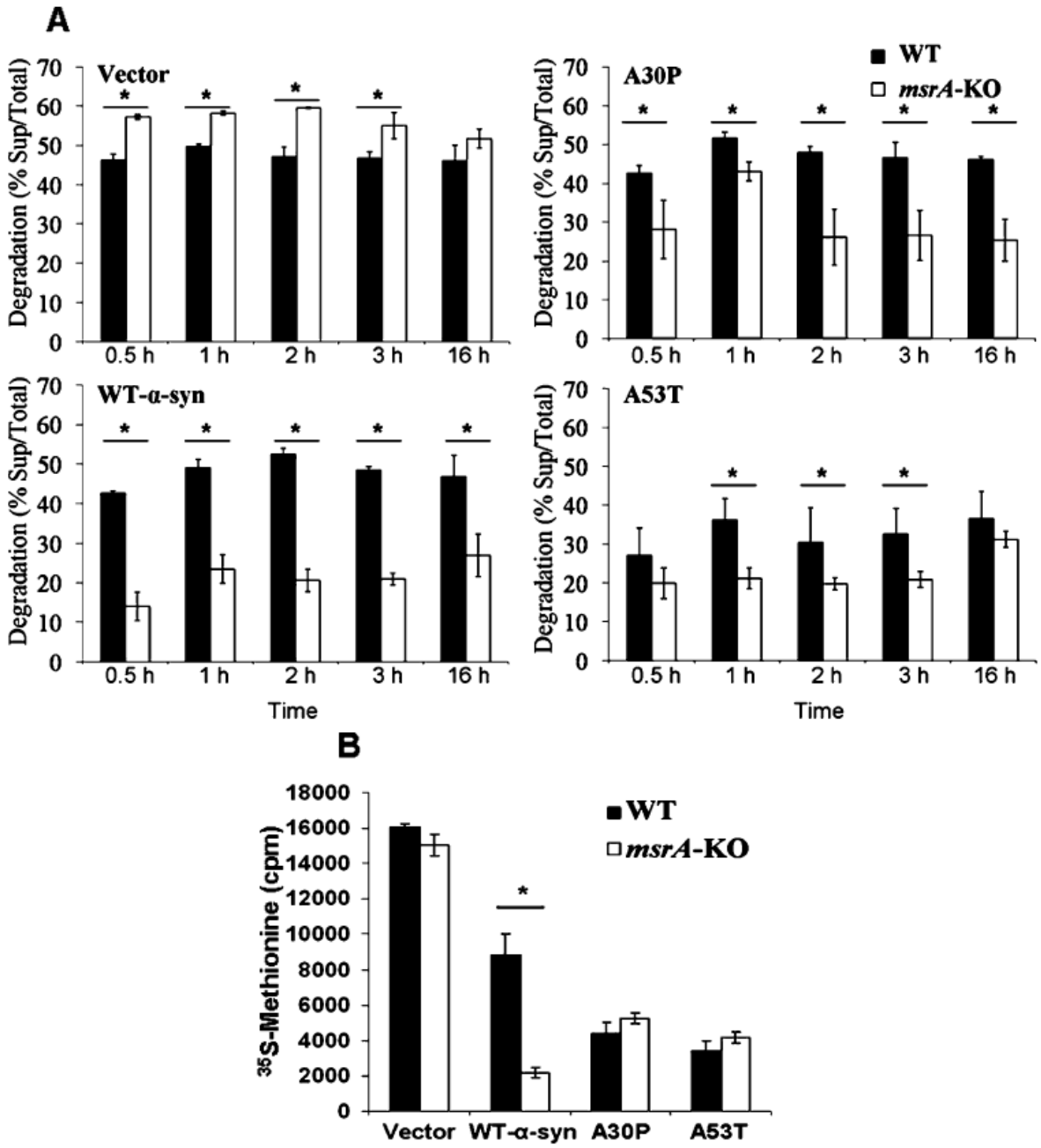

Figure 2. Total protein degradation and synthesis in *msrA*-KO and WT yeast cells. A) Total degradation of soluble cytosolic proteins. Soluble protein fraction was precipitated by TCA following pulse-chase labeling with [^{35}S]Met during alpha-synuclein protein induction. Values represent the percent of cpm of the TCA-soluble material divided by the total cpm values (TCA-soluble material plus precipitated TCA pellet at specified time points). *Black bars* represent WT

yeast cells; *white bars* represent *msrA*-KO yeast cells. *Top left*: Cells expressing sham vector. *Bottom Left*: Cells expressing α-synuclein (WT-α-syn). *Top right*: Cells expressing A30P α-synuclein. *Bottom right*: Cells expressing A53T α-synuclein. **B)** For quantification of protein synthesis, the radioactivity (cpm) in the TCA-insoluble material was measured following labeling with [^{35}S]Met. *Black bars* represent WT; *white bars* represent *msrA*-KO yeast cells. The annotation for the type of expression (vector or alpha-synuclein) is the same as in A. Error bars represent standard error of three experiments. * denotes $P < 0.05$

Accumulation of fibrillated proteins in yeast strains overexpressing alpha-synuclein

Fibrillation of protein in general and alpha-synuclein in particular, is associated with posttranslational or genetic modifications to a protein. The observations above, suggesting an inhibition of degradation and accumulation of oxidized protein in cells expressing alpha-synuclein, led us to examine the contribution of these events to alpha-synuclein -mediated fibril formation. Yeast cells were stained with Thioflavin T, which is commonly used for detection of fibrillated proteins (Hawe, Sutter, & Jiskoot, 2008). Cells were imaged by phase-contrast microscopy, and the staining of protein fibrils was detected with epifluorescence (Fig. 3A). In addition, quantification of stained cells per amount of cells present was determined (Fig. 3B). Expression of native alpha-synuclein in the WT strain that had no effect on the percentile of cells exhibiting protein fibrillation compared to the sham vector. However, expression of SynA30P, and to a lower extent SynA53T, increased the percentile of cells containing protein fibrillation. Additionally, the *msrA*-KO strain shows an increased effect on protein fibrillation over the WT values when SynA30P is expressed; and to a lower extent when native alpha-synuclein is expressed. In contrast, SynA53T expression had similar effect on the induction of protein fibrillation in both WT and *msrA*-KO strains. In general, it appears that expression of alpha-synuclein either with point mutations or in the absence of MsrA causes protein fibrillation.

Several posttranslational modifications can alter the solubility of alpha-synuclein. Oxidation will cause a Met residue to be more hydrophilic, but the overall MetO-protein may become more hydrophobic by exposing hidden hydrophobic residues (Chao, Ma, & Stadtman, 1997). Degradation of alpha-synuclein is inhibited in Parkinson's disease and thus it is a plausible theory that this inhibition (also shown in Figs. 1 & 2) decreases the clearance of alpha-synuclein and promotes its aggregation, especially when the protein undergoes modifications that reduce its solubility. All types of alpha-synuclein caused enhanced cellular fibrillation in the absence of MsrA compared to the vector, while SynA30P had the most effect on forming fibrils in the *msrA*-KO strain (Fig. 3). This result would be the expected outcome of enhanced inhibited degradation

of the alpha-synuclein A30P (Figs. 1 & 2). Since the SynA53T aggregation is less affected by the presence of MsrA (Fig. 3), it may reflect the enhanced aggregation found in Parkinson's disease patients carrying this mutation (Lee, Choi, & Lee, 2002; Ostrerova-Golts et al., 2000). However, a combination of a compromised Msr system (from mutations or lowered expression with age) and overexpression of SynA30P could cause even greater levels of alpha-synuclein fibrils in Parkinson's disease patients.

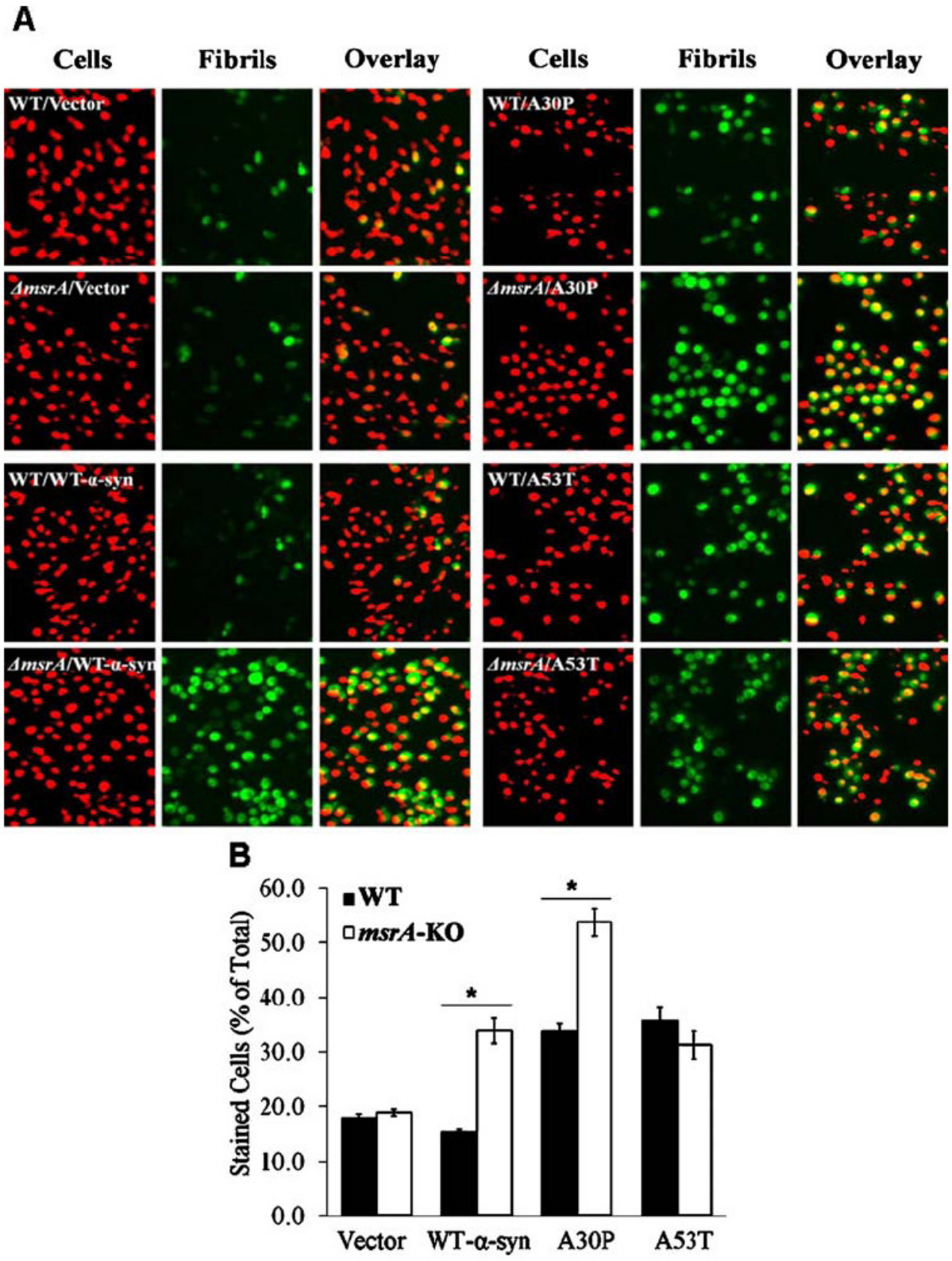
A
Cells
Fibrils
Overlay
Cells
Fibrils
Overlay
WT/Vector
WT/A30P
ΔmsrA/Vector
ΔmsrA/A30P
WT/WT-α-syn
WT/A53T
ΔmsrA/WT-α-syn
ΔmsrA/A53T
B
Stained Cells (% of Total)
60.0
50.0
40.0
30.0
20.0
10.0
0.0
WT
msrA-KO
*
*
Vector
WT-α-syn
A30P
A53T

Figure 3. Detection of fibrils present in msrA-KO and WT yeast cells by Thioflavin T staining. Yeast cells were stained with Thioflavin T after alpha-synuclein (WT-α-syn, A30P, A53T) induction of expression and transferring equal aliquots of cells into a 96-well plate. Cells were detected by phase-contrast microscopy and staining was detected with epifluorescence, both using a Nikon 40X objective of 1.3 N.A. and a standard DAPI/FitC/TxRed B filter set and dichroic (Brightline filters, Semrock). **A)** Representative images of cells collected by IN Cell Analyzer (GE Healthcare). For visualization, Image J software was used to make cells appear as red, fibrils appear as green, and to make an overlay image. **B)** Quantification of stained cells per number of cells present determined by IN Cell Analyzer provided software. Automated image segmentation was achieved independently on each image channel using the Otsu "global" method of thresholding. *Black bars* represent WT yeast cells; *white bars* represent *msrA*-KO yeast cells. Error bars represent standard deviation of six experiments. * denotes $P < 0.0001$

Phosphorylation of alpha-synuclein and its dependency on Msr

The functional role of phosphorylation to alpha-synuclein is not fully understood. Given our new data, it was intriguing to determine whether oxidation of Met could also affect the phosphorylation efficiency of alpha-synuclein. To follow the phosphorylation efficiency in both yeast strains expressing alpha-synuclein types, [^{32}P]ortho-phosphate was included in the expression induction media. Following the induction, the three types of alpha-synuclein protein were isolated from the corresponding yeast strains and phosphorylation was quantified by measuring the radiolabeling of the protein. All alpha-synuclein types isolated from *msrA*-KO cells showed significantly lower levels of phosphorylation relative to alpha-synuclein isolated from WT cells, especially in the native alpha-synuclein and SynA30P (Fig. 4A). The overall phosphorylation rate of SynA53T was significantly lower in both yeast strains, which may imply that this form of alpha-synuclein is more prone to oxidation even under normal function of the Msr system. Lower *in vivo* phosphorylation levels of α-synuclein in *msrA*-KO cells suggest that increased levels of MetO moiety in *msrA*-KO cells could partly inhibit the phosphorylation efficiency of alpha-synuclein. The two types of alpha-synuclein that are mostly affected by this phosphorylation decline in the *msrA*-KO strain are the native alpha-synuclein and SynA30P, similar to the effect of *msrA*-KO strain on protein fibrillation in the presence of these alpha-synuclein types (Fig. 3).

To further investigate the possibility that Met oxidation of alpha-synuclein may contribute to the phosphorylation inhibition, we used recombinant alpha-synuclein proteins in reduced and oxidized form, [^{32}P]ATP, and casein kinase 2 (a major kinase for alpha-synuclein Ser^{129} phosphorylation (Ishii et al., 2007)). To confirm that MetO formed in the oxidized alpha-synuclein is responsible for the observed effect on phosphorylation level, MsrA and PilB (naturally fused MsrA-MsrB protein from *Neisseria gonorrhoeae*) were added to the reaction mixture to reduce alpha-synuclein MetO residues. All samples were subjected to SDS-gel electrophoresis, gels were stained with GelCode Blue Stain (Fig. 4B), and phosphorylation was

visualized by autoradiography. The oxidation of the three types of alpha-synuclein inhibited the phosphorylation by casein kinase 2 (Fig. 4C), while both MsrA and PilB were able to reverse this inhibition via MetO reduction. Both of the mutant alpha-synuclein proteins were more phosphorylated when reduced by the Msr enzymes (Fig. 4C). Thus, it is possible that conformational changes that may occur in these alpha-synuclein mutants may also facilitate MetO reduction by the Msr system due to better accessibility of the enzyme to MetO residues. It is important to note that casein kinase 2 phosphorylation activities on control samples were not altered when Msr enzymes were added. This excludes the possibility that the enhanced alpha-synuclein phosphorylation, shown by Msr enzymes, is due to their reducing activity on casein kinase 2. Also, using MALDI-MS we have verified that the recombinant alpha-synucleins had elevated levels of oxidation relative to non-oxidized and Msr-reduced alpha-synucleins (data not shown).

The role of phosphorylation of alpha-synuclein (especially at Ser^{129}) is controversial. The phosphorylation alpha-synuclein at Ser^{129} by casein kinase 2 forms fibrils faster than unmodified alpha-synuclein i*n vitro* (Fujiwara et al., 2002) and increases the formation of cytoplasmic inclusion bodies in cell culture models of synucleinopathies (Smith et al., 2005). However, *in vivo* studies showed no obvious correlation between phosphorylated Ser^{129} and of alpha-synuclein fibril formation (L. Chen & Feany, 2005). In contrast, another study demonstrated that phosphorylation at Ser^{129} inhibits alpha-synuclein fibril formation *in vitro* (Paleologou et al., 2008). With regard to the vicinity of Met^{127} to Ser^{129}, we have examined the effect of MetO modifications on the rate of the *in vivo* phosphorylation of alpha-synuclein and casein kinase 2-mediated phosphorylation of alpha-synuclein. The observed decrease in alpha-synuclein phosphorylation due to MetO following MsrA ablation in cells (Fig. 4A) may be relevant to processes that regulate alpha-synuclein phosphorylation. As the provided yeast system is only a model to investigate the role of MsrA in maintaining alpha-synuclein function, further

investigations in a parallel mammalian system will greatly contribute to clarify the physiological role of MsrA on alpha-synuclein phosphorylation.

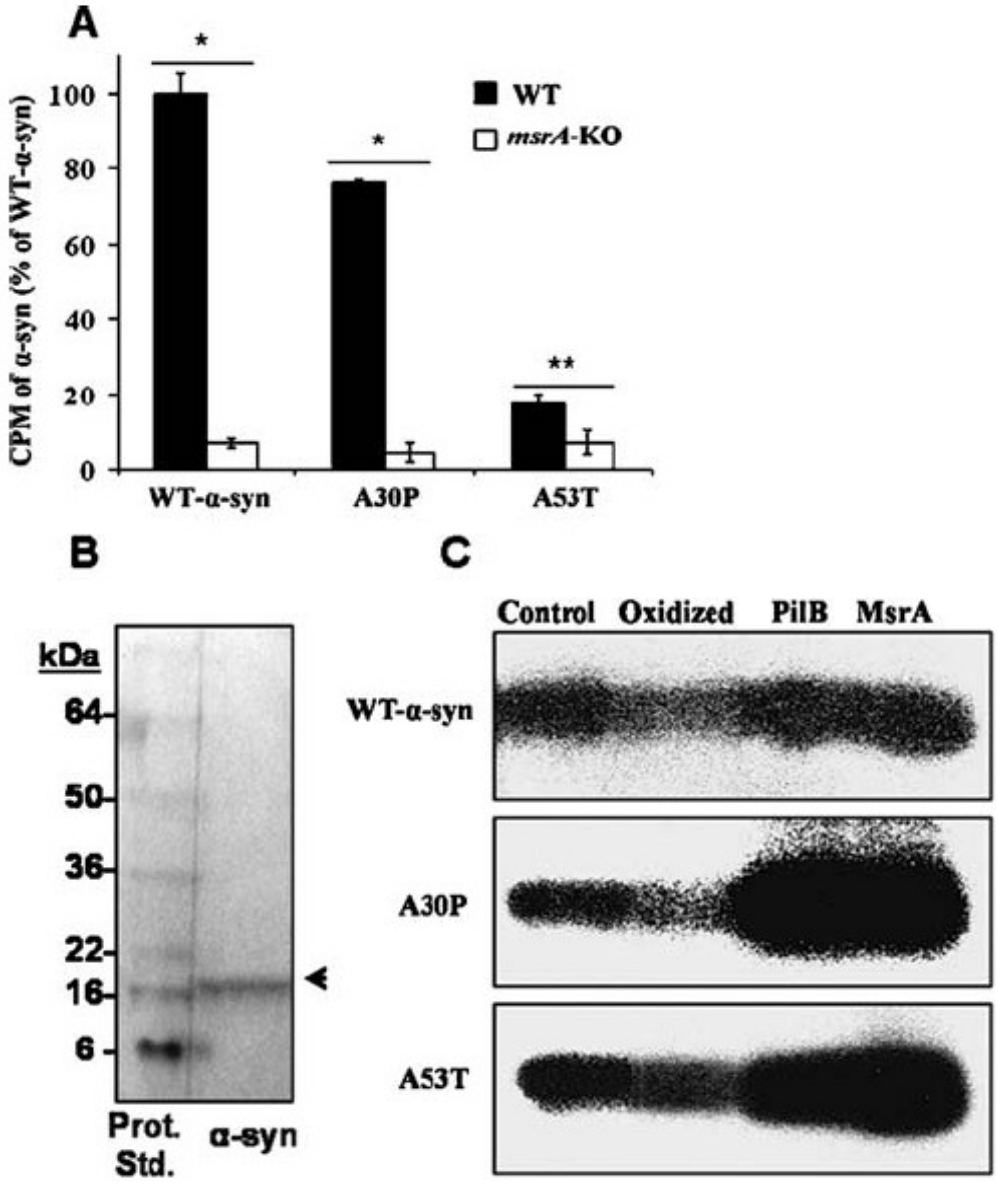

Figure 4. Phosphorylation of alpha-synuclein isolated from *msrA*-KO and WT yeast cells.

A) Each yeast strain expressing each alpha-synuclein type was induced and then incubated in medium containing ortho-[^{32}P]phosphoric acid. Expressed alpha-synuclein proteins (WT-α-syn, A30P, A53T) were isolated by resin binding and phosphorylation was detected by measuring cpm. Values represent percentage of cpm value relative to WT-α-syn cpm value in WT yeast cells. *Black bars* represent WT yeast cells; *white bars* represent *msrA*-KO yeast cells. Error bars represent standard error of four experiments. * denotes $P < 0.001$; ** denotes $P < 0.05$ **B)** A

representative gel stained with GelCode Blue Stain reagent. *Left lane:* SeeBlue Plus2 protein standard (Invitrogen). *Right lane:* typical separation of pure commercial recombinant human α alpha-synuclein proteins (WT-α-syn shown as a representative alpha-synuclein; *arrow* indicates the band corresponding to alpha-synuclein). **C)** Pure commercial recombinant human alpha-synuclein proteins (WT-α-syn, A30P, A53T) were exposed to H_2O_2 overnight (*Oxidized*). Oxidant was removed by catalase and Msr enzymes were added where indicated (PilB, MsrA). The removal of oxidants was verified by adding alpha-synuclein after oxidants were removed, and served as the non-oxidized form of alpha-synuclein (*Control*). All samples were phosphorylated with [γ-^{32}P]-ATP, and casein kinase 2. Equal amounts of alpha-synuclein proteins were subjected to an SDS-gel electrophoresis and the gel was exposed to X-ray film, followed by developing for visualization.

A functional Msr system and Met oxidation may have a role in regulating alpha-synuclein and the phosphorylation of other proteins. Recent studies suggested that MetO formation on inhibitory factor of NF-kappaB (IkBα) prevents its subsequent degradation. Similar to alpha-synuclein, the IkBα Met^{45} residue is close to the phosphorylation sites Ser^{32} and Ser^{36}. The MetO formation, particularly within helices, can cause major conformational rearrangements (Bigelow & Squier, 2005), and the oxidation of Met^{45} may cause a structural disruption that makes the protein a less effective kinase target (Kanayama, Inoue, Sugita-Konishi, Shimizu, & Miyamoto, 2002; Midwinter, Cheah, Moskovitz, Vissers, & Winterbourn, 2006; Mohri et al., 2002). In another recent study, MsrA was shown to suppress dopaminergic protein aggregation induced by mutant alpha-synuclein via MetO repair. The MsrA was able to reduce several oxidized Met residues in recombinant alpha-synuclein (Liu et al., 2008). Overall, it is suggested that oxidation of Met in alpha-synuclein inhibits phosphorylation, which may be involved in processes relevant to its degradation or aggregation depending on cellular environment.

In summary, both the nature of alpha-synuclein and presence of MsrA determined the overall protein and alpha-synuclein degradation in yeast. Furthermore, Met oxidation of alpha-synuclein inhibits alpha-synuclein phosphorylation. This occurs parallel to increasing protein fibrillation, especially when SynA30P is expressed in *msrA*-KO cells. To establish the relationships between alpha-synuclein overexpression and MsrA function in mammals, similar studies will be conducted in transgenic alpha-synuclein mice on an $MsrA^{-/-}$ background.

C. Met Oxidation of Proteins Associated with Neurodegenerative Diseases

The absence of MsrA appears to enhance markers for Alzheimer's disease in mice (Pal et al., 2007), alters the biochemical properties in yeast cells of alpha-synuclein which is known to be associated with Parkinson's disease (D. B. Oien, Shinogle et al., 2009), and various previously referenced systems. These effects are presumably from the accumulation of MetO. To identify MetO in proteins, polyclonal antibodies were developed (anti-MetO-DZS18) and characterized (D. B. Oien, Canello et al., 2009). As described below, these novel antibodies have been shown to detect MetO in blood serum proteins in the *MsrA*$^{-/-}$ mouse and patients diagnosed with Alzheimer's disease. In addition, carbonyl modifications can be detected as an alternative to the detection of MetO. Theoretically, oxidation of a residue to a carbonyl would follow the oxidation of any exposed methionines (D. B. Oien & Moskovitz, 2008). Msr null yeast cells have been shown to accumulate carbonyls (D. Oien & Moskovitz, 2007). This method has been applied to *msrA*-KO and WT yeast cells that express alpha-synuclein as shown below. Finally, anti-MetO-DZS18 antibodies have been used to detect MetO modifications in prions as shown below.

1. Blood Serum Proteins (D. B. Oien, Canello et al., 2009)

The major proteins in serum, mouse serum albumin (MSA) as well of intact IgG, were shown to react in western blot analysis with the anti-MetO-DZS18 antibodies (Fig. 1). The identification of the MSA was confirmed by mass spectrometry analysis using trypsin-digested peptides covering about 25% of the protein sequence. Among all peptides analyzed, Met572 was shown to be oxidized to MetO. Apparently, Met572 is conserved in all sequenced serum albumins and perhaps its structural location promotes its availability to oxidation. The identification of an intact IgG as the other target for Met oxidation (Fig. 1) was confirmed by probing a parallel western blot with primary rabbit anti-mouse IgG (data not shown). Further western blot analyses for Met oxidation in MSA and IgG were performed on serums from wild type and *MsrA*$^{-/-}$ mice taken at various ages. As shown in Fig. 2A, the oxidation of MSA and IgG in its intact form (~150 kDa) intensified in *MsrA*$^{-/-}$ compared to WT serums. The SDS-gel electrophoresis was performed in

the presence of β-mercaptoethanol that is expected to reduce the disulfide bonds between each IgG monomer as well as between the heavy (~50 kDa) and light (~25 kDa) chains of the protein. Accordingly, in serum of 6-month-old mice the IgG molecules were reduced to their monomeric components and shown to contain MetO by western blot analysis (Fig. 2A). In contrast, with older age, the disulfide bond reduction was inhibited and the relative oxidative levels of intact IgG (~150 kDa) and aggregated form of an unknown serum protein (~250 kDa suggested to be an aggregated form of IgG (Ag) were increased in both mouse strains as function of age (Fig. 2A). In comparison to WT, the Met oxidation of the Ag form of IgG was mostly pronounced in *MsrA*$^{-/-}$ serums (Fig. 2A). Densitometry analysis for the intensities of the corresponding MSA, IgG and AG bands have confirmed that the MetO levels of the selected proteins increases in *MsrA*$^{-/-}$ versus WT serums (Fig. 2B). Moreover, the levels of the MetO–Ag were increased in an age-dependent manner in both strains, while showing the highest levels in the *MsrA*$^{-/-}$ strain (Fig. 2B). The latter observation may be due to the common nature of aggregated proteins of being more resistant to degradation, which fosters their accumulation with age. Similar to the observed effects of age and lack of MsrA on IgG MetO levels, intact forms of IgGs in serums of patients with Alzheimer's disease were shown to contain MetO while none was observed in control serums, respectively (Fig. 3). It is noted that the limited number of human specimens analyzed for the presence of MetO in serum proteins requires further validation by larger group analyses.

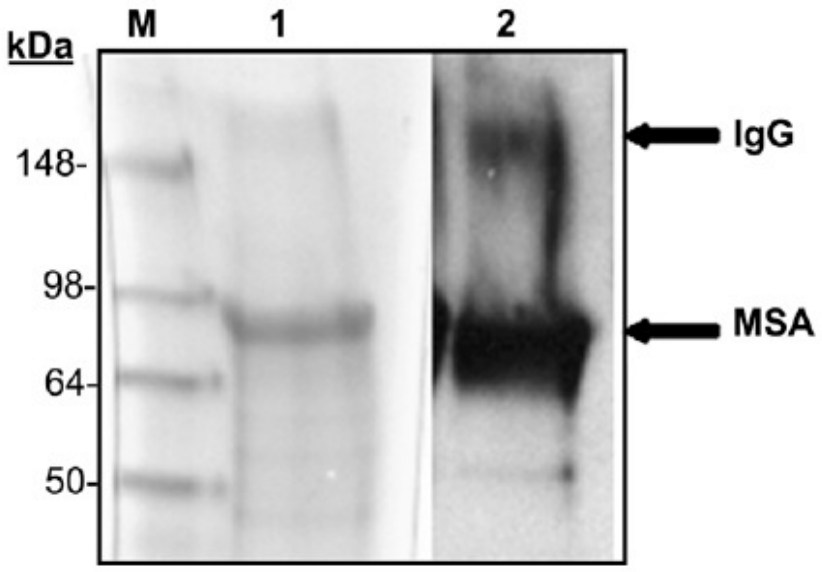

Figure 1. The anti-MetO-DZS18 antibodies detect methionine sulfoxide in mouse serum proteins. Fifty microgram of mouse serum proteins were subjected to SDS gel-electrophoresis and either stained with Coomassie blue (1), or probed with anti-MetO-DZS18 antibodies following western blot analysis (2). M, molecular mass markers (in kDa). IgG-Immunoglobulin G that was detected in a parallel gel by primary goat anti-mouse IgG antibodies (GenWay; data not shown). MSA, mouse serum albumin (detected by mass spectrometry analysis according to procedures previously described (D. B. Oien, Canello et al., 2009)). The presented data represents three independent experiments.

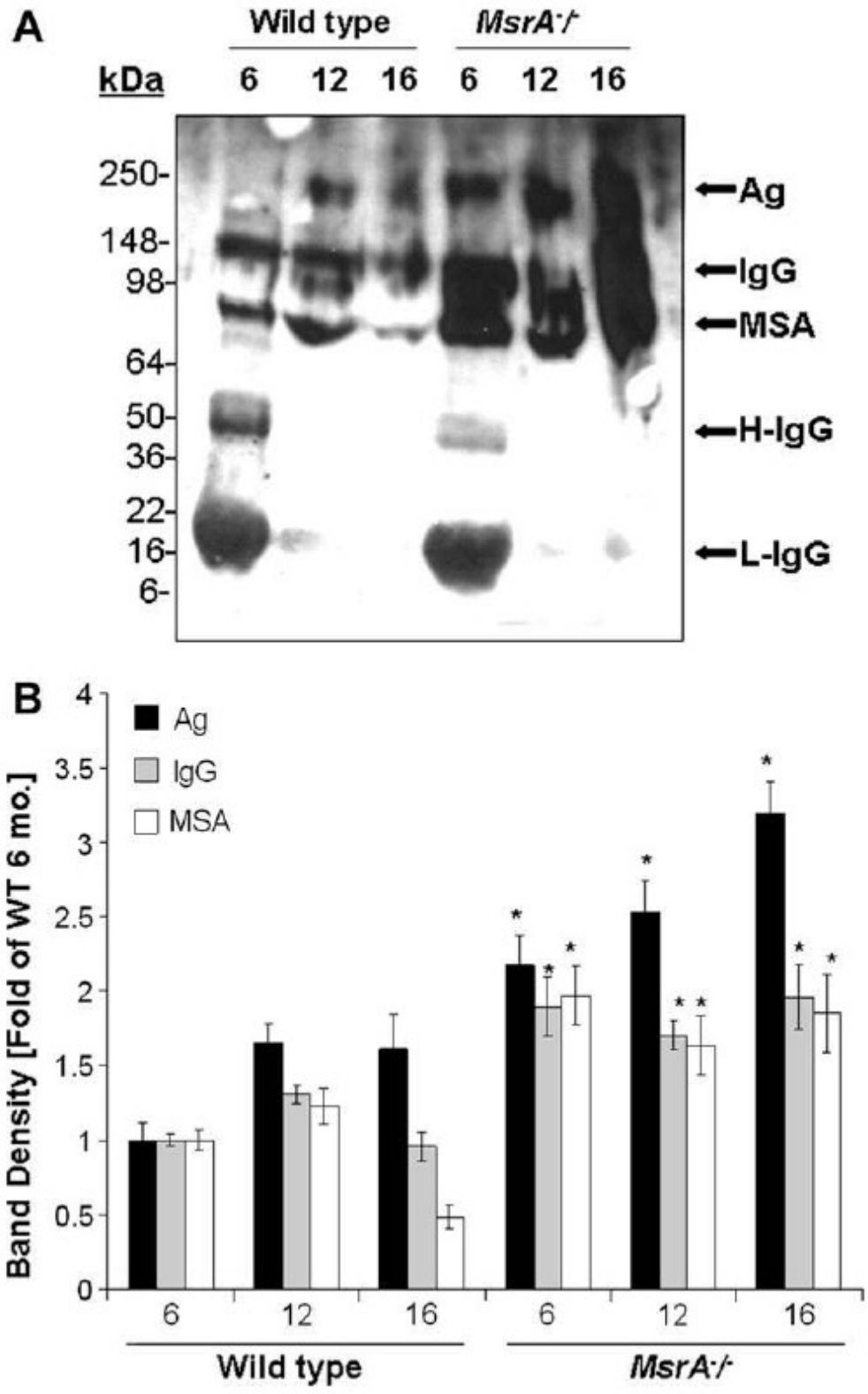
A
Wild type
MsrA-/-
kDa
6
12
16
6
12
16
250-
148-
98-
64-
50-
36-
22-
16-
6-
Ag
IgG
MSA
H-IgG
L-IgG
B
Ag
IgG
MSA
Band Density [Fold of WT 6 mo.]
4
3.5
3
2.5
2
1.5
1
0.5
0
6
12
16
6
12
16
Wild type
MsrA-/-

Figure 2. The anti-MetO-DZS18 antibodies detect methionine sulfoxide in mouse serum proteins in an age-dependent manner. A) Western blot analysis on mouse serums as function of age (6, 12 and 16, represent age in months) using the anti-MetO-DZS18 antibodies. Ag, aggregated form of serum protein. IgG, native form of IgG. H-IgG, heavy chain of IgG. L-IgG, light chain of IgG. MSA, mouse serum albumin. kDa, molecular mass indicators (in kDa). **B)** Densitometry analysis for the intensities of the MSA, IgG and Ag bands shown in panel A. The numbers 6, 12 and 16 represent age in months. The (*) symbol represents significant statistical difference ($P < 0.05$; t-test) between the age-matching bands of both mouse strains. Also, there were significant statistical differences ($P < 0.05$; t-test) within the relative levels of the Ag bands in each mouse strain: between all age groups of *MsrA*$^{-/-}$ and between 6 and 12 or 16 months old of WT mice. The shown data represent three independent experiments.

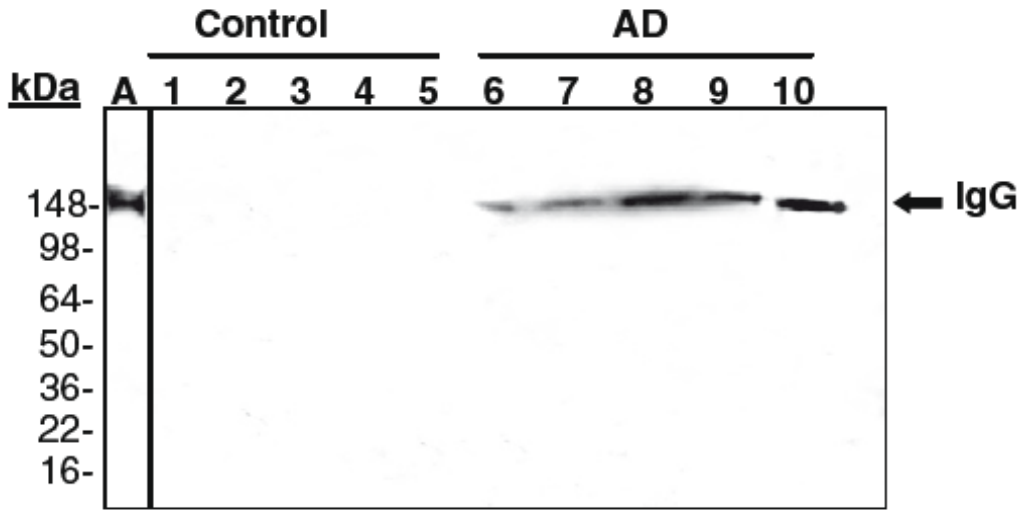

Figure 3. The anti-MetO-DZS18 antibodies detect methionine sulfoxide in IgG in serum proteins of Alzheimer's disease human subjects. Western blot analysis on human serums using the anti-MetO-DZS18 antibodies (1–5, samples from control human subjects; 6–10, samples of Alzheimer's disease patients; all samples are aged matched (70–80 years old). A. A representative sample of human serum probed with primary rabbit anti-human IgG antibodies (GenWay). kDa, molecular mass indicators (in kDa). The presented data represents three independent experiments.

2. Carbonylation of Alpha-Synuclein (J. Moskovitz & Oien)

To investigate the possible link between protein carbonylation, a compromised Msr system, and alpha-synuclein in the development of Parkinson's disease, we are presenting here new relevant data. Accordingly, to elucidate the effect of alpha-synuclein and its mutants on the accumulation of protein-carbonyl under conditions favoring Met oxidation, the proteins were expressed in both a WT stain and *msrA* null (MT) yeast strains (Yeast strains: The MT (*Mata* Δ*msrA*::*URA3 his6 leu2*) strain and its parent WT strain were obtained from previous studies by Moskovitz et al. (J. Moskovitz et al., 1997)).

The human alpha-synuclein protein and its mutants were overexpressed in MT and WT yeast strains. The expression vector pYES6 is designed for inducible expression of recombinant proteins in *Saccharomyces cerevisiae*. This vector harbors the yeast GAL1 promoter for high-level inducible protein expression in yeast by galactose and repression by glucose. In addition, it has a C-terminal peptide encoding V5 epitope and polyhistidine (6His) tag for detection and purification of the recombinant fusion protein (in this case alpha-synuclein). Additionally, the vector contains the ampicillin and blasticidin resistance genes for selection of bacteria and yeast colonies harboring the plasmid, respectively. Three forms of the human alpha-synuclein cDNA (wild type (alpha-synuclein) and naturally occurring mutants: Ala53Thr (SynA53T) and Ala30Pro (SynA30P)) were inserted into the pYES6 vector keeping the sequence in frame with the 6His peptide. For that purpose, suitable 5' forward and 3' reverse complement primers (harboring *Hind* III and *Xba* I restriction sites, respectively) were designed and used with each of the three alpha-synuclein cDNAs (kindly provided by Dr. Mikiei Tanaka, NIH, NHLBI) in a routine PCR procedure. Then, the resulting PCR products were sub-cloned into the suitable complementary restriction sites on the pYES6 and transformed into bacterial cells (DH5α). Each of the desired plasmids were isolated from bacterial cells, selectively grown on media containing ampicillin, and then transformed into WT and MT yeast strains. Vector-transformed cells served as controls for the alpha-synuclein expressed yeast cells. Following growth selection on media

containing blasticidin, all the transformed yeast strains (WT and MT containing either the vector only, vector containing alpha-synuclein, or vector containing either SynA53T or SynA30P) were grown in the presence of induction media containing 2% galactose and 1% raffinose for up to 24 hours. At various time points, equal amounts of cells were taken from each culture (as determined by optical density (OD_{600nm})) and extracted by glass beads and bead-beater homogenizer apparatus (BioSpec Products, OK). Finally, the alpha-synuclein proteins were purified from the corresponding extracts by using of ProBond™ Nickel-Chelating Resin following the commonly applied purification procedure (Invitrogen). Equal volumes of purified alpha-synuclein proteins were subjected to SDS-gel-electrophoresis and detected by western blotting using antibodies specific to the 6His tag.

Protein carbonyl determination.

Disrupted yeast cell protein extracts were monitored for their protein-carbonyl content by the use of the western blot-based carbonyl-assay kit manufactured by Cayman Chemical (Ann Arbor, MI). In brief, both yeast strains with the sham vector (control) and the three types of alpha-synuclein (Syn, SynA30P, SynA53T) were grown in the protein expression induction media for 2 h. Next, cells were precipitated and disrupted by glass beads in the presence of PBS and protease inhibitors cocktail (Roche). Following high speed centrifugation, equal amounts of the soluble protein extracts were reacted with 2,4-dinitrophenylhydrazine (DNPH), subjected to SDS-gel-electrophoresis, and detected by western blotting using antibodies specific to DNP. In addition, quantification of the relative amounts of the carbonylated proteins in the corresponding extracts was performed by monitoring the absorbance of the DNPH-protein derivatives at 370 nm.

Previously we have shown that following oxidative stress or non-replicative senescence, MT cells accumulate increased levels of protein carbonyl (D. Oien & Moskovitz, 2007). Moreover, accumulations of carbonylated proteins have been shown to cause inhibition of degradation with

age (Starke-Reed & Oliver, 1989). Together, it suggests that further protein oxidation prompted by Met oxidation may lead to the accumulation of carbonylated proteins especially in the alpha-synuclein-expressing MT strain. As shown in Fig. 4, compared to vector transformed yeast (control), a significant increase in the levels carbonylated proteins was observed when alpha-synuclein was expressed, especially in the MT strain expressing SynA30P. The latter massive accumulation of carbonylated proteins in the SynA30P expressed in MT correlates with the prominent inhibition of SynA30P degradation into shorter peptides (unpublished data). It is thus suggested that enhanced protein–carbonyl accumulations in MT strain may be due to an increased oxidation prompted by MetO (that may cause conformational changes to proteins, leading to further irreversible oxidation) along with alpha-synuclein inhibition of degradation (especially by the SynA30P type).

A

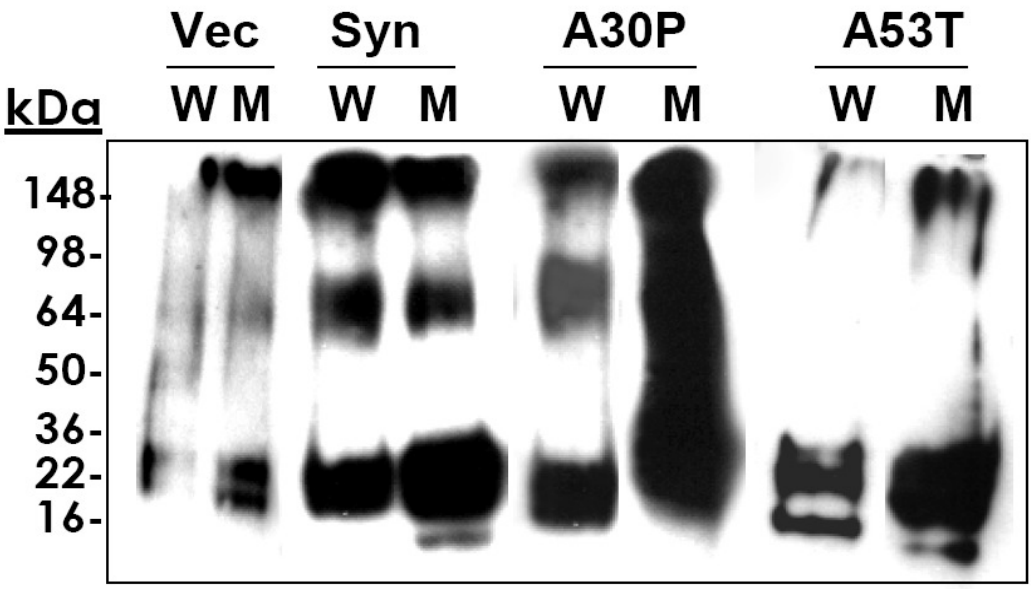
Vec
Syn
A30P
A53T
kDa
W M W M W M W M
148-
98-
64-
50-
36-
22-
16-

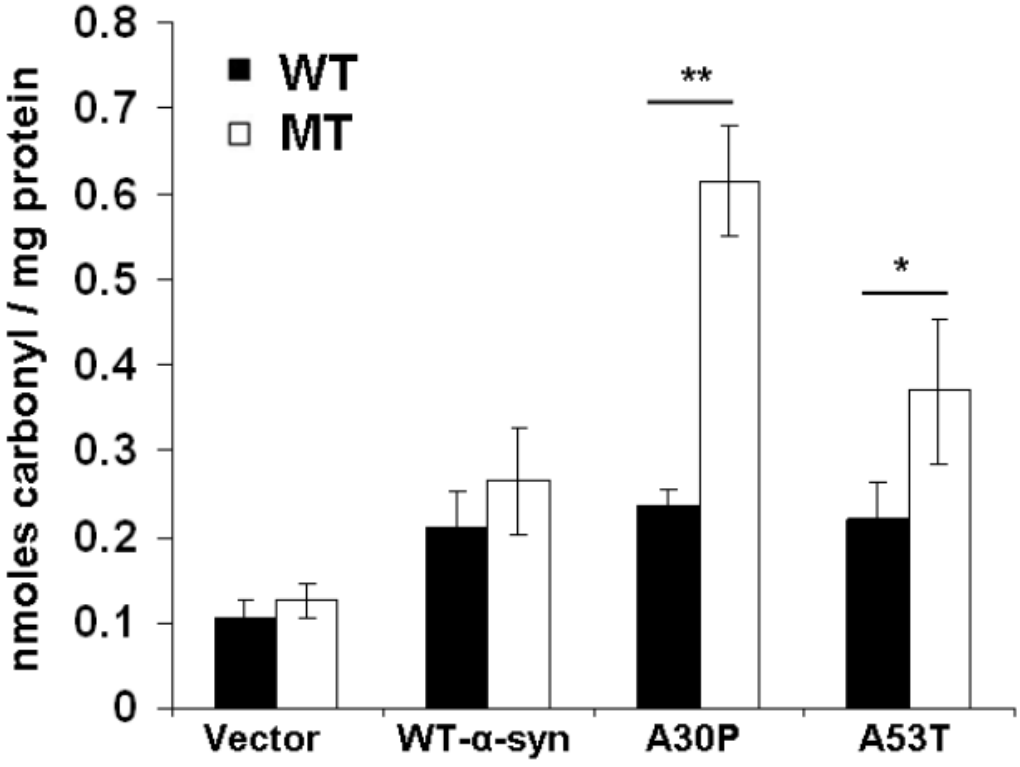
nmoles carbonyl / mg protein
0.8
0.7
0.6
0.5
0.4
0.3
0.2
0.1
0
WT
MT
**
*
Vector
WT-α-syn
A30P
A53T

B

Figure 4. Accumulation of carbonylated proteins in MT and WT yeast cells expressing alpha-synuclein and control vector. Both yeast strains with the sham vector control (Vec) and the three types of alpha-synuclein (Syn, A30P, A53T) were grown in the protein expression induction media for 2 h. Then, cells were precipitated and disrupted by glass beads in the presence of buffer and a protease inhibitor cocktail. Following high speed centrifugation, equal amounts of the soluble protein extracts were reacted with DNPH and subjected both to **A)** SDS-gel electrophoresis and detection by western blotting using antibodies specific to DNP (W, wild type yeast strain; M, *msrA* null MT yeast strain); and to **B)** readings by spectrophotometer at OD_{370nm}. Black bars represent WT yeast cells; white bars represent MT yeast cells. Vector, Syn, A30P, and A53T, represent sham vector, non-mutated, A30P, and A53T alpha-synuclein harboring cells respectively. Error bars represent standard error (n=3). * denotes $P < 0.05$ and ** denotes $P < 0.001$ (*t-test*).

Supportive evidence on the effect of SynA30P expression on protein carbonylation comes from a proteomic analysis of transgenic mice overexpressing SynA30P (Poon et al., 2005). In this study, it was shown that there were more than two-fold selective increases in specific carbonyl levels of three proteins in brains of SynA30P mice: carbonic anhydrase 2, alpha-enolase, and lactate dehydrogenase 2. Furthermore, Activity analyses of these oxidized proteins showed decreased functions in these enzymes as well. Accordingly, the authors suggested that proteins associated with impaired energy metabolism and mitochondria are particularly prone to oxidative stress associated with A30P-mutant alpha-synuclein (Poon et al., 2005). It is hypothesized that a cross between a transgenic mouse overexpressing SynA30P and the *MsrA*$^{-/-}$ mouse will exacerbate the increase in protein carbonyl levels, both in the above selected proteins and in other proteins yet to be identified.

3. Prion Protein (D. B. Oien, Canello et al., 2009)

The prion type PrPSc is the modified form of the membranal cellular prion protein (PrPC). PrPSc is considered to be a version of prion that is associated with transmissible spongiform encephalopathies. Stahl et al. have shown that either one or two Met residues (M206 and/or M213) were present in the form of MetO in PrPSc (Stahl et al., 1993). Additionally, PrPC has been assigned a role in the protection of cells from ROS (Brown, 2005; Nadal et al., 2007) and recombinant PrP (rPrP) was a target for oxidation (Redecke et al., 2007; Requena et al., 2004). Recently, it has been demonstrated by Gabizon et al. that brain PrPSc contains high levels of MetO, which are not detected in brain PrPC and its recombinant models (Canello et al., 2008). Accordingly, we have examined the possibility of detecting MetO in rPrP, oxidized rPrP and Proteinase K (PK) resistant hamster PrPSc by the anti-MetO-DZS18 antibodies. As shown in Fig. 5, the a-PrP mAb IPCV1 antibodies recognized all forms tested in the figure; a-PrP mAb IPC2 antibodies recognized PrP forms that were not oxidized at Met213 (Canello et al., 2008), and the anti-MetO-DZS18 antibodies recognized all forms of PrP tested, while exhibiting the

strongest reaction against the oxidized form of rPrP. As seen in Fig. 5, while a-PrP mAb IPC2 antibodies reacted with non-oxidized rPrP and with the lower forms of hamster PrPSc, the anti-MetO-DZS18 antibodies recognized all the additional PrP forms that react with a-PrP mAb IPCV1 antibodies. The fact that the silver stain pattern of PrPSc is similar to the a-PrP mAb IPCV1 pattern of PrP recognition suggests the anti-MetO-DZS18 antibodies indeed reacted with the fully glycosylated PrPSc form not recognized by a-PrP mAb IPC2 antibodies (primarily the ~36 kDa band that is mainly presented in the PrPSc form). It is important to note that the gel electrophoresis performed prior to the western blot using a-PrP mAb IPC2 antibodies was done in the absence of β-mercaptoethanol. This was due to the fact that a-PrP mAb IPC2 antibodies can recognize only PrP proteins with intact disulfide bridges (Canello et al., 2008). However, oxidation of PrP causing MetO formation interferes with the protein recognition by the a-PrP mAb IPC2 antibodies (Fig. 5). Complementary to this observation, it is suggested that the presence of β-mercaptoethanol causes the MetO at position 213 to be more surface exposed to facilitating its recognition by the anti-MetO-DZS18 antibodies (Fig. 5). These results are consistent with the recent publication (Canello et al., 2008) indicating that several Met residues are oxidized in PrPSc. This suggests that the anti-MetO-DZS18 antibodies can be an important tool to study this modification in prion protein.

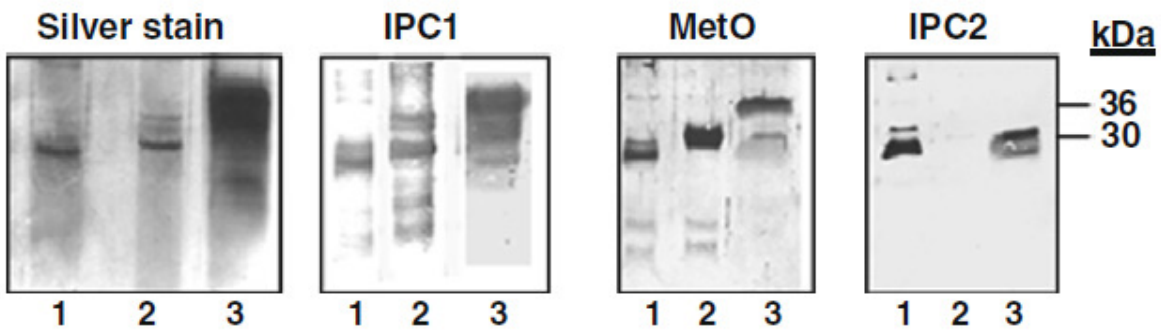

Figure 5. The anti-MetO-DZS18 antibodies detect MetO in prion protein. The following samples were subjected to SDS-gel electrophoresis followed by silver staining and immunoblotting with several antibodies. Full length polypeptide chains corresponding to the hamster PrP sequence, lacking the N- and C-terminal sequences (rSHaPrP (23–230; denoted as rPrP) were expressed and folded to their a-form as previously described (D. B. Oien, Canello et al., 2009). The rPrP was then incubated in the presence and absence of 50 mM H_2O_2 for 30 min. For the purified PK resistant PrPSc samples, membranes from scrapie infected hamster brain homogenates were purified. Following SDS-gel electrophoresis, all samples (1: rPrP; 2: oxidized rPrP; 3: PK resistant hamster PrPSc) were subjected to either silver staining or immunoblotting with: anti-PrP mAb IPCV1, which recognize all forms tested in the figure (IPC1); anti-PrP mAb IPC2, which recognize PrP forms that are non-oxidized at Met 213 (IPC2), as well as the anti-MetO-DZS18 antibodies, which recognize MetO in proteins (MetO). kDa, molecular mass indicators (in kDa). The presented data represents three independent experiments.

4. Summary

The evidence in this section supports an association between MetO oxidation (and carbonylation) and the neurodegenerative diseases of Alzheimer's disease, Parkinson's disease, and spongiform encephalopathies. To date, these three diseases still remain the leading frontiers for the antioxidant role of Met redox cycles in neurodegenerative diseases. The remainder of this document focuses on the Msr system in locomotor-associated dopamine

signaling. This research further supports a connection between Met redox cycles and Parkinson's disease. However, the direct relationship of the Msr system and Met oxidation to disease is yet to be determined.

D. References

Apelt, J., Bigl, M., Wunderlich, P., & Schliebs, R. (2004). Aging-related increase in oxidative stress correlates with developmental pattern of beta-secretase activity and beta-amyloid plaque formation in transgenic Tg2576 mice with Alzheimer-like pathology. *Int J Dev Neurosci, 22*(7), 475-484.

Ashwood, T. J., Lancaster, B., & Wheal, H. V. (1984). In vivo and in vitro studies on putative interneurones in the rat hippocampus: possible mediators of feed-forward inhibition. *Brain Res, 293*(2), 279-291.

Baba, M., Nakajo, S., Tu, P. H., Tomita, T., Nakaya, K., Lee, V. M., et al. (1998). Aggregation of alpha-synuclein in Lewy bodies of sporadic Parkinson's disease and dementia with Lewy bodies. *Am J Pathol, 152*(4), 879-884.

Barnham, K. J., Ciccotosto, G. D., Tickler, A. K., Ali, F. E., Smith, D. G., Williamson, N. A., et al. (2003). Neurotoxic, redox-competent Alzheimer's beta-amyloid is released from lipid membrane by methionine oxidation. *J Biol Chem, 278*(44), 42959-42965.

Berke, S. J., & Paulson, H. L. (2003). Protein aggregation and the ubiquitin proteasome pathway: gaining the UPPer hand on neurodegeneration. *Curr Opin Genet Dev, 13*(3), 253-261.

Bigelow, D. J., & Squier, T. C. (2005). Redox modulation of cellular signaling and metabolism through reversible oxidation of methionine sensors in calcium regulatory proteins. *Biochim Biophys Acta, 1703*(2), 121-134.

Blennow, K., Vanmechelen, E., & Hampel, H. (2001). CSF total tau, Abeta42 and phosphorylated tau protein as biomarkers for Alzheimer's disease. *Mol Neurobiol, 24*(1-3), 87-97.

Brandis, K. A., Holmes, I. F., England, S. J., Sharma, N., Kukreja, L., & DebBurman, S. K. (2006). alpha-Synuclein fission yeast model: concentration-dependent aggregation without plasma membrane localization or toxicity. *J Mol Neurosci, 28*(2), 179-191.

Breydo, L., Bocharova, O. V., Makarava, N., Salnikov, V. V., Anderson, M., & Baskakov, I. V. (2005). Methionine oxidation interferes with conversion of the prion protein into the fibrillar proteinase K-resistant conformation. *Biochemistry, 44*(47), 15534-15543.

Brown, D. R. (2005). Neurodegeneration and oxidative stress: prion disease results from loss of antioxidant defence. *Folia Neuropathol, 43*(4), 229-243.

Bussell, R., Jr., & Eliezer, D. (2003). A structural and functional role for 11-mer repeats in alpha-synuclein and other exchangeable lipid binding proteins. *J Mol Biol, 329*(4), 763-778.

Butterfield, D. A., & Boyd-Kimball, D. (2005). The critical role of methionine 35 in Alzheimer's amyloid beta-peptide (1-42)-induced oxidative stress and neurotoxicity. *Biochim Biophys Acta, 1703*(2), 149-156.

Canello, T., Engelstein, R., Moshel, O., Xanthopoulos, K., Juanes, M. E., Langeveld, J., et al. (2008). Methionine sulfoxides on PrPSc: a prion-specific covalent signature. *Biochemistry, 47*(34), 8866-8873.

Chao, C. C., Ma, Y. S., & Stadtman, E. R. (1997). Modification of protein surface hydrophobicity and methionine oxidation by oxidative systems. *Proc Natl Acad Sci U S A, 94*(7), 2969-2974.

Chen, L., & Feany, M. B. (2005). Alpha-synuclein phosphorylation controls neurotoxicity and inclusion formation in a Drosophila model of Parkinson disease. *Nat Neurosci, 8*(5), 657-663.

Chen, Q., Ding, Q., & Keller, J. N. (2005). The stationary phase model of aging in yeast for the study of oxidative stress and age-related neurodegeneration. *Biogerontology, 6*(1), 1-13.

Chen, Q., Thorpe, J., Ding, Q., El-Amouri, I. S., & Keller, J. N. (2004). Proteasome synthesis and assembly are required for survival during stationary phase. *Free Radic Biol Med, 37*(6), 859-868.

Choi, J., Sullards, M. C., Olzmann, J. A., Rees, H. D., Weintraub, S. T., Bostwick, D. E., et al. (2006). Oxidative damage of DJ-1 is linked to sporadic Parkinson and Alzheimer diseases. *J Biol Chem, 281*(16), 10816-10824.

Dong, J., Atwood, C. S., Anderson, V. E., Siedlak, S. L., Smith, M. A., Perry, G., et al. (2003). Metal binding and oxidation of amyloid-beta within isolated senile plaque cores: Raman microscopic evidence. *Biochemistry, 42*(10), 2768-2773.

Ferrer, I., Blanco, R., Carmona, M., Ribera, R., Goutan, E., Puig, B., et al. (2001). Phosphorylated map kinase (ERK1, ERK2) expression is associated with early tau deposition in neurones and glial cells, but not with increased nuclear DNA vulnerability and cell death, in Alzheimer disease, Pick's disease, progressive supranuclear palsy and corticobasal degeneration. *Brain Pathol, 11*(2), 144-158.

Fink, A. L. (2006). The aggregation and fibrillation of alpha-synuclein. *Acc Chem Res, 39*(9), 628-634.

Fujiwara, H., Hasegawa, M., Dohmae, N., Kawashima, A., Masliah, E., Goldberg, M. S., et al. (2002). alpha-Synuclein is phosphorylated in synucleinopathy lesions. *Nat Cell Biol, 4*(2), 160-164.

Gabbita, S. P., Aksenov, M. Y., Lovell, M. A., & Markesbery, W. R. (1999). Decrease in peptide methionine sulfoxide reductase in Alzheimer's disease brain. *J Neurochem, 73*(4), 1660-1666.

Gamrani, H., Onteniente, B., Seguela, P., Geffard, M., & Calas, A. (1986). Gamma-aminobutyric acid-immunoreactivity in the rat hippocampus. A light and electron microscopic study with anti-GABA antibodies. *Brain Res, 364*(1), 30-38.

Giasson, B. I., Duda, J. E., Murray, I. V., Chen, Q., Souza, J. M., Hurtig, H. I., et al. (2000). Oxidative damage linked to neurodegeneration by selective alpha-synuclein nitration in synucleinopathy lesions. *Science, 290*(5493), 985-989.

Giorgi, F. S., Bandettini di Poggio, A., Battaglia, G., Pellegrini, A., Murri, L., Ruggieri, S., et al. (2006). A short overview on the role of alpha-synuclein and proteasome in experimental models of Parkinson's disease. *J Neural Transm Suppl*(70), 105-109.

Glaser, C. B., Yamin, G., Uversky, V. N., & Fink, A. L. (2005). Methionine oxidation, alpha-synuclein and Parkinson's disease. *Biochim Biophys Acta, 1703*(2), 157-169.

Goedert, M., & Spillantini, M. G. (2006). A century of Alzheimer's disease. *Science, 314*(5800), 777-781.

Harris, F. M., Brecht, W. J., Xu, Q., Mahley, R. W., & Huang, Y. (2004). Increased tau phosphorylation in apolipoprotein E4 transgenic mice is associated with activation of extracellular signal-regulated kinase: modulation by zinc. *J Biol Chem, 279*(43), 44795-44801.

Hawe, A., Sutter, M., & Jiskoot, W. (2008). Extrinsic fluorescent dyes as tools for protein characterization. *Pharm Res, 25*(7), 1487-1499.

Hill, A. F., Joiner, S., Wadsworth, J. D., Sidle, K. C., Bell, J. E., Budka, H., et al. (2003). Molecular classification of sporadic Creutzfeldt-Jakob disease. *Brain, 126*(Pt 6), 1333-1346.

Hol, E. M., Roelofs, R. F., Moraal, E., Sonnemans, M. A., Sluijs, J. A., Proper, E. A., et al. (2003). Neuronal expression of GFAP in patients with Alzheimer pathology and identification of novel GFAP splice forms. *Mol Psychiatry, 8*(9), 786-796.

Hou, L., Kang, I., Marchant, R. E., & Zagorski, M. G. (2002). Methionine 35 oxidation reduces fibril assembly of the amyloid abeta-(1-42) peptide of Alzheimer's disease. *J Biol Chem, 277*(43), 40173-40176.

Hsu, L. J., Sagara, Y., Arroyo, A., Rockenstein, E., Sisk, A., Mallory, M., et al. (2000). alpha-synuclein promotes mitochondrial deficit and oxidative stress. *Am J Pathol, 157*(2), 401-410.

Hyman, B. T., Elvhage, T. E., & Reiter, J. (1994). Extracellular signal regulated kinases. Localization of protein and mRNA in the human hippocampal formation in Alzheimer's disease. *Am J Pathol, 144*(3), 565-572.

Hyman, B. T., Reiter, J., Moss, M., Rosene, D., & Pandya, D. (1994). Extracellular signal-regulated kinase (MAP kinase) immunoreactivity in the rhesus monkey brain. *Neurosci Lett, 166*(1), 113-116.

Ingelsson, M., Fukumoto, H., Newell, K. L., Growdon, J. H., Hedley-Whyte, E. T., Frosch, M. P., et al. (2004). Early Abeta accumulation and progressive synaptic loss, gliosis, and tangle formation in AD brain. *Neurology, 62*(6), 925-931.

Ishii, A., Nonaka, T., Taniguchi, S., Saito, T., Arai, T., Mann, D., et al. (2007). Casein kinase 2 is the major enzyme in brain that phosphorylates Ser129 of human alpha-synuclein: Implication for alpha-synucleinopathies. *FEBS Lett, 581*(24), 4711-4717.

Jackson, G. S., Hosszu, L. L., Power, A., Hill, A. F., Kenney, J., Saibil, H., et al. (1999). Reversible conversion of monomeric human prion protein between native and fibrilogenic conformations. *Science, 283*(5409), 1935-1937.

Jo, E., Fuller, N., Rand, R. P., St George-Hyslop, P., & Fraser, P. E. (2002). Defective membrane interactions of familial Parkinson's disease mutant A30P alpha-synuclein. *J Mol Biol, 315*(4), 799-807.

Jung, B., Lee, E. H., Chung, W. S., Lee, S. J., Shin, S. H., Joo, S. H., et al. (2003). Increased viability of PC12 cells exposed to amyloid-beta peptide by transduction with human TAT-methionine sulfoxide reductase. *Neuroreport, 14*(18), 2349-2353.

Kanayama, A., Inoue, J., Sugita-Konishi, Y., Shimizu, M., & Miyamoto, Y. (2002). Oxidation of Ikappa Balpha at methionine 45 is one cause of taurine chloramine-induced inhibition of NF-kappa B activation. *J Biol Chem, 277*(27), 24049-24056.

Karelson, E., Fernaeus, S., Reis, K., Bogdanovic, N., & Land, T. (2005). Stimulation of G-proteins in human control and Alzheimer's disease brain by FAD mutants of APP(714-723): implication of oxidative mechanisms. *J Neurosci Res, 79*(3), 368-374.

Knowles, W. D., & Schwartzkroin, P. A. (1981). Local circuit synaptic interactions in hippocampal brain slices. *J Neurosci, 1*(3), 318-322.

Kruger, R., Kuhn, W., Muller, T., Woitalla, D., Graeber, M., Kosel, S., et al. (1998). Ala30Pro mutation in the gene encoding alpha-synuclein in Parkinson's disease. *Nat Genet, 18*(2), 106-108.

Kunkel, D. D., Hendrickson, A. E., Wu, J. Y., & Schwartzkroin, P. A. (1986). Glutamic acid decarboxylase (GAD) immunocytochemistry of developing rabbit hippocampus. *J Neurosci, 6*(2), 541-552.

Lee, H. J., Choi, C., & Lee, S. J. (2002). Membrane-bound alpha-synuclein has a high aggregation propensity and the ability to seed the aggregation of the cytosolic form. *J Biol Chem, 277*(1), 671-678.

Lev, N., Roncevich, D., Ickowicz, D., Melamed, E., & Offen, D. (2006). Role of DJ-1 in Parkinson's disease. *J Mol Neurosci, 29*(3), 215-225.

Lindersson, E., Beedholm, R., Hojrup, P., Moos, T., Gai, W., Hendil, K. B., et al. (2004). Proteasomal inhibition by alpha-synuclein filaments and oligomers. *J Biol Chem, 279*(13), 12924-12934.

Liu, F., Hindupur, J., Nguyen, J. L., Ruf, K. J., Zhu, J., Schieler, J. L., et al. (2008). Methionine sulfoxide reductase A protects dopaminergic cells from Parkinson's disease-related insults. *Free Radic Biol Med, 45*(3), 242-255.

Lucking, C. B., & Brice, A. (2000). Alpha-synuclein and Parkinson's disease. *Cell Mol Life Sci, 57*(13-14), 1894-1908.

Midwinter, R. G., Cheah, F. C., Moskovitz, J., Vissers, M. C., & Winterbourn, C. C. (2006). IkappaB is a sensitive target for oxidation by cell-permeable chloramines: inhibition of NF-kappaB activity by glycine chloramine through methionine oxidation. *Biochem J, 396*(1), 71-78.

Mohri, M., Reinach, P. S., Kanayama, A., Shimizu, M., Moskovitz, J., Hisatsune, T., et al. (2002). Suppression of the TNFalpha-induced increase in IL-1alpha expression by hypochlorite in human corneal epithelial cells. *Invest Ophthalmol Vis Sci, 43*(10), 3190-3195.

Morris, J. C., Storandt, M., McKeel, D. W., Jr., Rubin, E. H., Price, J. L., Grant, E. A., et al. (1996). Cerebral amyloid deposition and diffuse plaques in "normal" aging: Evidence for presymptomatic and very mild Alzheimer's disease. *Neurology, 46*(3), 707-719.

Moskovitz, J. (2005). Methionine sulfoxide reductases: ubiquitous enzymes involved in antioxidant defense, protein regulation, and prevention of aging-associated diseases. *Biochim Biophys Acta, 1703*(2), 213-219.

Moskovitz, J., Bar-Noy, S., Williams, W. M., Requena, J., Berlett, B. S., & Stadtman, E. R. (2001). Methionine sulfoxide reductase (MsrA) is a regulator of antioxidant defense and lifespan in mammals. *Proc Natl Acad Sci U S A, 98*(23), 12920-12925.

Moskovitz, J., Berlett, B. S., Poston, J. M., & Stadtman, E. R. (1997). The yeast peptide-methionine sulfoxide reductase functions as an antioxidant in vivo. *Proc Natl Acad Sci U S A, 94*(18), 9585-9589.

Moskovitz, J., & Bush, A. I. (2005). Methionine Sulfoxide Reductase System: Possible Roles in Protection against Neurodegenerative Diseases. In Y. Luo & L. Packer (Eds.), *Oxidative Stress and Age-Related Neurodegeneration* (pp. 197-210): CRC.

Moskovitz, J., & Oien, D. B. Protein carbonyl and the methionine sulfoxide reductase system. *Antioxid Redox Signal, 12*(3), 405-415.

Mouser, P. E., Head, E., Ha, K. H., & Rohn, T. T. (2006). Caspase-mediated cleavage of glial fibrillary acidic protein within degenerating astrocytes of the Alzheimer's disease brain. *Am J Pathol, 168*(3), 936-946.

Munishkina, L. A., Henriques, J., Uversky, V. N., & Fink, A. L. (2004). Role of protein-water interactions and electrostatics in alpha-synuclein fibril formation. *Biochemistry, 43*(11), 3289-3300.

Nadal, R. C., Abdelraheim, S. R., Brazier, M. W., Rigby, S. E., Brown, D. R., & Viles, J. H. (2007). Prion protein does not redox-silence Cu2+, but is a sacrificial quencher of hydroxyl radicals. *Free Radic Biol Med, 42*(1), 79-89.

Oien, D., & Moskovitz, J. (2007). Protein-carbonyl accumulation in the non-replicative senescence of the methionine sulfoxide reductase A (msrA) knockout yeast strain. *Amino Acids, 32*(4), 603-606.

Oien, D. B., Canello, T., Gabizon, R., Gasset, M., Lundquist, B. L., Burns, J. M., et al. (2009). Detection of oxidized methionine in selected proteins, cellular extracts and blood serums by novel anti-methionine sulfoxide antibodies. *Arch Biochem Biophys, 485*(1), 35-40.

Oien, D. B., & Moskovitz, J. (2008). Substrates of the methionine sulfoxide reductase system and their physiological relevance. *Curr Top Dev Biol, 80*, 93-133.

Oien, D. B., Shinogle, H. E., Moore, D. S., & Moskovitz, J. (2009). Clearance and Phosphorylation of Alpha-Synuclein Are Inhibited in Methionine Sulfoxide Reductase A Null Yeast Cells. *J Mol Neurosci*, *In Press*.

Olry, A., Boschi-Muller, S., Marraud, M., Sanglier-Cianferani, S., Van Dorsselear, A., & Branlant, G. (2002). Characterization of the methionine sulfoxide reductase activities of PILB, a probable virulence factor from Neisseria meningitidis. *J Biol Chem, 277*(14), 12016-12022.

Ostrerova-Golts, N., Petrucelli, L., Hardy, J., Lee, J. M., Farer, M., & Wolozin, B. (2000). The A53T alpha-synuclein mutation increases iron-dependent aggregation and toxicity. *J Neurosci, 20*(16), 6048-6054.

Outeiro, T. F., & Lindquist, S. (2003). Yeast cells provide insight into alpha-synuclein biology and pathobiology. *Science, 302*(5651), 1772-1775.

Pal, R., Oien, D. B., Ersen, F. Y., & Moskovitz, J. (2007). Elevated levels of brain-pathologies associated with neurodegenerative diseases in the methionine sulfoxide reductase A knockout mouse. *Exp Brain Res, 180*(4), 765-774.

Paleologou, K. E., Schmid, A. W., Rospigliosi, C. C., Kim, H. Y., Lamberto, G. R., Fredenburg, R. A., et al. (2008). Phosphorylation at Ser-129 but not the phosphomimics S129E/D inhibits the fibrillation of alpha-synuclein. *J Biol Chem, 283*(24), 16895-16905.

Palmblad, M., Westlind-Danielsson, A., & Bergquist, J. (2002). Oxidation of methionine 35 attenuates formation of amyloid beta -peptide 1-40 oligomers. *J Biol Chem, 277*(22), 19506-19510.

Pei, J. J., Braak, H., An, W. L., Winblad, B., Cowburn, R. F., Iqbal, K., et al. (2002). Up-regulation of mitogen-activated protein kinases ERK1/2 and MEK1/2 is associated with the progression of neurofibrillary degeneration in Alzheimer's disease. *Brain Res Mol Brain Res, 109*(1-2), 45-55.

Perry, G., Roder, H., Nunomura, A., Takeda, A., Friedlich, A. L., Zhu, X., et al. (1999). Activation of neuronal extracellular receptor kinase (ERK) in Alzheimer disease links oxidative stress to abnormal phosphorylation. *Neuroreport, 10*(11), 2411-2415.

Pogocki, D. (2003). Alzheimer's beta-amyloid peptide as a source of neurotoxic free radicals: the role of structural effects. *Acta Neurobiol Exp (Wars), 63*(2), 131-145.

Polymeropoulos, M. H., Lavedan, C., Leroy, E., Ide, S. E., Dehejia, A., Dutra, A., et al. (1997). Mutation in the alpha-synuclein gene identified in families with Parkinson's disease. *Science, 276*(5321), 2045-2047.

Poon, H. F., Frasier, M., Shreve, N., Calabrese, V., Wolozin, B., & Butterfield, D. A. (2005). Mitochondrial associated metabolic proteins are selectively oxidized in A30P alpha-synuclein transgenic mice--a model of familial Parkinson's disease. *Neurobiol Dis, 18*(3), 492-498.

Rachidi, W., Vilette, D., Guiraud, P., Arlotto, M., Riondel, J., Laude, H., et al. (2003). Expression of prion protein increases cellular copper binding and antioxidant enzyme activities but not copper delivery. *J Biol Chem, 278*(11), 9064-9072.

Redecke, L., von Bergen, M., Clos, J., Konarev, P. V., Svergun, D. I., Fittschen, U. E., et al. (2007). Structural characterization of beta-sheeted oligomers formed on the pathway of oxidative prion protein aggregation in vitro. *J Struct Biol, 157*(2), 308-320.

Reis, K., Zharkovsky, A., Bogdanovic, N., Karelson, E., & Land, T. (2007). Critical role of methionine-722 in the stimulation of human brain G-proteins and neurotoxicity induced by London familial Alzheimer's disease (FAD) mutated V717G-APP(714-723). *Neuroscience, 144*(2), 571-578.

Requena, J. R., Dimitrova, M. N., Legname, G., Teijeira, S., Prusiner, S. B., & Levine, R. L. (2004). Oxidation of methionine residues in the prion protein by hydrogen peroxide. *Arch Biochem Biophys, 432*(2), 188-195.

Ribak, C. E., Vaughn, J. E., & Saito, K. (1978). Immunocytochemical localization of glutamic acid decarboxylase in neuronal somata following colchicine inhibition of axonal transport. *Brain Res, 140*(2), 315-332.

Sawada, H., Kohno, R., Kihara, T., Izumi, Y., Sakka, N., Ibi, M., et al. (2004). Proteasome mediates dopaminergic neuronal degeneration, and its inhibition causes alpha-synuclein inclusions. *J Biol Chem, 279*(11), 10710-10719.

Schoneich, C. (2005). Methionine oxidation by reactive oxygen species: reaction mechanisms and relevance to Alzheimer's disease. *Biochim Biophys Acta, 1703*(2), 111-119.

Schwartzkroin, P. A., & Mathers, L. H. (1978). Physiological and morphological identification of a nonpyramidal hippocampal cell type. *Brain Res, 157*(1), 1-10.

Sharma, N., Brandis, K. A., Herrera, S. K., Johnson, B. E., Vaidya, T., Shrestha, R., et al. (2006). alpha-Synuclein budding yeast model: toxicity enhanced by impaired proteasome and oxidative stress. *J Mol Neurosci, 28*(2), 161-178.

Singleton, A. B., Farrer, M., Johnson, J., Singleton, A., Hague, S., Kachergus, J., et al. (2003). alpha-Synuclein locus triplication causes Parkinson's disease. *Science, 302*(5646), 841.

Smith, W. W., Margolis, R. L., Li, X., Troncoso, J. C., Lee, M. K., Dawson, V. L., et al. (2005). Alpha-synuclein phosphorylation enhances eosinophilic cytoplasmic inclusion formation in SH-SY5Y cells. *J Neurosci, 25*(23), 5544-5552.

Snyder, H., Mensah, K., Hsu, C., Hashimoto, M., Surgucheva, I. G., Festoff, B., et al. (2005). beta-Synuclein reduces proteasomal inhibition by alpha-synuclein but not gamma-synuclein. *J Biol Chem, 280*(9), 7562-7569.

Stadtman, E. R., & Berlett, B. S. (1998). Reactive oxygen-mediated protein oxidation in aging and disease. *Drug Metab Rev, 30*(2), 225-243.

Stadtman, E. R., Moskovitz, J., & Levine, R. L. (2003). Oxidation of methionine residues of proteins: biological consequences. *Antioxid Redox Signal, 5*(5), 577-582.

Stahl, N., Baldwin, M. A., Teplow, D. B., Hood, L., Gibson, B. W., Burlingame, A. L., et al. (1993). Structural studies of the scrapie prion protein using mass spectrometry and amino acid sequencing. *Biochemistry, 32*(8), 1991-2002.

Starke-Reed, P. E., & Oliver, C. N. (1989). Protein oxidation and proteolysis during aging and oxidative stress. *Arch Biochem Biophys, 275*(2), 559-567.

Stoppini, L., Buchs, P. A., & Muller, D. (1991). A simple method for organotypic cultures of nervous tissue. *J Neurosci Methods, 37*(2), 173-182.

Su, Y., & Ni, B. (1998). Selective deposition of amyloid-beta protein in the entorhinal-dentate projection of a transgenic mouse model of Alzheimer's disease. *J Neurosci Res, 53*(2), 177-186.

Takeda, A., Mallory, M., Sundsmo, M., Honer, W., Hansen, L., & Masliah, E. (1998). Abnormal accumulation of NACP/alpha-synuclein in neurodegenerative disorders. *Am J Pathol, 152*(2), 367-372.

Trojanowski, J. Q., Mawal-Dewan, M., Schmidt, M. L., Martin, J., & Lee, V. M. (1993). Localization of the mitogen activated protein kinase ERK2 in Alzheimer's disease neurofibrillary tangles and senile plaque neurites. *Brain Res, 618*(2), 333-337.

Uversky, V. N., Gillespie, J. R., & Fink, A. L. (2000). Why are "natively unfolded" proteins unstructured under physiologic conditions? *Proteins, 41*(3), 415-427.

Uversky, V. N., Yamin, G., Souillac, P. O., Goers, J., Glaser, C. B., & Fink, A. L. (2002). Methionine oxidation inhibits fibrillation of human alpha-synuclein in vitro. *FEBS Lett, 517*(1-3), 239-244.

Vekrellis, K., Rideout, H. J., & Stefanis, L. (2004). Neurobiology of alpha-synuclein. *Mol Neurobiol, 30*(1), 1-21.

Williams, W. M., Stadtman, E. R., & Moskovitz, J. (2004). Ageing and exposure to oxidative stress in vivo differentially affect cellular levels of PrP in mouse cerebral microvessels and brain parenchyma. *Neuropathol Appl Neurobiol, 30*(2), 161-168.

Willingham, S., Outeiro, T. F., DeVit, M. J., Lindquist, S. L., & Muchowski, P. J. (2003). Yeast genes that enhance the toxicity of a mutant huntingtin fragment or alpha-synuclein. *Science, 302*(5651), 1769-1772.

Wong, B. S., Chen, S. G., Colucci, M., Xie, Z., Pan, T., Liu, T., et al. (2001). Aberrant metal binding by prion protein in human prion disease. *J Neurochem, 78*(6), 1400-1408.

Wong, B. S., Wang, H., Brown, D. R., & Jones, I. M. (1999). Selective oxidation of methionine residues in prion proteins. *Biochem Biophys Res Commun, 259*(2), 352-355.

Wood-Kaczmar, A., Gandhi, S., & Wood, N. W. (2006). Understanding the molecular causes of Parkinson's disease. *Trends Mol Med, 12*(11), 521-528.

Yamin, G., Glaser, C. B., Uversky, V. N., & Fink, A. L. (2003). Certain metals trigger fibrillation of methionine-oxidized alpha-synuclein. *J Biol Chem, 278*(30), 27630-27635.

III. MsrA Ablation Disrupts Locomotor-Associated DA Signaling

Shortly after the *MsrA*$^{-/-}$ mice were generated, it was observed that they displayed an abnormal walking pattern (Moskovitz et al., 2001). This was the first indication that mice lacking Msr would develop movement problems with age. It has since been determined that these locomotor abnormalities are related to changes in dopamine (DA) signaling. Furthermore, we suggest oxidation of the dopamine D2 receptor (D2DR) plays a central role in observed locomotor activities. The *MsrA*$^{-/-}$ mouse has reduced antioxidant capabilities and manifests abnormalities with age. Oxidative stress and aging are well known risk factors in some movement disorders such as Parkinson's disease. Parkinson's disease is also associated with abnormal DA signaling in addition to pathologies from Msr substrates, such as alpha-synuclein. A firm relationship between methionine redox cycles and any movement disorder has yet to have been established. However, the following research presented in this section postulates a theory of possible aging-associated movement abnormalities. The following article reviews the effects of MsrA ablation in mice and highlights genomic changes relevant to oxidative stress, neurodegeneration, and signal transduction.

A. Genomic and Proteomic Analyses of the MsrA Knockout Mouse

(D. Oien, Wang, & Moskovitz, 2008)

In this review we describe the effects of MsrA ablation in mouse tissues on the expression of various mRNAs and proteins, with an emphasis on brain tissues. Initially, the expression / activity levels of preselected proteins relevant to the Msr system in various tissues are discussed (the list of proteins contains: thioredoxin, thioredoxin reductase, MsrB, glucose-6-phosphate dehydrogenase, gluthathione peroxidase, selenoprotein P, and cysteine dioxygenase). Additionally, the consequences from lack of MsrA on protein oxidation (carbonylation and Met oxidation) are evaluated. Finally, newly generated unpublished data is presented on genomic and proteomic analyses, compared between *MsrA*$^{-/-}$ and WT control

brains. The gathered information is sorted out into three major protein groups that are linked to: 1) oxidative stress / apoptosis / degradation; 2) neuroregulation; and 3) signal transduction / transcription / elongation factors. In summary, the importance and relevance of MsrA in protecting against the development and progression of neurodegenerative diseases is reviewed.

1. Effects of MsrA ablation on the Expression Level of Proteins Related to the Msr System and Sulfur/Selenium Metabolism

Selenium and MsrA are positive protein expression regulators of the selenoprotein form of MsrB and Trr (Moskovitz et al., 2001; Moskovitz & Stadtman, 2003). In addition, following the selenium deficient (SD) diet the following enzymes declined especially in the *MsrA*$^{-/-}$ mouse: MsrB activity in cerebellum; thioredoxin reductase (Trr) activity mainly in liver, and kidneys; gluthathione peroxidase (GPx) in brains and livers. Consequently, higher protein-carbonyl adducts and protein-MetO were observed especially in *MsrA*$^{-/-}$ following the SD diet (Moskovitz, 2007). Elevated levels of these posttranslational protein modifications suggest an enhanced oxidative stress in *MsrA*$^{-/-}$ mouse fed with SD diet. Among all tested tissues only brain-cerebellum showed a major combined decrease in specific activities of MsrB, Trr, and GPx (Moskovitz, 2007). This observation may reflect a possible cerebellum malfunction associated with enhanced oxidative stress. It has been already noted that *MsrA*$^{-/-}$ mice exhibited an atypical “tip-toe” walking pattern that is exacerbated as a consequence of SD diet (Moskovitz et al., 2001; Moskovitz & Stadtman, 2003). Since the cerebellum is also responsible for certain motor functions, it is possible that this form of ataxia is at least partially due to the significant loss of the above antioxidant activities.

From these recent studies, it was concluded that enhanced protein oxidation occurs in the *MsrA*$^{-/-}$ mouse tissues following prolonged SD diet. Hearts and lungs of *MsrA*$^{-/-}$ mice that were subjected to the SD diet had significantly elevated expression and activity of glucose-6-phosphate dehydrogenase (G6PD), relative to control WT mice (Moskovitz, 2007). Both lungs

and heart are the first organs that are exposed to high level of oxygen. Thus, it is possible that elevated G6PD in these *MsrA*$^{-/-}$ tissues is an attempt to maintain sufficient reduction power (NADPH) to protect the *MsrA*$^{-/-}$ cells from extensive protein oxidation under selenium deficiency. One selenoprotein that is considered to be a good marker for selenium deficiency is the secreted protein selenoprotein P (SelP) (Burk & Hill, 2005). Surprisingly, the cellular levels of SelP were significantly higher in the *MsrA*$^{-/-}$ mice compared to control (Moskovitz, 2007). Normally, the SelP protein is secreted from cells to the plasma and one of its possible roles is to deliver selenium to tissues via its rich selenocysteine residue content (Burk & Hill, 2005; Schomburg et al., 2003). Another possible function of SelP is to act as an antioxidant by its potential reducing activity. Thus, it is suggested that, like G6PD, SelP may be part of a compensatory mechanism aiming at reducing the oxidative stress effects occurring when both MsrA and selenium levels are limited.

The enzyme cysteine deoxygenase (dioxygenase) (CDO) catalyzes the oxidation of Cys to Cys-sulfinic acid in the presence of Fe^{2+} that functions as a cofactor in mammals and yeast. The activity of CDO plays an important role in Cys catabolism, taurine synthesis, and accumulation of pyruvate and sulfate (Chai et al., 2005; Simmons, Hirschberger, Machi, & Stipanuk, 2006; Stipanuk, Dominy, Lee, & Coloso, 2006). The special significance of taurine synthesis, mediated by CDO, is mainly due to its involvement in bile salt synthesis, cardiac function, and protection of neuronal cells from ischemia–induced damage (Huxtable, 2000; Saransaari & Oja, 1996; Satoh, 1996). The cellular levels of the sulfur amino-acids Cys and Met regulate the expression level of CDO (Stipanuk et al., 2006). Thus, in the absence of MsrA, enhanced oxidation of Cys and Met will cause changes in Cys metabolism and CDO expression (especially when both MsrA and CDO are highly expressed in liver). Indeed, under selenium adequate (SA) diet the level of free thiol in the *MsrA*$^{-/-}$ was reduced to be a third of the level in WT mice, respectively (D. B. Oien & Moskovitz, 2007). Additionally, following SD diet, the absolute free thiol levels were reduced to about third of the corresponding levels following SA

diet. With respect to protein-thiol levels, no significant difference was observed between the WT and *MsrA*$^{-/-}$ mice under SA diet. However, following SD diet the level of protein-thiol decreased by 18% and 50% in WT and *MsrA*$^{-/-}$ mice, respectively. One possible explanation is that enhanced oxidation of free and protein-bound thiols in *MsrA*$^{-/-}$ mice seems like a reasonable occurrence, which is exacerbated under SD diet. The effect of thiol oxidation is more pronounced in the free thiols moiety because protein-bound thiols may not be as accessible to oxidation as free thiols (which are mostly present as L-Cys). Lower L-Cys can lead to decline in CDO expression via elevated ubiquitin-mediated degradation (Dominy, Hirschberger, Coloso, & Stipanuk, 2006). Similarly, the relative lower levels of free thiols in *MsrA*$^{-/-}$ mice following either SA or SD diet lead to a corresponding decline in CDO level, respectively (D. B. Oien & Moskovitz, 2007). A compromised Msr system (i.e. lack of MsrA) leads to enhanced oxidation of sulfur amino acids. Thus, there is an apparent need to lower the enzymatic oxidation of Cys by reduction of CDO expression. The indirect regulation of CDO by MsrA (D. B. Oien & Moskovitz, 2007) is predicted to involve other proteins that participate in maintaining adequate cellular redox balance. Identifying genes that are involved in the regulation of CDO in the *MsrA*$^{-/-}$ mice will provide more information about sulfur amino acids driven signal transduction events activated to protect cells from oxidative modifications to proteins.

2. Protein Substrates of the Msr System

Substrates or proteins that interact for the Msr system include MetO residues or methyl sulfoxide adducts, and their suitability as substrates for the Msr system was mainly described *in vitro* (D. B. Oien & Moskovitz, 2008). Only a limited number of proteins that interact with Msr enzymes or serve as substrates for the Msr system *in vivo* were identified. For example, in the gastric pathogen *Helicobacter pylori*, the following proteins: GroEL (chaperon), catalase (detoxification), SSR (DNA repair), thioredoxin-1 (Trx1, electron transport and a known reducer of Msr), seryl t-RNA synthase (protein synthesis), TolB precursor protein (colicine tolerance)

have shown to interact with Msr (a fused form of MsrA and MsrB) in a semi-*in vivo* system (Alamuri & Maier, 2006). Additionally, gluthathione perxoidase (Gpx3) showed to regulate the function of the yeast MsrA by interacting with MsrA through the formation of an intermolecular disulfide bond. Thus, upon an oxidative stress insult, the latter interaction is compromised and the free MsrA can reduce Met-oxidized proteins (Kho et al., 2006). Taken together, it is apparent that further identification of *in vivo* substrates for Msrs is required to determine the involvement of the Msr system in protein regulation and protection against oxidative modification to proteins. One possible approach to identify such proteins is by screening for potential proteins that have enhanced Met oxidation in the absence of Msr. The prediction is that proteins that their levels are elevated in a Msr knockout animal (compared to a WT control) may represent proteins that were extensively oxidized and inactivated, causing an increased synthesis of them as part of a compensatory response mechanism (demonstrated by increased mRNA synthesis). Complementary, a reduction in the levels of specific proteins in Msr knockout background (compared to control) may represent an enhanced degradation of proteins harboring elevated levels of MetO (demonstrated mainly by a reduced protein level while mRNA level remains unchanged). The mammalian model that we are currently investigating is the *MsrA*$^{-/-}$ mouse (Moskovitz et al., 2001). We have performed genomics and proteomics analyses on *MsrA*$^{-/-}$ and control WT brains.

3. Proteomics Analysis of *MsrA*$^{-/-}$ and WT Control Brains

Protein extracts from both mouse strains were loaded on 1-D gel followed by 2-D gel electrophoreses. The procedures for the gel electrophoresis assays were conducted according to previously published methods (Lopez et al., 2004). All reagents and precast gels were from Genomic Solutions (Ann Arbor, MI, USA), except IPG strips which were from Amersham (Piscataway, NJ, USA). Briefly, 18 cm pH 3–10 nonlinear IPG strips were rehydrated in sample diluted into a final volume of 400 mL thiourea sample buffer. The strips were focused for a total

of 100,000 Vh (maximum voltage, 5000 V; maximum current, 70 mA). The 2-D gels were stained with SYPRO Ruby Protein Gel Stain (PerkinElmer or Molecular Probes, Eugene, OR) or colloidal Coomassie Blue (Sigma Chemical). Gel images were acquired using a PerkinElmer Life Sciences ProXPRESS Proteomic Imaging System using optimized excitation (480/80) and emission (650/150) filters for SYPRO Ruby Protein Gel Stain, or white light converter for Coomassie Blue-stained gels. Images were acquired at 100 mm resolution.

Gel images were analyzed in Progenesis Discovery (Nonlinear Dynamics, Newcastle upon Tyne, UK). Spot presence in each sample was normalized between the two compared samples. Candidate differentially expressed protein spots identified by this process were validated by relocation on the original images in Progenesis. Only validated protein spots were excised for further analysis by mass spectrometry. We pre-selected protein spots that showed at least a 2x difference in their expression levels between the compared samples. Automated in-gel digestions, peptide extractions, desalting and concentration and spotting onto MALDI targets were carried out on a MultiProbe II Proteomic liquid handling workstation (PerkinElmer) using Montage Trypsin digestion kits and Zip Plate (Millipore, Bedford, MA, USA). Spectra were automatically acquired and analyzed on a prOTOF 2000 MALDI Mass Spectrometer (PerkinElmer). We have identified 21 proteins that their levels were altered in the *MsrA*$^{-/-}$ relative to WT brain, in which the expression of 19 were elevated and 2 were downregulated, respectively (Table 1). The presented list of proteins contains only abundant and identifiable proteins and it is not complete. Nevertheless, it provides initial information about physiological changes that may occur in the *MsrA*$^{-/-}$ brain. The fact that there are more degradation products and pI changes of various proteins in *MsrA*$^{-/-}$ brain, suggests that there is an enhanced protein posttranslational modification and degradation rate in *MsrA*$^{-/-}$ brain (Table 1).

The expression levels of certain proteins from the list are suggested to be part of response mechanisms to oxidative stress or neurodegenerative diseases: P63 is death inducing protein (Jacobs et al., 2005); alcohol toxicity induces dynamin expression (dynamin is a GTPase

protein and is important in endocytosis) (Saito, Smiley, Toth, & Vadasz, 2002), and metavanadate (causes oxidative stress) induces the expression of proliferin (an important protein in angiogenesis) (Parfett & Pilon, 1995). Transketolase (TK)-atrophy of murine thymus causes abnormality of transketolase (B12 dependent) in the brains of alcoholics. Also, lower activity of transketolase was shown in Alzheimer's disease as well (Gibson et al., 1988). Likewise, BB-creatine kinase (BBCK) is important for energy utilization and alteration of cytockeleton's proteins and its activity was shown to decrease in Alzheimer's disease, while having higher carbonyl content (Aksenov, Aksenova, Butterfield, & Markesbery, 2000). Higher cellular protein-carbonylation level under oxidative stress or Alzheimer's disease was also considered to be a factor involved in attenuating glyceraldehyde-3-phophate dehydrogenase (GAPDH) activity/expression (Opii et al., 2008). Dihydropyrimidinase-like 2 (DRP2) (Collapsin response mediator protein-2) hydrolyses adenine to form hypoxanthine and ammonia. The enzyme is part of metal dependent deaminases reaction. It is important for adenine utilization as a purine and also as nitrogen source. It was shown that the expression levels of DRP2 and dynamin-1 (DNM1, its role in maintaining neuronal function is yet to be understood) were among proteins in which their expression levels were significantly increased in brains of old versus young mice (Poon, Vaishnav, Getchell, Getchell, & Butterfield, 2006). Taken together, it is possible that the observed elevated level of TK, BBCK, DRP2, DNM1 and GAPDH in *MsrA*$^{-/-}$ brain is part of a general compensatory mechanism for lower enzyme activity due to enhanced oxidative damage (e.g. increased protein-carbonyl /MetO moiety). The Kallikrein–Kinin system influences the permeability of the blood-brain barrier and is activated in stroke. Plasma concentrations of tissue kallikrein–Kinin are then elevated. Accordingly, it is possible that increased level of tissue kallikrein in *MsrA*$^{-/-}$ brain is due to increased strokes or stroke–related events. Likewise, elevation of *MsrA*$^{-/-}$ brain CDC16 may be a response to elevated stress promoting neurodegeneration, as lack of it causes defects in the proliferation of brain neuroblasts and results in the absence of identified neuronal lineages in central and peripheral

nervous systems. Only two proteins were identified as downregulated proteins in the *MsrA*$^{-/-}$ brain: Heat shock protein 70 (HSP70) and serine protease inhibitor (SPI). Attenuation of HSP70 is associated with stress conditions and apoptosis whereas changes in the levels of SPI can be monitored in various biological systems. It is possible that the reduced level of brain-SPI contributes to the enhanced accumulation of degraded proteins observed in the 2D-protein analysis of *MsrA*$^{-/-}$ brain.

Table 1. **Proteomics analysis of *MsrA*$^{-/-}$ versus WT brain.** Only top-scored proteins were selected and each protein-identification was based on at least 5-6 peptides. We used Mascot Software as a search engine and NCBI as the database source.

Upregulated Proteins *MsrA*$^{-/-}$ vs. wild-Type Brain (x Fold)	**Accession #**	**pI and/or Molecular Weight (M.W), if Different than Normal Value (X)**
TA*p63 alpha (2.83)	AF075436	
Dynamin (2.02)	L31395	
Transketolase (2.17)	AF195533	
Dihydropyrimidinase-like 2; Collapsin response mediator protein 2 (3.04)	NP_034085.1	
Novel protein (ortholog of human C22orf1) (2.76)	AL513354	
Tubulin beta 4 (2.40)	NP_033477.1	
Tubulin beta 3 (2.81)	NP_075768.1	
Tubulin beta 5 (2.14)	NP_035785.1	
Creatine kinase, (3.56)	NP_067248.1	
Gamma actin (3.21)	X13055	
Aldolase 1, A form (2.02)	NP_031464.1	
Degradation product of Dihydropyrimidinase (3.00)	NP_034085.1	M.W.: ~30kDa (63kDa); pI: 8.8 (6.0)
Tissue Kallikrein (2.50)	NP_034245.1	
Topoisomerase (DNA) III (2.12)	NP_035754.1	
Glyceraldehyde-3-phosphate dehydrogenase (2.09)	NP_032110.1	
Degradation product of Exonuclease 1 (6.72)	NP_036142.1	M.W.: ~30kDa (94kDa)
Degradation product of Topoisomerase (DNA) III (6.95)	NP_035754.1	M.W: 30kDa (99kDa)
Proliferin-related protein (5.80)	A22722	pI: 9.5 (4.9)
Putative; cell division cycle16 homolog (yeast) (5.34)	AK013213	pI: 8.7 (4.9)
Downregulated proteins *MsrA*$^{-/-}$ vs. wild-type brain (xFold)		
Heat shock 70kDa protein 8 (0.2)	AK004608 or NP_112442.1	
Serine protease inhibitor (0.1)	NP_033278.2	

4. Genomics Analysis of *MsrA*$^{-/-}$ and WT Control Brains

To further evaluate protein expression levels in *MsrA*$^{-/-}$ in comparison to WT brain, genomic analyses were performed on 3 mouse brains from each strain. The mRNA was isolated from the 6-month-old animals and probed for analyses (using Affymetrix Mouse Genome 430 2.0 Array, Affymetrix GeneChip System). One of the advantages of using the genomic approach is that it facilitates the detection of mRNA levels of low abundant proteins. From a list of 300 genes that showed significant expression level changes between the two strains (with statistical significance of $P < 0.05$), genes were selected and sorted into three groups with relevancy to either neurodegeneration (group A), oxidative-stress / apoptosis / degradation (group B), or signal transduction & transcription / elongation factors (group C) (groups A-C correspond to Table 2A-C, respectively). Comparison of the mRNA levels of the genes in the *MsrA*$^{-/-}$ relative to WT brain revealed that: in group A, 6 genes were up regulated and 10 genes were downregulated; in group B, 15 genes were up regulated and 9 genes were downregulated; and in group C, 12 genes were up regulated and 31 genes were downregulated (Table 2A-C, respectively). Amyotrophic lateral sclerosis (ALS) is a progressive neurodegenerative disease that manifests as selective upper and lower motor neuron degeneration. From the upregulated genes in *MsrA*$^{-/-}$ brain listed in Table 2A, it is worth noting the genes *MPP4* and *Als2cr3* (which are two potential gene-homologues) are suggested to be involved in the disease ALS type 2. Homer proteins regulate signal transduction, synaptogenesis and receptor trafficking, in addition to maintaining and regulating extracellular glutamate levels in limbo-corticostriatal brain regions. Homer isoforms are involved in behavioral pathologies associated with neuropsychiatric disorders (Szumlinski, Kalivas, & Worley, 2006). The upregulation of Homer homolog 2 in *MsrA*$^{-/-}$ brain listed in Table 2A, may indicate abnormal responses that could be linked to abnormal behavior of the *MsrA*$^{-/-}$ mouse manifested by its altered walking pattern (Moskovitz et al., 2001).

In relation to behavioral traits, the upregulation of the tyrosine hydroxylase activating protein gene (Ywhaz) may suggest an increase in dopamine synthesis that may also affect motor

behavior. From the list of downregulated genes in Table 2A, glutamate receptor, ionotropic, kainate 1 (*Grik 1*) was the most affected gene; while lower expression of GABA receptor gene (*Gabra6*) was also observed. It is possible that the expression changes in these receptors, which are involved in neurotransmitter regulation, may contribute to the abnormal locomotor activity observed in the *MsrA*$^{-/-}$ mouse (unpublished results).

With respect to oxidative stress, it is suggested that the genes participating in cellular redox regulation (dehydrogenase/reductase (SDR family) member 8, carbonic anhydrase 8, peroxiredoxin, superoxide dismutase 3, and Succinate dehydrogenase complex, subunit A) are upregulated in the *MsrA*$^{-/-}$ mouse as a response to enhanced oxidative stress (Table 2B). It is hypothesized that this response is an attempt of the *MsrA*$^{-/-}$ brain cells to reduce the level of the oxidative modification to proteins, which may be increased in the absence of MsrA. In contrast, the levels of the Heat shock protein 1A and Ataxia telangiectasia mutated homolog (ATM) are reduced in the *MsrA*$^{-/-}$ brain, thus reducing the cellular protection against ROS mediated damage (Table 2B). Caspase 12 and Tial 1, and SPI are considered to be inducing factors for apoptotic events. SPI was also shown to be downregulated *MsrA*$^{-/-}$ brain on the protein level (Table 1) and thus confirms the respective genomic data. The downregulation of these genes in the *MsrA*$^{-/-}$ brain in conjunction with the elevated expression of antioxidant proteins may reflect an attempt to prolong neuronal survival under increased oxidative conditions. The altered gene expression in the *MsrA*$^{-/-}$ brain in Table 2C may be mediated by oxidation of specific proteins that play an important role in signaling processes and synthesis of key proteins in various pathways. It is still not yet known how multiple processes are either simultaneously affected by Met oxidation or the mechanisms controlling the net expressed cellular effect in a specific pathway.

Table 2A. Genomic analysis of genes involved in *MsrA*$^{-/-}$ versus WT brain.

Oxidative-Stress/ Apoptosis/ Degradation Gene Name	Fold Change	*P* Value	Description
Prdx2	13.39	0.00222	Peroxiredoxin
1200011D03Rik	8.844	0.0492	Aldehyde oxidase 3
Dhrs8	6.332	0.00147	Dehydrogenase/reductase (SDR family) member 8
Mpp4	4.436	0.0103	ALS2 homolog
Car8	3.643	0.000459	Carbonic anhydrase 8
Alox15b	2.805	0.0175	Arachidonate 15-lipoxygenase, 2nd type
A930001K02Rik	2.464	0.0109	N-myristoyltransferase 2
1500032O14Rik	2.175	0.0169	Succinate dehydrogenase complex, subunit A, flavoprotein (Fp)
Stk3	2.116	0.0184	Serine/threonine kinase 3 (Ste20, yeast homolog) (MST)
SOD3	2.065	0.00147	Superoxide dismutase 3, extracellular
Xdh	1.6	0.01	Xanthine dehydrogenase
Bcl2l2	1.5	0.0054	Bcl2-like 2
Txnip	1.5	0.0137	Thioredoxin interacting protein
Pipox	1.5	0.0387	Pipecolic acid oxidase
Nos1	1.5	0.0137	Nitric oxide synthase 1, neuronal
Diablo	0.666	0.0122	Diablo homolog
C630049M13	0.473	0.0317	Prenylcysteine oxidase 1 like
B230207H15Rik	0.467	0.000339	Malic enzyme 3, NADP(+)-dependent, mitochondrial
Wwox	0.416	0.0000947	WW domain-containing oxidoreductase
Casp12	0.387	0.0311	Caspase 12
Atm	0.351	0.000589	Ataxia telangiectasia mutated homolog (human)
Hspa1b	0.286	0.0000594	Heat shock protein 1A
Serpina3n	0.0909	0.000543	Serine (or cysteine) proteinase inhibitor
Tial1	0.0367	0.00491	Tial1 cytotoxic granule-associated RNA binding protein-like 1

Table 2B. Genomic analysis of genes involved in oxidative stress in *MsrA*$^{-/-}$ versus WT brain.

Neuroregulation Gene name	Fold Change	*P* value	Description
Mpp4	4.436	0.0103	ALS2 homolog
9130022E09Rik	4.098	0.000204	BB357317, cortactin binding protein 2 ;cerebellum
Ywhaz	4.03	0.000908	Tyrosine/trptophan hydroxylase activating protein
Homer2	2.881	0.00521	Homer homolog 2
Als2cr3	2.691	0.00493	ALS2 homolog
Kcnj9	1.5	0.0387	Potassium channel
Gabra6	0.625	0.0667	GABA receptor
Fkrp	0.495	0.00746	Fukutin related protein
1500001L15Rik	0.477	0.00036	EIF4E binding protein
Npb	0.455	0.0309	Neuropeptide B
Dao1	0.421	0.00224	D-amino oxidase
Wwox	0.416	0.0000947	WW domain-containing oxidoreductase
9630011N22Rik	0.408	0.00739	Phosphodiesterase 4D, cAMP specific
Sox8	0.402	0.00841	SRY-box containing gene 8
Sv2	0.346	0.0282	Synaptic vesicle glycoprotein 2c
Grik1	0.112	0.0456	Glutamate receptor, ionotropic, kainate 1

Table 2C. Genomic analysis of genes involved in signal transduction and transcription in *MsrA*$^{-/-}$ versus WT brain.

Signal Transduction & Transcription/ Elongation Factors Gene Name	Fold Change	*P* Value	Description
Rbm7	5.015	0.0257	RNA binding motif protein 7
Ywhaz	4.03	0.000908	Tyrosine/trptophan hydroxylase activating protein
Efhd2	3.848	0.00272	EF hand domain containing 2
Zfp617	3.757	0.003	zinc finger protein s11-6
5830437M04Rik	3.691	0.00464	Jakmip1, gamma-aminobutyric acid (GABA-B) receptor binding protein
Limd1	2.607	0.00117	LIM domains containing 1
Garnl1	2.122	0.0268	GTPase activating RANGAP domain-like 1

Table 2C (continued).

Signal Transduction & Transcription/ Elongation Factors Gene Name	Fold Change	*P* Value	Description
Camk2d	2.117	0.0144	Calcium/calmodulin-dependent protein kinase II, delta
Stk3	2.116	0.0184	Serine/threonine kinase 3 (Ste20, yeast homolog) (MST)
Gak	1.6	0.012	cyclin G associated kinase
Eif2s2	1.5	0.00574	Eukaryotic translation initiation factor 2, subunit 2 (beta)
Bclaf1	1.5	0.0226	BCL2-associated transcription factor 1
Klf4	0.667	0.0102	Kruppel-like factor 4
Zfp236	0.667	0.0226	Zinc finger protein 236
Idb1	0.667	0.0122	Inhibitor of DNA binding 1
Sbk	0.667	0.0387	SH3-binding kinase
Dusp1	0.667	0.0226	Dual specificity phosphatase 1
Zfr	0.667	0.00574	Zinc finger RNA binding protein
A530094I17Rik	0. 588	0.00574	Zinc finger protein 72
Zfp248	0.499	0.000463	Zinc finger protein 248
LOC224598	0.497	0.00055	Similar to zinc finger protein 40
Nrk	0.438	0.0469	Serine/Threonine protein kinases
Zfp53	0.495	0.0169	Zinc finger protein 118
Eprs	0.482	0.00007	Glutamyl-prolyl-tRNA synthetase
Sdf2l1	0.470	0.00518	Stromal cell-derived factor 2-like 1
Hmg20a	0.469	0.00494	High mobility group 20A
Arid4a	0.467	0.00228	AT rich interactive domain 4A (Rbp1 like)
1200013I08Rik	0.465	0.000364	Ring finger protein (C3H2C3 type) 6
Sbk	0.462	0.00184	SH3-binding kinase
Tll	0.449	0.0284	Tolloid-like
1700073K01Rik	0.435	0.0365	EF-hand calcium binding domain 2
Mint	0.428	0.0000723	Msx2 interacting nuclear target protein
Cpg21 like	0.404	0/00527	Similar to Map-kinase phosphates (cpg21)
Sox8	0.402	0.00841	SRY-box containing gene 8
Riok2	0.379	0.000513	Rio kinase 2 (yeast)
Hnrpl	0.363	0.00236	Hnrpl
Khsrp	0.351	0.0128	KH-typesplicing regulatory protein
6330416L07Rik	0.3	0.00507	Similar to zinc finger protein 91
Zfp52	0.274	0.00189	Zinc finger protein 52
Depdc6	0.248	0.00235	DEP domain containing 6
Paip1	0.14	0.0207	Polyadenylate binding protein-interacting protein 1
Pim1	0.0368	0.00955	Proviral integration site 1
Tial1	0.0367	0.00491	Tial1 cytotoxic granule-associated RNA binding protein-like 1

5. Conclusions

In this review we have presented evidence that MsrA is mainly associated with the expression of specific genes/proteins that are involved in pathways that are important for cellular antioxidant and redox status. Significant changes found in expression levels may be relevant to the processes of neurodegeneration, oxidative-stress / apoptosis / degradation, and signal transduction & transcription / elongation factors. Obviously, more detailed research is required to better elucidate the role of Met oxidation to specific proteins *in vivo*. Additionally, a more clear understanding of the regulating function of the Msr system may enable future intervention in controlling its expression and function under stages of cellular stress/disease.

B. The *MsrA* Knockout Mouse Exhibits Abnormal Behavior and Brain DA Levels

(D. B. Oien, Osterhaus et al., 2008)

Recent evidence has found oxidized methionine residues in neurodegenerative conditions. Previously, we have described elevated levels of brain pathologies and an abnormal walking pattern in the *MsrA*$^{-/-}$ mouse. Here we show that *MsrA*$^{-/-}$ mice have compromised complex task learning capabilities relative to WT mice. Likewise, *MsrA*$^{-/-}$ mice exhibit lower locomotor activity and altered gait that exacerbated with age. Furthermore, *MsrA*$^{-/-}$ mice were less responsive to amphetamine treatment. Consequently, brain DA levels were determined. Surprisingly, relative to WT mice, *MsrA*$^{-/-}$ brains contained significantly higher levels of DA up to 12 months of age, while lower level of DA was observed at 16 months of age. Moreover, striatal regions of *MsrA*$^{-/-}$ mice showed an increase of DA release parallel to observed DA levels. Similarly, the expression pattern of tyrosine hydroxylase activating protein correlated with the age-dependent DA levels. Thus, it is suggested that DA regulation and signaling pathway are impaired in *MsrA*$^{-/-}$ mice, which may contribute to their abnormal bio-behavior. These observations may be relevant to age-related neurological diseases associated with oxidative stress.

1. Introduction

Given the hippocampal sensitivity to oxidative stress and markers of Alzheimer's disease in the *MsrA*$^{-/-}$ mouse (Pal, Oien, Ersen, & Moskovitz, 2007a), we analyzed this mouse for a decline of complex task learning capability in the current study. The previously described "tip toe" walking pattern described for *MsrA*$^{-/-}$ mouse prompted us to look into Parkinson's disease-associated bio-behavioral traits in this mouse strain. In Parkinson's disease, neurodegeneration (especially in the dopaminergic neurons of the substantia nigra) and altered DA levels have been linked to abnormal motor behavior, including walking distance and gait. Thus, locomotor activity and gait performance of the *MsrA*$^{-/-}$ mouse, compared to WT mouse, were monitored as function of age. The direct natural cause for these neuronal deaths in Parkinson's disease is yet to be revealed, but toxins can produce Parkinsonism via ROS and have been used to create animal models for Parkinson's disease. For example, both 1-methyl-4-phenyl-1,2,3,6-tetrahydropyridine (MPTP) and 6-hydroxydopamine (6-OHDA, a neurotransmitter analogue toxic to dopaminergic neurons) reduces DA levels in the brain and results in Parkinson's disease-like motor syndromes. While 6-OHDA may cause direct elevation of ROS, MPTP is converted to MPP+, which by its inhibitory action on mitochondrial complex 1 may elevate ROS production. Therefore, behavioral characteristics of MPTP-treated mice served as a guide to demonstrating Parkinson's-related abnormal locomotor behavior in *MsrA*$^{-/-}$ mice. Since DA is an important signaling molecule involved in motor regulation, we also determined the level of brain dopamine (post-mortem assay) and electrically stimulated brain DA secretion and reuptake in striatal neurons (*in vitro,* brain slice preparation). Additionally, the response of the mice to amphetamine was determined because 1) amphetamine blocks the DA transporter (DAT) ability to clear DA from the synaptic space, and 2) amphetamine is transported into the cell which contibutes to the DA efflux (Fleckenstein, Volz, Riddle, Gibb, & Hanson, 2007). Together, the current observations show significant differences between *MsrA*$^{-/-}$ and WT mice with regard to bio-behavioral traits and

brain DA levels, thereby providing a potential linkage between MetO, abnormal behavior, and age-related neurodegenerative diseases.

2. Materials and Methods

Operant learning procedures

Eight *MsrA*$^{-/-}$ mice and 7 WT mice were exposed to operant conditioning procedures in which the mice first acquired the capacity to press a lever to obtain small portions of condensed milk such that each lever press produced a reward (this procedure is termed fixed ratio 1 or FR1). The initial training, managed entirely by a computer program (McKerchar, Zarcone, & Fowler, 2005), occurred when the mice were 1 year old (mean ages of 12.9 months and 12.2 months for *MsrA*$^{-/-}$ and WT mice, respectively; not significantly different). Briefly, the computer-controlled lever-pressing training procedure used mouse operant chambers that were supplied by Med Associates (St. Albans, VT) and programmed to present condensed milk on concurrent FR1 and noncontingent variable time schedules of milk reinforcement in two consecutive-day, 2 h sessions. These two sessions were followed by 4 consecutive-day FR1 training sessions 30 min in duration. The mice were returned to their home cages for a period of about 3.5 months with no training, but with daily restriction of food intake. Then the mice were retested for 7 consecutive daily sessions on FR1. The mice were then exposed to a computer-implemented shaping procedure aimed at gradually introducing increasingly greater task demands until they reached FR20 (i.e., 20 lever presses per reward). The FR-shaping procedure individually monitored each mouse's behavior, and the FR requirement was increased only if the last two interresponse times of the preceding ratio were less than 1 s each. The training procedure was stopped after training session 32 when all WT mice reached the FR20 criterion. The dependent variable for describing the difference in learning was the number of sessions required by each mouse to reach the criterion. Mice not reaching the FR20 criterion were assigned a score of 32 sessions. Our FR shaping procedure was not a type of progressive ratio that is commonly used

in experiments designed to reflect motivation to obtain a reward. In the conventional progressive ratio the trained animal is presented with a series of monotonically increasing ratios such that each completed ratio results in a reinforcer (reward) and the requirement for obtaining the reinforcer is increased in increments, eventually making the ratio of reinforcers to responses smaller and smaller until the animal "gives up"- the break point. Importantly, the criterion for reinforcement grows steadily without taking account how well the animal is progressing. In the procedure we used, the animal was shaped to move on to increasing ratios; if it did not make two responses in moderately quick succession (two responses following one another each in less than 1 s), it could remain indefinitely at whatever ratio it was on and continue to be reinforced. We see our task as measuring the mouse's sensitivity to the reinforcement contingency, which unimpaired animals learn quickly.

Locomotor activity

Locomotor activity and other behavioral attributes were assessed with four concurrently operative force-plate actometers (Fowler et al., 2001b). The actometer and associated peripherals, as well as the methods of data collection and analysis, were used as described previously (Fowler et al., 2001b). In the current studies, mouse locomotor activity was measured for 30 min. Six mice of each genotype (*MsrA*$^{-/-}$ or WT) and age (6- or 12-month-old) were used for the analyses.

Gait dynamics

The DigiGait system (Mouse Specifics, Inc., MA) provides numerous spatial and temporal indices of gait dynamics and posture, including: stride length, stance width, stance duration, swing duration, braking duration, propulsion duration, stride frequency, and paw angle. The mouse observation compartment is constructed of clear polycarbonate of fixed width with adjustable front and rear walls. The DigiGait apparatus performs ventral plane videography of

rodents walking on a motorized transparent treadmill belt. A high-speed digital video camera continuously images the underside of the walking animals. DigiGait software generates “digital paw prints” to measure gait indices, representing the temporal record of paw placement relative to the treadmill belt. The gait signal of each limb comprises the stride duration, which includes the stance duration when the paw of a limb is in contact with the walking surface, plus the swing duration when the paw of the same limb is not in contact with the walking surface. Stance duration is subdivided into braking duration (increasing paw contact area over time) and propulsion duration (decreasing paw contact area over time). More than twenty gait indices are reported by the software, including the sciatic functional index (SFI), stance factor, and the step-sequence pattern. The incline of treadmill belt is fixed at horizontal. Imaging and analysis software automatically quantifies spatial and temporal indices of gait in walking or running animals. Additional details have been published previously (Amende et al., 2005; Hampton, Stasko, Kale, Amende, & Costa, 2004; Wooley et al., 2005). The experimental design was similar to the locomotor activity measurements except that only one measurement session was conducted at each of the two age points. The experiments were conducted on the same mice (n=6 for each mouse genotype and age) a week after the actometer measurements. The belt speed was adjusted to the animals’ ability to walk without moving backwards. Belt speeds were kept constant for each age group.

Behavioral effects of amphetamine administration

In the amphetamine experiment, the doses studied were 5.0, 2.5, and 0.0 mg/kg (in this order, administered i.p. in a volume of 5 mL/kg) with 7 to 10 days separating treatments. Doses specified are in terms of the d-amphetamine sulfate salt (Sigma-Aldrich, St. Louis, MO). Amphetamine was administered 15 min before placement in the actometers. The primary behavioral measurement was distance traveled and secondary measurement was stereotypy.

DA levels in post-mortem brains

Animals were sacrificed and their brains were dissected out and stored at –80℃ until analysis. The DA analysis was performed on whole isolated brain. On the day of the assay, the brain was sonicated in 10 volumes (weight/volume), of 0.1 M perchloric acid containing 50 ng/mL dihydrobenzylamine as internal standard. After centrifugation at 15,000 X *g* for 15 min at 4℃, 20 µL of supernatant was injected onto a C18 reverse-phase HR-80 catecholamine column (ESA Inc., Bedford, MA, USA). The mobile phase consisted of 94% 50 mM sodium phosphate/0.2 mM EDTA/1.2 mM heptanesulfonic acid (pH 3.2) solution and 6% methanol. The flow rate was 1.5 mL/min. Peaks were detected by an ESA 8 Channel CoulArray system. Data was collected and processed using the CoulArray data analysis program.

Release and reuptake of DA in the striatum

Brain slices. Mice were deeply anesthetized by isoflurane inhalation and decapitated. The brains were immediately removed and placed in oxygen-saturated ice cold aCSF. From each brain, the cerebellum was excised and the cerebrum was glued on a Teflon block. Coronal slices of 300 µm thick were made using an NVSL vibratome (World Precision Instruments, Sarasota, FL). Brain slices containing the striatum, obtained at +0.3 to +1.5 mm from bregma, were stored in ice cold aCSF. A single slice was submerged under aCSF maintained at 34ºC and continuously flowing (2 mL/min) through a superfusion chamber (Warner Instruments, Hamden, CT). Each brain slice was equilibrated for 30 minutes prior to obtaining measurements.

Electrochemistry. The procedure was based on method previously described by Bath et al. (Bath et al., 2000). Carbon-fiber cylinder microelectrodes were made as previously described using T650 carbon fibers (Amoco, Greenville, SC) cut to a length of 25 µm. A triangular waveform, starting at -0.4 V, increasing to 1.0 V, and scanning back to -0.4 V (versus Ag/AgCl reference electrode), was applied to the carbon-fiber working electrode at a scan rate of 300 V/s

and an update rate of 10 cyclic voltammograms/s. The carbon-fiber was inserted until the tip reached 100 µm below the surface of the brain slice in the dorsolateral caudate region of the striatum between the prongs of a bipolar stimulating electrode (FHC, Bowdoinham, ME), situated 200 µm apart. To evoke DA release, a single, biphasic stimulating current pulse (2 ms each phase, 350 µA in amplitude), was applied to the stimulating electrode. Successive cyclic voltammograms were collected every 20 s. The current arising from DA oxidation (at about 0.6 V) was measured and plotted versus time. To account for the naturally occurring heterogeneity of DA terminals in the striatum, DA release readings were obtained at four different randomly selected locations in the dorsolateral caudate and the resulting data were averaged and counted as a single reading. Electrodes were calibrated against DA standards of known concentrations in a flow cell before and after each brain slice experiment. The averages of these pre- and post-calibration measurements were used to calibrate the electrode.

Genomic and western blot analyses

Genomic analysis. The mRNAs from three brains of each mouse genotype at 6 months of age were purified using the RNeasy Mini Kit (Qiagen, Valencia, CA). The purified mRNA from each brain was used for genomic screening analyses probing with Affymetrix Mouse Genome 430 2.0 Array (using Affymetrix GeneChip System at the University of Kansas Genomic Facility). Only the tyrosine hydroxylase (*TH*) and TH-activating protein (*Ywhaz*) genes were evaluated for the current study.

Western blot analysis. Protein-expression levels of TH and TH-activating protein (Ywhaz) were detected by extracting protein from a pool of 5 mouse brains. For each sample, 30 micrograms of soluble protein were subjected to gel-electrophoresis, followed by western blot analysis using primary antibodies against Ywhaz (Abcam) and TH (Millipore).

Statistical analysis.

Data presented are the mean ± standard deviation of the mean. Statistical analysis was carried out using paired or unpaired student's t-test to determine if the observed changes between the two mouse strains had a significant effect ($P<0.05$). For locomotor activity, the distance traveled was analyzed with a repeated measures 2-way ANOVA with genotype as the between groups factor and 5-min time block as the repeated measures factor.

3. Results

Behavioral effects of MsrA targeted deletion

Assessment of operant learning. Eight *MsrA*$^{-/-}$ mice and 7 WT mice were exposed to operant conditioning procedures. The mice first acquired the capacity to press a lever to obtain small portions of condensed milk such that each lever press produced a reward (FR1). During initial training, the two types of mice were not significantly different, but numerically the *MsrA*$^{-/-}$ mice lagged behind the WT mice. The mice were returned to their home cages for a period of about four months with no training in this interval. Then the mice were retested for seven consecutive daily sessions on FR1. All mice showed evidence of relearning the task and attained similar lever press rates on the seventh day. The mice were then exposed to a second computer-implemented shaping procedure aimed at gradually introducing increasingly greater task demand until the requirement for reward was FR20 (i.e., 20 lever presses per reward). This increase in demand revealed striking differences between the *MsrA*$^{-/-}$ and WT mice. The WT mice learned the FR20 task significantly faster than the *MsrA*$^{-/-}$ mice (Fig. 1). Over the 32 training sessions, the mean number of training sessions to reach FR20 was 10.9 for the WT mice and 30.6 for the *MsrA*$^{-/-}$ mice, $t_{13}=6.142$, $P<0.001$ (t_{13} refers to a "between-groups" t-test with 13 degrees of freedom). It is important to note that the *MsrA*$^{-/-}$ mice continued to lever press for reward during the FR shaping procedure (i.e., they did not "extinguish"). Therefore, the deficit of the *MsrA*$^{-/-}$ mice was not failure to perform a previously acquired habit, but, instead, was a failure to learn a new habit. These results clearly support the hypothesis that the *MsrA*$^{-/-}$ mice have functional behavioral/cognitive impairments at about 16

months of age compared to WT control mice, which may be related to the enhanced hippocampal neurodegeneration observed in the 12-month-old *MsrA*$^{-/-}$ mice (Pal et al., 2007a).

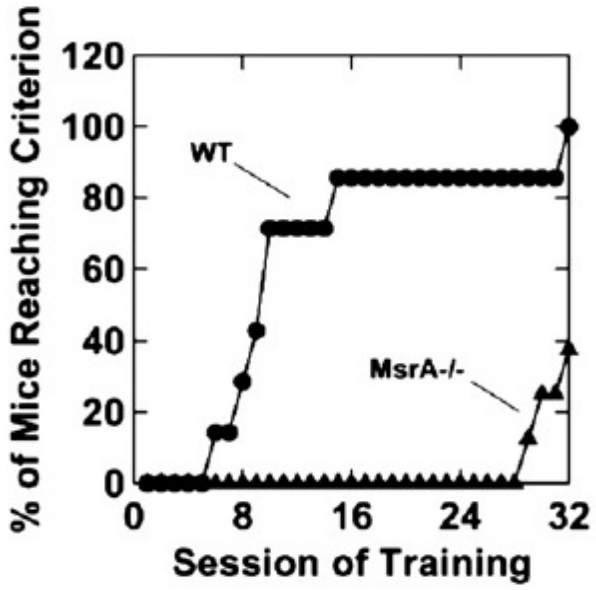

Figure 1. Operant task in both mouse strains. At the age of ~16 months, the control mice quickly learned to transition from FR1 to FR20 schedule of milk reward (WT), but the *MsrA*$^{-/-}$ mice lagged significantly behind the WT mice in learning to perform under these conditions (despite the fact that they were not different when the task demand was FR1). WT, n=7; *MsrA*$^{-/-}$, n=8. Over the 32 training sessions shown, the mean number of training sessions to reach FR20 was 10.9 for the WT mice and 30.6 for the *MsrA*$^{-/-}$ mice, t_{13}=6.142, P<0.001(t_{13} refers to a "between-groups" t-test with 13 degrees of freedom).

Locomotor activity. At 12 months of age, the *MsrA*$^{-/-}$ were less active by up to ~50% relative to control mice (Fig. 2). However, no obvious difference in locomotor activity between the two mouse strains was detected at 6 months of age (data not shown). Decreased spontaneous motor activity was also observed in mice that were shown to have signs of Parkinson's or Alzheimer's disease (Crocker et al., 2003; Lee et al., 2004).

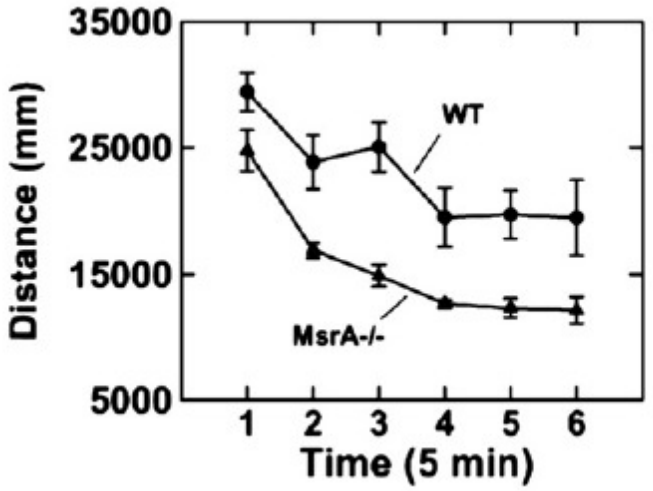

Figure 2. Spontaneous locomotor activity of *MsrA*$^{-/-}$ and WT control mice measured in a force-plate actometer apparatus. Five WT and 5 *MsrA*$^{-/-}$ mice (12 months old) were individually placed in a dark force-plate actometer apparatus and their behavior was recorded for 30 min. The effect of genotype was significant: $F(1, 8) = 12.106$, $P = 0.008$ as was the effect of time block: $F(5, 40) = 43.259$, $P < 0.001$. The interaction effect: $F(5, 40) = 1.752$, $P = 0.145$, was not significant.

Gait dynamics. Gait disturbances including shortened stride length (Salarian et al., 2004; Weller et al., 1993) and abnormal stride frequency (Bartolic, Pirtosek, Rozman, & Ribaric, 2005) are symptomatic of Parkinson's disease. A ventral plane videography apparatus using a clear treadmill (Amende et al., 2005; Kale, Amende, Meyer, Crabbe, & Hampton, 2004) was chosen to analyze the gait indices of mice at a constant speed (Fig. 3), compared to traditional "paw painting" techniques that do not control speed. The *MsrA*$^{-/-}$ displayed significant differences in stride length, frequency and duration relative to WT control mice (Fig. 3). Specifically, we observed a reduced stride length and stride duration as well as an increased stride frequency in *MsrA*$^{-/-}$ mice. The decreased parameters suggest a lack of motor control, and the increase frequency occurs to maintain the animal's speed as governed by the constant rate of the belt. Moreover, this novel technology has been previously used to analyze the gait dynamics of MPTP-injected mice (Amende et al., 2005), a common Parkinson's disease mouse model (shown in Table 1 for comparison). The gait data were pooled from all four limbs for analysis, as was done in previous analyses (Amende et al., 2005). The values in the graph (Fig. 3) show the differences by genotype and age relative to the 6-month-old control mice (WT young mice normalized to 100%). Actual numbers of the averaged values are given in Table 1. All stride indices were significantly different between the two types of mice, and these differences increased with age (aged mice are approximately 16 months of age). Also, Table 1 shows the percent change relative to the corresponding genotype. Reduced stride length is indicative of basal ganglia dysfunction (Fernagut, Diguet, Labattu, & Tison, 2002). Indeed, the current results for *MsrA*$^{-/-}$ mice are comparable in magnitude to the data reported by Amende et al. (Amende et al., 2005) for MPTP-treated C57BL/6 mice (Table 1). There is no evidence that MPTP administration and *MsrA* ablation affect the same biochemical pathway. However, the gait abnormalities found in the PD mouse model using MPTP administration and the *MsrA*$^{-/-}$ mouse may be indicative of some similarities in brain function/s of both mouse types, which may affect gait performance.

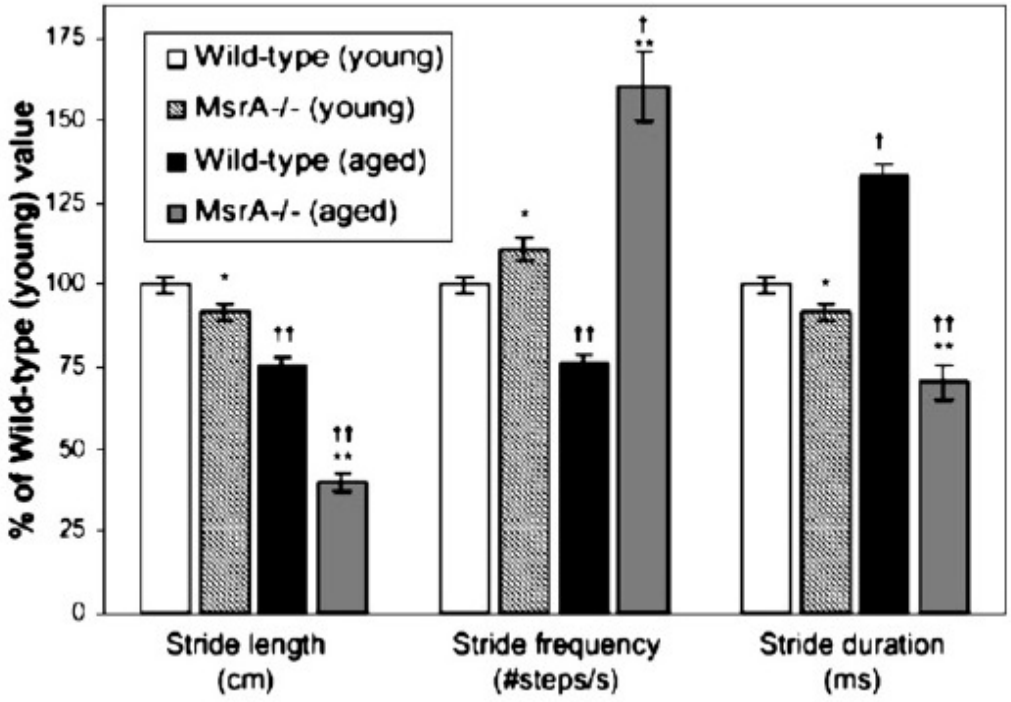

Figure 3. Gait dynamics of *MsrA*$^{-/-}$ and WT control mice. The horizontal axis represents the type of mouse and the dependent variables from the DigiGait Imaging System. The graphic shows differences in stride dynamics of *MsrA*$^{-/-}$ mice at two age points, 6 months (young, slashes) and 16 months (aged, gray solid) versus young and aged WT controls (white and black, respectively). Values are given as a percentage relative to the WT young value to show progression of abnormalities with age. The DigiGait-treadmill speed: young mice: 26 cm/s; aged mice: 15 cm/s, MPTP-injected mice: 34 cm/s. Significance was determined by *t*-test and indicated between strains by * ($P < 0.05$) or ** ($P < 0.001$); and between age groups in each strain by † ($P < 0.05$) or †† ($P < 0.005$). Each strain, n = 6.

Table 1
Stride dynamics of *MsrA*$^{-/-}$ versus wild-type (WT) and MPTP mice

Strain	Stride length (cm)	Stride frequency (steps/second)	Stride duration (ms)
WT (young)	7.24±0.18	3.67±0.10	257±7
MsrA$^{-/-}$ (young)	6.63±0.18	4.06±0.13	252±7
WT (aged)	5.50±0.13	2.80±0.07	367±9
MsrA$^{-/-}$ (aged)	2.90±0.21	5.90±0.39	194±1
MsrA$^{-/-}$ vs WT (young)	91.5%	110.7%	91.6%
MsrA$^{-/-}$ vs WT (aged)	52.8%	209.8%	52.9%
MPTP vs saline	93%	108%	93.7%

The mean value from actual numbers determined by DigiGait Analysis in Fig. 3 expressed as percentile of *MsrA*$^{-/-}$ or MPTP value [14] of WT or saline control, respectively.

Behavioral effects of amphetamine administration

Force-plate actometers were used to measure the locomotor-activating effects of amphetamine in *MsrA*$^{-/-}$ mice and WT controls. Numerical data for distance traveled are shown in Fig. 4 and tracings of movement trajectories are shown in Fig. 5. Analysis of variance indicated a significant difference between the two types of mice ($F(1,9)=7.104$, $P=0.026$). The dose effect was also significant ($F(2,18)=36.932$, $P<0.001$), as was the dose-by-type interaction effect ($F(2,18)=8.245$, $P=0.003$)). A significant three-way interaction (dose X time block X type of mouse) was also obtained, ($F(10,90)=15.393$, $P<0.001$). The statistical interaction effects were the result of the marked divergence of the behavior in the two types of mice at the 5.0 mg/kg dose, with the WT mice increasing their activity and the *MsrA*$^{-/-}$ mice decreasing in activity as session time passed. Because it is known that higher doses of amphetamine can induce in rodents focused stereotypies that reduce amount of locomotion (Lyon & Robbins, 1975), it is important to examine the behavior for indications of the potential occurrence of focused stereotypy in response to amphetamine. Data shown in Fig. 5 (examples for 4 animals per mouse strain) can be used to address this issue. Consistent with Figure 4 at the 5.0 mg/kg dose of amphetamine, the WT mice exhibited a high degree of locomotor stimulation which was accompanied by partial spatial confinement in mice number 3 and number 5, whereas the *MsrA*$^{-/-}$ mice showed declining stimulation with time but no spatial confinement of the kind seen for the WT mice. There was no focused sterotypies observed at 0.0 dose of amphetamine for either mouse strain. Intensified spatial confinement was observed for the WT mice when treated with amphetamine 2.5 mg/kg, which was the second dose treatment. The *MsrA*$^{-/-}$ mice also showed evidence of spatial confinement after the 2.5 mg/kg dose, but less than the WT mice. The somewhat greater spatial confinement effect in the second dose (even though it was lower than the first dose) is consistent with the idea that both types of mice were capable of expressing behavioral sensitization. At the 5.0 mg/kg dose the data suggest a deficient ability of the *MsrA*$^{-/-}$ to sustain motor response to amphetamine that may be related to an abnormality in the mouse's

DA neurotransmitter system, which is the predominate modality through which amphetamine produces its increase in locomotor activity.

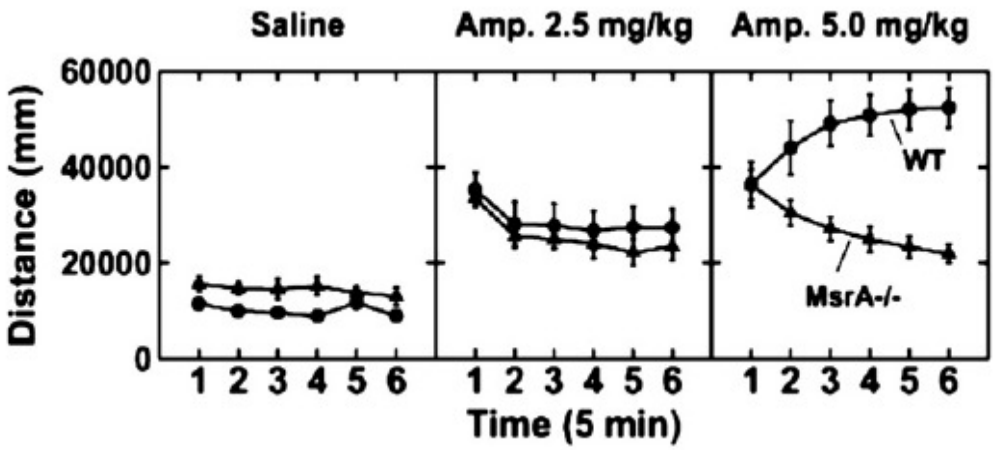

Figure 4. Response to amphetamine administered to both mouse strains. Distance traveled by *MsrA*$^{-/-}$ mice (filled circles, n=5) and controls (triangles, n=6) in response to the indicated doses of d-amphetamine sulfate (Amp) given i.p. The drug was administered 15 min before the 30-min recording session in a force-plate actometer. Mice were about 16 months old. Analysis of variance indicated a significant difference between the two types of mice ($F(1,9)=7.104$, $P=0.026$). The dose effect was also significant ($F(2,18)=36.932$, $P<0.001$), as was the dose-by-type interaction effect ($F(2,18)=8.245$, $P=0.003$)). A significant three-way ANOVA interaction (dose X time block X type of mouse) was also obtained, ($F(10,90)=15.393$, $P<0.001$).

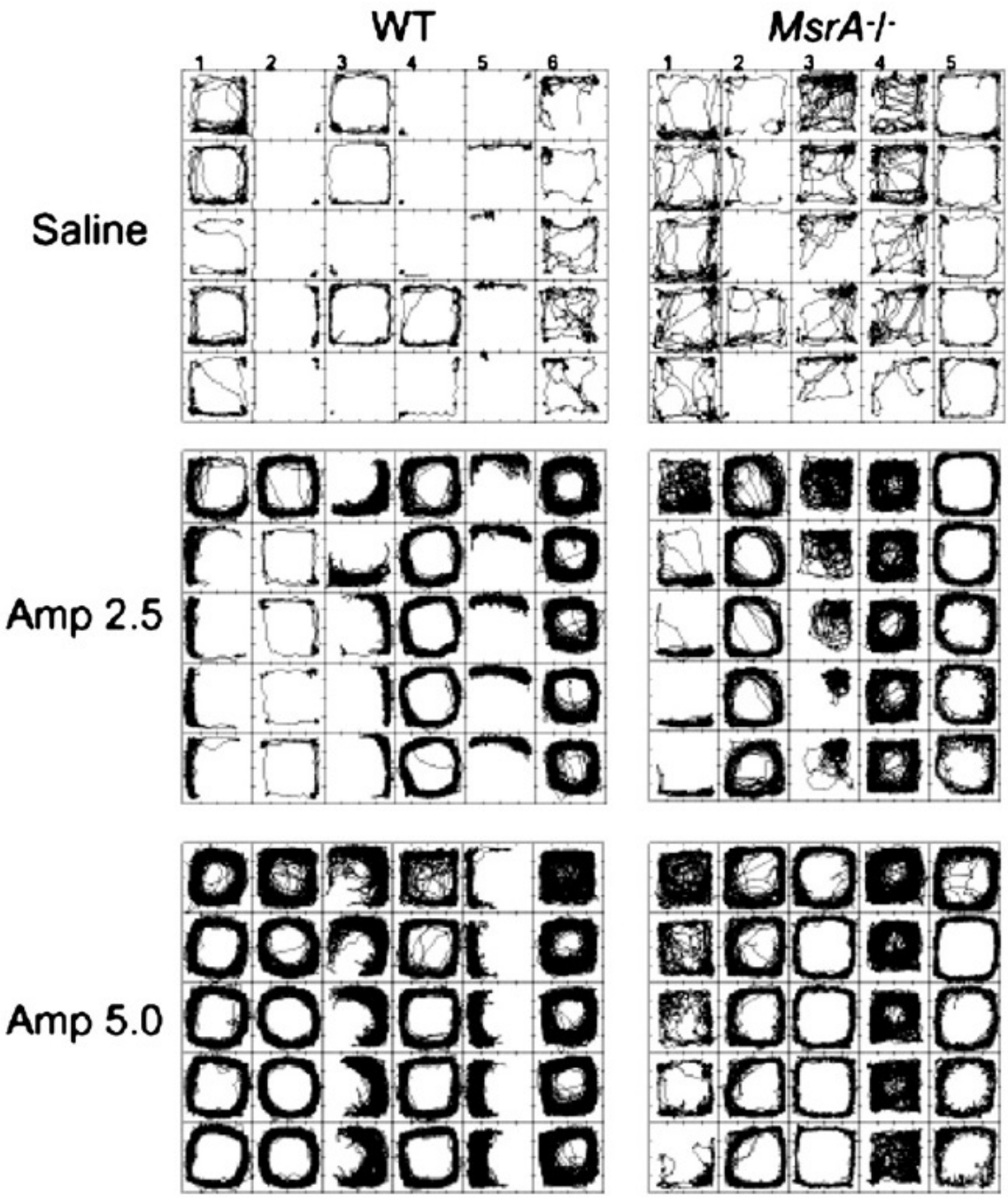

Figure 5. **Movement trajectories for the data shown in Figure 4.** Each square represents 6 min of recording. The top row for each treatment occurred first in time.These mice were approximately 16 months old.

Assessment of the molecular changes in MsrA$^{-/-}$ mouse brain

DA levels in post-mortem brains. Changes in brain DA levels are associated with abnormal motor behavior. Thus, we measured DA level in total brain extracts of 6-, 12-, and 16-month-old mice using reverse-phase HPLC-column linked to an electrochemical detector. Surprisingly, brains of the *MsrA*$^{-/-}$ mice exhibited 47% and 63% more dopamine compared to their counterpart WT brains at 6- and 12-month-old brains, respectively (Fig. 6). However, at older age (16 months), there was a ~50% decline in DA level in *MsrA*$^{-/-}$ compared to WT mice. It is important to note that the DA level in WT brain increased at 16 months of age to the DA level observed in *MsrA*$^{-/-}$ at 12 months. Consequently, it was important to evaluate the possibility of enhanced DA synthesis and release as shown by monitoring the expression levels of tyrosine hydroxylase (TH), TH-activating protein (TH has been reported to require binding of 14-3-3 proteins (Ywhaz) for optimal activation by phosphorylation (Kleppe, Toska, & Haavik, 2001), and DA release/reuptake in striatum of brain slices *in vitro*, as shown below.

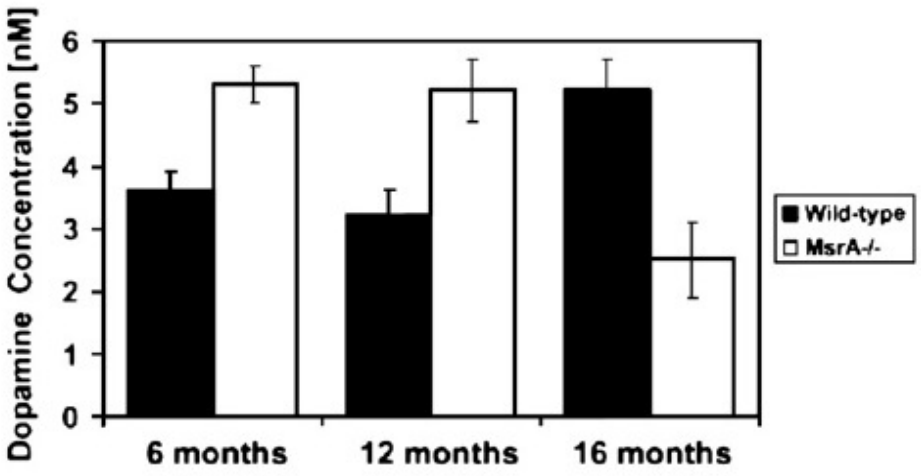

Figure 6. Concentration of brain DA in *MsrA*$^{-/-}$ and WT control mice at various ages. Neurotransmitter level was assayed by HPLC with electrochemical detection. Dopamine levels in the *MsrA*$^{-/-}$ brains were significantly higher than in the WT mice at ages of 6 and 12 months and lower than WT at 16 months of age, respectively, as determined by *t*-test, $P<0.01$. The higher DA level in WT at age of 16 months relative to ages of 6 and 12 months was also significant, as determined by *t*-test, $P<0.01$. Each strain, n=6.

Release and reuptake of DA in the striatum of brain slices

To gain insight into presynaptic dopaminergic malfunctions that may occur in *MsrA*$^{-/-}$ mice, we measured electrically evoked DA release and reuptake in striatal brain slices using fast-scan cyclic voltammetry (FSCV) at carbon-fiber microelectrodes. Electrodes were placed in the dorsolateral caudate because dopaminergic innervation in this brain region comes almost exclusively from the nigrostriatal pathway (Gerfen, Herkenham, & Thibault, 1987). As shown in a representative concentration-time plot (Fig. 7), a sharp increase in DA concentration is measured at the electrode upon application of a single stimulus pulse. This increase is followed by a more gradual decrease as DA is taken up by DAT (Jones, Gainetdinov, Wightman, & Caron, 1998a). Cyclic voltammograms (upper right in Fig. 7) obtained at the maxima confirm the detection of DA. Amplitudes of stimulated DA release obtained from brain slices of *MsrA*$^{-/-}$ mice are dramatically increased (272% of WT on average, aggregated data are shown in Table 2). Plots of stimulated DA release at carbon-fiber microelectrodes in brain slices may be distorted by diffusional contributions and DA reuptake by DAT (Bath et al., 2000). To account for these contributions, concentrations of DA released per stimulus pulse ([DA]p) were estimated by modeling the concentration–time curves (Fig. 7). The curved line superimposed over the points of the sample DA release plot represents best-fit curve derived using curve-fitting software (Wu, Reith, Wightman, Kawagoe, & Garris, 2001). On average, [DA]p was significantly increased (333% of WT, $P < 0.05$, n = 3 mice per genotype, 12 month-old mice) in brain slices harvested from *MsrA*$^{-/-}$ mice (Fig. 8). [DA]p progressively decreased with increasing time in culture of the *MsrA*$^{-/-}$ brain-slices, while remaining flat in the first 90 min for the WT brain slices and increasing by 200% at 180 min time point (Fig. 8).

From the analysis of the stimulated release curves we also determined V_{max}, a kinetic parameter describing the maximum rate of DA reuptake by DAT. The average values determined from *MsrA*$^{-/-}$ and WT mice were consistent with previously published values of V_{max} (4 lM/s) in mice (Jones, Joseph, Barak, Caron, & Wightman, 1999). No significant difference in

V_{max} between *MsrA*$^{-/-}$ mice and aged-matched WT littermates was found n= 3 mice per genotype, data not shown). The K_M for reuptake is the concentration of extracellular DA at which DAT functions at ½V_{max}. The K_M serves as a measure of DAT efficiency, whereas, V_{max} is directly proportional to DAT concentration. Values of K_M in the absence of reuptake inhibitors have been determined in synaptosomal preparations to be approximately 0.2 M (Jones, Garris, Kilts, & Wightman, 1995). Dopamine reuptake follows Michaelis–Menten kinetics (Jones et al., 1995; Kawagoe, Garris, Wiedemann, & Wightman, 1992; Wightman et al., 1988). Therefore, the rate of DA reuptake in a given plot of stimulated DA release is dependent upon DA concentration and is independent of the time point in the curve at which the concentration is measured. Thus, to qualitatively assess DA reuptake efficiency, we overlaid the averaged *MsrA*$^{-/-}$ and WT DA reuptake curves, time shifted so that the initial concentrations were approximately equal, from brain slice data obtained. This approach to observing relative DAT efficiency has been employed previously (Jones et al., 1995). The *MsrA*$^{-/-}$ curves are not statistically different from their respective WT curves in the concentration range of K_M (0.2 μM; $p > 0.05$, Mann–Whitney, n = 3, each genotype, 12-month-old *MsrA*$^{-/-}$ vs. age-matched WT; graphic not shown). This suggests that the K_M, and therefore the efficiency of DA reuptake by DAT, is similar in *MsrA*$^{-/-}$ and WT mice.

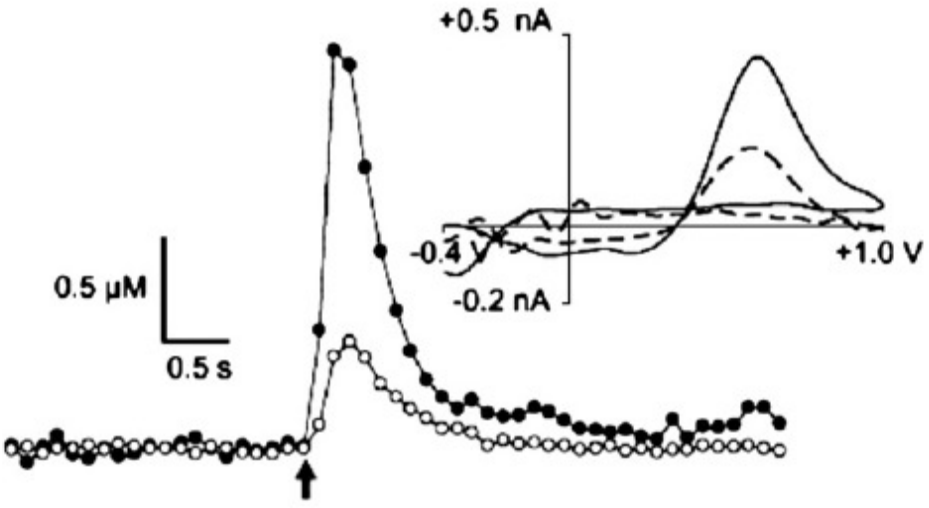

Figure 7. DA release in striatal brain slices of *MsrA*$^{-/-}$ and WT control mice. A representative stimulated DA release plot generated from measurements obtained from striatal brain slices (from 12-month-old post-mortem brains). FSCV was used to collect DA release measurements. The cyclic voltammograms plots (shown above and to the right) confirm the presence of DA. Legend: *MsrA*$^{-/-}$, closed symbols on release plot, solid line on cyclic voltammogram; WT, open symbols on release plot, dashed line on cyclic voltammograms.

Table 2
Peak dopamine release from brain slices harvested from *MsrA*$^{-/-}$ and WT control mice

Genotype	$[DA]_{max}$
MsrA$^{-/-}$	2.07 ± 0.49 µM
WT	0.76 ± 0.07 µM

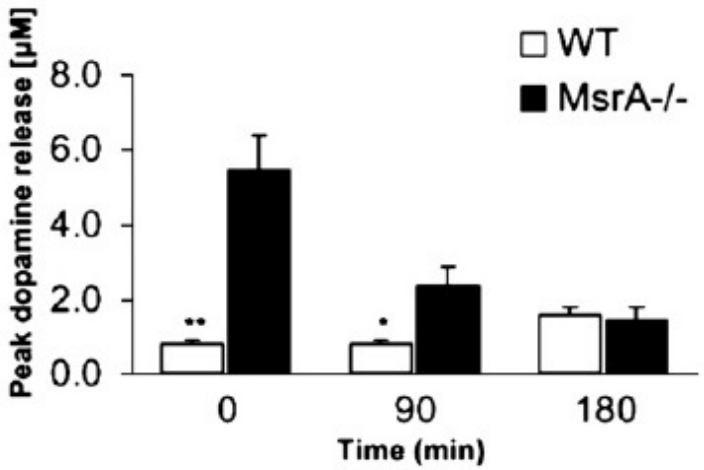

Figure 8. Peak dopamine release presented from the WT and *MsrA*$^{-/-}$ slices. Successive measurements were collected from striatal brain slices of *MsrA*$^{-/-}$, and WT mice 90 min apart. Bar graph values represent the average of release measurements collected from four different locations within the ventral lateral caudate/putamen. DA release from *MsrA*$^{-/-}$ brain slices diminished over time, whereas it did not diminish in WT slices. Error bars represent ±SEM. Significance determined by *t*-test: * $P < 0.05$, ** $P < 0.001$.

Analyses of TH and TH-activating protein

Increased DA levels observed may be attributed to elevated DA synthesis. We performed brain genomic screening analyses and found that the *MsrA*$^{-/-}$ brain had about 4-fold induction in *Ywhaz* (TH-activating protein) mRNA content over the WT brain gene at age of 6 months, respectively (P<0.001). The up-regulation of the *Ywhaz* gene in *MsrA*$^{-/-}$ brain was confirmed on the protein level following western blot analysis of *MsrA*$^{-/-}$ and WT brain extracts at ages of 6 and 12 months (Fig, 9A). Additionally, the protein level of Ywhaz was reduced at 16 months versus 12 months of age in the *MsrA*$^{-/-}$ brain and elevated in WT brain at 16 months of age compared to 12 months of age, respectively (Fig. 9A). Thus, there is a good correlation between the expression of *Ywhaz* gene and brain DA levels across the monitored strains and age. This correlation implies that *Ywhaz* may play an important role in the regulating brain DA synthesis as a function of age and performance of the Msr system. Differences in dopaminergic neuron quantities can alter the TH-activating protein content. However, the relative expression level of TH in both mouse strains was similar across all monitored ages (mRNA data not shown; and Fig. 9B for the protein expression level). The unchanged TH level suggests no significant age-dependent neurodegeneration in *MsrA*$^{-/-}$ dopaminergic neurons compared to WT, respectively.

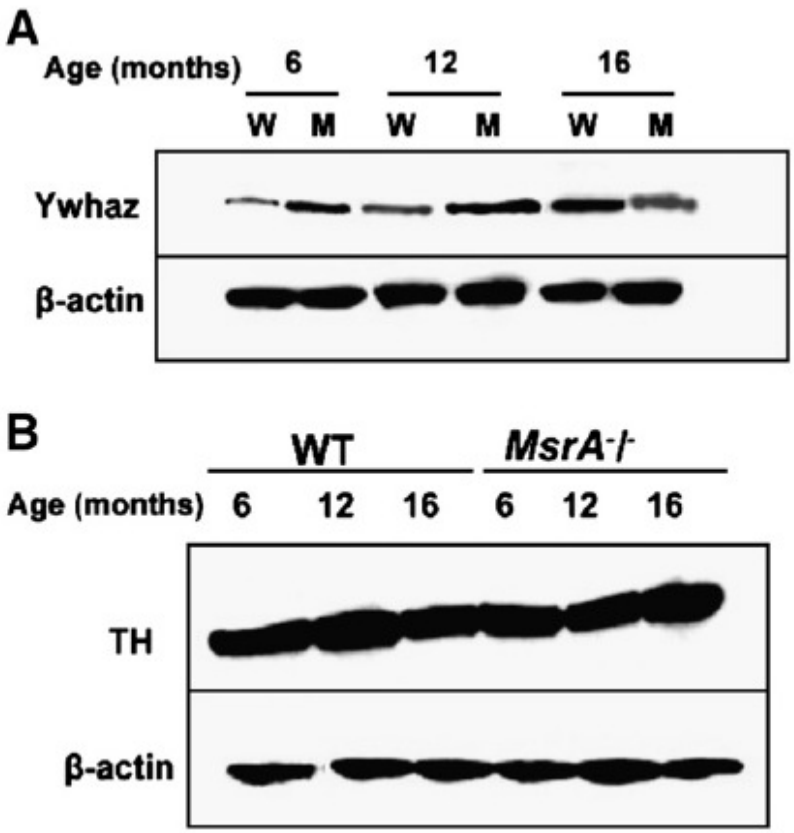

Figure 9. Protein-expression levels of TH and Ywhaz in WT and *MsrA*$^{-/-}$ brains. Pool of 5 mouse brain extracts were subjected to gel-electrophoresis, followed by western blot analyses. Thirty microgram of soluble brain proteins were loaded in each lane. **A)** Expression levels of Ywhaz (TH-activating protein) in both mouse strains as function of age (6, 12, and 16 months). **B)** Expression levels of TH as function of age (6, 12, and 16 months). Respectively, β-actin levels for each lane are shown in Panel A and panel B.

4. Discussion

In our previous studies we have found that *MsrA*$^{-/-}$ mice display elevated brain pathologies and a "tip-toe" walking pattern. Here we show evidence that the *MsrA*$^{-/-}$ mouse exhibits abnormal cognitive and locomotor behaviors reminiscent of age-related neurodegenerative diseases. In addition, the mice lacking MsrA display atypical dopamine regulation. The initial increased *MsrA*$^{-/-}$ DA levels are a finding that, to our knowledge, has only been reported in studies not related to oxidative stress. The *MsrA*$^{-/-}$ mouse was shown to be more vulnerable to oxidative stress and showed enhanced neurodegeneration in the hippocampus. Thus, it is possible that the general observed hypersensitivity of the *MsrA*$^{-/-}$ to oxidative stress may affect the function of specific proteins that are involved in DA physiology.

Lower locomotor activity present as early as 12 months of age in *MsrA*$^{-/-}$ relative to WT mice (Fig. 2), and measurable gait disturbances detected at 6 months and worsening with age in *MsrA*$^{-/-}$ (Fig. 3), suggests that the motor deficiencies in the *MsrA*$^{-/-}$ are exacerbated with age; relative to WT declining locomotor activity. The data presented in Fig. 3 and Table 1 suggests a magnitude of gait abnormality in the *MsrA*$^{-/-}$ mice that is comparable to what is seen in MPTP treated mice. The gait abnormalities found in the PD mouse model using MPTP administration, which has also been demonstrated in *MsrA*$^{-/-}$ mouse, may be a consequence of a common response to direct or indirect effects prompted by the ablation of *MsrA* and MPP+ action in the brain. Studies of gait in mouse models will help establish parallels with human pathologies, and these parallels may be useful in identifying therapeutic approaches to human neurological diseases. Alteration in DA metabolism is strongly associated with abnormal locomotor activity. The drug amphetamine blocks the re-uptake of already released DA, by blocking DAT function, and thus was used to treat the mice to elevate their locomotor activity.

Surprisingly, the presented data showed that amphetamine-treated *MsrA*$^{-/-}$ mice have a compromised response to this treatment (Figs. 4 and 5) at 5.0 mg/kg. From the results obtained on DA release and re-uptake from the striatum, using FSCV (Figs. 7 and 8, Table 2), it appears

that the DAT in *MsrA*$^{-/-}$ mice functions properly, while a dramatic increase in DA release is observed. Thereby, it is unlikely that the observed high levels of *MsrA*$^{-/-}$ brain DA at ages of 6 and 12 months (Fig. 6) are the outcome of insufficient reuptake of DA. Rather, these findings imply that the measured high level of *MsrA*$^{-/-}$ brain DA (Fig. 6) is related to an enhancement in DA synthesis. Supportive evidence to this hypothesis arises from the fact that the upregulation or downregulation of the activating enzyme of TH (TH-activating protein, Ywhaz) correlate with the levels of brain-DA in both mouse strains (Fig. 9A and Fig 6). At an age of 16 months, *MsrA*$^{-/-}$ mice showed reduction in DA level compared to the previous ages (50%), while the WT reached the DA levels of the *MsrA*$^{-/-}$ at ages of 6 and 12 months (Fig. 6). One possible explanation for this observation is that, relative to WT, the *MsrA*$^{-/-}$ brain is functioning under oxidative stress conditions from an early age and it is responding by elevating DA levels (possibly as a compensatory response). However, at an older age this response mechanism to oxidative stress may fail in the *MsrA*$^{-/-}$ brain. In contrast, MsrA expression and activity in WT brains decline only at older ages (Petropoulos, Mary, Perichon, & Friguet, 2001; Stadtman, Moskovitz, Berlett, & Levine, 2002). The increase of DA content in 16-month-old WT mice may reflect, in light of the DA-data presented for the MsrA KO mice, an enhanced oxidative stress at older age before dopaminergic neurodegeneration occurs. Thus, the same phenomenon may occur in WT, but it is delayed until MsrA levels are decreased in normal aging.

The unchanged levels of TH in *MsrA*$^{-/-}$ relative to WT brain (Fig. 9B) reduce the possibility of enhanced dopaminergic neurodegeneration in *MsrA*$^{-/-}$ brain up to 16 months of age. Similarly, lack of an obvious *in vivo* dopaminergic neurodegeneration was shown in major genetic mouse models for Parkinson's disease; for example, in the DJ-1 knockout mouse (Yamaguchi & Shen, 2007) and in various types of mouse models overexpressing alpha-synuclein (Chesselet, 2007). The different promoters and mouse transgenes of alpha-synuclein lead to a wide variety of phenotypes accompanied by nonexistent, late onset, or non-specific neurodegeneration (Chesselet, 2007). Thus, it is proposed enhanced level of dopaminergic neurodegeneration is

probably an outcome of multi-component events manifested at late stages of cell death; whereas MetO participates in earlier stages of neurodegeneration. Nevertheless, the type of brain cell having a compromised MsrA system may determine the level of neurodegeneration. For example, it seems that certain cells of the hippocampus are more sensitive to neurodegeneration (Pal et al., 2007a) compared to dopaminergic neurons (Fig. 9B).

The inability of high DA levels in the *MsrA*$^{-/-}$ mice to increase their locomotor and gait performances (in the absence of DAT abnormality) supports the hypothesis that malfunction of downstream signaling events (due to MetO) may be the rate-limiting factors in attenuating the *MsrA*$^{-/-}$ response to DA. Moreover, the increased bio-behavior abnormalities observed in the aged *MsrA*$^{-/-}$ mice may be due to the additional age-dependent general decline in antioxidant defense. For example, it is speculated that the DA receptors in *MsrA*$^{-/-}$ mice may be more affected by MetO with age, thereby causing either lower efficiency in DA receptors binding to DA, downregulation of DA-receptors expression, or both.

The *MsrA*$^{-/-}$ mice exhibited a compromised learning capability when challenged with increased task demands. As shown in Fig. 1, the WT mice learned the FR20 task significantly faster than the *MsrA*$^{-/-}$ mice. Given the older age of these mice (16 months), this observed difference in learning is possibly the result of having malfunctioning proteins involved in the learning processes as oxidative damage increases with age. Reduced operant capability is indicative of problems residing within the cortico-striatal-thalamo-cortical loops. Thus, it is possible that irregularities in DA physiology may contribute to the altered learning capacity in the *MsrA*$^{-/-}$ mice, in addition to the already demonstrated pathologies in the *MsrA*$^{-/-}$ hippocampus (Pal et al., 2007a).

The FSCV results (Figs. 7 and 8, Table 2) clearly suggest that there is a rapid exaggerated release of DA in *MsrA*$^{-/-}$ brain upon stimulation. It is well established that DA plays a pivotal role in motor behavior activity and that the rate of DA release from dopaminergic neurons contributes significantly to its potential action on targeted receptors. Dopaminergic neurons

have the capacity to release DA not only from their axon terminals, but also from their somatodendritic compartment. The endoplasmic reticulum and its associated tubulovesicles have been proposed as possible storage sites for somatodendritic DA. These structures indeed appear to contain DA (Groves & Linder, 1983; Hattori, McGeer, & McGeer, 1979; Linder, Klemfuss, & Groves, 1987), and similar structures have been shown to express proteins of the SNAP-receptor (SNARE) complex, otherwise known to be essential for exocytosis. Consequently, one possible explanation for the observed increased DA release in *MsrA*$^{-/-}$ brain is an upregulation of the expression levels of the proteins participating in DA release mechanisms.

In summary, elevated protein oxidation at older age may cause irreversible MetO leading to protein malfunction and/or abnormal accumulation. Thus, irregularities in various physiological processes may occur, including abnormalities in neurological functions manifested by attenuated locomotor behavior and reduced learning capabilities. The molecular basis for such events may involve altered DA synthesis and release (this study) and post-synaptic physiology (future studies), which are associated with age-dependent reduction in the proper function of the Msr system. Accordingly, it is proposed to use the *MsrA*$^{-/-}$ mouse as a model to further studies on the relationships between MetO, neuronal metabolism, behavioral functions, and aging.

C. Caloric Restriction Alleviates Abnormal Locomotor Activity and Dopamine Levels in the Brain of the MsrA Knockout Mouse

(D. B. Oien, Osterhaus, Lundquist, Fowler, & Moskovitz, 2010)

Oxidative stress is associated with the aging process, a risk factor for neurodegenerative diseases, and decreased by reduced energy intake. Oxidative modifications can affect protein function; the sulfur-containing amino acids, including methionine, are particularly susceptible to oxidation. A MetO can be enzymatically reduced by the Msr system. Previously, we have shown that *MsrA*$^{-/-}$ mice exhibit altered locomotor activity and brain DA levels as function of age.

Previous studies have demonstrated that a caloric restriction enhances antioxidant defense and reduces the action of ROS. Here we examine locomotor behavior and DA levels of *MsrA*$^{-/-}$ mice after caloric restriction (CR) starting at 8 months of age and ending at 17 months. The *MsrA*$^{-/-}$ mice did not have any significant difference in spontaneous distance traveled when compared to controls at 17 months of age. In contrast, our previous report showed decreased locomotor activity in the *MsrA*$^{-/-}$ mice at 12 months of age and older when fed *ad libitum*. After completion of the CR diet, DA levels were comparable to control mice. This differs from the abnormal DA levels previously observed in *MsrA*$^{-/-}$ mice fed *ad libitum*. Thus, CR had a neutralization effect on MsrA ablation. In summary, it is suggested that CR alleviates abnormal locomotor activity and DA levels in the brain of the *MsrA*$^{-/-}$ mouse.

1. Introduction

Reduced energy intake is known to decrease free radical production and oxidative damage in mammals, extend life-span, and slow age-related health problems in multiple species (Martin, Golden, Egan, Mattson, & Maudsley, 2007). An ongoing study with rhesus monkeys supports the latter concept (Colman et al., 2009). Furthermore, CR is neuroprotective (Maalouf, Rho, & Mattson, 2009) and has benefits that oppose brain aging, including oxidative stress pathways and related pathological states (Contestabile, 2009). In rodents, feeding conditions have been found to affect locomotor activity (Govic, Levay, Kent, & Paolini, 2009; Minor et al., 2008), and restrictive diets can increase DA signaling (Carr, Tsimberg, Berman, & Yamamoto, 2003; Gelegen et al., 2008).

Previously, it was shown that *MsrA*$^{-/-}$ mice exhibit lower locomotor activity with age (D. B. Oien & Moskovitz, 2008). The *MsrA*$^{-/-}$ brains contained significantly higher levels of DA up to 12 months of age relative to WT control mice, while lower levels of DA were observed at 16 months of age. Moreover, *MsrA*$^{-/-}$ mice were less responsive to amphetamine, the release of DA was increased in the striatal regions, and the expression pattern of tyrosine hydroxylase activating

protein correlated with age-dependent DA levels. Thus, it was suggested that DA regulation and signaling pathways are impaired in *MsrA*$^{-/-}$ mice, which may contribute to their abnormal behavior. Here we describe *MsrA*$^{-/-}$ mice on CR conditions and compare the results to our recent experiments showing abnormal locomotor behavior and DA levels in brain (D. B. Oien & Moskovitz, 2008). The *MsrA*$^{-/-}$ mice were placed on feeding restrictions starting at eight months of age, and these restrictions were continued until up to the age of 17 months. The mice were analyzed for locomotor behavior and brain DA levels.

2. Materials and Methods

The *MsrA*$^{-/-}$ mice have been previously described (Moskovitz et al., 2001; D. B. Oien & Moskovitz, 2008). The methods for reduction in food availability, locomotor measurements, and euthanasia were approved by the KU Institutional Animal Care and Use Committee.

Caloric restriction

The *MsrA*$^{-/-}$ and WT control mice were both fed on an *ad libitum* (AL) diet until they reached eight months of age. Initial weights prior to caloric restriction were calculated by taking the average weight over three days for each mouse. Each mouse was then fed daily an amount of chow equal to 10% body weight until the weight of the mouse was reduced by 15%. All mice achieved this reduction within the first two weeks of restriction. Each mouse was maintained at this body weight for the duration of the experiment by adjusting food availability. The average weight losses within each mouse type and between the mouse groups did not significantly differ (P<0.05; data not shown). Likewise, it was previously reported that the weights of *MsrA*$^{-/-}$ and WT mice are not different, and there are no differences between the groups with age on an AL diet (Moskovitz et al., 2001).

Total distance traveled

Locomotor activity was assessed with four concurrently operative force-plate actometers (Fowler et al., 2001b). The actometer and associated peripherals, including the methods of data collection and analysis, were used as described previously (Fowler et al., 2001b). In this study, the total distance traveled for each *MsrA*$^{-/-}$ and WT control mouse on CR was measured for 30 minutes. Measurements were taken before CR at the age of eight months and each subsequent month while mice were on CR. Measurements were taken at the same time of day each month. Data presented are the mean ±standard deviation. The distance traveled was analyzed with a repeated-measures two-way ANOVA with genotype as the between-groups factor and month as the repeated-measures factor. Significance was further determined by the polynomial trend order 2 post-hoc test.

DA concentrations in brain tissue

The concentration of DA in the brain tissue was analyzed when mice on CR were 12 months old and 17 months old. The DA concentrations in *MsrA*$^{-/-}$ and WT control mice were measured immediately after the respective analysis of distance traveled by methods described previously (D. B. Oien & Moskovitz, 2008). Briefly, postmortem brain was dissected and cerebrum was weighed after olfactory bulb and cerebellum removal. The cerebrum was homogenized with in a solution containing 0.2 M perchloric acid and dihydrobenzylamine as the internal standard. Insoluble material was removed by centrifugation and supernatants were injected into a C18 reverse-phase HR-80 catecholamine column (ESA Inc., Bedford, MA). The mobile phase consisted of 94% 50 mM sodium phosphate/0.2 mM EDTA/1.2 mM heptanesulfonic acid (pH 3.2) solution and 6% methanol. The flow rate was 1.5 mL/min. Peaks were detected by an ESA 8 Channel CoulArray system. Data were collected and processed using CoulArray data analysis. Data presented are the mean ±standard deviation. Statistical analysis was carried out using *Student's t-test* to determine if the observed changes between the two mouse types had a significant effect ($P<0.05$).

Detection of methionine sulfoxide proteins and tyrosine hydroxylase

Post-mortem brains (cerebra) from both mouse types at 12 months of age, fed either CR (four months) or AL diets were homogenized in buffer, and following centrifugation the corresponding supernatants were collected. Equal protein amounts (50 µg) from each brain extract were separated by gel-electrophoresis in 4-20% SDS-gel followed by western blot analysis using the primary anti-MetAO antibodies or anti-tyrosine hydroxylase antibodies, as previously described (D. B. Oien, Canello et al., 2009).

3. Results

Total distance traveled of MsrA$^{-/-}$ and WT mice on reduced food availability

Changes in spontaneous locomotor activity can be indicative of neuronal dysfunction and neurodegenerative diseases (Hausdorff et al., 2000). In a previous study, the *MsrA*$^{-/-}$ mice showed significantly less locomotor activity when compared to WT mice, including the spontaneous distance traveled. There was no significant difference between *MsrA*$^{-/-}$ and WT mice for distance traveled in the overall experiment (Fig. 1; P=0.661, main effect). Also, there were no significant differences found between distances traveled among the genotypes during both the beginning and the end months of the CR diet (Fig. 1). The *MsrA*$^{-/-}$ mice traveled significantly more only in the intermediate months as judged by the polynomial trend order 2 post-hoc test (P=0.001, month-by-type interaction effect). The lack of difference before the CR diet (when mice were fed AL at 8 months of age; Fig. 1) is comparable to the distances traveled by *MsrA*$^{-/-}$ and WT mice at 6 months of age that were also fed on an AL diet (D. B. Oien & Moskovitz, 2008). The increase and later non-significant difference of *MsrA*$^{-/-}$ mice on a CR diet is a contrast to the ~50% decrease in distance traveled by *MsrA*$^{-/-}$ mice when on an AL diet at the age of 12 months (D. B. Oien & Moskovitz, 2008).

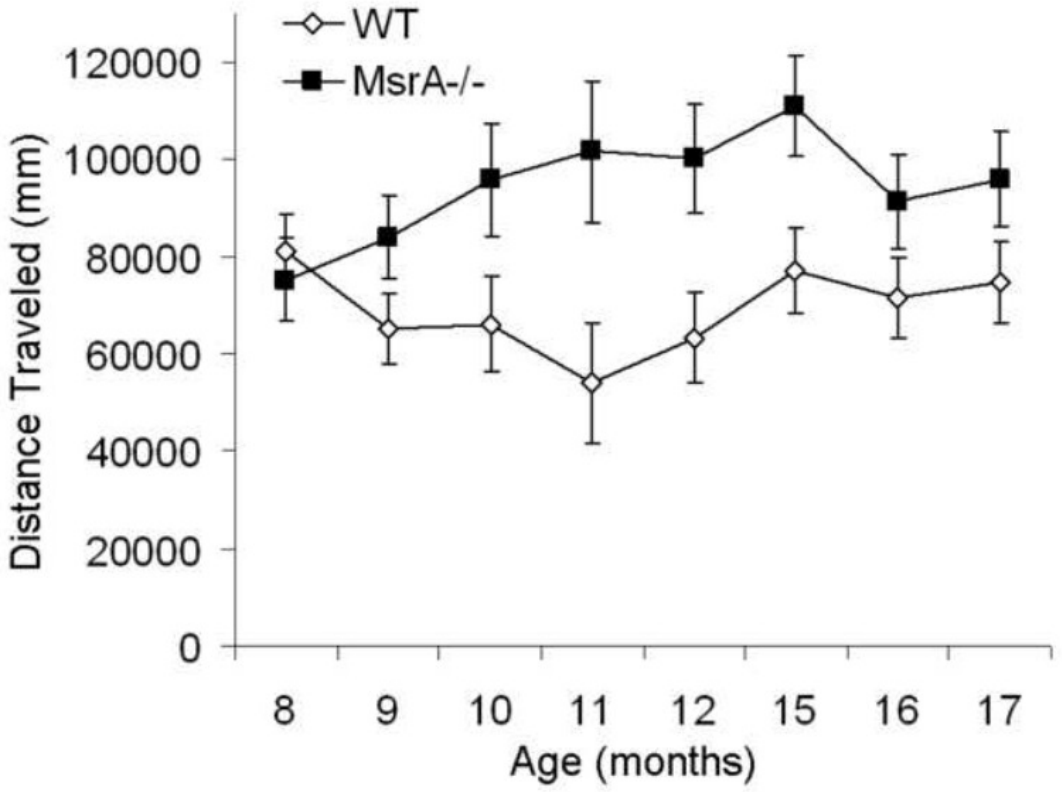

Figure 1. Total distance traveled by *MsrA*$^{-/-}$ mice on caloric restriction diet. Mouse spontaneous locomotor activity was measured starting before feeding the CR diet (8 months). These measurements were continued at the end of each month of the CR diet. Locomotor activity was measured as total distance traveled in a force-plate actometer for 30 minutes. Values represent average distance traveled of *MsrA*$^{-/-}$ mice (*filled squares*) and WT mice (*open diamonds*). Error bars represent standard deviation. The *MsrA*$^{-/-}$ mice traveled significantly more only in the intermediate months as judged by the polynomial trend order 2 post-hoc test (*P*=0.661, main effect; *P*=0.001, month*type interaction effect).

DA concentrations in brain tissues of MsrA$^{-/-}$ and WT mice on reduced food availability

DA levels from the nigrostriatal pathway can influence the direct and indirect movement pathways. In a previous study, abnormal DA levels in the brain tissue of *MsrA*$^{-/-}$ mice were found, relative to WT mice (D. B. Oien & Moskovitz, 2008). The concentration of DA in the brain tissue of *MsrA*$^{-/-}$ and WT mice did not significantly differ at the ages of 12 months and 17 months (Fig. 2) when on CR. There was a small, non-significant relative decline in DA levels of *MsrA*$^{-/-}$ mice at 17 months of age, which may be similar to the significant decrease between *MsrA*$^{-/-}$ and WT mice when fed on an AL diet (Table 1) (D. B. Oien & Moskovitz, 2008). This latter observation suggests that the positive effect of the CR diet on *MsrA*$^{-/-}$ DA levels may be limited in advancing age. Furthermore, the increased DA concentration of 16-month-old WT control mice on an AL diet (D. B. Oien & Moskovitz, 2008) was not detected in WT mice fed on a CR diet at 17 months of age. This observation suggests that the CR diet reduced brain oxidative stress below levels that normally prompt DA elevation (D. B. Oien & Moskovitz, 2008).

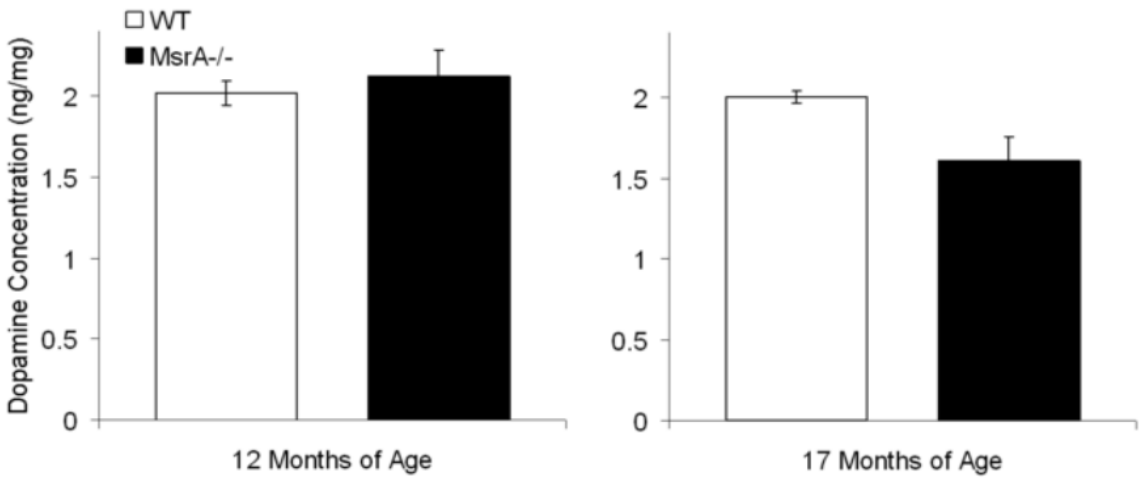

Figure 2. DA concentration in the brain tissue of *MsrA*$^{-/-}$ mice on CR diet.

Cerebral DA levels were determined for *MsrA*$^{-/-}$ mice (*filled*) and WT mice (*open*) after reduced food intake as described in "Materials and Methods". Values represent the amount of DA per weight of cerebral brain tissue after four months of caloric restriction diet (*left*), or after nine months of caloric restriction diet (*right*). Error bars represent standard deviation of 6 *MsrA*$^{-/-}$ mice and 5 WT mice at four months and 5 *MsrA*$^{-/-}$ mice and 7 WT mice at nine months. *P*=0.597 and *P*=0.054, respectively, by the *student's t-test*.

Age (months)	6		12		16-17	
Genotype	WT	*MsrA*$^{-/-}$	WT	*MsrA*$^{-/-}$	WT	*MsrA*$^{-/-}$
AL diet*	100±8	148±8	89±10	144±14	144±14	69±17
CR diet			90±7	94±16	89±4	72±15

Table 1. Comparison of dopamine levels in brain tissue of *MsrA*$^{-/-}$ mice on caloric restriction diet and *ad libitum* diet. Cerebral DA levels are listed by the respective age after reduced food intake (CR diet) or on *ad libitum* feeding (AL diet) from our previous study* (D. B. Oien & Moskovitz, 2008). Relative DA values and standard deviations are depicted as percentage of DA levels in WT control mice at 6 months of age fed on an AL diet. Variance (±) represents standard deviation of 5-7 mice per group.

Met oxidation of 15 kDa protein in brain tissue of MsrA$^{-/-}$ and WT mice on CR and AD diet

We have applied our novel anti-MetO antibodies (D. B. Oien, Canello et al., 2009) to identify MetO proteins in brain extracts of both mouse types under AL and CR diets. There was an enhanced Met oxidation in a ~15 kDa brain protein from *MsrA*$^{-/-}$ mice under AL diet, and to lesser extent in WT mice (Fig. 3). Interestingly, under CR diet, the levels of Met oxidation in this protein were reduced in both mouse types. Other MetO-containing proteins were detected in the western blot analysis, but their band intensities were not sufficient to determine the effect of CR diet due to the assay sensitivity limits. Further purification and enrichment of this protein will be performed to facilitate the identification of this protein by mass spectrometry analysis. Also, we have shown no change in tyrosine hydroxlase expression in all cases, which serves both as an internal control for protein loading and evidence for lack of obvious neurodegeneration in the brains of both mouse types.

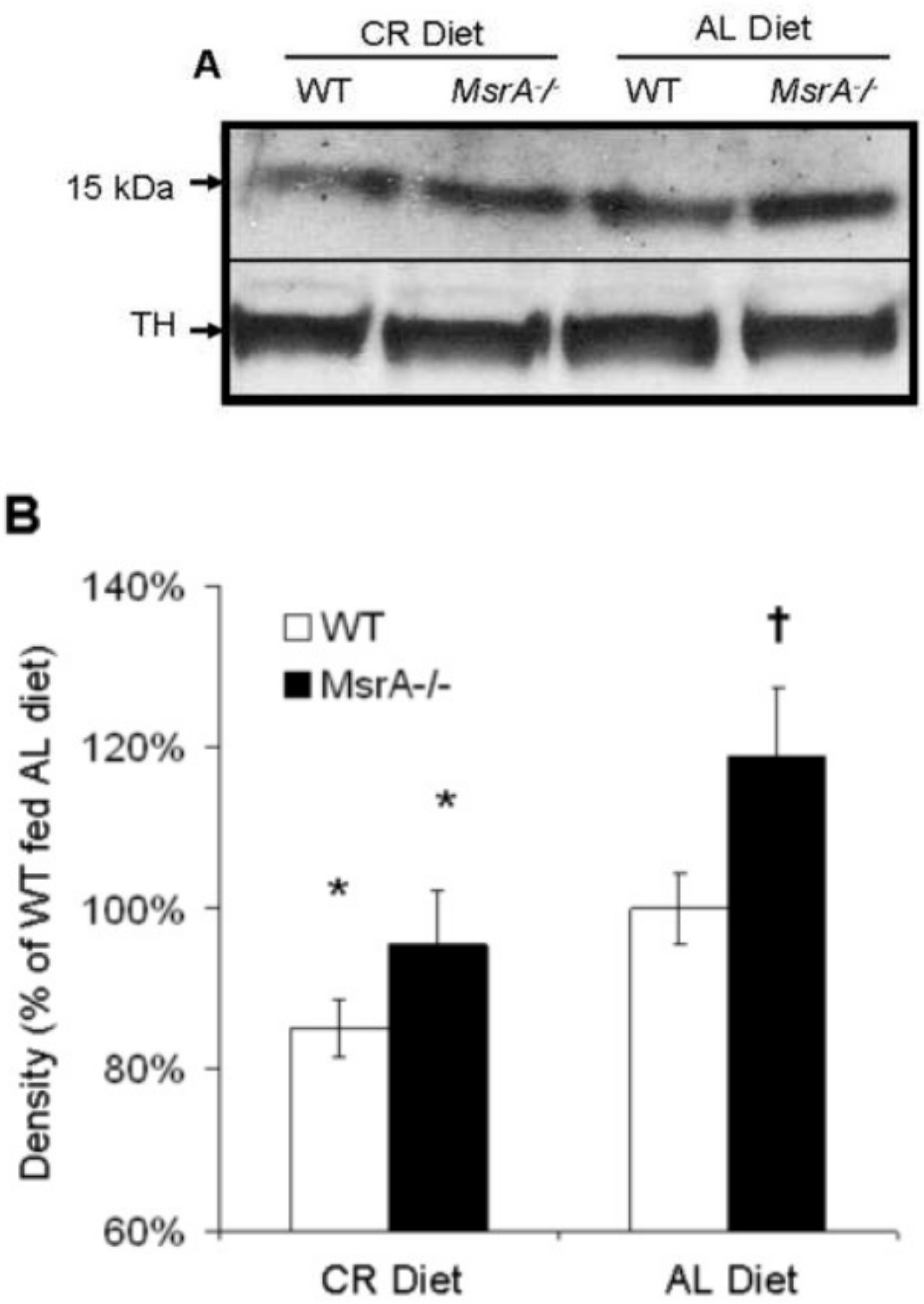

Figure 3. MetO detection in a 15 kDa protein from brain tissues of *MsrA*$^{-/-}$ and WT mice on CR and AD diet. Soluble protein extracts were made from *MsrA*$^{-/-}$ and WT brain tissue of 12-month-old mice after four months of restricted feeding (CR diet) and from age-matched mice maintained with no feeding restrictions (AL diet). Equal protein amounts from each brain extract were separated by gel-electrophoresis followed by western blot analysis using the primary anti-

MetO antibodies or anti-tyrosine hydroxylase (TH) antibodies, as previously described (D. B. Oien, Canello et al., 2009). **A)** Representative gel showing an unidentified protein with a mass of ~15kDa (mass estimated by the separation of prestained molecular mass markers; data not shown). TH is shown as a loading control. **B)** Average density of the 15 kDa protein. Density was determined by using the densitometry ImageJ (NIH). Error bars represent standard deviation of three brains per group. $^{*}P<0.05$ for the effect from diet and $^{\dagger}P<0.05$ for the effect of genotype on the AL diet, *student's t-test*.

4. Discussion

The *MsrA*$^{-/-}$ mice are hypersensitive to oxidative stress and exhibit accelerated age-related pathologies (Moskovitz & Oien, 2009; D. B. Oien & Moskovitz, 2008; Pal, Oien, Ersen, & Moskovitz, 2007b). We have previously reported that the *MsrA*$^{-/-}$ mice exhibit decreased locomotor activity and abnormal DA levels in the brain tissue. Here, it is demonstrated that reduced availability of food can alleviate abnormal locomotor activity and DA levels in the brain of *MsrA*$^{-/-}$ mice. However, there is a lack of solid evidence for mechanisms involved in alteration of MetO content and DA signaling via Met oxidation. Thus, it is still difficult to predict if a decrease in reactive oxygen species or compensatory response prompted by the CR diet, or both, are responsible for the observed changes.

The reduced availability of food and corresponding loss of body weight has been shown to correspond to a reduction of oxidative stress and reactive oxygen species (Martin et al., 2007). In this study, the mice had reduced access to the same food that was given when fed on an AL diet. No differences in the feeding habits of *MsrA*$^{-/-}$ and WT mice were observed, and this is further supported by a previous report demonstrating that the weights of *MsrA*$^{-/-}$ and WT mice are not different on an AL diet (Moskovitz et al., 2001). In addition, there is not a difference of body weight between these mice with age (Moskovitz et al., 2001). Furthermore, a 20% reduction in body weight has been shown to improve DA receptor signaling in rodents (Carr et al., 2003). The *MsrA*$^{-/-}$ mice have been previously reported to exhibit decreased locomotor activity and abnormal DA levels in the brain tissue relative to WT mice (D. B. Oien & Moskovitz, 2008). In this study, it is shown that *MsrA*$^{-/-}$ mice after nine months of caloric restriction do not significantly differ from the WT mice (Fig. 1). This supports the idea that the reduced energy intake decreases the activity of ROS, whereas normally fed *MsrA*$^{-/-}$ mice are hypersensitive to oxidative stress (Moskovitz et al., 2001; Pal et al., 2007b). However, *MsrA*$^{-/-}$ mice were significantly more active than the WT mice before the end of the experiment (Fig. 1). This latter finding supports the concept that the food restriction had an effect by reducing MetO-mediated

cellular changes while increasing the function of already up-regulated genes in *MsrA*$^{-/-}$ brain (D. Oien, Wang et al., 2008); alternatively, this could also be by activating specific compensatory mechanisms yet to be discovered. Regarding DA levels, it has been determined in this study (Fig. 2) that CR significantly alleviated the differences in DA levels observed between the *MsrA*$^{-/-}$ and WT mice when fed AL (D. B. Oien & Moskovitz, 2008). Thus, it may be that this is a result reflects the hypothesis above, which suggests the CR effects on cellular metabolism are linked to Met oxidation via the absence of MsrA. It is important to note that in contrast to the elevated DA levels in 16-month-old WT mice fed on an AL diet, the WT mice fed on a CR diet at 17 months of age had a decreased concentration of DA in their brain tissue (Table 1). If indeed higher DA levels represent a response to elevated oxidative stress conditions, the latter decrease in DA levels in the WT brain may reflect lower oxidative stress conditions in older WT mice on food restriction.

The efficacy of CR diet in reducing the accumulations of MetO in specific brain proteins is evident from the data presented in Fig. 3, showing an example of one protein in which its MetO moiety can be reduced by the diet. Other tissues can be analyzed for the presence and reduction of MetO under AL diet versus CR diet using the anti-MetO antibodies; the positive effect of CR in lowering methionine sulfoxide content is probably not limited to brain. The data in Fig. 3 suggest that up-regulation of antioxidants during the course of the CR diet is a valid possible explanation for the prevention of brain abnormalities associated with oxidative stress in general, and Met oxidation in particular.

Oxidative stress and Met oxidation have been implicated in neurodegenerative movement disorders such as Parkinson's disease (Choi et al., 2006; Dong et al., 2003; Moskovitz & Oien, 2009). In Parkinson's disease, the DA-mediated movement pathways are disrupted. Dietary restriction has been shown to improve the behavioral outcome and reduce neurodegeneration of the MPTP rodent model of this disease (Duan & Mattson, 1999). Furthermore, the addition of MsrA has been shown to prevent Parkinson's disease-like symptoms in *Drosophila* when alpha-

synuclein is expressed (Wassef et al., 2007). Alpha-synuclein, a protein that binds to DA and is associated with the pathogenesis of Parkinson's disease, is a substrate for Msr (D. B. Oien & Moskovitz, 2008; D. B. Oien, Shinogle, Moore, & Moskovitz, 2009b). Despite a growing body of evidence, the association between Met oxidation, DA, and alpha-synuclein in movement disorders is still not clear. However, it is a plausible hypothesis that ROS are causing modifications to Met residues of proteins, including or excluding alpha-synuclein, involved in DA signaling (D. B. Oien & Moskovitz, 2008).

In summary, we suggest that CR reduces oxidative stress effects, including Met oxidation. Furthermore, our studies support the concept that Met oxidation alters protein function, which may contribute to neurological diseases associated with oxidative stress and aging.

D. Reserve Pool DA Mobilization in Msr Null Mice

(Ortiz, Oien, Moskovitz, & Johnson, Manuscript)

Abnormal DA regulation has been associated with multiple neurodegenerative disease states. Nevertheless, the role of DA reserve pool storage and mobilization in many of these pathologies has not been fully investigated. *MsrA*$^{-/-}$ mice suffer from increased oxidative stress and have previously been found to have chronically elevated brain DA content levels relative to control mice. Additionally, these high levels parallel increased presynaptic DA release. In this work, FSCV at carbon-fiber microelectrodes was used to provide evidence that the DA reserve pool is enhanced in the striatum and that this increase correlates with increased DA levels in knockout mice. Amphetamine-induced DA efflux was measured in brain slices from knockout and WT mice in the presence of α-methyl-p-tyrosine, a DA synthesis inhibitor. Additionally, the stimulated release of reserve pool DA, mobilized by cocaine, was measured. Both efflux and stimulated release measurements where enhanced in slices from knockout mice suggesting that these mice have greater reserve pool DA stores than WT and that these stores are effectively

mobilized. Moreover, differences in release were likely not caused by altered calcium response or a difference in the levels of DAT protein molecules.

1. Introduction

The abnormal regulation of DA has been associated with multiple neurodegenerative disease states (Bird & Iversen, 1974; Morgan, May, & Finch, 1987), yet the role of DA reserve pool storage and mobilization in the pathophysiology is now just being revealed. For example, previous studies have shown that in Huntington's disease (HD) model R6/2 mice stimulated DA release is impaired and the number of DA reserve pool vesicles is diminished (Ortiz, Kurth, Osterhaus, & Johnson, 2010). Basal levels of striatal DA in this mouse model are 40% less than respective control mice (Johnson, Rajan, Miller, & Wightman, 2006). Theoretically, the overall amount of DA within presynaptic terminals may be dependent upon the overall number of vesicles.

A key trigger for exocytosis is calcium (Nachshen & Sanchez-Armass, 1987) and presynaptic DA release is dependent on available calcium (Kume-Kick & Rice, 1998). The movement between neurotransmitter release-ready vesicle pools and reserve pools is also thought to require calcium (Rose et al., 2002). In addition, plasma membrane calcium ATPase modulates calcium levels associated with neurotransmitter release (Palacios, Sepulveda, Lee, & Mata, 2004). In aging tissues, the activity of the calmodulin, a calcium regulatory protein, decreases when acting on the plasma membrane calcium ATPase (Michaelis et al., 1996). The oxidation of specific Met in calmodulin results in about a 50% reduction of plasma membrane calcium ATPase activation (Bartlett et al., 2003). Oxidized calmodulin can accumulate in brain tissues as a result of low antioxidant levels and it is speculated that oxidation of Met on calmodulin may be acting as a molecular switch in calcium regulation and oxidative stress (Bigelow & Squier, 2005). Furthermore, oxidants can modulate synaptic DA release and this regulation is dependent on the available calcium (Chen, Avshalumov, & Rice, 2001). In contrast,

Met oxidation of calcium/calmoduilin kinase II can cause calcium-independent activation of calcium channels (Erickson et al., 2008). Moreover, neuronal activity and blocking calcium channels can regulate DAT function via calcium/calmoduilin kinase II signaling (Padmanabhan & Prasad, 2009).

Here, we used FSCV at carbon-fiber microelectrodes to study the mobilization and efflux of reserve pool DA in striatal brain slices from *MsrA*$^{-/-}$ mice and WT control mice. In order to measure reserve pool DA, brain slices were treated with alpha-methyl-p-tyrosine (aMPT), a DA synthesis inhibitor, and then with amphetamine (AMPH), which induces DA efflux. To measure exocytotic DA release from mobilized reserve pool vesicles, slices were treated with aMPT and then cocaine (COC), which mobilizes reserve pool vesicles. Stimulated DA release was then measured. There were no differences in DAT levels and calcium regulation, suggesting that DA in reserve pool vesicles accumulate in the *MsrA*$^{-/-}$ striatum.

2. Materials and Methods

Animals

The *MsrA*$^{-/-}$ and WT control mice have been described previously (Moskovitz et al., 2001). All mice used in these experiments were fed *ad libitum*, housed with 12 h of light per day, and caged individually. All procedures and conditions of live mice, including euthanasia, were approved by the University of Kansas Institutional Animal Care and Use Committee.

Brain Slice Preparation

Brain slices of 12-week-old *MsrA*$^{-/-}$ mice and age-matched WT mice were prepared as previously described (Johnson et al., 2006). Mice were anesthetized by isoflurane inhalation and then decapitated. The brain was immediately removed and placed in ice cold artificial cerebrospinal fluid (aCSF) consisting of (mM): NaCl 126, KCl 2.5, NaH_2PO_4 1.2, $CaCl_2$ 2.4, $MgCl_2$ 1.2, $NaHCO_3$ 25, HEPES 20, and D-Glucose 11. Using 1 M HCl, the pH of the aCSF was

adjusted to 7.4. The cerebellum was removed from the brain using a razor blade and the brain was then mounted on an aluminum block. A vibratome slicer (Leica, Wetzlar, Germany) was used to make 300 µm thick coronal slices. Each brain slice was equilibrated in the superfusion chamber which was maintained at 34℃, through which aCSF flowed at a continuous rate of 2 mL/min, prior to obtaining measurements.

DA Release in Brain Slices

Caron-fiber microelectrodes were fabricated using a single 7 µm diameter carbon-fiber (Goodfellow Cambridge Ltd, Huntingdon, U.K.) that was aspirated through a glass capillary tube (1.2 mm outer diameter, 0.68 mm inner diameter, 20 mm long, A-M Systems, Inc. Carlsborg, WA), and was pulled using a heated coil puller (Narishige International USA, Inc., East Meadow, NY) (Kraft, Osterhaus, Ortiz, Garris, & Johnson, 2009). The carbon-fiber was trimmed to about 25 µM and further insulated using with epoxy resin (EPON resin 815C, EPIKURE 3234 curing agent, Miller-Stephenson, Danbury, CT, USA), and then cured at 100°C for 1 h. The electrodes were backfilled with 0.5 M potassium acetate to provide an electrical connection between the carbon fiber and an inserted silver wire.

A triangular waveform was applied to the carbon-fiber electrode starting at -0.4 V, increasing to +1.0 V, and then back down to -0.4 V. A scan rate of 300 V/s and an update rate of 60 V/s were used. A headstage amplifier (UNC Chemistry Department Electronics Design Facility, Chapel Hill, NC) was interfaced with a computer via a breakout box and custom software provided by R.M. Wightman and M.L.A.V. Heien (University of North Carolina, Chapel Hill). A Ag/AgCl reference electrode consisted of a choridated silver wire. The carbon fiber microelectrode was inserted 100 µm into the dorsolateral caudate-putamen region of the striatum between the prongs of a bipolar stimulation electrode (Plastics One, Roanoke, VA), which was separated by a distance of 200 µm. A single pulse at 60 Hz was applied to the brain slice and the current was then measured at the peak oxidation potential for DA (about +0.6 V

versus Ag/AgCl reference electrode). Working electrodes were calibrated with DA standards of known concentration in a flow cell before and after each use. The average of pre- and post-calibration measurements was used as the calibration factor.

After a location with stable DA release was found, 50 µM aMPT was added into the aCSF using a three-way valve. Stimulated DA release was measured every 5 min until the DA release diminished. Once the DA release was diminished 20 µM AMPH was added to the aCSF/aMPT solution. A 25 min long file was then collected using a scan rate of 300 V/s and an uptake rate of 5 V/s.

In order to mobilize DA reserve pools, a similar study was done using aMPT and COC. The slice was perfused with of 50 µM aMPT and stimulated DA release was measured every 5 min until the DA release was diminished. Next, 20 µM COC was added to the slice and a single-pulse stimulation was continuously applied every 5 min and the reserve pool DA was measured.

Calcium sensitivity of DA release

To measure changes in the sensitivity to calcium in *MsrA*$^{-/-}$ mice the slices were treated with aCSF that contained 0 mM calcium. Once the DA release was diminished, the brain slices were treated with aCSF containing 0.6, 1.2, 1.8, and 2.4 mM calcium. Each concentration was exposed to the slice for 15 min, with files collected every five 5 min using a single pulse stimulation.

Immunoblotting

MsrA$^{-/-}$ and WT brains were dissected from post-mortem mice. Each cerebrum was placed in a glass tube and homogenized with Teflon in 50 mM HEPES buffer pH 7.4 plus protease inhibitors (Roche) at 4℃. Homogenized extract was centrifuged for 20 min to separate the membrane fraction. Buffer containing 50 mM HEPES, 0.62% CHAPS, and 150 mM NaCl was added to each membrane fraction and agitated for 30 min. Each fraction was centrifuged for 20

min. Protein concentration of the supernatant was determined by BCA Protein Assay Kit (Pierce). Equal protein amounts (20 µg) of each soluble membrane fraction was loaded into a HEPES 4-20% Protein Gel (Pierce) and submitted to electrophoresis. Proteins were transferred to a nitrocellulose membrane and blocked overnight in 5% dry milk in buffer. Protein was detected using rabbit anti-DAT antibody (1:1000; Chemicon). Primary antibodies were detected by horseradish peroxide-conjugated goat-anti-rabbit secondary antibodies (1:2000; Bio-Rad). Protein bands were visualized by chemiluminescent substrate and exposure to autoradiography film. Densitometry analysis was done using ImageJ software (NIH).

Statistical Analyses

Data were analyzed by ANOVA or students t-test. All numerical values are represented as mean ± SEM.

3. Results

Reserve Pool DA Levels

It has been previously demonstrated that, in *MsrA*$^{-/-}$ mice, stimulated DA release evoked by a single-pulse electrical stimulation is significantly higher than WT controls (D. B. Oien, Osterhaus et al., 2008). To determine if reserve pool DA is similarly more abundant in 12-month-old *MsrA*$^{-/-}$ mice, striatal brain slices were subjected to treatment with aMPT and AMPH induced efflux was measured. Each slice was treated with 50 µM aMPT to inhibit tyrosine hydroxylase, the rate limiting enzyme in DA synthesis. A stimulus pulse was then applied to the slice every 5 min until the DA release was diminished. At this point, DA remaining in terminals consisted of reserve pool DA. The slices were then exposed to 20 µM AMPH, a competitive DAT inhibitor that causes DA efflux from vesicles inside the pre-synaptic terminals. AMPH enters the pre-synaptic terminals in one of two ways: either by lipophilic diffusion through membranes or by passage through DAT protein molecules (Fischer & Cho, 1979; Liang & Rutledge, 1982). AMPH also

displaces vesicular DA into the cytoplasm where it can be released by reverse transport caused when AMPH enters through the DAT causing allosteric translocation of the transporters (Chiueh & Moore, 1975; Jones, Gainetdinov, Wightman, & Caron, 1998b). The AMPH induced efflux of DA was measured over the course of 25 min and the amplitude of the DA peak ($[DA]_{AMPH}$) was used to determine the amount of DA released (Fig.1a). In 12-month-old *MsrA*$^{-/-}$ mice there was a significant increase in the amount of AMPH-induced DA efflux after treatment with aMPT (Fig. 1b; $P = 0.022$; *MsrA*$^{-/-}$, 7.02 ± 1.42 µM, n = 5 mice; WT, 5.63 ± 0.33 µM, n = 4).

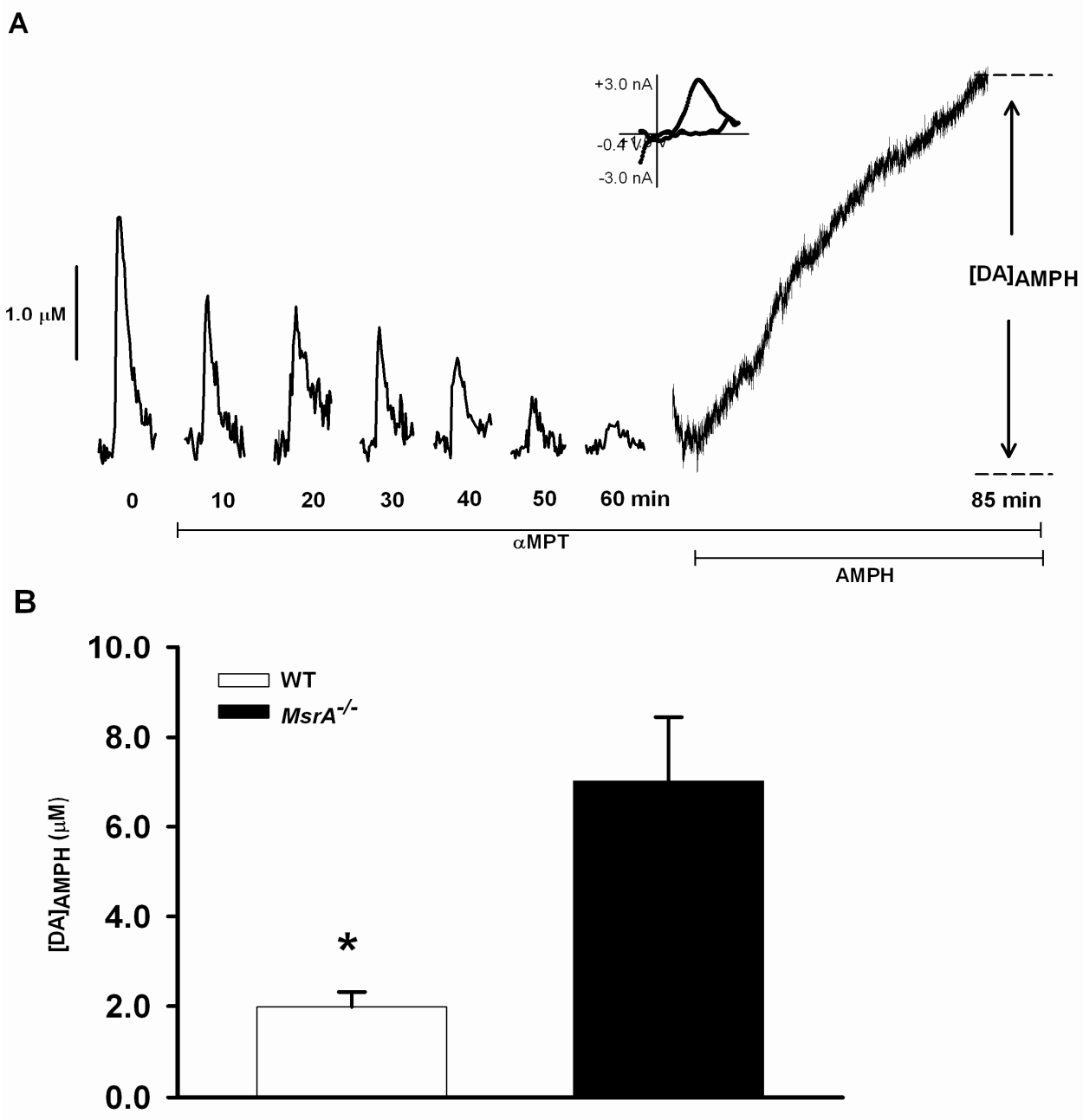

Figure 1. AMPH induced DA efflux is increased in 12-month-old *MsrA*$^{-/-}$ mice in comparion with age-matched WT mice. A) Representative data from 12-month-old WT mice. The brain slice was exposed to 50 μM aMPT while applying a single stimulus pulse every 5 min until the DA release diminished. The slice was then exposed to 20 μM AMPH for 25 min, and $[DA]_{AMPH}$ was measured. A CV is provided from the time of peak release, and confirms the release of DA.

B) In 12-month-old *MsrA*$^{-/-}$, $[DA]_{AMPH}$ is significantly higher than in WT mice ($^{*}P = 0.022$; *MsrA*$^{-/-}$, 7.02 ± 1.42 µM, n = 5 mice; WT, 5.63 ± 0.33 µM, n = 4).

Mobilization of Reserve Pool DA

To determine if the DA reserve pools mobilize differently in 12-month-old *MsrA*$^{-/-}$ mice compared to age-matched WT mice, aMPT and COC was used. COC has previously been shown to mobilize reserve pool DA (Venton et al., 2006). Using a single electrical stimulus pulse, DA release was measured using FSCV (Fig. 2a). Once the DA release was constant, 50 µM aMPT was added to the brain slice in order to stop DA synthesis and the slice was continuously stimulated every 5 min. After the DA release was diminished, 20 µM COC was added into the aMPT/aCSF solution and the slice continued to be stimulated every 5 min. This caused the DA release to reappear for a longer amount of time in the *MsrA*$^{-/-}$ mice then in the WT mice (Fig. 2b). The WT slices were treated for a shorter amount of time (90 min) after the addition of COC compared to *MsrA*$^{-/-}$ mice (120 min; Fig. 2b), but there was not a significant difference in the peak DA release between the two sets of mice.

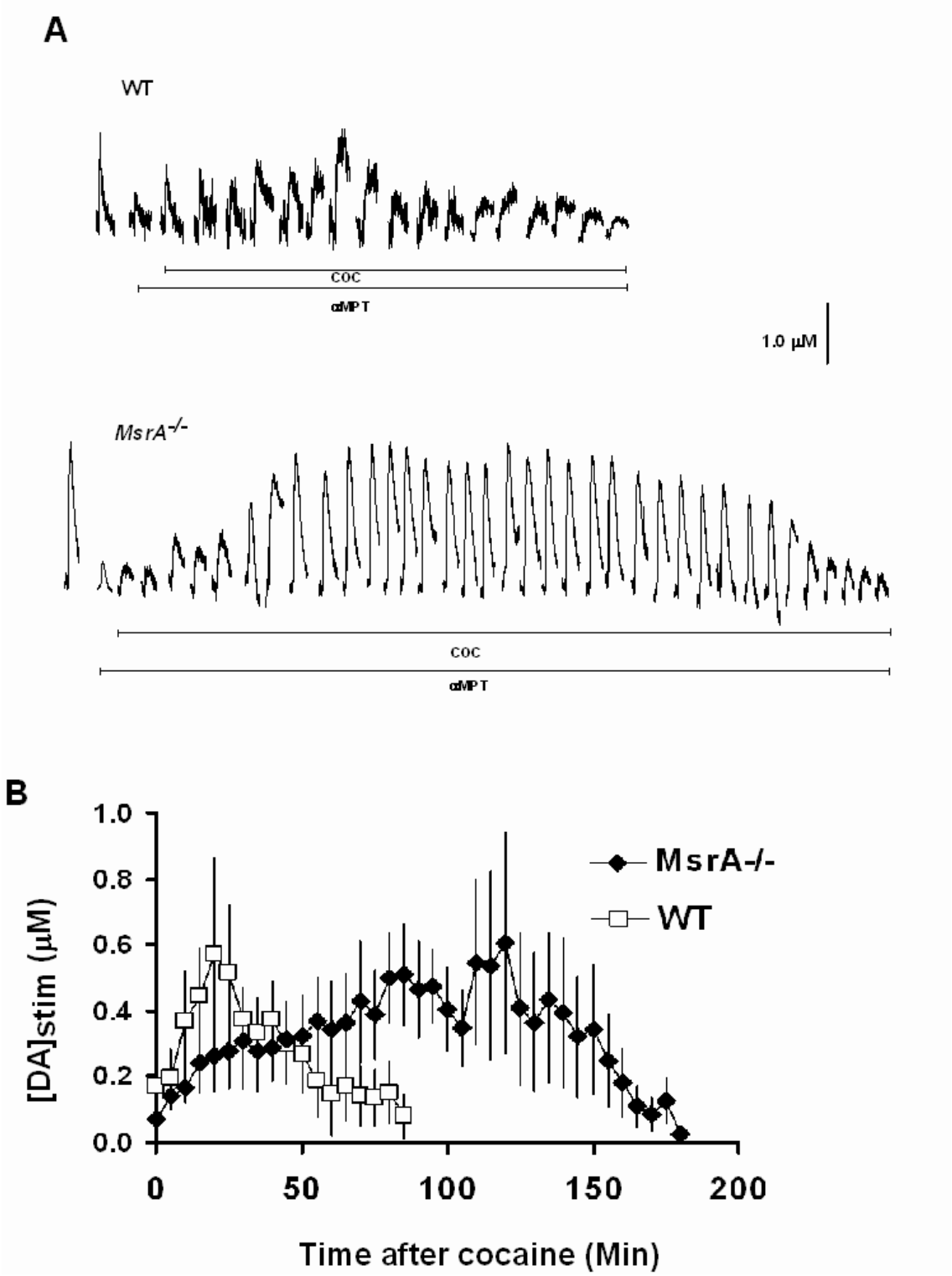

Figure 2. The mobilization of reserve pools lasts for a longer duration of time in *MsrA*$^{-/-}$ mice in comparion with WT mice. Slices from 12-month-old *MsrA*$^{-/-}$ and WT mice were exposed to 50 µM aMPT while applying a single-pulse stimulus every 5 min. Once the DA

release disappeared, 20 μM COC was added to the slice and the application of a single-pulse stimulation continued to be applied every 5 min to the brain slice. **A)** Representative data from *MsrA*$^{-/-}$ and WT slices. The addition of COC after pretreatment with aMPT resulted in an increase in stimulated DA release. Stimulated plots taken immediately after the addition of aMPT, during the time that DA release was diminished have been omitted for clarity. **B)** Pooled data from *MsrA*$^{-/-}$ and WT mice after the addition of COC. Each data point represents the average value (± SEM) of [DA]stim obtained from 5 *MsrA*$^{-/-}$ mice and 6 WT mice.

DAT Protein Levels

The DAT is a transmembrane protein that moves DA from the synaptic cleft into the presynaptic neuron. It is also well known to interact with COC and AMPH. In membrane fractions of *MsrA*$^{-/-}$ and WT mice, no difference in DAT protein levels was detected (Fig. 3). These data are consistent with a previous report that showed synaptic DA clearance was similar between *MsrA*$^{-/-}$ and WT mice (Oien et al., 2008).

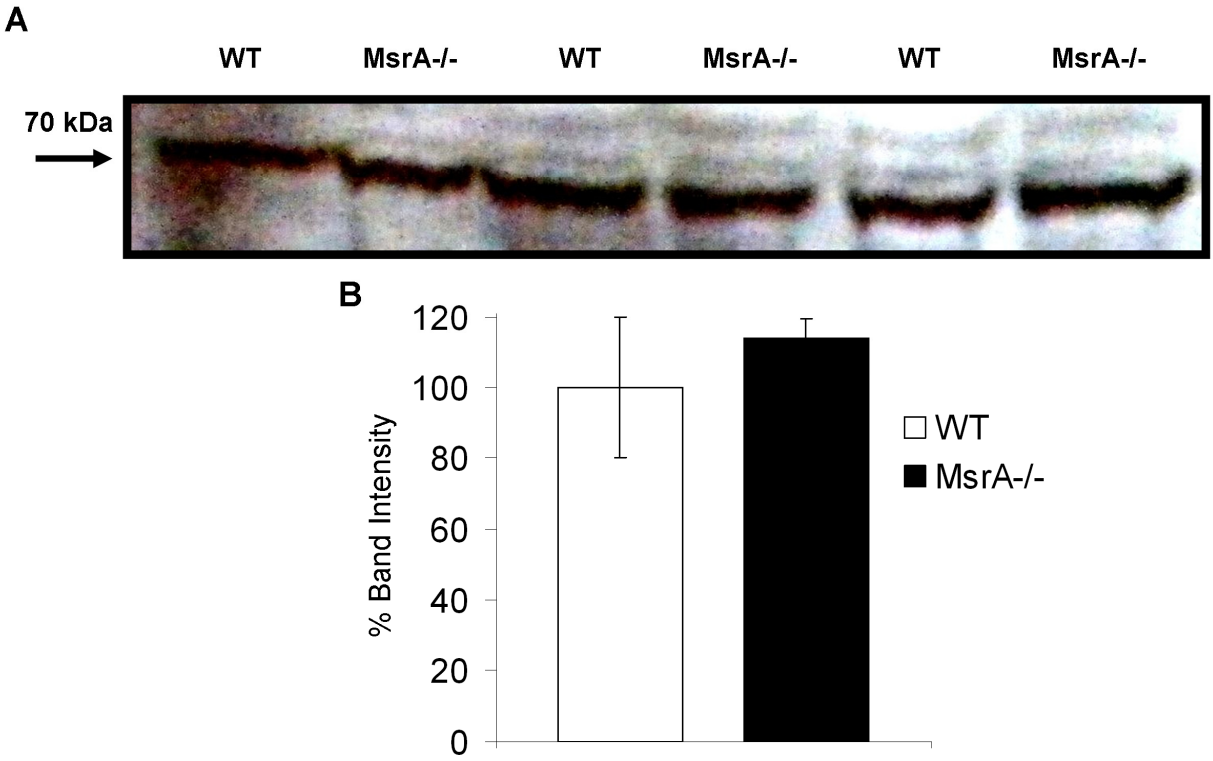

Figure 3. DAT protein levels are unchanged in *MsrA*$^{-/-}$ mice. *MsrA*$^{-/-}$ and WT cerebral membrane fractions were solubilized and equal amounts of protein were separated by gel electrophoresis. **A)** Protein bands detected by anti-DAT antibodies indicate similar amounts of the protein at about 70 kDa. **B)** Densitometry of protein bands shown as an average density from *MsrA*$^{-/-}$ (*black*) and WT (*white*) bands. Error bars represent SEM.

Extracellular Calcium Sensitivity

Calcium levels are associated with the movement of vesicles between storage pools (Rose et al., 2002), change the ability of oxidants to modulate synaptic DA release (Chen et al., 2001), and can interfere with DA release measurements by FSCV (Jones, Mickelson, Collins, Kawagoe, & Wightman, 1994). In order to evaluate whether calcium-dependent release was altered in 12-month-old *MsrA*$^{-/-}$ mice, brain slices were treated with various concentrations of extracellular calcium and the stimulated DA release was measured (Fig. 4). DA release was normalized to the peak DA release at 2.4 mM calcium. DA release was not detected in the absence of calcium. At all calcium concentrations used there was not a significant difference in DA release between the *MsrA*$^{-/-}$ and WT mice (Fig. 4; $P > 0.05$; MsrA$^{-/-}$, n = 4 mice, WT, n = 6 mice).

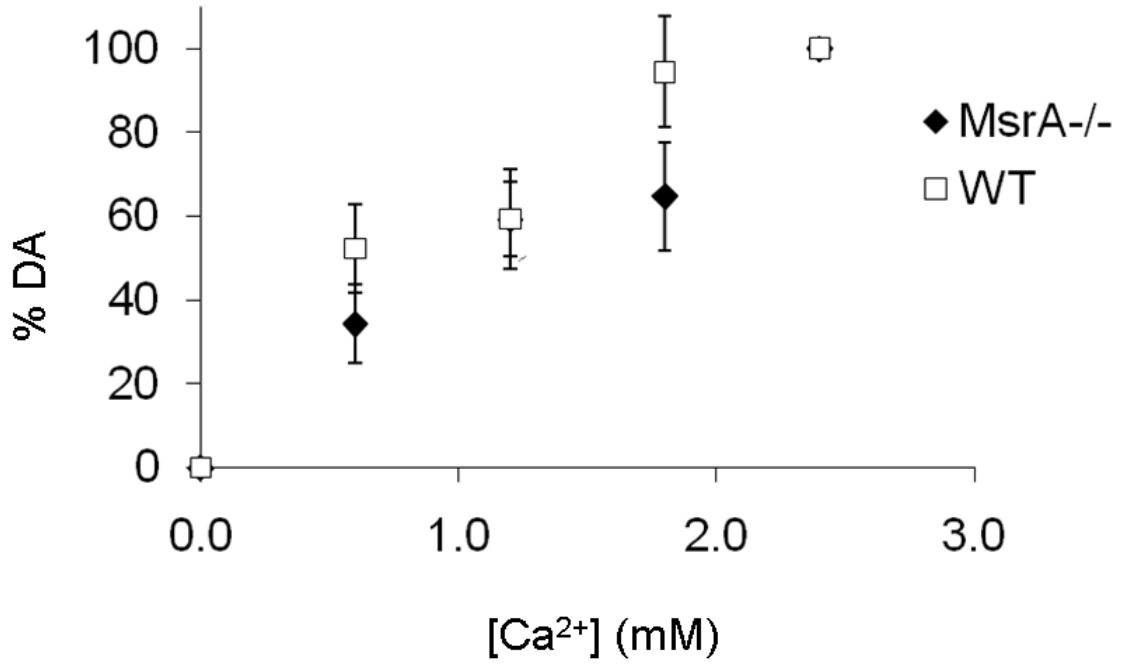

Figure 4. Calcium-dependent release was unchanged in 12-month-old *MsrA*$^{-/-}$ mice in comparion with age-matched WT mice. Brain slices were treated with 0, 0.6, 1.8, and 2.4 mM concentrations of extracellular calcium and the stimulated DA release was measured for 15 min at each concentration. DA release was normalized to the peak DA release at 2.4 mM calcium. At 0 mM calcium no DA release was detected. At all calcium concentrations used there was not a significant difference in DA release between the *MsrA*$^{-/-}$ and WT mice ($P > 0.05$; MsrA$^{-/-}$, n = 4 mice, WT, n = 6 mice).

4. Discussion

Previous studies using *MsrA*$^{-/-}$ have shown that DA release evoked using a single-pulse stimulation is increased (D. B. Oien, Osterhaus et al., 2008). This is in contrast to 12-week-old R6/2 mice where the stimulated release was inhibited, as was the amount of vesicles in the reserve pool (Ortiz et al., 2010). In this study, differences in DA reserve pool storage and mobilization in striatal brain slices from *MsrA*$^{-/-}$ mice were examined. AMPH-induced DA efflux was increased in 12-month-old *MsrA*$^{-/-}$ brain slices after treatment with aMPT compared to age-matched WT mice. Furthermore our data suggest that a greater amount of DA reserve pool vesicles were mobilized after COC treatment in *MsrA*$^{-/-}$ mice compare to WT controls. Thus, a greater number of reserve pool vesicles are present in the *MsrA*$^{-/-}$ striatum and it is possible to make a correlation between the amount of RRP DA and the reserve pool DA. Enhanced DA release likely did not arise either from altered sensitivity to extracellular calcium or from a change in the number of DAT protein molecules.

Experiments were aimed at determining if alterations in either DAT or calcium regulation preferentially enhance release in *MsrA*$^{-/-}$ mice. A previous report suggested that the efficiency of DA reuptake by DAT is similar in *MsrA*$^{-/-}$ and WT mice (D. B. Oien, Osterhaus et al., 2008). The data used to support this conclusion was based on similar FSCV measurements after *in vitro* stimulation. Furthermore, here we show that DAT protein levels are similar in *MsrA*$^{-/-}$ and WT mice (Fig. 3). This result further supports the concept that DAT function and protein levels are not altered in the absence of *MsrA*. Therefore, we predict that COC and AMPH effects on the DAT would be similar in both mice genotypes.

Calcium modulation can affect oxidant regulation of DA release (Chen et al., 2001) and movement between RRP and reserve pools (Rose et al., 2002). The release of DA during synaptic transmission is mediated by calcium-dependent fusion with the active zone (Kavalali, 2006). An increase in the intrasynaptic calcium levels causes the vesicles to fuse to the active site, where DA is released and then the vesicles collapse onto the plasma membrane (Heuser

and Reese, 1973; Cremona and De Camilli, 1997). Furthermore, Met oxidation of calcium regulatory proteins, such as calmodulin (Michaelis et al., 1996) and calcium/calmodulin kinase II (Erickson et al., 2008), would suggest that this is associated with the increase of DA reserve pools in the *MsrA*$^{-/-}$ mice (Figs. 1 & 2). By changing the extracellular calcium concentrations, the lack of significant differences between *MsrA*$^{-/-}$ and WT mice suggests that calcium regulatory proteins in both mice are functioning in a similar manner (Fig. 4). Furthermore, the similarity of measurements between both mouse types is important for the integrity of FSCV measurements of DA release (Jones et al., 1994; Kume-Kick & Rice, 1998) and the normal functioning of DAT. The DAT function and abundance is dependent on calcium and calcium/calmodulin kinase II (Padmanabhan & Prasad, 2009). Also, the AMPH-induced efflux of DA through the DAT is associated with calcium levels and calcium/calmodulin kinase II activity (Kantor, Zhang, Guptaroy, Park, & Gnegy, 2004). Overall, the lack of changes in *MsrA*$^{-/-}$ DAT (Fig. 3 & Oien et al., 2008b) and calcium regulation (Fig. 4) support our DA reserve pool studies (Figs. 1 & 2), and further narrow down the possibilities of an underlying mechanism for DA associated abnormalities in *MsrA*$^{-/-}$ mice.

The DA reserve pools were examined using various pharmacological agents. Treating the brain slices with aMPT coupled with electrical stimulation depletes the DA in the RRP vesicles, and DA in the extracellular space will be packaged and also released, leaving only DA in the reserve pool vesicles (Ortiz et al., 2010). Upon the addition of AMPH, the DAT is reversed and the DA in the reverse pool vesicles is leaked out and we are able to measure the DA efflux. We found that 12-month-old *MsrA*$^{-/-}$ mice have an increased AMPH induced DA efflux after treatment with aMPT, indicating that *MsrA*$^{-/-}$ mice have an increased supply of reserve pool dopamine. This increase parallels both the enhancement of stimulated DA release and the increase in striatal DA content found previously in *MsrA*$^{-/-}$ mice (D. B. Oien, Osterhaus et al., 2008).

COC was also used to mobilize the reserve pool DA. COC is commonly known to block the DAT and inhibit DA uptake. By treating the slices with aMPT and COC the differences in DA release in the *MsrA*$^{-/-}$ and WT mice would arise from differences in the number of reserve pool vesicles. The peak DA release evoked by single-pulse stimulation after treatment with aMPT and COC is the same between the *MsrA*$^{-/-}$ and WT mice, implying that there are the same number of DA molecules contained in each mobilized reserve pool vesicle. Additionally, because the peak DA release is attained earlier in WT mice than in MsrA$^{-/-}$ mice, impaired mobilization of reserve pool vesicles in the *MsrA*$^{-/-}$ cannot be ruled out.

One potential cause of increased stimulated DA release found previously in *MsrA*$^{-/-}$ mice is a mechanism by which enhanced reserve pool DA levels result incease the number of vesicles available for stimulated DA release. Vesicles containing DA are thought to be in one of three distinct vesicle pools: the RRP, the recycling pool, and the reserve pool. On average, within presynaptic terminals, the RRP consists of 1-2% of the total vesicles. In contrast, the reserve pool makes up about 80 to 90% of vesicles (Neves & Lagnado, 1999; Zucker & Regehr, 2002). Thus, the large amount of reserve pool DA vesicles could be transferred into the RRP, which then undergoes exocytosis upon application of a mild electrical stimulus pulse applied by our electrochemical system. This mild pulse is intended to simulate the occurrence of a natural action potential; therefore, this increase in reserve pool vesicles likely enhances naturally occurring DA release events in *MsrA*$^{-/-}$ mice.

The mechanism of the chronically increased DA levels in *MsrA*$^{-/-}$ mice is still unknown. The abnormally high brain DA in *MsrA*$^{-/-}$ mice can be alleviated by caloric restriction (D. B. Oien et al., 2010), suggesting metabolism and oxidative stress related mechanisms are involved in this phenomenon. Previous studies suggest an increase of the tyrosine hydroxylase activating protein 14-3-3zeta mRNA (D. Oien, Wang et al., 2008) and protein (D. B. Oien, Osterhaus et al., 2008) may be associated with the increased levels of DA by enhanced DA synthesis. In addition, we have recently reported that Met oxidation of the dopamine D2 receptor may

participate in DA signaling in *MsrA*$^{-/-}$ mice (Derek B. Oien et al., In Press-b), which may include the presynaptic D2 autoreceptor isoform. Another possible explanation for this abnormal DA regulation is increased methionine sulfoxide levels in alpha-synuclein that may interfere with its interaction with DA (D. B. Oien & Moskovitz, 2008; D. B. Oien, Shinogle, Moore, & Moskovitz, 2009a; Outeiro et al., 2009). This theory is further supported by defective mobilization of DA from reserve pools in alpha-synuclein knockout mice and A30P mutated alpha-synuclein transgenic mice (Yavich et al., 2005; Yavich, Tanila, Vepsalainen, & Jakala, 2004).

In summary, the increased AMPH induced efflux in *MsrA*$^{-/-}$ mice after treatment with aMPT in 12-month-old mice, versus age-matched WT mice, indicates that *MsrA*$^{-/-}$ mice have more striatal reserve pool DA. The stimulated release of reserve pool DA, mobilized by treatment with COC, was longer lasting in *MsrA*$^{-/-}$ slices compared to WT slices, indicating that *MsrA*$^{-/-}$ mice have a greater number of DA reserve pool vesicles. Thus, this study identifies *MsrA*$^{-/-}$ mice as a model of neurodegeneration in which the DA system is overactive.

E. D2DR Function is Compromised in the Brain of the MsrA Knockout Mouse

(DB Oien et al., In Press-a)

Previous research suggests that brain oxidative stress and altered rodent locomotor behavior are linked. We observed bio-behavioral changes in *MsrA*$^{-/-}$ mice associated with abnormal DA signaling. Compromised ability of these knockout mice to reduce MetO enhances accumulation of sulfoxides in proteins. We examined the D2DR function and expression, which has an atypical arrangement and quantity of Met residues. Indeed, protein expression levels of D2DR were higher in knockout mice compared with WT. However, the binding of D2DR agonist was compromised in the same fractions of knockout mice. Coupling efficiency of D2DR to G-proteins was also significantly reduced in knockout mice, supporting the compromised agonist binding. Furthermore, presynaptic DA release in knockout striatal sections was less responsive than control sections to D2DR ligands. Behaviorally, the locomotor activity of knockout mice was less

responsive to the inhibitory effect of quinpirole than WT mice. Involvement of specific Met residue oxidation in the D2DR third intracellular loop is suggested by *in vitro* studies. We conclude that ablation of Msr can affect DA signaling through altering D2DR physiology and may be related to symptoms associated with neurological disorders and diseases.

1. Introduction

The *MsrA*$^{-/-}$ mouse exhibits age-dependent lower locomotor activity and abnormal gait indices (D. B. Oien, Osterhaus et al., 2008) relative to control mice. Lower DA levels are associated with altered motor performance (Carlsson, Bjorklund, & Kirik, 2007). Surprisingly, our recent observations showed that *MsrA*$^{-/-}$ brains in adult mice contained significantly higher levels of DA (D. B. Oien, Osterhaus et al., 2008). Moreover, presynaptic neuronal DA in *MsrA*$^{-/-}$ striatal slices is released at higher DA pulses than WT slices as measured by FSCV. These results raise the possibility that DA function is impaired in *MsrA*$^{-/-}$ mice. Moreover, *MsrA*$^{-/-}$ mice were less responsive to amphetamine treatment as assayed by locomotor activity and stereotypy, suggesting alteration of DA signaling. Dysfunctions of the corpus striatum and dopaminergic signaling are linked to a range of disorders including Parkinson's disease (Hornykiewicz, 1962), Huntington's disease (Hickey, Reynolds, & Morton, 2002), schizophrenia, and obsessive-compulsive disorder (Saxena, Brody, Schwartz, & Baxter, 1998).

The observed *MsrA*$^{-/-}$ locomotor deficits and DA abnormalities prompted us to further examine DA signaling events that are associated with striatal movement pathways. The dopamine D1 receptor (D1DR) and D2DR are closely associated with movement regulation, and theoretically are the DA receptors most related to the *MsrA*$^{-/-}$ locomotor phenotypes (D. B. Oien, Osterhaus et al., 2008). Additionally, D2DR is also expressed in its short form ($D2DR_S$) that serves as an autoreceptor for dopaminergic neurons. Thus, Met oxidation in either the long form of D2DR or $D2DR_S$ or a combination of both may be related to the elevation in DA levels observed in *MsrA*$^{-/-}$ brains (D. B. Oien, Osterhaus et al., 2008). In the current study we

investigate the ligand-binding capabilities of DA receptors and their coupling efficiency to G-proteins in *MsrA*$^{-/-}$ versus WT mice. The presented data support the hypothesis that MetO modification to D2DRs participates in the *MsrA*$^{-/-}$ behavioral and biochemical phenotypes.

2. Materials and Methods

Materials

The radioligands [^{3}H]SCH23390 (85 Ci/mmol), [^{3}H]raclopride (84 Ci/mmol), [^{3}H]quinpirole (50 Ci/mmol), were purchased from Perkin Elmer. Non-radioactive sulpiride, quinpirole, SKF82958, and GTPγS were purchased from Sigma. Mouse and goat antibodies against D2DR were purchased from Abcam. Mouse β-actin antibodies were purchased from Molecular Probes.

Mice

Mice used in these studies were WT (C57BL6/129 Sv) and *MsrA*$^{-/-}$ on the same genetic background at an age of 6-8 months unless otherwise noted. Both types of mice were littermates born to *MsrA*$^{+/-}$ heterozygous parents (Moskovitz et al 2001). All procedures using mice were performed within guidelines of the NIH and KU Institutional Animal Care and Use Committee.

Immunohistochemistry analysis

Coronal brain sections from 12-month-old WT and *MsrA*$^{-/-}$ mice were processed as 20 µm-thick brain sections. Sections were treated with 3% H_2O_2 in methanol for 30 min. After blocking with 1% bovine serum albumin and 3% horse serum in PBS, the sections were incubated for 24 h with primary goat antibodies against D2DR (1:500 dilution, stock concentration of 1.5 mg/mL). Sections were then incubated with biotinylated mouse anti-goat IgG antibodies (Santa Cruz Biotechnology), avidin–horseradish peroxide solution, 0.015% diaminobenzidine, 0.001% H_2O_2,

and finally counterstained with hematoxylin. The brain slides were washed, dehydrated, mounted, and visualized using a brightfield microscope with a 100X objective lens.

Immunoblot analysis

Equal amounts of striatal membranal protein extracts or cytosolic brain proteins (extracted as described below for receptors fraction) were subjected to SDS-gel electrophoresis. Immunoblot analyses with anti-goat D2DR antibodies (1:1000 dilution, stock concentration of 1.5 mg/mL) were performed according to common procedures. β-actin (loading control) was detected by primary anti-β-actin mouse antibodies.

Antagonists and agonists binding of D1DR and D2DR ligands

Saturation curves of receptor binding were determined by using the common membrane filtration assay (Bylund & Toews, 1993). Briefly, brains (striatal region of each mouse type) were dissected and glass-Teflon homogenized in PBS with protease inhibitor cocktail (Roche). Following centrifugal precipitation at 20,000xg for 20 min, the supernatant was removed and saved (cytosolic fraction in immunoblots), and the membranal pellet was washed and precipitated again by centrifugation. Final pellet was homogenized in 1.0 mL of 50 mM Tris pH 7.4. Membranal protein fractions of 100 µg were used per assay, determined by BCA Protein Assay Kit (Thermo Scientific). Total ligand binding was determined following incubation of membranal fractions with incrementing concentrations of radioligand for 2 h at room temperature. Non-specific ligand binding was determined using the same conditions with the addition of non-radioactive ligands, 1 mM DA for D1DR and 1 µM sulpiride for D2DR. Bound radioligand was separated using a Brandel harvester (Brandel). Radioligand bound to the filter was measured by liquid scintillation counting. Specific ligand binding values were calculated by subtracting non-specific ligand binding from total ligand binding. The ligands used in the tests were: [^{3}H]SCH23390 and [^{3}H]raclopride as D1DR and D2DR antagonists, respectively, and

[^{3}H]quinpirole as a D2DR agonist. The range for radioactive materials used was between 0.03-4.0 nM (increments by serial dilution).

The effect of MsrA enzyme on quinpirole and raclopride binding was tested by using recombinant yeast MsrA (10 µg) (Moskovitz, Berlett, Poston, & Stadtman, 1997) with 15 mM dithiothreitol (DTT; this alone did not affect binding). D1DR binding to the agonist SKF82958 was determined using the same conditions above, except for the addition of 2 nM [^{3}H]SCH23390 to quantify the competitive binding of non-radiolabeled SKF82958 ligand (performed due to limited sources of commercially available radiolabeled D1DR agonists).

GTPγS-induced inhibition of radiolabeled quinpirole binding to D2DR

The ability of agonists to stimulate the dissociation of GDP and association of GTP from G-protein was assessed using GTPγS, a non-hydrolyzable analogue of GTP (Y. Zhang et al., 2001). When the agonist binds to the receptor, GDP is released from the G-protein and GTPγS binds (Harrison & Traynor, 2003). The G-protein uncoupling on [^{3}H]quinpirole binding to the D2DR was investigated by measuring the inhibition of [^{3}H]quinpirole binding at incrementing GTPγS concentrations. The membrane portion of homogenized striatal regions were isolated and lysed in 5 mM Tris buffer by glass-Teflon homogenation. Membranal extracts (30 mg/mL; 80 µg per assay) were incubated with [^{3}H]quinpirole (1 nM) and GTPγS (0.1, 1, 10, 100, and 1000 nM) in 50 mM Tris buffer for 2 h at room temperature in a total volume of 1 mL. To determine non-specific binding, identical assays were performed in the presence of sulpiride (1 µM; racemic mixture). Unbound ligand was removed by Brandel filtration and the remaining bound ligand was quantified by liquid scintillation counting.

Stimulated release of DA in striatal brain sections in the presence of quinpirole and sulpiride measured by FSCV

Brain sections were prepared as previously described (Johnson et al., 2006). Mice were anesthetized by isoflurane inhalation. The brain was immediately removed and placed in ice cold artificial CSF. Artificial CSF consisted of 126 mM NaCl, 2.5 mM KCl, 1.2 mM NaH_2PO_4, 2.4 mM $CaCl_2$, 1.2 mM $MgCl_2$, 25 mM $NaHCO_3$, 20 mM HEPES, and 11 mM D-Glucose at pH 7.4 and was continuously saturated with 95% O_2/5% CO_2 throughout the experiment. Coronal sections of 300 µm in thickness were made using a vibratome slicer (Leica). A single section was placed in the superfusion chamber with artificial CSF flowing at 34°C and a continuous rate of 2 mL/min. Each brain section was equilibrated for 60 min prior to obtaining measurements. Quinpirole and sulpiride in artificial CSF were maintained in a separate reservoir and introduced through a three-way valve.

Carbon-fiber microelectrodes were fabricated as previously described (Kraft et al., 2009). A single carbon-fiber with a 7 µm diameter (Goodfellow Cambridge Ltd.) was aspirated through a glass capillary tube (1.2 mm outer diameter, 0.68 mm inner diameter, 4 inches long, A-M Systems, Inc.) and pulled using a heated coil puller (Narishige International USA, Inc.). Electrodes were trimmed to 20 µm from the glass seal, further insulated with epoxy resin (EPON resin 815C, EPIKURE 3234 curing agent, Miller-Stephenson), and then cured at 100°C for 1 h. Prior to experimentation, electrodes were backfilled with 0.5 M potassium acetate.

A triangular waveform starting at -0.4 V, increasing to +1.0 V, and scanning back to -0.4 V was applied at the carbon-fiber working electrode. A scan rate of 300 V/s was used with an update rate of 10 Hz. A head-stage amplifier (UNC Chemistry Department Electronics Design) was interfaced with a computer via breakout box and custom software provided by R.M. Wightman and M.L.A.V. Heien. A choridated silver wire was used as an Ag/AgCl reference electrode. The carbon fiber was inserted 100 µm into the dorsolateral caudate-putamen region of the striatum. The fiber was between the prongs of a bipolar stimulation electrode (Plastics One), which were separated by 200 µm. Current was measured at 0.6 V, which is the oxidation potential for DA. DA release was measured in the presence of either 1 µM quinpirole or 5 µM

sulpiride as previously described (Fawaz, Martel, Leo, & Trudeau, 2009) using a 30-pulse stimulus train at a stimulation frequency of 60 Hz. During stimulation and DA release, stabilized scans of 15 s were collected every 2 min and averaged as 4 min time blocks.

Locomotor activity measured by force-plate actometer

The force-plate actometer and methods of data analysis have been previously described (Fowler et al., 2001a). Briefly, the force-plate actometer consists of a low mass and highly stiff 5 mm thick plate (28 cm X 28 cm). This plate is supported by four Sensotec Model 31 load cells (0-250 g range). Each force plate is positioned below a Plexiglas cage that confines the mouse to the force-sensing plate and is encased in sound-attenuating cubicle. Horizontal movements of the mouse were recorded along the sensing surface with a spatial resolution of 1 mm and a temporal resolution of 0.01 s.

The duration of recording sessions was based upon preliminary experiments and relevant literature assessing spontaneous locomotor activity (Geter-Douglass, Katz, Alling, Acri, & Witkin, 1997; Usiello et al., 2000; Wang et al., 2000). The effects of the drugs used on locomotor activity were apparent within the initial period of 45 min following drug injection. Thus, 45 min periods were determined to be sufficient to monitor the locomotor response to the performed treatments. Total distance traveled per animal was measured and analyzed by 2-way ANOVA (2 mouse types) with repeated measures on the time block and session factors.

Administration of agonists of D1DR and D2DR for locomotor activity analyses

Prior to treating the mice with D1DR or D2DR agonists, the WT and *MsrA*$^{-/-}$ mice received intraperitoneal injection with 0.9% saline as a vehicle control and spontaneous locomotor activity was monitored for 45 min using force-plate actometers. After 4 days, the same mice were injected with either quinpirole (D2DR agonist, 0.1 and 0.5 mg/kg) or SKF82958 (D1DR agonist, 0.3 and 1.0 mg/kg) and locomotor activity was monitored for 45 min. A minimum of 4

days between trials was used to minimize potential carryover effects. Different sets of animals were used for each drug to prevent cross-reactivity and carryover effects between drugs. The drugs were administered at volume of 5 mL/kg.

MetO residues in recombinant long form of D2DR third intracellular loop

The long form of rat D2DR third intracellular loop ($D2DR_L$-IC_3) was expressed as a GST fusion protein in bacteria (gift from Dr. Kim Neve, Oregon Health & Science University) and purified according to published procedures (Lan, Liu, Bell, Gurevich, & Neve, 2009). The protein was oxidized overnight with 200 mM H_2O_2 and excess oxidants were removed by catalase. In parallel, oxidized protein was reduced with recombinant poly-His-tagged yeast MsrA (10 µg) (Moskovitz et al., 1997) in the presence of 20 mM DTT for 1 h at 37°C (DTT alone does not reduce MetO residues under these conditions). After reduction, all proteins (non-treated, H_2O_2-treated, and MsrA-reduced) were subjected to gel-electrophoresis followed by Commassie blue staining for the isolation of the corresponding GST-$D2DR_L$-IC_3. Bands corresponding to the predicted weight of ~54 kDa were excised and protein was isolated. The protein was subjected to tryptic digestion prior to analysis by a LCT Premier electrospray ionization tandem mass spectrometer (Waters Corp.). The mass spectrometry analyses of the peptides and their MetO content were performed according to previously published methods (L. Zhang et al., 2010).

3. Results

Expression levels and ligand binding capabilities of D2DR in $MsrA^{-/-}$ striatum

Post-mortem brain sections from *$MsrA^{-/-}$* and WT mice were immunostained with anti-D2DR antibodies. The *$MsrA^{-/-}$* striatal region exhibited higher reaction levels with the antibodies compared with this region in WT mice (Fig. 1A). D2DR expression levels were quantified by immunoblot analysis on brain extracts followed by densitometry analysis (Fig. 1B). Similar to the increase of DA in *$MsrA^{-/-}$* brains (D. B. Oien, Osterhaus et al., 2008), the upregulation of the

D2DR may be part of compensatory response for the dysfunction of the DA system in the *MsrA*$^{-/-}$ brain.

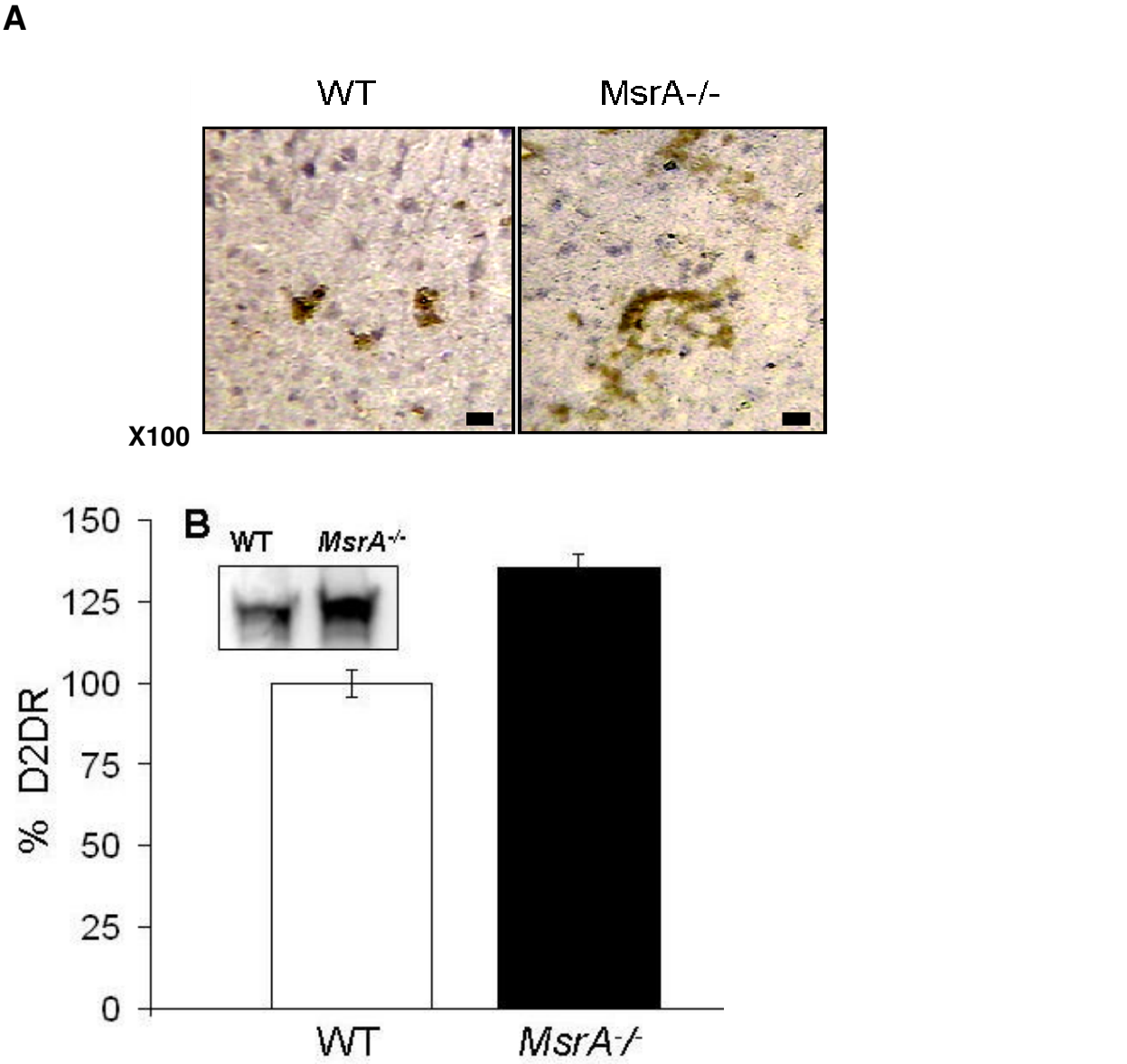

Figure 1. Immunohistochemistry and immunoblot analyses of D2DR in *MsrA*$^{-/-}$ and WT striatum. A) Immunohistochemistry of coronal brain sections using primary antibodies against D2DR. Slides were visualized using light microscope with a 100X objective lens. Brownish structures correspond to the presence of D2DR. Scale bars represent 10 µm. **B)** Immunoblot analysis using primary antibodies against D2DR. Representative bands are shown in the small window followed by densitometry analysis for the corresponding D2DR band in each extract (relative density in WT represents 100%; $P<0.01$, *t*-test). The densities of D2DR were corrected for the relative densities of β-actin.

The binding of the D2DR to appropriate ligands can reflect their expression levels and function in signaling. Binding of the D2DR antagonists are independent of G-protein coupling and more reflective of D2DR expression levels. Binding of the D2DR agonists are dependent on G-protein coupling and more reflective of D2DR function in signaling. Accordingly, the calculated Bmax value of D2DR antagonist [^{3}H]raclopride was higher in *MsrA*$^{-/-}$ membranal fractions (250 ±20 fmole/mg protein) compared with the value of WT (140 ±4 fmole/mg protein) (Fig. 2A). In addition, the Kd value for [^{3}H]raclopride in both mouse types was similar (Kd of 0.70 ±0.10 nM), suggesting no difference in the binding affinity of the bound antagonists to D2DR (it is noteworthy that the Kd values in these mice are different than rats, see "Discussion"). The [^{3}H]raclopride Bmax values also provide further supportive evidence to the observed elevated levels of the D2DR in *MsrA*$^{-/-}$ brain (Fig. 1). The calculated Bmax value of D2DR agonist [^{3}H]quinpirole was lower in *MsrA*$^{-/-}$ membranal fractions (56 ±7 fmole/mg protein) when compared with the value of the WT (140 ±10 fmole/mg protein), while the Kd value for [^{3}H]quinpirole binding was similar in both mouse types (0.40 ±0.05 nM) (Fig. 2A). These observations suggest that the coupling ability of the *MsrA*$^{-/-}$ D2DR to the respective G-proteins is compromised, in spite of the higher number of receptors in *MsrA*$^{-/-}$ mice (Fig. 1). Additionally, adding recombinant MsrA to the binding reaction mixture caused significant recovery of the *MsrA*$^{-/-}$ [^{3}H]quinpirole Bmax value to the WT Bmax value (Fig. 2B). This latter result strengthens the hypothesis that lack of MsrA enhances MetO formation in D2DR, which affects D2DR function and expression. In contrast to relative D2DR agonist-to-antagonist Bmax differences between the two mouse types (Fig. 2A & 2B), no significant differences were found for D1DR ligand binding to the antagonist SCH23390 or agonist SKF82958 between these mouse types (Figs. 2C & 2D). At relatively high concentrations, [^{3}H]SCH23390 was bound to *MsrA*$^{-/-}$ and WT striatal fractions to a similar extent (Fig. 2C). Similar results were found when SKF82958 was used (Fig. 2D). The SKF82958 ligand was not radiolabeled, thus binding efficiency was determined by its competitive binding in the presence of 2 nM [^{3}H]SCH23390 as previously

described (Nwaneshiudu & Unterwald, 2009). The amounts of [^{3}H]SCH23390 bound to the striatal fractions were significantly decreased (P<0.05) by the presence of 16 nM of SKF82958. This supports the hypothesis that *MsrA* ablation primarily impacts the D2DR.

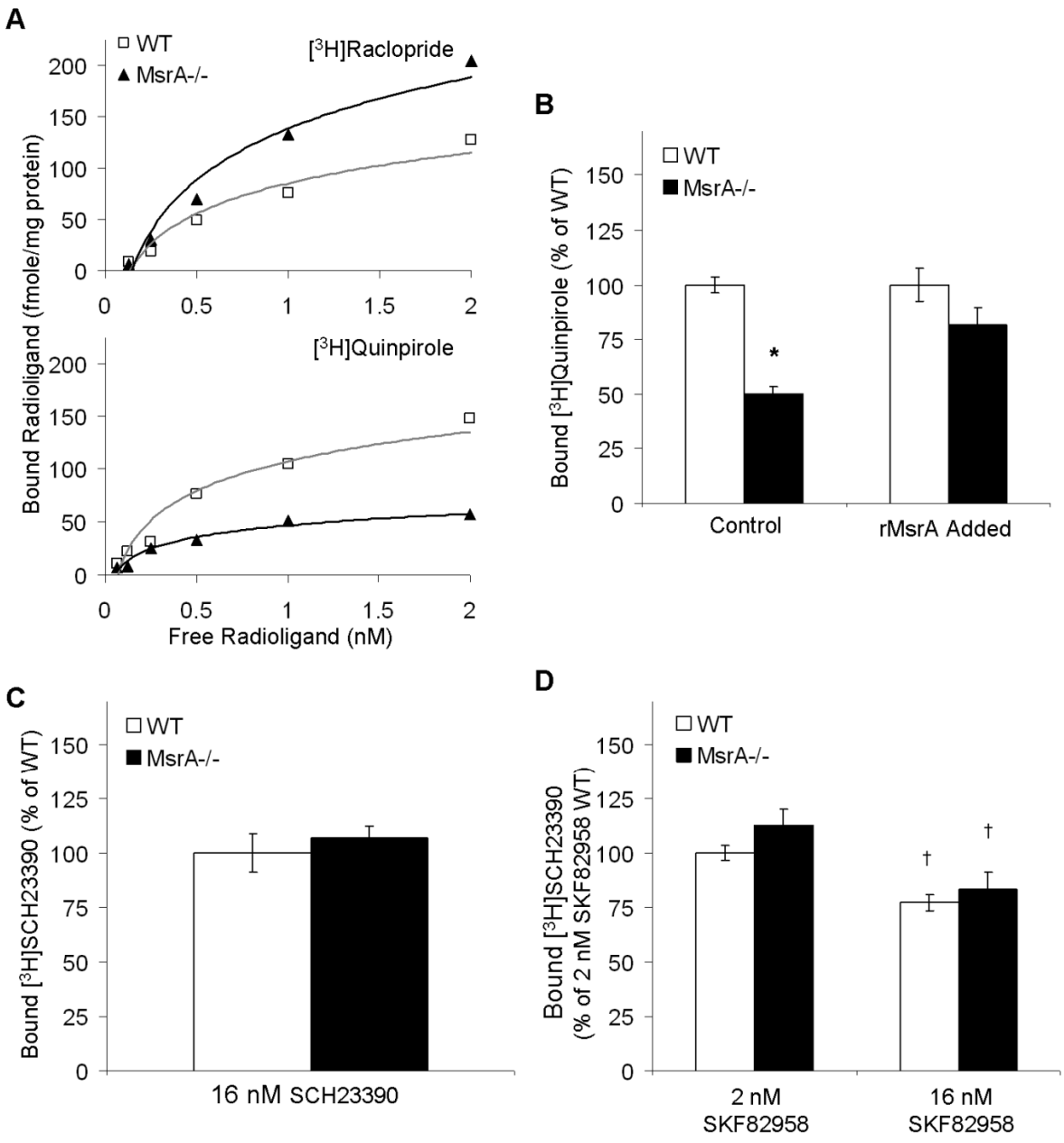

Figure 2. Binding efficiency of ligands to D2DR and D1DR in *MsrA*$^{-/-}$ and WT membranes. Specific ligand binding was calculated from subtracting non-specific ligand binding from total ligand binding as described in "Materials and Methods". **A)** Representative [^{3}H]raclopride and [^{3}H]quinpirole specific ligand binding curves of D2DR. **B)** Bmax of [^{3}H]quinpirole binding presented as percent of WT Bmax value (represents 100% binding) in the absence (Control) and presence of recombinant yeast MsrA (rMsrA Added). **C)** Binding of [^{3}H]SCH23390 at a

saturating concentration (Bmax value WT, under these conditions, represents 100% binding). (D) Relative binding of [^{3}H]SCH23390 at a concentration of 2 nM (as in panel C) in the presence of 2 nM and 16 nM SKF82958 concentrations. For all graphs, n=3. Significance is denoted by * or † indicating $P<0.05$ using *t*-test for difference by mouse type or by condition, respectively.

G-protein coupling efficiency to D2DR in MsrA$^{-/-}$ striatum

The non-hydrolyzable GTPγS analog will reduce the binding of [^{3}H]quinpirole to D2DR (quinpirole binds with lower affinity to uncoupled D2DR compared with coupled receptors). Consequently, competition curves were performed by inhibiting [^{3}H]quinpirole binding with increasing concentrations of GTPγS. Accordingly, the maximal inhibition from the competition curve reflects the number of D2DR coupled to G-proteins, while the 50% binding inhibition concentration (IC_{50}) from the curve reflects the potency of GTPγS to dissociate the D2DR and G-protein complex. The maximum binding of [^{3}H]quinpirole to D2DR in *MsrA*$^{-/-}$ was ~50% of the maximum binding of the agonist to the receptors in the WT brain (Fig. 3; WT = 50 ±6 and *MsrA*$^{-/-}$ = 26 ±3 fmole/mg protein in the presence of 1μM [^{3}H]quinpirole). The IC_{50} was found to be similar for both mouse types (10 ±1 nM), which is in agreement with current literature (Y. Zhang et al., 2001). These data suggest reduced G-protein and D2DR coupling in the *MsrA*$^{-/-}$ brain. Moreover, the similar IC_{50} in both mouse types suggests that the dissociation rates of the receptors from the G-proteins are similar. The reduced interaction of G-proteins with D2DR in *MsrA*$^{-/-}$ brains could be a consequence of either lower G-protein expression or interference in the initial binding of G-proteins to the third intracellular loop of D2DR. There was no significant difference in expression of $G\alpha_{i/o}$ proteins between the two mouse types (Fig. S1), suggesting that the observed limitation in *MsrA*$^{-/-}$ D2DR agonist binding is probably not because of reduced $G\alpha_{i/o}$ levels. Since the expression levels of these G-proteins seem to be similar in the two mouse types (Fig. S1), data in Fig. 3 are supportive of compromised D2DR agonist binding in *MsrA*$^{-/-}$ brains (Fig. 2A) and also may reflect interference in binding of *MsrA*$^{-/-}$ G-proteins to the third intracellular loop of D2DR.

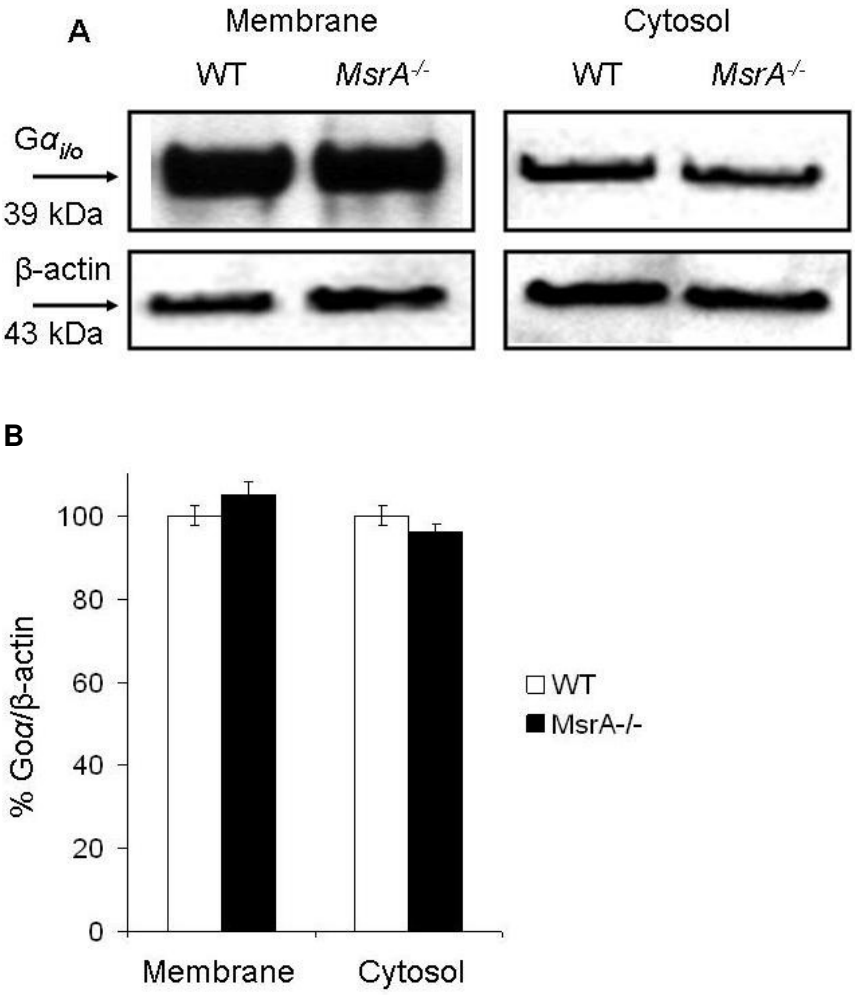

Figure S1. $G\alpha_{i/o}$ protein expression levels in *MsrA*$^{-/-}$ and WT brains. A) Membranal and cytosolic protein extracts of the striatal region (25 µg each from 6 month-old-mice) were subjected to SDS gel-electrophoresis, followed by immunoblot using primary antibodies against $G\alpha_{i/o}$ (rabbit antibodies, 1:1000 dilution, stock concentration for both forms: 0.2 mg/mL; Santa Cruz Biotechnology) and secondary HRP-conjugated goat ant-rabbit antibodies (Bio-rad). **B)** The relative densities of the protein bands were determined by densitometry analysis using ImageJ (NIH). The same immunoblot was probed for the levels of β-actin that were used as loading controls. The densities of $G\alpha_{i/o}$ were corrected for the relative densities of β-actin. The relative densities of the $G\alpha_{i/o}$ in *MsrA*$^{-/-}$ mouse were presented as percentage of density in WT (represents 100%).

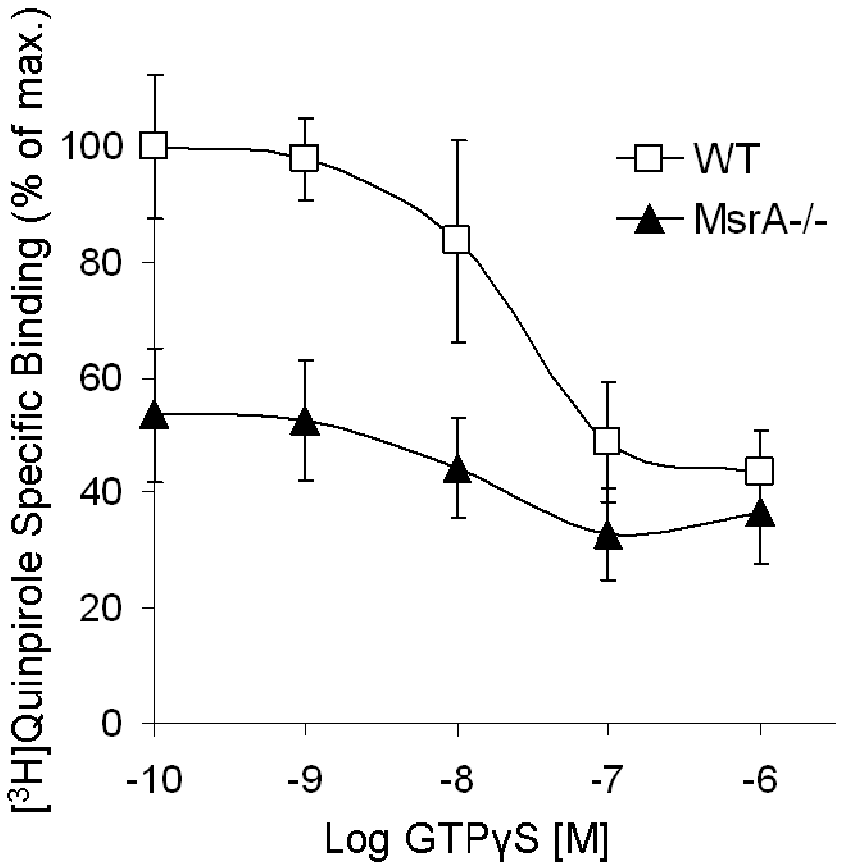

Figure 3. Inhibition of D2DR agonist binding in striatal membrane extracts of *MsrA*$^{-/-}$ and WT mice in the presence of GTPγS. The Y axis values of the graph represent the specific binding percentage of [^{3}H]quinpirole at GTPγS concentrations of 0.1, 1, 10, 100, and 1000 nM. The value at 100% specific binding represents maximum binding of WT D2DR to [^{3}H]quinpirole at 0.1 nM GTPγS. The maximum binding values were not significantly different from values obtained in the absence of GTPγS; data not shown. n=3.

Presynaptic stimulated dopamine release of MsrA$^{-/-}$ striatal tissue sections in response to D2DR ligands

A shorter form of the DRD2 receptor, D2DR$_S$, serves as an autoreceptor on the presynaptic membrane of dopaminergic neurons. This receptor has a third intracellular loop that is truncated by 29 amino acids, but still retains four of the eight Met residues. D2DR$_S$ has been previously demonstrated to respond to the D2DR agonist quinpirole and D2DR antagonist sulpiride by decreasing and increasing the presynaptic release of DA, respectively (Fawaz et al., 2009). Using a similar experimental design as Fawaz et al., the presynaptic DA release in the striatal area from *MsrA*$^{-/-}$ and WT coronal sections was measured in the presence of quinpirole (Fig. 4A & 4B) and sulpiride (Fig. 4C & 4D). Presynaptic DA release was detected by FSCS every 2 min, initially without any treatment and followed by treatment with a saturating dose of quinpirole. In the presence of quinpirole, *MsrA*$^{-/-}$ sections were less responsive than WT sections when both were compared to the respective initial stimulation and detection without the presence of drug. The DA release of the *MsrA*$^{-/-}$ presynaptic neurons was significantly higher than the decreased release of the WT presynaptic neurons (P<0.05; two-way repeated measures ANOVA). Moreover, the *MsrA*$^{-/-}$ presynaptic neurons were also less responsive to sulpiride than WT. After sulpiride treatment, the changes in DA concentration from the initial non-treated measurement of *MsrA*$^{-/-}$ sections were significantly lower than the increased DA concentration changes of the WT (P<0.05). These results suggest that the D2DR$_S$ signaling is disrupted in *MsrA*$^{-/-}$ mice.

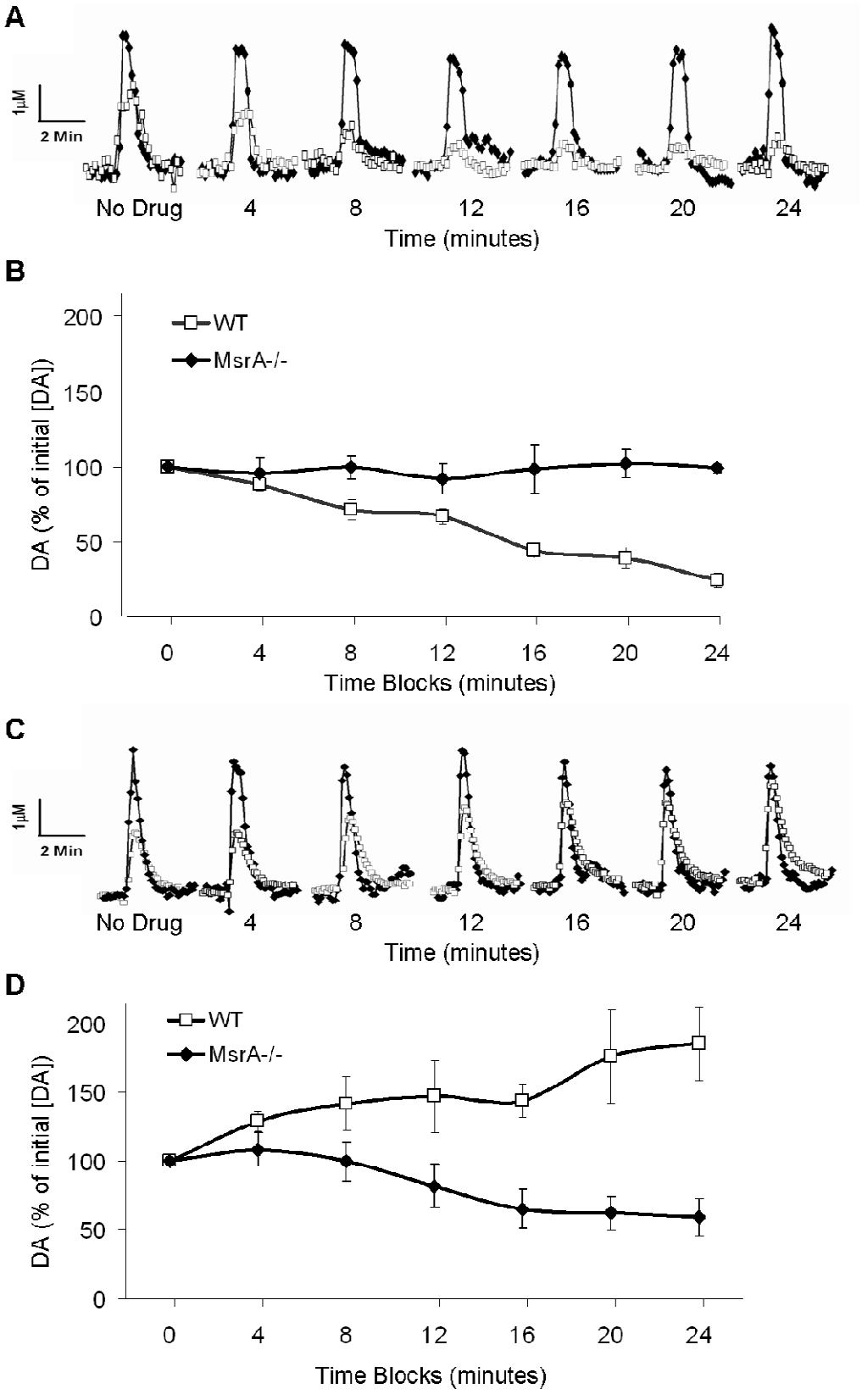
A
1μM
2 Min
No Drug
4
8
12
16
20
24
Time (minutes)
B
WT
MsrA-/-
DA (% of initial [DA])
200
150
100
50
0
0
4
8
12
16
20
24
Time Blocks (minutes)
C
1μM
2 Min
No Drug
4
8
12
16
20
24
Time (minutes)
D
WT
MsrA-/-
DA (% of initial [DA])
200
150
100
50
0
0
4
8
12
16
20
24
Time Blocks (minutes)

Figure 4. DA release in striatal sections from *MsrA*$^{-/-}$ and WT mice treated with D2DR agonist and antagonist. Coronal sections were stimulated using a 30 pulse-stimulus train and DA scans were collected by fast scan cyclic voltammetry. **A)** A representative stimulated DA release plot generated from measurements in the presence and absence of quinpirole. WT, *open squares; MsrA*$^{-/-}$, *filled diamonds*. **B)** The DA release measured in 4 min time blocks of WT and *MsrA*$^{-/-}$ sections in the presence of quinpirole. The basal initial measurements without drug treatment (time block 0) were set to 100%. All subsequent measurements with quinpirole are represented as a percentage of this value. **C)** A representative stimulated DA release plot generated from measurements obtained in the presence and absence of sulpiride. WT, *open squares; MsrA*$^{-/-}$, *filled diamonds*. **D)** The DA release measured in 4 min time blocks of WT and *MsrA*$^{-/-}$ sections in the presence of sulpiride. The initial basal measurements without treatment (time block 0) were set to 100%. All subsequent measurements with sulpiride are represented as a percentage of the initial 100% values. For both experiments, n=3 and $P<0.05$ for genotype determined by two-way repeated measures ANOVA. The basal DA concentrations in the absence of drug were WT=1.63 ±0.44 µM and *MsrA*$^{-/-}$ =5.47 ±0.36 µM.

Locomotor activity of MsrA$^{-/-}$ mice after injections of dopamine receptor agonists

The *in vitro* and brain section findings suggest functional changes in the DA system that should be expressed at the behavioral level. Consequently, we investigated the behavioral effects of D1DR and D2DR selective agonists on locomotor activity in *MsrA*$^{-/-}$ and WT mice. A significant difference in locomotor activity was observed between the mouse strains when injected with quinpirole. At a dose of 0.5 mg/kg, the *MsrA*$^{-/-}$ exhibited ~40% more locomotor activity than WT, and at a dose of 0.1 mg/kg the *MsrA*$^{-/-}$ exhibited ~35% more locomotor activity than WT (Fig. 5A; repeated measures ANOVA for mouse type effect, $P<0.02$). No significant difference in locomotor activity was observed between the two mouse types when injected with saline (Fig. 5), which is consistent with previous experiments (D. B. Oien, Osterhaus et al., 2008). Given the higher expression level of the D2DR in *MsrA*$^{-/-}$ mice, these data suggest that the compromised responsiveness of the *MsrA*$^{-/-}$ D2DRs to the inhibitory effect of quinpirole may be due to irregularities in either DA binding or abnormal function of further downstream signaling events. Moreover, the lack of a significant dose effect in the quinpirole concentrations used is consistent with published data, illustrating by similar analyses that there was no dose effect in mice even at broader and higher dose ranges (Wang et al., 2000).

Additionally, *MsrA*$^{-/-}$ and WT mice were injected with two doses of the D1DR agonist SKF82958, and ensuing locomotor activity behavioral effects were assessed in 45 min sessions (Fig. 5B). The ANOVA applied to these distance traveled data indicated no effect of mouse type, a significant effect of SKF82958 dose effect (repeated measures ANOVA; $P<0.01$), and no dose-by-type interaction. These data show that the D1DR agonist did not differentially affect the two types of mice (no type effect, no interaction effect). As expected from the literature for several types of inbred mice, SKF82958 substantially increased locomotor activity in the dose range used here (Niimi, Takahashi, & Itakura, 2009). These data strengthen the idea that methionine oxidation in the D2DR third cytoplasmic loop plays an important role in the *MsrA*$^{-/-}$ phenotype (the D2DR third intracellular loop contains eight methionines, and the D1DR C-

terminus cytoplasmic region contains only one methionine; both of these regions are directly involved in signal transduction).

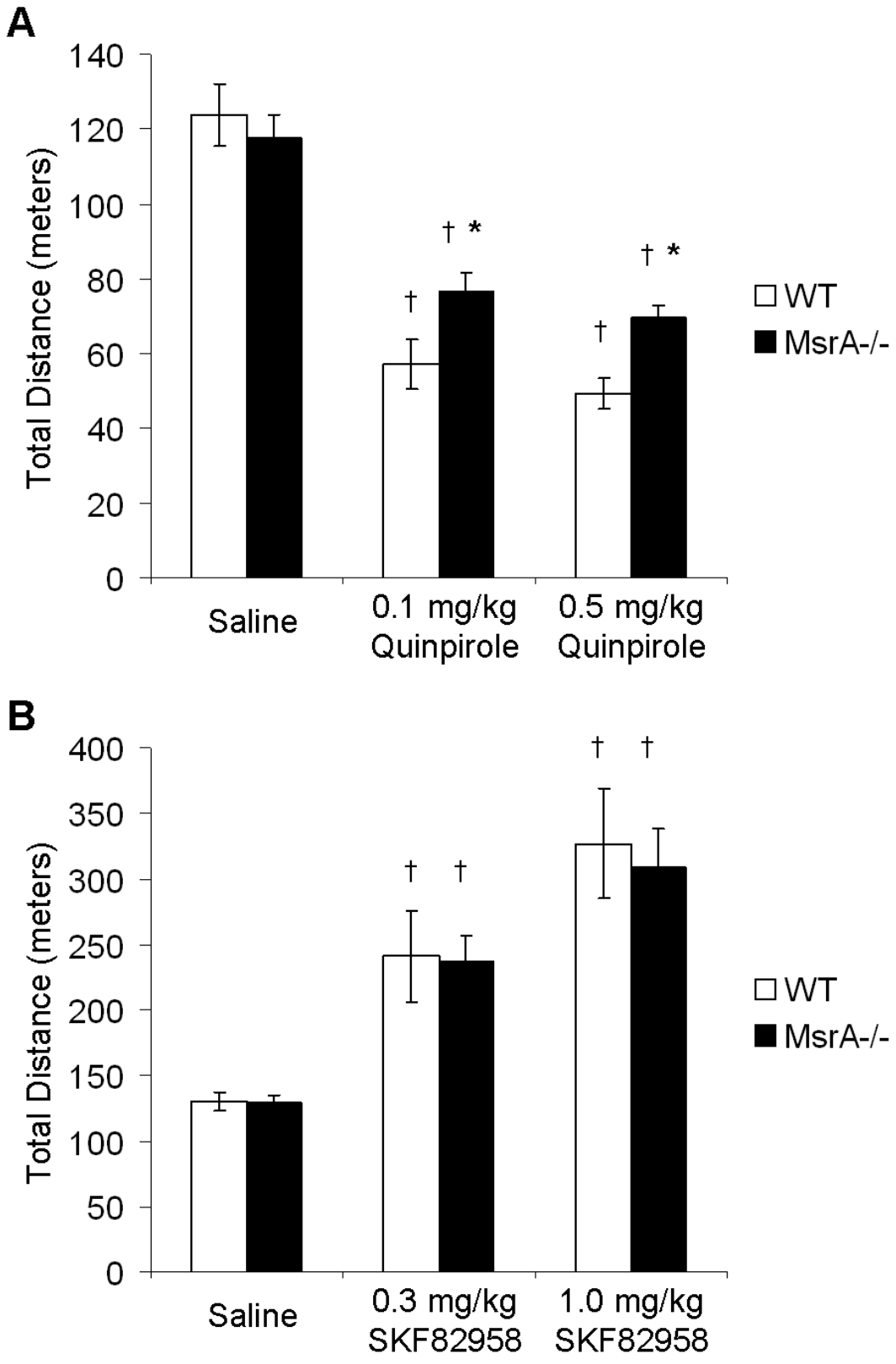
A
Total Distance (meters)
140
120
100
80
60
40
20
0
† *
† *
†
†
Saline
0.1 mg/kg Quinpirole
0.5 mg/kg Quinpirole
WT
MsrA-/-
B
Total Distance (meters)
400
350
300
250
200
150
100
50
0
† †
† †
Saline
0.3 mg/kg SKF82958
1.0 mg/kg SKF82958
WT
MsrA-/-

Figure 5. Locomotor activity after D2DR and D1DR agonist administration in *MsrA*$^{-/-}$ and WT mice. Total distance traveled was measured for 45 min after intraperitoneal injections of saline (vehicle) or indicated drug. **A)** Quinpirole injection at doses of 0.5 mg/kg and 0.1 mg/kg. WT, n=7; *MsrA*$^{-/-}$, n=10. $^{\dagger}P<0.01$ for quinpirole effect and $^{*}P<0.02$ for the genotype effect, determined by ANOVA. **B)** SKF82958 injection at doses of 0.3 mg/kg and 1.0 mg/kg. WT, n=7; *MsrA*$^{-/-}$, n=10. There was no significant effect of mouse type on SKF82958 effect, SKF82958 increased locomotor activity in the dose range used ($^{\dagger}P<0.01$) and no dose-by-type interaction was detected; determined by ANOVA.

MetO residues in recombinant long form D2DR third intracellular loop

Oxidation vulnerability was examined with recombinant GST-D2DR$_L$-IC$_3$ and peroxide exposure. Non-H_2O_2 oxidized GST-D2DR$_L$-IC$_3$ protein, H_2O_2 oxidized GST-D2DR$_L$-IC$_3$ protein, and H_2O_2 oxidized GST-D2DR$_L$-IC$_3$ proteins treated with MsrA were all subjected to mass spectrometry analysis following gel-electrophoresis separation and tryptic digestion. The procedure used to detect peptides by this mass spectrometry analysis (L. Zhang et al., 2010) normally causes some Met oxidation. To compensate for this, averaged MetO levels detected in the non-H_2O_2 oxidized GST-D2DR$_L$-IC$_3$ peptides were subtracted from the H_2O_2 oxidized forms of the protein (+/- MsrA and DTT). A 17-amino-acid peptide produced by collision-induced dissociation was found to contain the highest quantity of oxidized Met (276-AQELEMEMLSSTSPPER-292; Fig. 6). Furthermore, the Met283 residue (present in daughter ion Y10) of the peptide was found to be relatively more oxidized in comparison with the Met281 residue (present in daughter ion Y12; data not shown). The net oxidation level of Met283 treated with H_2O_2 *in vitro* was on average 2% (Fig 6). This oxidation level resembles the basal physiological level of MetO in unpublished observations and in yeast cells without H_2O_2 in the growth media (Moskovitz et al., 1997). Accordingly, the current *in vitro* condition of oxidation may resemble physiological Met oxidation. The addition of MsrA and DTT to oxidized GST-D2DR$_L$-IC$_3$ protein was able to reduce the sulfoxide of Met283 by 60% (Fig. 6). The MsrA enzyme can reduce only the *S*-form of MetO. Empirically, the distribution ratio of *S* to *R* forms of MetO is 1:1 (D. B. Oien & Moskovitz, 2008). Typically, we observed that *in vitro* oxidation of Met by H_2O_2 results in 60% *S*-MetO and 40% *R*-MetO (determined by amino acid analysis separation; unpublished results). Thus, the ability of the MsrA to reduce 60% of the total oxidized Met283 reflects the expected maximum reduction capability of the enzyme in an expected MetO racemic mixture of *R* and *S* forms following Met oxidation by H_2O_2. In addition, the preferred oxidation of Met283 suggests this residue is more vulnerable to oxidation and also readily accessible to the reducing function of MsrA.

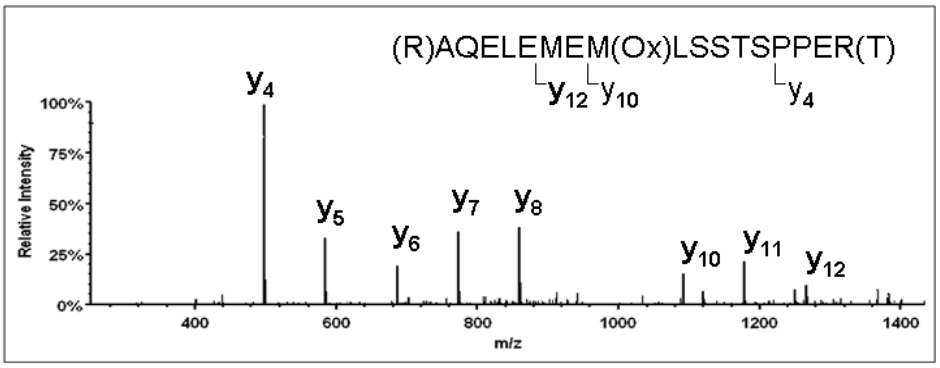

D2DR third intracellular loop sequence (amino acids: 211-375):

211kiyivlrkrrkrvntkrssrafranlktplkgncthpedmklctvimksngsfpvnrrrmdaarr(aqelememlsstsppe
r)tryspippshhqltlpdpshhglhsnpdspakpeknghakivnpriakffeiqtmpngktrtslktmsrrklsqqkekkatq
m375

Percent Met (Y10) oxidation (-blank)

+H_2O_2: 2.00±0.10

+H_2O_2 + rMsrA: 0.80±0.05

Figure 6. Oxidized Met residues in D2DR$_L$-IC$_3$ recombinant protein. The short and long form D2DR differ by a 29-amino-acid region in the third cytoplasmic loop, which begins after amino acid 241 in the rat sequence (underlined). The Mets (m) are in bold. The corresponding recombinant fusion protein GST-D2DR$_L$-IC$_3$ was isolated and resulting peptides were subjected to tandem mass spectrometry after trypsin digestion. The sequence of the major oxidized peptide identified is shown and also indicated in the sequence by parenthesis. Representative relative signal levels for the daughter ions of the major peptide detected after collision-induced fragmentation are presented as relative intensity of each ion. The difference in percent Met (Y10) oxidation between the presence and absence of rMsrA was found to be significant (3 experiments, $P<0.05$ by *t*-test).

4. Discussion

This study describes for the first time the possible effects of Met oxidation on DA receptor function *in vivo* by using *MsrA*$^{-/-}$ mice. Previously, we observed an inverse relationship between abnormally high levels of DA accompanied by lowered locomotor activity in *MsrA*$^{-/-}$ mice (D. B. Oien, Osterhaus et al., 2008). This is paradoxical because chronically low levels of brain DA are associated with Parkinson's disease-like motor effects including low levels of locomotor activity. These unexpected results led us to investigate the possibility that alteration of DA receptor function and expression may be involved.

Both the D1DR and the D2DR modulate striatal information processing that is integral to the translation of cortical plans into actions by providing for the expression of selected motor responses with concurrent suppression of unwanted responses ("responses" may be cognitive or motor). The D2DR are of particular clinical interest because of their role in neuropsychiatric disorders, such as schizophrenia, where D2DR antagonists are therapeutic (Lieberman et al., 2008), or their role in the movement disorder, Parkinson's disease, where D2DR agonists are known to benefit patients (Pahwa, Lyons, & Hauser, 2004). Thus, we predicted a reduced expression of striatal D2DR in *MsrA*$^{-/-}$ mice to explain the relative lower locomotor activity (D. B. Oien, Osterhaus et al., 2008). Surprisingly, there was an increase of D2DR expression in *MsrA*$^{-/-}$ mice (Fig. 1). Higher levels of [^{3}H]raclopride binding to D2DR confirmed this increase (Fig. 2). The higher protein levels of the D2DR in *MsrA*$^{-/-}$ may be part of a compensatory mechanism for the accumulation of oxidized D2DR. In spite of the higher D2DR levels observed, the binding of [^{3}H]quinpirole suggests a compromised agonist binding of the D2DR in *MsrA*$^{-/-}$ brain (Fig. 2A). Supportive *in vivo* data to this phenomenon are demonstrated by the lesser D2DR agonist inhibitory effect on locomotor function in *MsrA*$^{-/-}$ mice (Fig. 5A). Agonist occupation of G-protein coupled receptors leads to a cellular response that wanes, or desensitizes, with prolonged agonist exposure. MetO in the intracellular loops of the D2DR may cause a conformational change that may result in uncoupling of the receptor to G-protein subunits. The relative

compromised binding of the D2DR to [^{3}H]quinpirole suggests lower efficiency in D2DR-G-protein coupling. Indeed, our data show that although the levels of $G\alpha_{i/o}$ are similar in both mouse types (Fig. S1), the coupling of D2DR to G-proteins is reduced by ~50% in *MsrA*$^{-/-}$ relative to WT brain (Fig. 3). This suggests that the total $G\alpha_{i/o}$ coupling capacity is reduced in *MsrA*$^{-/-}$ brain rather than their coupling affinity to D2DR.

The ability of MsrA to restore D2DR agonist binding in *MsrA*$^{-/-}$ striatal extracts (Fig. 2B) supports the theory that methionine oxidation of D2DR occurs in the *MsrA*$^{-/-}$ brain. Accordingly, it may be beneficial to cause striatal overexpression of Msr to prevent MetO related abnormalities manifested by oxidized D2DR. Furthermore, the selectivity of the effect of Met oxidation on D2DR (by MsrA ablation) was demonstrated by the similar binding of D1DR to striatal extracts in both mouse types (Figs. 2C & 2D). Data presented in Fig. 4 suggest the autoreceptor function of D2DR in *MsrA*$^{-/-}$ striatum is compromised in its functional response to quinpirole and sulpiride compared to WT $D2DR_S$. The *in vivo* observation that *MsrA*$^{-/-}$ mice are less responsive to the inhibitory effect of quinpirole on locomotor activity (Fig. 5A) supports the conclusion that there is a general malfunction of *MsrA*$^{-/-}$ D2DR. Furthermore, the *in vivo* specificity of the MsrA ablation effect for D2DR is strengthened by the similar response of both mouse types to D1DR agonist (Fig. 5B). According to the literature, the use of the administrated doses of 0.1 and 0.5 mg/kg quinpirole are within the common range used in mice. In mice, there is no increased locomotor response as the dose is increased; instead, a suppression of locomotor activity is observed (Geter-Douglass et al., 1997; Usiello et al., 2000; Wang et al., 2000). Mice are different from rats in their response to quinpirole. In rats there is an increase of locomotor response with a higher quinpirole dose (Eilam, Clements, & Szechtman, 1991; Koeltzow, Austin, & Vezina, 2003). This observation may be linked to the observed difference in the ligand Kd values in rats (Levant, Grigoriadis, & DeSouza, 1992) versus mice (current study).

Taken together, it is suggested that lack of MsrA leads to Met oxidation in both long and short forms of D2DR and diminishes their overall function. The generally lowered *MsrA*$^{-/-}$

response to quinpirole, both *in vitro* and *in vivo* (Figs. 2 & 5) implies that conserved regions of both D2DR subtypes are primarily affected in the *MsrA*$^{-/-}$ mouse (this does not exclude involvement of the 29 amino acid sequence that is not present in the $D2DR_S$). The compromised G-protein coupling in *MsrA*$^{-/-}$ may be a result of oxidative modification of specific Met residues, especially in the cytoplasmic loops of the D2DR that are important for G-proteins coupling (i.e. $D2DR_L$-IC_3) (Ilani et al., 2002; Montmayeur, Guiramand, & Borrelli, 1993). To assess the possibility of Met oxidation in $D2DR_L$-IC_3 and reversal by MsrA *in vitro*, a recombinant GST-$D2DR_L$-IC_3 protein was oxidized and treated with recombinant MsrA. An oxidation of a specific Met (Met283) in recombinant GST-$D2DR_L$-IC_3 protein occurred and was reduced to Met by 60% with MsrA (Fig 6). Met283 is present in both subtypes of D2DR and may be an important target for oxidation that affects the general function of this receptor. Future experiments are underway to monitor *in vivo* MetO levels and location in the D2DR of *MsrA*$^{-/-}$ mice. Overall, the collective evidence indicates that primarily D2DR related signaling is affected in *MsrA*$^{-/-}$ mice. However, the contributions of other signaling events to the observed abnormalities will still need further investigations.

Mechanistically, we suggest that oxidation of specific Metresidues may also affect phosphorylation of adjacent amino acids in $D2DR_L$-IC_3, thereby altering DA signal transduction pathways. For example, a regulatory role of MetO in protein phosphorylation was recently reported (Emes, 2009; Hardin, Larue, Oh, Jain, & Huber, 2009; D. B. Oien, Shinogle et al., 2009a). Accordingly, it is possible that specific MetO residues in $D2DR_L$-IC_3 inhibit phosphorylation events that are important for proper coupling of the receptor to G-proteins as well (Namkung, Dipace, Javitch, & Sibley, 2009).

Our data can be interpreted to suggest that lack of MsrA in mouse brain causes D2DR malfunction via G-protein uncoupling leading to the production of higher DA levels (as a potential compensatory mechanism), reduced locomotor activity, and diminished behavioral responsiveness to D2DR agonists (D. B. Oien, Osterhaus et al., 2008). Understanding the role

of MsrA and MetO in DA physiology may result in identifying other proteins and neurotransmitter receptors that are altered by oxidative modification of Met.

Recently it was reported that mutations in the upstream region of *MsrA* may be potential markers for schizophrenia. If this proves true, research clearly supports the relevance of the *MsrA*$^{-/-}$ DA system to the occurrence of DA-related abnormal behavior (Walss-Bass et al., 2009).

F. References

Aksenov, M., Aksenova, M., Butterfield, D. A., & Markesbery, W. R. (2000). Oxidative modification of creatine kinase BB in Alzheimer's disease brain. *J Neurochem, 74*(6), 2520-2527.

Alamuri, P., & Maier, R. J. (2006). Methionine sulfoxide reductase in Helicobacter pylori: interaction with methionine-rich proteins and stress-induced expression. *J Bacteriol, 188*(16), 5839-5850.

Amende, I., Kale, A., McCue, S., Glazier, S., Morgan James, P., & Hampton Thomas, G. (2005). Gait dynamics in mouse models of Parkinson's disease and Huntington's disease. *J Neuroengineering Rehabil FIELD Full Journal Title:Journal of neuroengineering and rehabilitation, 2*, 20.

Bartlett, R. K., Bieber Urbauer, R. J., Anbanandam, A., Smallwood, H. S., Urbauer, J. L., & Squier, T. C. (2003). Oxidation of Met144 and Met145 in calmodulin blocks calmodulin dependent activation of the plasma membrane Ca-ATPase. *Biochemistry, 42*(11), 3231-3238.

Bartolic, A., Pirtosek, Z., Rozman, J., & Ribaric, S. (2005). Postural stability of Parkinson's disease patients is improved by decreasing rigidity. *European Journal of Neurology, 12*(2), 156-159.

Bath, B. D., Michael, D. J., Trafton, B. J., Joseph, J. D., Runnels, P. L., & Wightman, R. M. (2000). Subsecond adsorption and desorption of dopamine at carbon-fiber microelectrodes. *Analytical Chemistry, 72*(24), 5994-6002.

Bigelow, D. J., & Squier, T. C. (2005). Redox modulation of cellular signaling and metabolism through reversible oxidation of methionine sensors in calcium regulatory proteins. *Biochim Biophys Acta, 1703*(2), 121-134.

Bird, E. D., & Iversen, L. L. (1974). Huntington's chorea. Post-mortem measurement of glutamic acid decarboxylase, choline acetyltransferase and dopamine in basal ganglia. *Brain, 97*(3), 457-472.

Burk, R. F., & Hill, K. E. (2005). Selenoprotein P: an extracellular protein with unique physical characteristics and a role in selenium homeostasis. *Annu Rev Nutr, 25*, 215-235.

Bylund, D. B., & Toews, M. L. (1993). Radioligand binding methods: practical guide and tips. *Am J Physiol, 265*(5 Pt 1), L421-429.

Carlsson, T., Bjorklund, T., & Kirik, D. (2007). Restoration of the striatal dopamine synthesis for Parkinson's disease: viral vector-mediated enzyme replacement strategy. *Curr Gene Ther, 7*(2), 109-120.

Carr, K. D., Tsimberg, Y., Berman, Y., & Yamamoto, N. (2003). Evidence of increased dopamine receptor signaling in food-restricted rats. *Neuroscience, 119*(4), 1157-1167.

Chai, S. C., Jerkins, A. A., Banik, J. J., Shalev, I., Pinkham, J. L., Uden, P. C., et al. (2005). Heterologous expression, purification, and characterization of recombinant rat cysteine dioxygenase. *J Biol Chem, 280*(11), 9865-9869.

Chen, B. T., Avshalumov, M. V., & Rice, M. E. (2001). H(2)O(2) is a novel, endogenous modulator of synaptic dopamine release. *J Neurophysiol, 85*(6), 2468-2476.

Chesselet, M. F. (2007). In vivo alpha-synuclein overexpression in rodents: A useful model of Parkinson's disease? *Exp Neurol*.

Chiueh, C. C., & Moore, K. E. (1975). D-amphetamine-induced release of "newly synthesized" and "stored" dopamine from the caudate nucleus in vivo. *J Pharmacol Exp Ther, 192*(3), 642-653.

Choi, J., Sullards, M. C., Olzmann, J. A., Rees, H. D., Weintraub, S. T., Bostwick, D. E., et al. (2006). Oxidative damage of DJ-1 is linked to sporadic Parkinson and Alzheimer diseases. *Journal of Biological Chemistry, 281*(16), 10816-10824.

Colman, R. J., Anderson, R. M., Johnson, S. C., Kastman, E. K., Kosmatka, K. J., Beasley, T. M., et al. (2009). Caloric restriction delays disease onset and mortality in rhesus monkeys. *Science, 325*(5937), 201-204.

Contestabile, A. (2009). Benefits of caloric restriction on brain aging and related pathological States: understanding mechanisms to devise novel therapies. *Curr Med Chem, 16*(3), 350-361.

Crocker, S. J., Smith, P. D., Jackson-Lewis, V., Lamba, W. R., Hayley, S. P., Grimm, E., et al. (2003). Inhibition of calpains prevents neuronal and behavioral deficits in an MPTP mouse model of Parkinson's disease. *Journal of Neuroscience, 23*(10), 4081-4091.

Dominy, J. E., Jr., Hirschberger, L. L., Coloso, R. M., & Stipanuk, M. H. (2006). Regulation of cysteine dioxygenase degradation is mediated by intracellular cysteine levels and the ubiquitin-26 S proteasome system in the living rat. *Biochem J, 394*(Pt 1), 267-273.

Dong, J., Atwood, C. S., Anderson, V. E., Siedlak, S. L., Smith, M. A., Perry, G., et al. (2003). Metal binding and oxidation of amyloid-beta within isolated senile plaque cores: Raman microscopic evidence. *Biochemistry, 42*(10), 2768-2773.

Duan, W., & Mattson, M. P. (1999). Dietary restriction and 2-deoxyglucose administration improve behavioral outcome and reduce degeneration of dopaminergic neurons in models of Parkinson's disease. *J Neurosci Res, 57*(2), 195-206.

Eilam, D., Clements, K. V., & Szechtman, H. (1991). Differential effects of D1 and D2 dopamine agonists on stereotyped locomotion in rats. *Behav Brain Res, 45*(2), 117-124.

Emes, M. J. (2009). Oxidation of methionine residues: the missing link between stress and signalling responses in plants. *Biochem J, 422*(2), e1-2.

Erickson, J. R., Joiner, M. L., Guan, X., Kutschke, W., Yang, J., Oddis, C. V., et al. (2008). A dynamic pathway for calcium-independent activation of CaMKII by methionine oxidation. *Cell, 133*(3), 462-474.

Fawaz, C. S., Martel, P., Leo, D., & Trudeau, L. E. (2009). Presynaptic action of neurotensin on dopamine release through inhibition of D(2) receptor function. *BMC Neurosci, 10*, 96.

Fernagut, P. O., Diguet, E., Labattu, B., & Tison, F. (2002). A simple method to measure stride length as an index of nigrostriatal dysfunction in mice. *Journal of Neuroscience Methods, 113*(2), 123-130.

Fischer, J. F., & Cho, A. K. (1979). Chemical release of dopamine from striatal homogenates: evidence for an exchange diffusion model. *J Pharmacol Exp Ther, 208*(2), 203-209.

Fleckenstein, A. E., Volz, T. J., Riddle, E. L., Gibb, J. W., & Hanson, G. R. (2007). New insights into the mechanism of action of amphetamines. *Annu Rev Pharmacol Toxicol, 47*, 681-698.

Fowler, S. C., Birkestrand, B. R., Chen, R., Moss, S. J., Vorontsova, E., Wang, G., et al. (2001a). A force-plate actometer for quantitating rodent behaviors: illustrative data on locomotion, rotation, spatial patterning, stereotypies, and tremor. *J Neurosci Methods, 107*(1-2), 107-124.

Fowler, S. C., Birkestrand, B. R., Chen, R., Moss, S. J., Vorontsova, E., Wang, G., et al. (2001b). A force-plate actometer for quantitating rodent behaviors: illustrative data on locomotion, rotation, spatial patterning, stereotypies, and tremor. *Journal of Neuroscience Methods, 107*(1-2), 107-124.

Gelegen, C., van den Heuvel, J., Collier, D. A., Campbell, I. C., Oppelaar, H., Hessel, E., et al. (2008). Dopaminergic and brain-derived neurotrophic factor signalling in inbred mice exposed to a restricted feeding schedule. *Genes Brain Behav, 7*(5), 552-559.

Gerfen, C. R., Herkenham, M., & Thibault, J. (1987). The Neostriatal Mosaic .2. Patch-Directed and Matrix-Directed Mesostriatal Dopaminergic and Nondopaminergic Systems. *Journal of Neuroscience, 7*(12), 3915-3934.

Geter-Douglass, B., Katz, J. L., Alling, K., Acri, J. B., & Witkin, J. M. (1997). Characterization of unconditioned behavioral effects of dopamine D3/D2 receptor agonists. *J Pharmacol Exp Ther, 283*(1), 7-15.

Gibson, G. E., Sheu, K. F., Blass, J. P., Baker, A., Carlson, K. C., Harding, B., et al. (1988). Reduced activities of thiamine-dependent enzymes in the brains and peripheral tissues of patients with Alzheimer's disease. *Arch Neurol, 45*(8), 836-840.

Govic, A., Levay, E. A., Kent, S., & Paolini, A. G. (2009). The social behavior of male rats administered an adult-onset calorie restriction regimen. *Physiol Behav, 96*(4-5), 581-585.

Groves, P. M., & Linder, J. C. (1983). Dendro-Dendritic Synapses in Substantia-Nigra - Descriptions Based on Analysis of Serial Sections. *Experimental Brain Research, 49*(2), 209-217.

Hampton, T. G., Stasko, M. R., Kale, A., Amende, I., & Costa, A. C. S. (2004). Gait dynamics in trisomic mice: quantitative neurological traits of Down syndrome. *Physiology & Behavior, 82*(2-3), 381-389.

Hardin, S. C., Larue, C. T., Oh, M. H., Jain, V., & Huber, S. C. (2009). Coupling oxidative signals to protein phosphorylation via methionine oxidation in Arabidopsis. *Biochem J, 422*(2), 305-312.

Harrison, C., & Traynor, J. R. (2003). The [35S]GTPgammaS binding assay: approaches and applications in pharmacology. *Life Sci, 74*(4), 489-508.

Hattori, T., McGeer, P. L., & McGeer, E. G. (1979). Dendro axonic neurotransmission. II. Morphological sites for the synthesis, binding and release of neurotransmitters in dopaminergic dendrites in the substantia nigra and cholinergic dendrites in the neostriatum. *Brain Res. FIELD Full Journal Title:Brain Research, 170*(1), 71-83.

Hausdorff, J. M., Lertratanakul, A., Cudkowicz, M. E., Peterson, A. L., Kaliton, D., & Goldberger, A. L. (2000). Dynamic markers of altered gait rhythm in amyotrophic lateral sclerosis. *J Appl Physiol, 88*(6), 2045-2053.

Hickey, M. A., Reynolds, G. P., & Morton, A. J. (2002). The role of dopamine in motor symptoms in the R6/2 transgenic mouse model of Huntington's disease. *J Neurochem, 81*(1), 46-59.

Hornykiewicz, O. (1962). [Dopamine (3-hydroxytyramine) in the central nervous system and its relation to the Parkinson syndrome in man.]. *Dtsch Med Wochenschr, 87*, 1807-1810.

Huxtable, R. J. (2000). Expanding the circle 1975-1999: sulfur biochemistry and insights on the biological functions of taurine. *Adv Exp Med Biol, 483*, 1-25.

Ilani, T., Fishburn, C. S., Levavi-Sivan, B., Carmon, S., Raveh, L., & Fuchs, S. (2002). Coupling of dopamine receptors to G proteins: studies with chimeric D2/D3 dopamine receptors. *Cell Mol Neurobiol, 22*(1), 47-56.

Jacobs, W. B., Govoni, G., Ho, D., Atwal, J. K., Barnabe-Heider, F., Keyes, W. M., et al. (2005). p63 is an essential proapoptotic protein during neural development. *Neuron, 48*(5), 743-756.

Johnson, M. A., Rajan, V., Miller, C. E., & Wightman, R. M. (2006). Dopamine release is severely compromised in the R6/2 mouse model of Huntington's disease. *J Neurochem, 97*(3), 737-746.

Jones, S. R., Gainetdinov, R. R., Wightman, R. M., & Caron, M. G. (1998a). Mechanisms of amphetamine action revealed in mice lacking the dopamine transporter. *Journal of Neuroscience, 18*(6), 1979-1986.

Jones, S. R., Gainetdinov, R. R., Wightman, R. M., & Caron, M. G. (1998b). Mechanisms of amphetamine action revealed in mice lacking the dopamine transporter. *J Neurosci, 18*(6), 1979-1986.

Jones, S. R., Garris, P. A., Kilts, C. D., & Wightman, R. M. (1995). Comparison of Dopamine Uptake in the Basolateral Amygdaloid Nucleus, Caudate-Putamen, and Nucleus-Accumbens of the Rat. *Journal of Neurochemistry, 64*(6), 2581-2589.

Jones, S. R., Joseph, J. D., Barak, L. S., Caron, M. G., & Wightman, R. M. (1999). Dopamine neuronal transport kinetics and effects of amphetamine. *Journal of Neurochemistry, 73*(6), 2406-2414.

Jones, S. R., Mickelson, G. E., Collins, L. B., Kawagoe, K. T., & Wightman, R. M. (1994). Interference by pH and Ca2+ ions during measurements of catecholamine release in slices of rat amygdala with fast-scan cyclic voltammetry. *J Neurosci Methods, 52*(1), 1-10.

Kale, A., Amende, N., Meyer, G. P., Crabbe, J. C., & Hampton, T. G. (2004). Ethanol's effects on gait dynamics in mice investigated by ventral plane videography. *Alcoholism-Clinical and Experimental Research, 28*(12), 1839-1848.

Kantor, L., Zhang, M., Guptaroy, B., Park, Y. H., & Gnegy, M. E. (2004). Repeated amphetamine couples norepinephrine transporter and calcium channel activities in PC12 cells. *J Pharmacol Exp Ther, 311*(3), 1044-1051.

Kawagoe, K. T., Garris, P. A., Wiedemann, D. J., & Wightman, R. M. (1992). Regulation of Transient Dopamine Concentration Gradients in the Microenvironment Surrounding Nerve-Terminals in the Rat Striatum. *Neuroscience, 51*(1), 55-64.

Kho, C. W., Lee, P. Y., Bae, K. H., Cho, S., Lee, Z. W., Park, B. C., et al. (2006). Glutathione peroxidase 3 of Saccharomyces cerevisiae regulates the activity of methionine sulfoxide reductase in a redox state-dependent way. *Biochem Biophys Res Commun, 348*(1), 25-35.

Kleppe, R., Toska, K., & Haavik, J. (2001). Interaction of phosphorylated tyrosine hydroxylase with 14-3-3 proteins: evidence for a phosphoserine 40-dependent association. *J Neurochem, 77*(4), 1097-1107.

Koeltzow, T. E., Austin, J. D., & Vezina, P. (2003). Behavioral sensitization to quinpirole is not associated with increased nucleus accumbens dopamine overflow. *Neuropharmacology, 44*(1), 102-110.

Kraft, J. C., Osterhaus, G. L., Ortiz, A. N., Garris, P. A., & Johnson, M. A. (2009). In vivo dopamine release and uptake impairments in rats treated with 3-nitropropionic acid. *Neuroscience, 161*(3), 940-949.

Kume-Kick, J., & Rice, M. E. (1998). Dependence of dopamine calibration factors on media Ca2+ and Mg2+ at carbon-fiber microelectrodes used with fast-scan cyclic voltammetry. *J Neurosci Methods, 84*(1-2), 55-62.

Lan, H., Liu, Y., Bell, M. I., Gurevich, V. V., & Neve, K. A. (2009). A dopamine D2 receptor mutant capable of G protein-mediated signaling but deficient in arrestin binding. *Mol Pharmacol, 75*(1), 113-123.

Lee, K. W., Lee, S. H., Kim, H., Song, J. S., Yang, S. D., Paik, S. G., et al. (2004). Progressive cognitive impairment and anxiety induction in the absence of plaque deposition in C57BL/6 inbred mice expressing transgenic amyloid precursor protein. *Journal of Neuroscience Research, 76*(4), 572-580.

Levant, B., Grigoriadis, D. E., & DeSouza, E. B. (1992). Characterization of [3H]quinpirole binding to D2-like dopamine receptors in rat brain. *J Pharmacol Exp Ther, 262*(3), 929-935.

Liang, N. Y., & Rutledge, C. O. (1982). Evidence for carrier-mediated efflux of dopamine from corpus striatum. *Biochem Pharmacol, 31*(15), 2479-2484.

Lieberman, J. A., Bymaster, F. P., Meltzer, H. Y., Deutch, A. Y., Duncan, G. E., Marx, C. E., et al. (2008). Antipsychotic drugs: comparison in animal models of efficacy, neurotransmitter regulation, and neuroprotection. *Pharmacol Rev, 60*(3), 358-403.

Linder, J. C., Klemfuss, H., & Groves, P. M. (1987). Acute Ultrastructural and Behavioral-Effects of 1-Methyl-4-Phenyl-1,2,3,6-Tetrahydropyridine (Mptp) in Mice. *Neuroscience Letters, 82*(2), 221-226.

Lopez, M. F., Mikulskis, A., Golenko, E., Melov, S., Bennett, D., Cherkasskiy, A., et al. (2004). Microscale fractionation facilitates detection of differentially expressed proteins in Alzheimer's disease brain samples. *Electrophoresis, 25*(15), 2557-2563.

Lyon, M., & Robbins, T. (1975). The action of central nervous stimulant drugs: A general theory concerning amphetamine effects. In E. W & V. L (Eds.), *Current Developments in Psychopharmacology* (Vol. 2, pp. 79-163). New York: Spectrum.

Maalouf, M., Rho, J. M., & Mattson, M. P. (2009). The neuroprotective properties of calorie restriction, the ketogenic diet, and ketone bodies. *Brain Res Rev, 59*(2), 293-315.

Martin, B., Golden, E., Egan, J. M., Mattson, M. P., & Maudsley, S. (2007). Reduced energy intake: the secret to a long and healthy life? *IBS J Sci, 2*(2), 35-39.

McKerchar, T. L., Zarcone, T. J., & Fowler, S. C. (2005). Differential acquisition of lever pressing in inbred and outbred mice: Comparison of one-lever and two-lever procedures and correlation with differences in locomotor activity. *Journal of the Experimental Analysis of Behavior, 84*(3), 339-356.

Michaelis, M. L., Bigelow, D. J., Schoneich, C., Williams, T. D., Ramonda, L., Yin, D., et al. (1996). Decreased plasma membrane calcium transport activity in aging brain. *Life Sci, 59*(5-6), 405-412.

Minor, R. K., Villarreal, J., McGraw, M., Percival, S. S., Ingram, D. K., & de Cabo, R. (2008). Calorie restriction alters physical performance but not cognition in two models of altered neuroendocrine signaling. *Behav Brain Res, 189*(1), 202-211.

Montmayeur, J. P., Guiramand, J., & Borrelli, E. (1993). Preferential coupling between dopamine D2 receptors and G-proteins. *Mol Endocrinol, 7*(2), 161-170.

Morgan, D. G., May, P. C., & Finch, C. E. (1987). Dopamine and serotonin systems in human and rodent brain: effects of age and neurodegenerative disease. *J Am Geriatr Soc, 35*(4), 334-345.

Moskovitz, J. (2007). Prolonged selenium-deficient diet in MsrA knockout mice causes enhanced oxidative modification to proteins and affects the levels of antioxidant enzymes in a tissue-specific manner. *Free Radic Res, 41*(2), 162-171.

Moskovitz, J., Bar-Noy, S., Williams, W. M., Requena, J., Berlett, B. S., & Stadtman, E. R. (2001). Methionine sulfoxide reductase (MsrA) is a regulator of antioxidant defense and lifespan in mammals. *Proc Natl Acad Sci U S A, 98*(23), 12920-12925.

Moskovitz, J., Berlett, B. S., Poston, J. M., & Stadtman, E. R. (1997). The yeast peptide-methionine sulfoxide reductase functions as an antioxidant in vivo. *Proc Natl Acad Sci U S A, 94*(18), 9585-9589.

Moskovitz, J., & Oien, D. B. (2009). Methionine Oxidation: Implication in Protein Regulation, Aging and Aging-Associated Diseases. In M. R & M. G (Eds.), *Glutathione and Sulfur Amino Acids in Human Heath and Disease*: John Wiley & Sons, Inc.

Moskovitz, J., & Stadtman, E. R. (2003). Selenium-deficient diet enhances protein oxidation and affects methionine sulfoxide reductase (MsrB) protein level in certain mouse tissues. *Proc Natl Acad Sci U S A, 100*(13), 7486-7490.

Nachshen, D. A., & Sanchez-Armass, S. (1987). Co-operative action of calcium ions in dopamine release from rat brain synaptosomes. *J Physiol, 387*, 415-423.

Namkung, Y., Dipace, C., Javitch, J. A., & Sibley, D. R. (2009). G protein-coupled receptor kinase-mediated phosphorylation regulates post-endocytic trafficking of the D2 dopamine receptor. *J Biol Chem, 284*(22), 15038-15051.

Neves, G., & Lagnado, L. (1999). The kinetics of exocytosis and endocytosis in the synaptic terminal of goldfish retinal bipolar cells. *J Physiol, 515 (Pt 1)*, 181-202.

Niimi, K., Takahashi, E., & Itakura, C. (2009). Age dependence of motor activity and sensitivity to dopamine receptor 1 agonist, SKF82958, of inbred AKR/J, BALB/c, C57BL/6J, SAMR1, and SAMP6 strains. *Brain Res, 1250*, 175-182.

Nwaneshiudu, C. A., & Unterwald, E. M. (2009). Blockade of neurokinin-3 receptors modulates dopamine-mediated behavioral hyperactivity. *Neuropharmacology, 57*(3), 295-301.

Oien, D., Ortiz, A., Rittel, A., Dobrowsky, R., Johnson, M., Levant, B., et al. (In Press-a). Dopamine D2 Receptor Function is Compromised in the Brain of the Methionine Sulfoxide Reductase A Knockout Mouse. *Journal of Neurochemistry*.

Oien, D., Wang, X., & Moskovitz, J. (2008). Genomic and Proteomic Analyses of the Methionine Sulfoxide Reductase A Knockout Mouse. *Current Proteomics, 5*(2), 96-103.

Oien, D. B., Canello, T., Gabizon, R., Gasset, M., Lundquist, B. L., Burns, J. M., et al. (2009). Detection of oxidized methionine in selected proteins, cellular extracts and blood serums by novel anti-methionine sulfoxide antibodies. *Arch Biochem Biophys, 485*(1), 35-40.

Oien, D. B., & Moskovitz, J. (2007). Ablation of the mammalian methionine sulfoxide reductase A affects the expression level of cysteine deoxygenase. *Biochem Biophys Res Commun, 352*(2), 556-559.

Oien, D. B., & Moskovitz, J. (2008). Substrates of the methionine sulfoxide reductase system and their physiological relevance. *Curr Top Dev Biol, 80*, 93-133.

Oien, D. B., Ortiz, A. N., Rittel, A. G., Dobrowsky, R. T., Johnson, M. A., Levant, B., et al. (In Press-b). Dopamine D2 Receptor Function is Compromised in the Brain of the Methionine Sulfoxide Reductase A Knockout Mouse. *Journal of Neurochemistry*.

Oien, D. B., Osterhaus, G. L., Latif, S. A., Pinkston, J. W., Fulks, J., Johnson, M., et al. (2008). MsrA knockout mouse exhibits abnormal behavior and brain dopamine levels. *Free Radic Biol Med, 45*(2), 193-200.

Oien, D. B., Osterhaus, G. L., Lundquist, B. L., Fowler, S. C., & Moskovitz, J. (2010). Caloric restriction alleviates abnormal locomotor activity and dopamine levels in the brain of the methionine sulfoxide reductase A knockout mouse. *Neurosci Lett, 468*(1), 38-41.

Oien, D. B., Shinogle, H. E., Moore, D. S., & Moskovitz, J. (2009a). Clearance and phosphorylation of alpha-synuclein are inhibited in methionine sulfoxide reductase a null yeast cells. *J Mol Neurosci, 39*(3), 323-332.

Oien, D. B., Shinogle, H. E., Moore, D. S., & Moskovitz, J. (2009b). Clearance and Phosphorylation of Alpha-Synuclein Are Inhibited in Methionine Sulfoxide Reductase A Null Yeast Cells. *J Mol Neurosci*, *In Press*.

Opii, W. O., Joshi, G., Head, E., Milgram, N. W., Muggenburg, B. A., Klein, J. B., et al. (2008). Proteomic identification of brain proteins in the canine model of human aging following a long-term treatment with antioxidants and a program of behavioral enrichment: relevance to Alzheimer's disease. *Neurobiol Aging, 29*(1), 51-70.

Ortiz, A. N., Kurth, B. J., Osterhaus, G. L., & Johnson, M. A. (2010). Dysregulation of intracellular dopamine stores revealed in the R6/2 mouse striatum. *J Neurochem, 112*(3), 755-761.

Ortiz, A. N., Oien, D. B., Moskovitz, J., & Johnson, M. A. (Manuscript). Reserve Pool Dopamine Mobilization in Msr Null Mice.

Outeiro, T. F., Klucken, J., Bercury, K., Tetzlaff, J., Putcha, P., Oliveira, L. M., et al. (2009). Dopamine-induced conformational changes in alpha-synuclein. *PLoS One, 4*(9), e6906.

Padmanabhan, S., & Prasad, B. M. (2009). Sustained depolarization decreases calcium/calmodulin-dependent protein kinase II activity and gene expression in dopamine neurons. *Neuroscience, 163*(1), 277-285.

Pahwa, R., Lyons, K. E., & Hauser, R. A. (2004). Ropinirole therapy for Parkinson's disease. *Expert Rev Neurother, 4*(4), 581-588.

Pal, R., Oien, D. B., Ersen, F. Y., & Moskovitz, J. (2007a). Elevated levels of brain-pathologies associated with neurodegenerative diseases in the methionine sulfoxide reductase A knockout mouse. *Experimental Brain Research, 180*(4), 765-774.

Pal, R., Oien, D. B., Ersen, F. Y., & Moskovitz, J. (2007b). Elevated levels of brain-pathologies associated with neurodegenerative diseases in the methionine sulfoxide reductase A knockout mouse. *Exp Brain Res, 180*(4), 765-774.

Palacios, J., Sepulveda, M. R., Lee, A. G., & Mata, A. M. (2004). Ca2+ transport by the synaptosomal plasma membrane Ca2+-ATPase and the effect of thioridazine. *Biochemistry, 43*(8), 2353-2358.

Parfett, C. L., & Pilon, R. (1995). Oxidative stress-regulated gene expression and promotion of morphological transformation induced in C3H/10T1/2 cells by ammonium metavanadate. *Food Chem Toxicol, 33*(4), 301-308.

Petropoulos, I., Mary, J., Perichon, M., & Friguet, B. (2001). Rat peptide methionine sulphoxide reductase: cloning of the cDNA, and down-regulation of gene expression and enzyme activity during aging. *Biochem J, 355*(Pt 3), 819-825.

Poon, H. F., Vaishnav, R. A., Getchell, T. V., Getchell, M. L., & Butterfield, D. A. (2006). Quantitative proteomics analysis of differential protein expression and oxidative modification of specific proteins in the brains of old mice. *Neurobiol Aging, 27*(7), 1010-1019.

Rose, S. D., Lejen, T., Casaletti, L., Larson, R. E., Pene, T. D., & Trifaro, J. M. (2002). Molecular motors involved in chromaffin cell secretion. *Ann N Y Acad Sci, 971*, 222-231.

Saito, M., Smiley, J., Toth, R., & Vadasz, C. (2002). Microarray analysis of gene expression in rat hippocampus after chronic ethanol treatment. *Neurochem Res, 27*(10), 1221-1229.

Salarian, A., Russmann, H., Vingerhoets, F. J. G., Dehollain, C., Blanc, Y., Burkhard, P. R., et al. (2004). Gait assessment in Parkinson's disease: Toward an ambulatory system for long-term monitoring. *Ieee Transactions on Biomedical Engineering, 51*(8), 1434-1443.

Saransaari, P., & Oja, S. S. (1996). Taurine and neural cell damage. Transport of taurine in adult and developing mice. *Adv Exp Med Biol, 403*, 481-490.

Satoh, H. (1996). Direct inhibition by taurine of the ATP-sensitive k+ channel in guinea pig ventricular cardiomyocytes. *Gen Pharmacol, 27*(4), 625-627.

Saxena, S., Brody, A. L., Schwartz, J. M., & Baxter, L. R. (1998). Neuroimaging and frontal-subcortical circuitry in obsessive-compulsive disorder. *Br J Psychiatry Suppl*(35), 26-37.

Schomburg, L., Schweizer, U., Holtmann, B., Flohe, L., Sendtner, M., & Kohrle, J. (2003). Gene disruption discloses role of selenoprotein P in selenium delivery to target tissues. *Biochem J, 370*(Pt 2), 397-402.

Simmons, C. R., Hirschberger, L. L., Machi, M. S., & Stipanuk, M. H. (2006). Expression, purification, and kinetic characterization of recombinant rat cysteine dioxygenase, a non-heme metalloenzyme necessary for regulation of cellular cysteine levels. *Protein Expr Purif, 47*(1), 74-81.

Stadtman, E. R., Moskovitz, J., Berlett, B. S., & Levine, R. L. (2002). Cyclic oxidation and reduction of protein methionine residues is an important antioxidant mechanism. *Mol Cell Biochem, 234-235*(1-2), 3-9.

Stipanuk, M. H., Dominy, J. E., Jr., Lee, J. I., & Coloso, R. M. (2006). Mammalian cysteine metabolism: new insights into regulation of cysteine metabolism. *J Nutr, 136*(6 Suppl), 1652S-1659S.

Szumlinski, K. K., Kalivas, P. W., & Worley, P. F. (2006). Homer proteins: implications for neuropsychiatric disorders. *Curr Opin Neurobiol, 16*(3), 251-257.

Usiello, A., Baik, J. H., Rouge-Pont, F., Picetti, R., Dierich, A., LeMeur, M., et al. (2000). Distinct functions of the two isoforms of dopamine D2 receptors. *Nature, 408*(6809), 199-203.

Venton, B. J., Seipel, A. T., Phillips, P. E., Wetsel, W. C., Gitler, D., Greengard, P., et al. (2006). Cocaine increases dopamine release by mobilization of a synapsin-dependent reserve pool. *J Neurosci, 26*(12), 3206-3209.

Walss-Bass, C., Soto-Bernardini, M. C., Johnson-Pais, T., Leach, R. J., Ontiveros, A., Nicolini, H., et al. (2009). Methionine sulfoxide reductase: a novel schizophrenia candidate gene. *Am J Med Genet B Neuropsychiatr Genet, 150B*(2), 219-225.

Wang, Y., Xu, R., Sasaoka, T., Tonegawa, S., Kung, M. P., & Sankoorikal, E. B. (2000). Dopamine D2 long receptor-deficient mice display alterations in striatum-dependent functions. *J Neurosci, 20*(22), 8305-8314.

Wassef, R., Haenold, R., Hansel, A., Brot, N., Heinemann, S. H., & Hoshi, T. (2007). Methionine sulfoxide reductase A and a dietary supplement S-methyl-L-cysteine prevent Parkinson's-like symptoms. *J Neurosci, 27*(47), 12808-12816.

Weller, C., Oneill, C. J. A., Charlett, A., Bowes, S. G., Purkiss, A., Nicholson, P. W., et al. (1993). Defining Small Differences in Efficacy between Anti-Parkinsonian Agents Using Gait Analysis - a Comparison of 2 Controlled Release Formulations of Levodopa Decarboxylase Inhibitor. *British Journal of Clinical Pharmacology, 35*(4), 379-385.

Wightman, R. M., Amatore, C., Engstrom, R. C., Hale, P. D., Kristensen, E. W., Kuhr, W. G., et al. (1988). Real-Time Characterization of Dopamine Overflow and Uptake in the Rat Striatum. *Neuroscience, 25*(2), 513-523.

Wooley, C. M., Sher, R. B., Kale, A., Frankel, W. N., Cox, G. A., & Seburn, K. L. (2005). Gait analysis detects early changes in transgenic SOD1(G93A) mice. *Muscle & Nerve, 32*(1), 43-50.

Wu, Q., Reith, M. E. A., Wightman, R. M., Kawagoe, K. T., & Garris, P. A. (2001). Determination of release and uptake parameters from electrically evoked dopamine dynamics measured by real-time voltammetry. *Journal of Neuroscience Methods, 112*(2), 119-133.

Yamaguchi, H., & Shen, J. (2007). Absence of dopaminergic neuronal degeneration and oxidative damage in aged DJ-1-deficient mice. *Mol Neurodegener, 2*, 10.

Yavich, L., Oksman, M., Tanila, H., Kerokoski, P., Hiltunen, M., van Groen, T., et al. (2005). Locomotor activity and evoked dopamine release are reduced in mice overexpressing A30P-mutated human alpha-synuclein. *Neurobiol Dis, 20*(2), 303-313.

Yavich, L., Tanila, H., Vepsalainen, S., & Jakala, P. (2004). Role of alpha-synuclein in presynaptic dopamine recruitment. *J Neurosci, 24*(49), 11165-11170.

Zhang, L., Yu, C., Vasquez, F. E., Galeva, N., Onyango, I., Swerdlow, R. H., et al. (2010). Hyperglycemia alters the schwann cell mitochondrial proteome and decreases coupled respiration in the absence of superoxide production. *J Proteome Res, 9*(1), 458-471.

Zhang, Y., D'Souza, D., Raap, D. K., Garcia, F., Battaglia, G., Muma, N. A., et al. (2001). Characterization of the functional heterologous desensitization of hypothalamic 5-HT(1A) receptors after 5-HT(2A) receptor activation. *J Neurosci, 21*(20), 7919-7927.

Zucker, R. S., & Regehr, W. G. (2002). Short-term synaptic plasticity. *Annu Rev Physiol, 64*, 355-405.

IV. Conclusions and Future Directions

One of the main foci of our laboratory is Met redox cycling as a means for cell signal regulation. Theoretically, this means that ROS normally oxidize Met residues and they are reduced by Msr. Furthermore, there is an inherent layer of modulation of protein function by ROS, as a natural product or byproduct, and a reversal via Msr. Ultimately, this may act as a molecular switch, turning protein functions on and off, or switching proteins from one function to another. Possibly, one aspect of this regulation may be a compensatory mechanism to deal with abnormal sources of ROS, arising from genetic, lifestyle, and environmental impacts. Evidence to support Met redox cycles as a method of cell signal regulation comes from potential benefits from Msr substrate-methionine sulfoxide formation and from an ROS scavenging role in other Msr-substrates (D. B. Oien & Moskovitz, 2008). Moreover, there is evidence to suggest that Msr expression is increased in the presence of Met oxidation in peptides (ongoing study; unpublished observations). The Msr system of higher-order organisms is seemingly more evolutionarily complex, possibly as a result of more complex environmental hazards, different lifestyles, and longer life spans. Extrapolating from these theories and the Free Radical Theory of Aging, some aging-related diseases could be associated with increases in ROS and inadequate antioxidant systems. Neurodegenerative diseases associated with age and oxidative stress are the basis of my research. Determining the mechanisms of disease signs and symptoms related to the Msr system may lead to new pharmaceutical approaches in the future.

A. Conclusions

In summary, we have found multiple pathologies in the absence of MsrA that correlate to neurodegenerative diseases. We have found elevated brain pathologies related to Alzheimer's disease biomarkers in the hippocampal regions of the *MsrA*$^{-/-}$ mouse (Pal, Oien, Ersen, & Moskovitz, 2007). Furthermore, bio-behavioral differences in complex task learning were detected in the *MsrA*$^{-/-}$ mouse (D. B. Oien et al., 2008). The latter results may or may not be

related to the former results. Alternatively, any hippocampal region-associated results may be attributed to changes in the D2DR (discussed below), as this receptor is known to be highly expressed in that region. These results need further exploration, and indicate a major future direction. Separately, we have found novel changes in the clearance and phosphorylation of alpha-synuclein when expressed in *MsrA* null yeast cells (D. B. Oien, Shinogle, Moore, & Moskovitz, 2009a). These results may be associated with Parkinson's disease and other synuclienopathies. It was interesting that total degradation was inhibited in these cells, in addition to the clearance of alpha-synuclein. This may provide evidence of a mechanism by which alpha-synuclein accumulates as fibrils in these cells and in the Lewy bodies of Parkinson's disease. Also, the cell survival rate changed in the same *MsrA* null yeast cells when exposed to oxidants.

Survival of yeast strains overexpressing alpha-synuclein (unpublished). In attempt to evaluate the effect of oxidative stress on alpha-synuclein expressing cells, the cells were exposed to either H_2O_2 or paraquat and their survival rate was monitored by their consequential growth levels (which represent the amount of living cells). Previously it was shown that *msrA*-KO yeast cells were most sensitive to H_2O_2 compared to WT (H_2O_2 has a minor specificity for sulfur amino acids (Moskovitz, Berlett, Poston, & Stadtman, 1997; Moskovitz et al., 1998)). As expected, following exposure to H_2O_2 the *msrA*-KO harboring the sham vector showed much lower survival rate compared to the WT strain, respectively (Fig. 1). The expression of all forms of alpha-synuclein showed enhanced survival rate in the WT strain under all conditions tested compared to the control (vector expressing cells in each condition) (Fig. 1). However, this survival enhancement was less pronounced in *msrA*-KO cells expressing alpha-synuclein and was shown to be effective mainly in H_2O_2 treated cells (Fig. 1). Interestingly, under oxidative stress mediated treatment (H_2O_2 or paraquat) the highest survival difference between WT and *msrA*-KO alpha-synuclein -expressing cells was observed when SynA30P was expressed followed by SynA53T expression, respectively (Fig. 1). The latter result is consistent with the

lower degradation rate, enhanced protein oxidation, and aggregation levels when SynA30P is expressed in *msrA*-KO cells (D. B. Oien et al., 2009a). This result seems inconsistent with the degenerating neurons in the Parkinson's disease pathology. However, a recent study in our lab indicates an increase of Msr expression in the presence of oxidized peptides (unpublished results). This may explain the increased survival rates of alpha-synuclein expressing cells, and the decrease in survival of *msrA*-KO cells. This idea could further be extrapolated to a mechanism in which Parkinson's disease is age-related. Thus, as Msr decreases with age, human brains may not be able to handle oxidative stress.

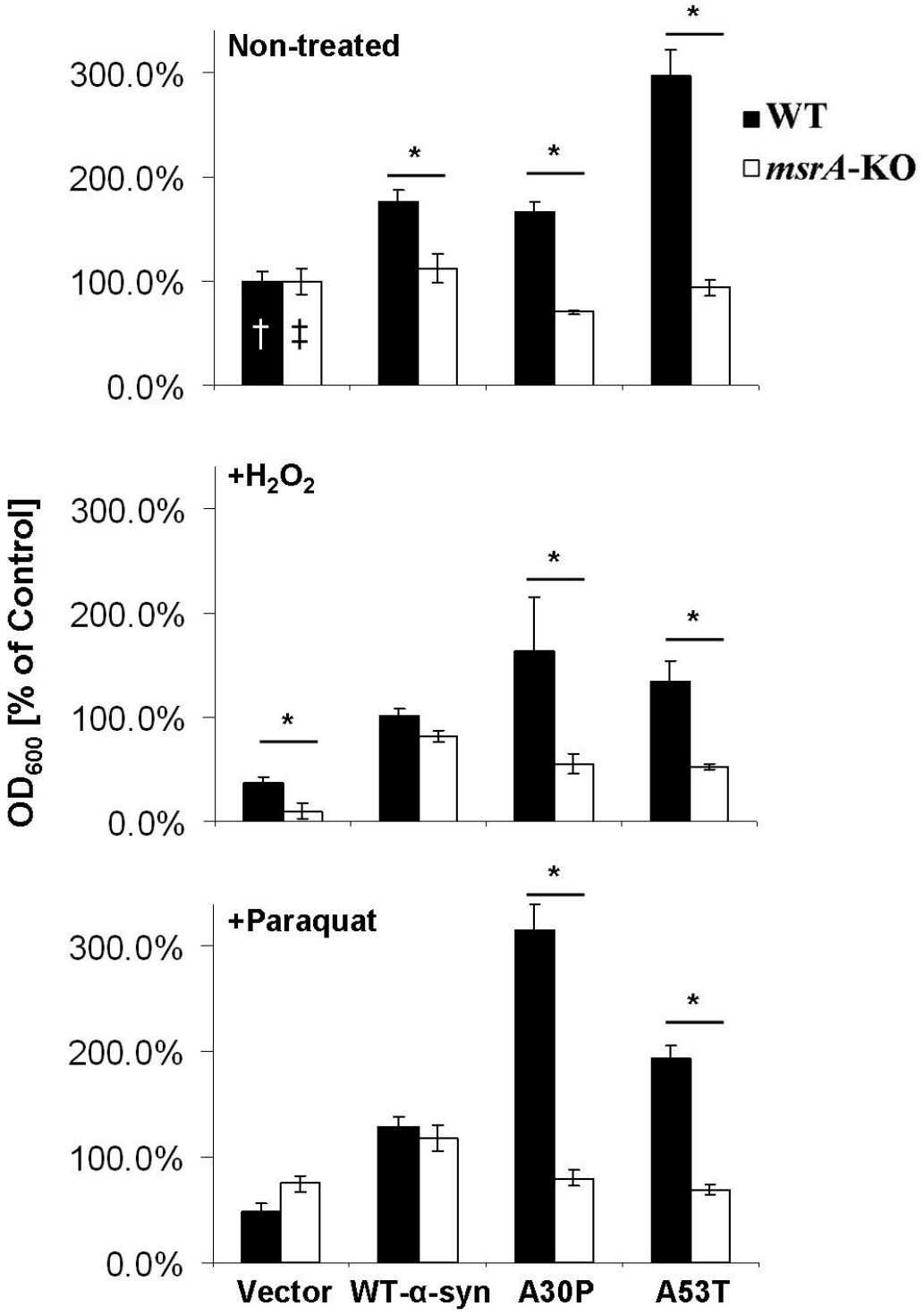

Figure 1. Survival of *msrA*-KO and WT yeast cells expressing alpha-synuclein and control vector. Yeast cells (at logarithmic growth phase) expressing the three types of alpha-

synuclein and control vector were subjected to the induction media for 2 h and then incubated with either 10 mM H_2O_2, 10 mM paraquat, or only media (control) for an additional 1 h at 30℃. The relative survival rate was monitored by inoculating each culture (1:500 dilutions) into a complete synthetic media followed by monitoring growth levels in logarithmic phase by measuring OD_{600nm}. The percent survival rate of each culture represents the percent of optical density measurements at the same time for each culture relative to the corresponding WT (†) or *msrA*-KO (‡) cells, harboring the sham vector in non-treated media. Error bars represent standard deviation, number of experiments = 3. * denotes $p < 0.01$ (*t-test*) between WT and *msrA*-KO.

The role of Met redox cycles in transmissible encephalopathies has not been established to the extent of Alzheimer's and Parkinson's disease. We have detected an increase of MetO in the scapie prion, compared to the non-infectious cellular prion protein. However, other reports of specific Met residue oxidation, Met213, claim that this modification is probably not associated with the disease (Silva et al., 2010). In contrast, other reports state that the sulfoxide on Met213 can destabilize the structure of the cellular prion protein, which may be essential for the pathogenic conversion (Colombo, Meli, Morra, Gabizon, & Gasset, 2009). This report also claims another Met modified to sulfoxide, M206, can cause similar structural changes. The role of this Met, and all other Mets, in prion-related disease has yet to be determined.

After creation of the *MsrA*$^{-/-}$ mouse, several characteristics were noticed including an abnormal "tip-toe" walking pattern (Moskovitz et al., 2001). We later performed a gene array (D. B. Oien & Moskovitz, 2008) and behavioral tests (D. B. Oien et al., 2008) concurrently to better characterize this genotype. After genomic analysis, we found that 14-3-3zeta expression was changed in 6-month-old *MsrA*$^{-/-}$ mice. This protein is an activating protein for tyrosine hydroxylase, and key enzyme in DA synthesis. Together with locomotor behavior deficits and a decreased response to amphetamine injection, we concluded there was a possible problem in DA signaling. Surprisingly, DA levels were elevated in younger *MsrA*$^{-/-}$ mice. The abnormal locomotor and DA levels were alleviated when the mice were on a CR diet (D. B. Oien, Osterhaus, Lundquist, Fowler, & Moskovitz, 2010). Food restriction theoretically reduces oxidative stress, and in our experiments reduced DA levels in WT mice and increased DA levels in *MsrA*$^{-/-}$ mice. There are several methods of restricting the diet in mice. We choose a common method of basing the diet on body weight (Fig. 2). This method also resulted in reduced MetO content of several proteins, including an unknown 15 kDa protein. These proteins have not been identified, however immunoblotting confirmed the 15 kDa protein is not alpha-synuclein.

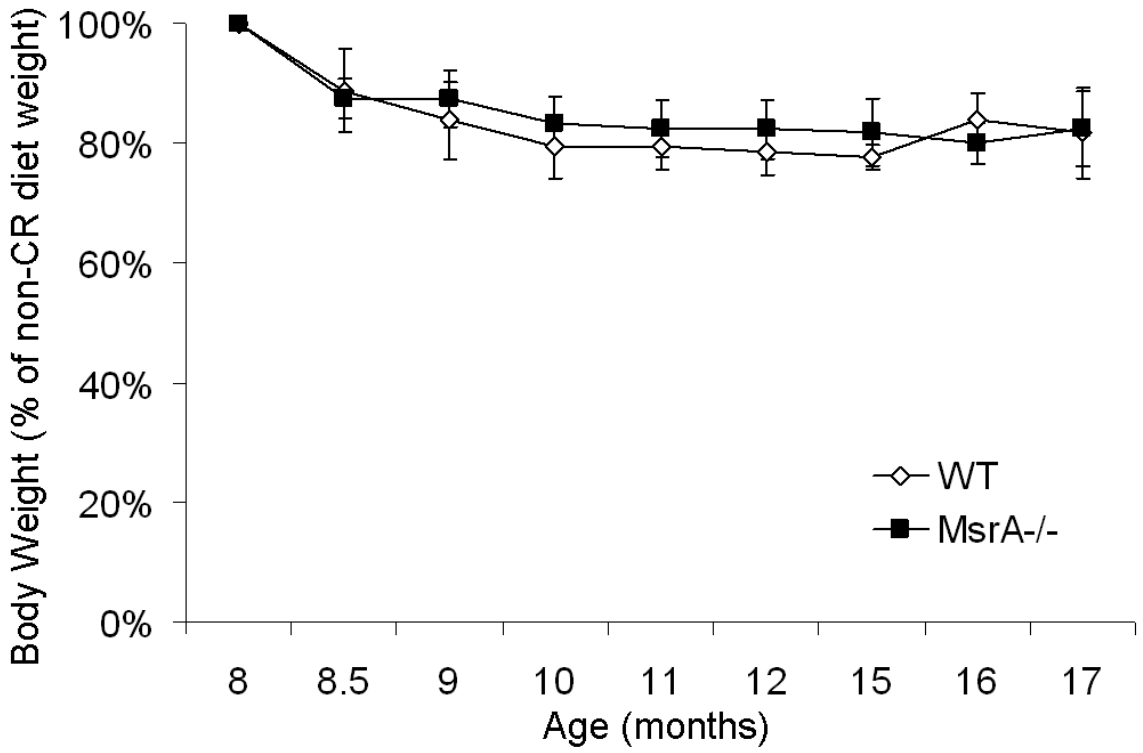

Figure 2. The average body weight of the *MsrA*$^{-/-}$ mice on CR diet by percent of *ad libitum* starting weight. The amount of food available to each mouse was restricted after eight months of age as described in "Materials and Methods" (D. B. Oien et al., 2010). Mice were fed an amount of food proportional to their *ad libitum* starting weight (8 months) until each achieved a loss of 15% original body weight, which occurred within 15 days (8.5 months). Based on semiweekly weight monitoring, each mouse was maintained at 15-20% of the respective original weight by adjusting the daily available food. The monthly average body weight of the *MsrA*$^{-/-}$ mice on CR diet as a percent of the *ad libitum* starting weight. *Y axis* represents the average by percent of original weight for each mouse. *X axis* represents each month of the CR diet. *Black squares* - *MsrA*$^{-/-}$ mice. *Open diamonds* – WT control mice. No significant difference was detected by repeated measures ANOVA. The three-month body weight average of the *MsrA*$^{-/-}$ mice on CR diet. The three-month average body weight in grams at 8 months (Pre-CR diet), and at 4 and 9 months of CR diet (12 month- and 17 month-old mice, respectively) was

determined by semiweekly monitoring. Bars represent average of *MsrA*$^{-/-}$ mice (*filled*) and WT mice (*open*). No significant difference was detected between mouse genotypes within respective age groups by the Student's t-test. Error bars represent standard deviation of 11-13 mice per genotype in both graphs.

Presynaptic DA levels were also increased in coronal brain sections of *MsrA*$^{-/-}$ mice (D. B. Oien et al., 2008). Further studies indicated that DA reserve pools were increased (Ortiz, Oien, Johnson, & Moskovitz, Manuscript). These results and prior data indicate that there is an increase in DA synthesis. Importantly, presynaptic DA release of *MsrA*$^{-/-}$ mice was also examined in the presence of incrementing calcium levels. No significant change was observed, suggesting that calcium regulatory proteins in *MsrA*$^{-/-}$ mice were functioning properly. The significance of this target comes from multiple literature sources that have noted calcium regulatory proteins, such as calmodulin and calcium/calmodulin kinase II, as Msr substrates. As calcium levels are involved in vesicle mobilization and release, this result further suggests that natural physiological DA release is not increasing or decreasing, at least based on calcium level regulation. The increase in DA synthesis may be due to a lack of autoreceptor signaling, which is modulated via a D2DR isoform.

Several results indicated a potential abnormality in D2DR signaling. Decreased locomotor activity, cognitive deficits, and unresponsiveness to increases in extracellular DA (via amphetamine injection) (D. B. Oien et al., 2008) can all be all be related to poor DA receptor signaling. In addition to increased synthesis, the *MsrA*$^{-/-}$ mice were later found to be less responsive to the D2DR agonist quinpirole indicating poor D2DR autoreceptor signaling (quinpirole is known to decrease locomotor activity in mice at the concentrations used, presumably by decreasing presynaptic DA) (DB Oien et al., In Press). All together, these results indicate a problem with D2DR signaling. This was confirmed by receptor binding studies in which a D2DR agonist bound to receptors with less affinity than a D2DR antagonist. In contrast, receptor binding results with a D1DR agonist and antagonist did not show any significant difference in the *MsrA*$^{-/-}$ mice, suggesting a particular specificity for the D2DR. The D2DR has more Met residues where G-proteins couple (third intracellular loop) than other DA receptors. Indeed, D2DR agonist binding could be restored by the addition of Msr and G-protein coupling

was decreased in *MsrA*$^{-/-}$ mice (DB Oien et al., In Press), suggesting MetO formation in the D2DR third intracellular loop. D2DR purification experiments to detect MetO were unsuccessful.

B. Hypotheses and Future Directions

The role of the Msr system in neurodegenerative diseases is still being evaluated. We have found that Alzheimer's disease-related biomarkers were elevated in *MsrA*$^{-/-}$ mice (Pal et al., 2007). In addition, Met oxidation of the amyloid-beta peptide, known to form amyloid plaques in Alzheimer's disease, can be neurotoxic (Schoneich, 2005). This is in contrast to increases in (yeast) cell survival in when an Msr substrate (alpha-synuclein) was overexpressed in WT cells (as shown in Fig. 1). However, an ongoing study has shown evidence that Met oxidation of substrates can increase Msr expression (new results; data not shown). Based on previous reports that show Msr expression decreases in aging tissues, including brain tissues (Petropoulos, Mary, Perichon, & Friguet, 2001; Stadtman, Moskovitz, Berlett, & Levine, 2002), we hypothesize that Met redox cycles are disrupted in Alzheimer's disease. This hypothesis includes the aging component of this neurodegenerative disease; thus, the genetic, lifestyle, and environmental impacts are negligible until an older age is reached and Msr capability has decreased. This concept is supported by reports of decreased Msr in Alzheimer's disease brains (Gabbita, Aksenov, Lovell, & Markesbery, 1999). Obviously, there are many more factors that may affect the etiology of Alzheimer's disease, but the role of the Msr system in Alzheimer's disease, and to what extent this role is, remains a future direction.

The role of the Msr system in Parkinson's disease and other synucleinopathies may be similar to that hypothesized for Alzheimer's disease. However, a decrease of Msr expression and activity has not been shown in Parkinson's disease patients to date. In spite of this missing information (that is major future direction), our studies (D. B. Oien, Shinogle, Moore, & Moskovitz, 2009b) and studies from other groups support the need for a better understanding of alpha-synuclein and corresponding Met oxidation. One challenge of studying alpha-synuclein in

mice, including *MsrA*$^{-/-}$ mice, is that the protein has a few different residues at the primary structure than that of human alpha-synuclein. One difference between human and murine alpha-synuclein is the threonine at position 53, which is also found in the A53T genetic form of Parkinson's disease. To overcome this, I have proposed to express human alpha-synuclein in *MsrA*$^{-/-}$ mice, which would create a model for studying Met redox cycles and the alpha-synuclein substrate. Integrative knowledge from our research group and others lead us to propose the central hypothesis that the Parkinsonian characteristics of substantia nigral neurodegeneration, gait and locomotor activity deficits, and alpha-synuclein modification and aggregation will develop progressively over time in mice that lack Msr with nigrostriatal-targeted overexpression of human alpha-synuclein (from my comprehensive example proposal). The overall goal of the following proposed experiments will be to analyze this mouse as a potential model of Parkinson's disease.

In addition to studies on alpha-synuclein, we have discovered that *MsrA* ablation disrupts DA signaling and the D2DR is a substrate for Msr (DB Oien et al., In Press). One major difficulty in this study was the purification of the mouse D2DR, which still remains to be accomplished. Once the D2DR is purified from *MsrA*$^{-/-}$ mice, mass spectrometry analysis may indicate which methionine residues in the receptor are oxidized. This information, and purification of D2DR from Parkinson's disease patients, will provide for a possible new area of research based on abnormal DA signaling and associated molecular mechanisms. One possibility may be changes to D2DR phoshorylation.

Phosphorylation is a well-accepted method of regulation via posttranslational modifications. We have found new evidence for methionine sulfoxides that inhibit phosphorylation on alpha-synuclein (D. B. Oien et al., 2009b). This may be more of a general phenomenon, and remains to be investigated in the D2DR and other physiological systems. Overall, our research has been inspired by the hypothesis that Met redox cycles have a physiological role in cellular regulation, from scavenging ROS to changing the functions of Msr substrates. One method to uncover this

possibility is by examining when the Msr system is compromised, and this also assists in the understanding of abnormalities in Met redox cycles and disease.

C. Other Relevant Research of the Msr System

In contrast to the previous research presented, the Msr system and its respective impact extend far beyond the nervous system. There are several reports on the Msr system in other fields of research. Two of our studies on the Msr system are presented below. These studies were never continued, but like many other orphan reports on Msr they may become more important as new information on the Msr system in uncovered.

1. MsrA and Cystiene Dioxygenase

(D. B. Oien & Moskovitz, 2007b)

Msrs are able to reduce MetO to Met both in proteins and free amino acids. By their action it is possible to regulate the function of specific proteins and the cellular antioxidant defense against oxidative damage. Similarly, cysteine dioxygenase (CDO) may be involved in the regulation of protein function and antioxidant defense mechanisms by its ability to oxidized Cys residues. The two enzymes' involvement in sulfur amino-acids metabolism seems to be connected. Lack of MsrA in liver of *MsrA*$^{-/-}$ led to a significant drop in the cellular level of thiol groups and lowered the CDO level of expression. Moreover, following selenium deficient diet (applied to decrease the expression levels of selenoproteins like MsrB), the latter effect was maintained while the basal levels of thiol decreased in both mouse strains. We suggest that both enzymes are working in coordination to balance cellular antioxidant defense.

2. MsrA and Non-Replicative Senescence of Yeast

(D. Oien & Moskovitz, 2007a)

The major enzyme of the Msr system is MsrA. Senescing msrA knockout mother yeast cells accumulated significant amounts of protein-carbonyl both at 5 generation-old (young) and 21 generation-old (old) cultures, while the control mother cells showed significant levels of protein-carbonyl mainly in the old culture. The Msr activities of both yeast strains declined with age and exposure of cells to H_2O_2 caused an accumulation of protein-carbonyl especially in the msrA knockout strain. It is suggested that a compromised MsrA activity may serve as a marker for non-replicative aging.

D. References

Colombo, G., Meli, M., Morra, G., Gabizon, R., & Gasset, M. (2009). Methionine sulfoxides on prion protein Helix-3 switch on the alpha-fold destabilization required for conversion. *PLoS One, 4*(1), e4296.

Gabbita, S. P., Aksenov, M. Y., Lovell, M. A., & Markesbery, W. R. (1999). Decrease in peptide methionine sulfoxide reductase in Alzheimer's disease brain. *Journal of Neurochemistry, 73*(4), 1660-1666.

Moskovitz, J., Bar-Noy, S., Williams, W. M., Requena, J., Berlett, B. S., & Stadtman, E. R. (2001). Methionine sulfoxide reductase (MsrA) is a regulator of antioxidant defense and lifespan in mammals. *Proc Natl Acad Sci U S A, 98*(23), 12920-12925.

Moskovitz, J., Berlett, B. S., Poston, J. M., & Stadtman, E. R. (1997). The yeast peptide-methionine sulfoxide reductase functions as an antioxidant in vivo. *Proc Natl Acad Sci U S A, 94*(18), 9585-9589.

Moskovitz, J., Flescher, E., Berlett, B. S., Azare, J., Poston, J. M., & Stadtman, E. R. (1998). Overexpression of peptide-methionine sulfoxide reductase in Saccharomyces cerevisiae and human T cells provides them with high resistance to oxidative stress. *Proc Natl Acad Sci U S A, 95*(24), 14071-14075.

Oien, D., & Moskovitz, J. (2007a). Protein-carbonyl accumulation in the non-replicative senescence of the methionine sulfoxide reductase A (msrA) knockout yeast strain. *Amino Acids, 32*(4), 603-606.

Oien, D., Ortiz, A., Rittel, A., Dobrowsky, R., Johnson, M., Levant, B., et al. (In Press). Dopamine D2 Receptor Function is Compromised in the Brain of the Methionine Sulfoxide Reductase A Knockout Mouse. *Journal of Neurochemistry*.

Oien, D. B., & Moskovitz, J. (2007b). Ablation of the mammalian methionine sulfoxide reductase A affects the expression level of cysteine dioxygenase. *Biochem Biophys Res Commun, 352*(2), 556-559.

Oien, D. B., & Moskovitz, J. (2008). Substrates of the methionine sulfoxide reductase system and their physiological relevance. *Curr Top Dev Biol, 80*, 93-133.

Oien, D. B., Osterhaus, G. L., Latif, S. A., Pinkston, J. W., Fulks, J., Johnson, M., et al. (2008). MsrA knockout mouse exhibits abnormal behavior and brain dopamine levels. *Free Radic Biol Med, 45*(2), 193-200.

Oien, D. B., Osterhaus, G. L., Lundquist, B. L., Fowler, S. C., & Moskovitz, J. (2010). Caloric restriction alleviates abnormal locomotor activity and dopamine levels in the brain of the methionine sulfoxide reductase A knockout mouse. *Neurosci Lett, 468*(1), 38-41.

Oien, D. B., Shinogle, H. E., Moore, D. S., & Moskovitz, J. (2009a). Clearance and phosphorylation of alpha-synuclein are inhibited in methionine sulfoxide reductase a null yeast cells. *J Mol Neurosci, 39*(3), 323-332.

Oien, D. B., Shinogle, H. E., Moore, D. S., & Moskovitz, J. (2009b). Clearance and Phosphorylation of Alpha-Synuclein Are Inhibited in Methionine Sulfoxide Reductase A Null Yeast Cells. *J Mol Neurosci*, *In Press*.

Ortiz, A. N., Oien, D. B., Johnson, M. A., & Moskovitz, J. (Manuscript). Dopamine Reserve Pool Mobilization in Methionine Sulfoxide Reductase Null Mice.

Pal, R., Oien, D. B., Ersen, F. Y., & Moskovitz, J. (2007). Elevated levels of brain-pathologies associated with neurodegenerative diseases in the methionine sulfoxide reductase A knockout mouse. *Exp Brain Res, 180*(4), 765-774.

Petropoulos, I., Mary, J., Perichon, M., & Friguet, B. (2001). Rat peptide methionine sulphoxide reductase: cloning of the cDNA, and down-regulation of gene expression and enzyme activity during aging. *Biochem J, 355*(Pt 3), 819-825.

Schoneich, C. (2005). Methionine oxidation by reactive oxygen species: reaction mechanisms and relevance to Alzheimer's disease. *Biochim Biophys Acta, 1703*(2), 111-119.

Silva, C. J., Onisko, B. C., Dynin, I., Erickson, M. L., Vensel, W. H., Requena, J. R., et al. (2010). Assessing the role of oxidized methionine at position 213 in the formation of prions in hamsters. *Biochemistry, 49*(9), 1854-1861.

Stadtman, E. R., Moskovitz, J., Berlett, B. S., & Levine, R. L. (2002). Cyclic oxidation and reduction of protein methionine residues is an important antioxidant mechanism. *Mol Cell Biochem, 234-235*(1-2), 3-9.